Influence of the chemical modification of the interface on the dispersion of lignocellulosic reinforcements in Green Wood Plastic Composites GWPC : numerical model contribution on the optimization of the mechanical properties

Erica Rodi

Thèse de Doctorat

Présentée par :

Erica Gea RODI

Pour obtenir le grade de Docteur de l'Université Paris-Est

École doctorale Sciences, Ingénierie et Environnement

Spécialité : Sciences des matériaux

Influence de la modification chimique de l'interface sur la dispersion des renforts lignocellulosiques dans les Green Wood Plastic Composites (GWPC) : apport de la modélisation sur l'optimisation des propriétés mécaniques.

Soutenue le 13 décembre 2017

Rapporteur	Emmanuel RICHAUD	Professeur, Arts et Métiers ParisTech
Rapporteur	Marco GIGLIOTTI	Professeur, Université de Poitiers, ISAE-ENSMA
Examinateur	Salah RAMTANI	Professeur, Université Paris 13, CSPBAT
Directeur de thèse	Valérie LANGLOIS	Professeur, Université Paris-Est, ICMPE
Co-directeur	Thibault LEMAIRE	Professeur, Université Paris-Est, MSME
Co-encadrant	Vittorio SANSALONE	Professeur, Université Paris-Est, MSME

Thèse de Doctorat

Présentée par :

Erica Gea RODI

Pour obtenir le grade de Docteur de l'Université Paris-Est

École doctorale Sciences, Ingénierie et Environnement

Spécialité : Sciences des matériaux

Influence de la modification chimique de l'interface sur la dispersion des renforts lignocellulosiques dans les Green Wood Plastic Composites (GWPC) : apport de la modélisation sur l'optimisation des propriétés mécaniques.

Soutenue devant le jury composé de :

Rapporteur	Emmanuel RICHAUD	Professeur, Arts et Métiers ParisTech
Rapporteur	Marco GIGLIOTTI	Professeur, Université de Poitiers, ISAE-ENSMA
Examinateur	Salah RAMTANI	Professeur, Université Paris 13, CSPBAT
Directeur de thèse	Valérie LANGLOIS	Professeur, Université Paris-Est, ICMPE
Co-directeur	Thibault LEMAIRE	Professeur, Université Paris-Est, MSME
Co-encadrant	Vittorio SANSALONE	Professeur, Université Paris-Est, MSME

II

Acknowledgments

"Gratitude is not only the greatest of virtues, but the mother of all the others"; this is what Cicero said in I century B.C. Now, by saying "thank you" I want to express my gratitude to all those persons who have contributed to this work and I want to return the affection received during these long three years.

First of all, I would like to thank the directors of the two laboratories, the professor Michel Latroche of the ICMPE and the professor Salah Naili of the MSME for having hosting me in their institutes and allowing me to work in the best conditions, as well as the LABEX MMCD for funding this work and the "École doctorale ED-SIE" for all the proposed courses that have enriched me. I would like to thank also the members of the jury, Professors Richaud and Gigliotti who have done me the honor of evaluating my thesis, giving precise advises and useful suggestions about the work. A great thanks goes also to Professor Ramtani for his kindness and availability to accept the role of examiner in the committee.

I would like to express all my gratitude to my supervisor Valérie Langlois. She was constantly engaged with energy in this project, conducting this work with optimism and allowing me to always see the positive side of doing research. I would like to thank my co-supervisor, Estelle Renard for her generosity and also for her extraordinary good mood. Thanks also to my other co-supervisor Vittorio Sansalone for his prompt intervention in solving all problems presented during this work and for the discussions in our mother tongue that have often reassured me. I would like to express my endless gratitude to my other supervisor, Thibault Lemaire, excellent teacher and source of inspiration. Thank you, Thibault, for accepting my strange professional profile in your research team, thank you for guiding me in this path with the irony and sympathy that I needed and finally thank you for believing in me.

I would like to thank Luca Andena and Francesco Briatico for hosting me in the department "Giulio Natta" at the Polytechnic of Milan, directing my work carefully and integrating me into a solid and intellectually stimulating research group. A great thanks goes also to Professor Andrea Pavan for his valuable tips. I will always remember "my Milanese period" with a great smile!

I would like to thank all the members of the administrative team and in particular Isabelle of the MSME, whose "joie de vivre" has been for me as a drug delivered every morning and Marcelle of the ICMPE whose affection makes me feel at home. A great "thank you" goes to all the technicians and lecturers of the three laboratories who have contributed to this work from the beginning. I would like to express my gratitude also to all the professors of the three laboratories for their unconditional help and to all the interns who have worked by my side and who have contributed in a decisive way for the result of this work.

A great thanks goes to my colleagues all, companions of adventure, some of them became friends during this long journey. I will never forget the endless hours spent with my dear friend Etienne in front of the extruder or the memorable evenings with Antoine B., Sarra, Etienne, Romain P., Azad, little Alina and Pierre. I will never forget the extraordinary days with Ilaria, Romain V. and Antoine T. and our aperitifs in the afternoon to have the necessary "energy" to work or the good times spent with Carine and Tina in our office and lastly the Milanese colleagues, true gentlemen. I

To Maria Foresi,

whose doubtful mind and pure soul,

have inspired my best thoughts and

consolidated my deepest certainties.

Table of contents

Chapter II

List of figures and schemes

General Introduction

Chapter V

Chapter VI

List of tables

"How much truth can a spirit endure,
how much truth can it dare?
This became for me more and more
the actual test of value.
Error (the belief in the ideal) is not blindness;
error is cowardice.
Every conquest,
every step forward in knowledge
is the outcome of courage, of hardness towards one's self;
of cleanliness towards one's self."

(Friedrich Nietzsche)

GENERAL INTRODUCTION

The manufacturing and characterization of green composite materials constituted by bio-based and biodegradable polymers as matrixes and vegetal fibers as reinforcement represents the general context of this work. Growing environmental consciousness and changes in public policy have led to an increasing demand for environmental eco-friendly materials with a subsequent progress in the field of material science and an improvement of the associated technology. More precisely, in the recent years, many efforts have been carried out from industries and researchers in different fields such as organic chemistry, chemical engineering and process to improve the properties of such biocomposites. The goals are to find new green materials by optimizing the processing steps necessary to their manufacture and trying to control their mechanical behavior. Nowadays, the high specific strength, the lightweight, the biodegradability and the eco-friendly character of natural fiber reinforced polymer composites should be preferred to the traditional composites derived from petroleum resources, these last being not eco-friendly due to their low degradability level. Many efforts have been made to improve the characteristics of the biocomposites, typically acting on their mechanical resistance and their thermal stability, in order to make them competitive with the traditional ones.

Notwithstanding their green character, biocomposites present a series of concerns that affect their final application. Some of these problems are related to the cost, which remains relatively high at present and to the difficulty in processability of certain bio-based matrixes when compared to traditional ones. A second concern is related to the physical incompatibility between the hydrophilic vegetal fibers and the hydrophobic matrixes, which causes a lack of adhesion between the constituents at their interface, inducing poor dispersion of reinforcement in the continuous phase, fibers pulling out, mechanical properties and resistance to environmental aging of the composite worse than those in which the contact matrix/fibers is good. In this context important challenges include the good homogenization of fibers in the matrix, the improvement of the adhesion between fibers and matrix, the reduction of the processing impact on the degradation of polymer and on the fibers structure, and the full understanding of all those mechanisms related to the environmental conditions to which a biocomposite could be subjected during his life-cycle. Undoubtedly, the combined action of a good treatment of natural fibers, the appropriate choice of the matrix and an adequate processing method are the key factors for the realization of biocomposites that meet the criteria of sustainability, biodegradability and compostability required these last years (figure I-0). Among all existing matrixes, this work takes into account the thermoplastic polymers and among these last, the aliphatic

biodegradable polyesters were chosen thanks to their great availability, biodegradability and pretty good mechanical properties. More precisely, this thesis focuses on the realization and characterization of biocomposites made of poly(ε-caprolactone) (PCL), poly(3-hydroxybutyrate-*co*-3-hydroxyvalerate) (PHBHV) and poly (lactic acid) (PLA), as matrixes and Miscanthus *giganteus* (MIS) fibers as reinforcement. The thesis has been organized as a set of articles in which different aspects of biocomposites were taken into account and studied.

The first chapter constitutes a general overview on the existing literature about composites materials, with peculiar attention to the mechanical and thermal properties of the biopolymers and the effect of fiber's type and arrangement on the characteristics of the final composite. The properties of each constituent were taken into account in order to choose appropriate matrixes and reinforcement for the experimental section. Moreover, particular attention was given to the processing methods and to all those chemical treatments that could improve the mechanical properties of the final material. In addition, an overview on analytical and numerical models was made in order to choose an appropriate model that could help in designing the mechanical behavior of the biocomposites.

The second chapter focuses on the effect of chemical modification of fibers based on a two-steps procedure. The first step consists on a thiol-ene reaction carried out between the double bonds present in the lignin of fibers and the thiol groups characterizing the reactive used. The second step consists in the grafting of the polyester, in this case PCL, to the vegetal fibers using a peroxide. The originality of this method relies on the fact that it directly modifies vegetable fibers without using pre-treatments and it acts on the unsaturated bonds present in the fibers instead of cellulose, this last being largely studied in literature. This part has allowed us to find a green chemical modification method applicable to any polyester. The identified chemical treatment will be able to improve the mechanical properties of the final material maintaining the green character of the composite.

The third, fourth and fifth chapters are dedicated to the characterization of biocomposites realized with the most innovative bio-based matrix used in this work, the PHBHV. In the third chapter the effect of filler content was investigated and a micromechanical approach was used to identify a model that could approximate the mechanical behavior of the final material. More precisely, a homogenization approach was used and fibers modeled as cylindrical inclusions in a perfect contact with the matrix seems to well approximate the experimental mechanical behavior of the biocomposites.

Once defined processing parameters, the effect of reinforcement sizes and arrangement were investigated in the fourth chapter by 2D and 3D numerical models aiming at determining not only the effective mechanical behavior of the biocomposites but also the distribution of the stress in the material, giving by this way important information on the non-linear behavior. The fifth chapter focuses on the combined effect of fibers size and chemical treatment using reactive extrusion on the PHBHV-based composites. The aim of this chapter was to understand the mechanism behind the reactive process and to try to provide a quantification of the cross-linking phenomenon occurring during the reactive extrusion.

The last chapter focuses on the effect of processing, chemical modification of fibers and photo-oxidative aging on PLA-based composites. At this stage, a more pragmatic approach was considered, taking into account the reduction of the total cost by the use of a less expensive matrix such as the PLA and the possibility to use other processing methods that can minimize the polymer degradation. Moreover, a preliminary study of the long term behavior of the PLA/MIS composites allowed us to a present a full characterization of the biocomposites, establishing relations between the mechanical properties and the microstructural changes of the polymer matrix.
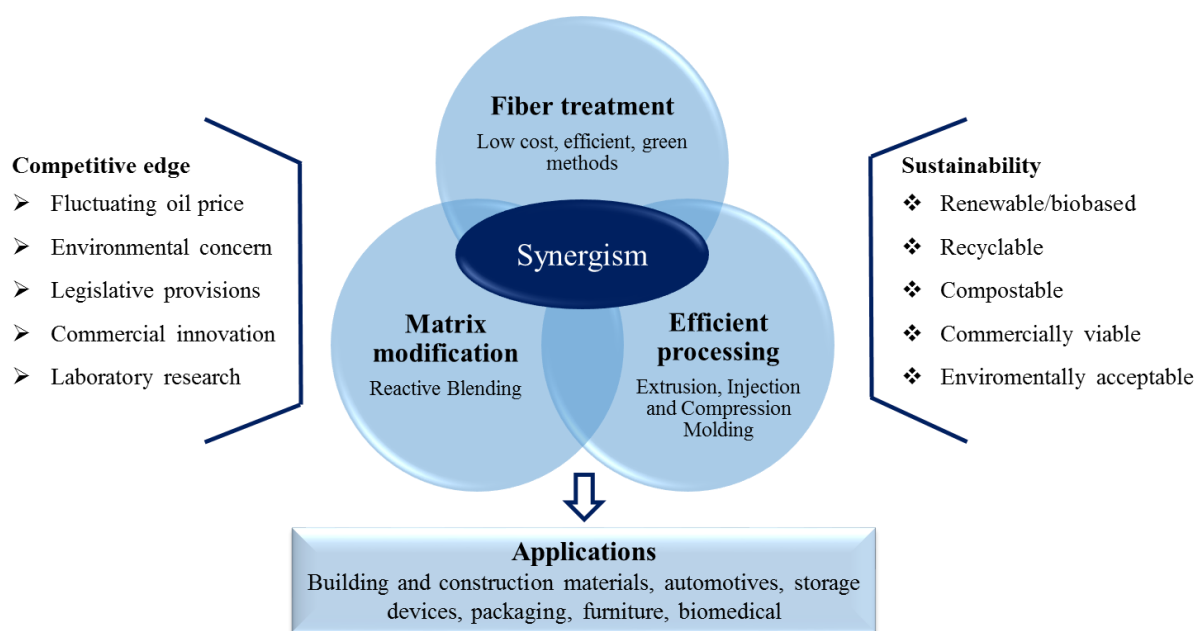
Figure I-0. Performance, competitiveness, sustainability balance and applications of biocomposites (adapted from [1]).

Chapter I:

Green Wood Plastic Composites

I-1. AN OVERVIEW ON COMPOSITES MATERIALS

The term "composite" refers to a material obtained by combining two or more constituents, by adhesion or cohesion, different in shape and chemical composition and separated by an interface. The final product has properties that are different from those of the individual constituents [2]. This concept is very old. For instance, the ancients mixed straw and mud to get a building material and Mongol warriors used biocomposites made of natural fibers and pine resins to craft swifter and more powerful archery bows [3]. However, the word "composite" was first introduced only in the 1950's. Today one of the most used composites in the construction field, the reinforced concrete, belongs to this type of materials.

In general, composites are constituted by a continuous phase called "matrix" and a discontinuous one called "reinforcement". This last is in general responsible of the strength and stiffness of the final material, while the matrix is used to transfer the applied external loads by adhering to the discontinuous phase. Furthermore, the matrix has the function to give a shape to the finished object, holding together the type of reinforcement used (particles or fibers) [4]. A more accurate analysis of the composition and internal structure of composite materials shows that, in addition to those phases previously mentioned (matrix and fibers), there is also a third phase, located between the matrix and the reinforcement, called interface. This last can be seen as a separation surface between the different phases that constitute the composite material. However, the microscopic observation of the areas near to the interface shows that this part have not only different structure but also different properties. For this reason, in such cases, the word interface is substituted by the word interphase, which corresponds to a defined area with specific chemical structure produced during the processing step or created voluntarily to protect the reinforcement. This fact means that a composite cannot be considered as a homogeneous material from a microscopic point of view because of the presence of different phases and also of an interphase [5].

The constituents of a composite exhibit very different performances and according to the principle of the combined actions, the optimization of properties (mechanical, cost etc.) are achieved by the careful combination of two or more different materials. For instance, in the case of mechanical properties, the addition of fibers with high tensile modulus to a matrix highly deformable results in a composite with intermediary properties between those of the two constituents, like showed in the figure I-1.
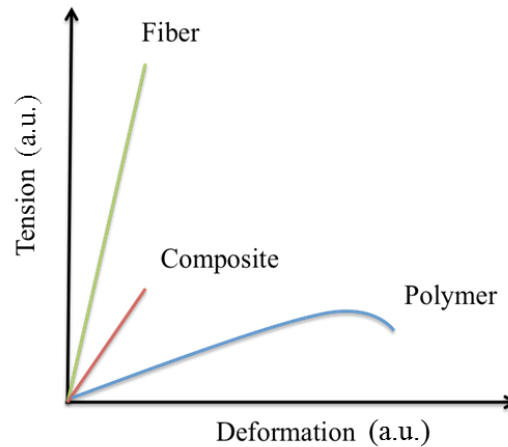
Figure I-1. Principle of combined actions for the mechanical resistance of a composite material constituted by a fiber reinforced polymeric matrix.

Composites can be classified using different criteria. One of this is based on the reinforcing type and its orientation in the polymer matrix (see figure I-2). More precisely, we can distinguish fibrous or particulate reinforcements. The fibrous one can be organized in a discontinuous or in a continuous way. In the first case, short fibers are used with a random or a partial orientation, while in the second case long fibers are preferred, resulting in unidirectional or bidirectional composites [5].
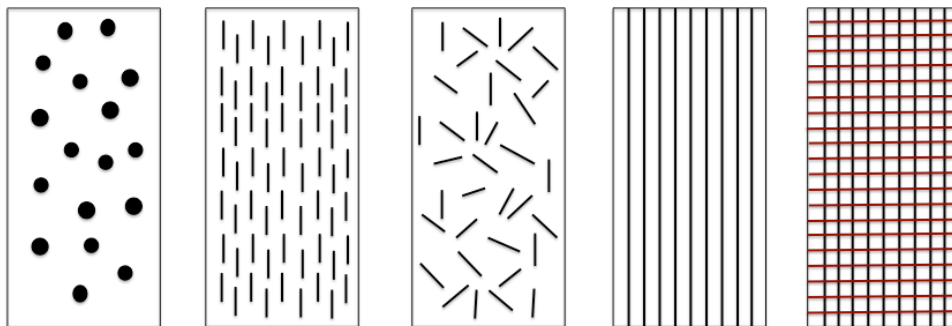
Figure I-2. Example of reinforcement in the matrix. From left to right: particulate random, discontinuous fibers (unidirectional), discontinuous fibers (randomly arranged), continuous fibers (unidirectional) and continuous fibers (bidirectional) (adapted from [5]).

Undoubtedly one of the most important classification is based on the type of matrix used, this last being the continuous phase present in greater quantity in the blend. Matrixes can be polymeric, metallic or ceramic [6]. The possibility to be processed at temperatures lower than 250°C by using conventional techniques, the combination of low density and good mechanical properties, the relatively low cost and the great availability and variability of matrixes, often makes of polymers the good candidates for the realization of composite materials [5, 7, 8]. For all these reasons, this work

is restricted on polymer matrix composites (PMCs), classifiable by different criteria [9], typically one of these is that based on the polymer type. According to this last, we can distinguish two great categories of polymers: thermosets and thermoplastics as shown in figure I-3.

Thermoplastics   **Thermosets**

Semicrystalline   **Amorphous**

Polyolefin (PE, PP…)   PVC   Epoxy resins
Biodegradable Polyesters   PS   Phenolic resins
                                        PC   Amino resins
                                        PMMA   Polyimides
                                                            Unsaturated polyesters
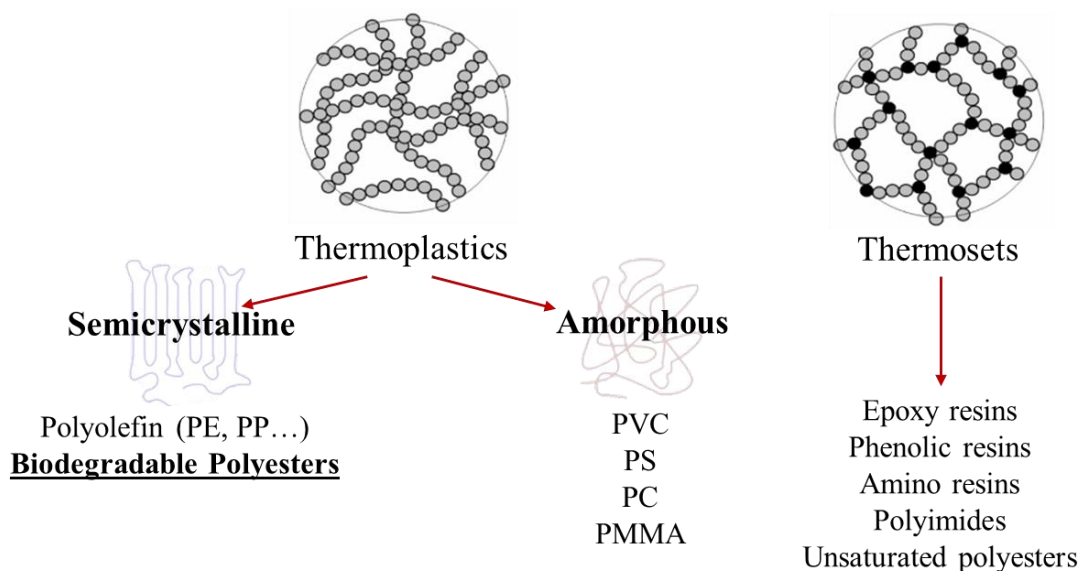
Figure I-3. Common polymers classification.

To the first category belong all those polymers whose polymerization process induces a cross-linking phenomenon. This process takes place directly in a mold and it is irreversible, causing insolubility, infusibility and high stiffness [10]. Thermosets resins have been largely used for the realization of high performant composite materials for different reasons. First of all, the liquid form of these resins before curing promotes the impregnation of the reinforcement at room temperature. Second of all, the final composite can be used for high temperature applications, keeping its shape due to the covalent bonds formed between the polymer chains. However the improvement of the hardness of these materials causes a consequent increase in brittleness. Thermoplastics are linear or slightly branched polymers. They can be processed with different techniques and re-heated more than one time. Actually, they can be modeled under the action of heat without changing their chemical composition and thus to form various shapes after cooling. They can be considered as ductile materials compared to the first category. Polymers belonging to the class of thermoplastics are a great number of polyolefin such as polyethylene (PE) and polypropylene (PP), polyesters and many others [11-16]. An important group of thermoplastics which is fundamental in the realization of biocomposites is that of aliphatic biodegradable polyesters, produced both from renewable and petrochemical resources. After cooling, thermoplastics result in amorphous or semicrystalline polymers. The first are constituted by randomly arranged chains and the second are constituted both

by amorphous domains and by compacted polymer chains called crystalline regions (see figure I-4). Two different temperatures are fundamental in order to well understand the properties of these two categories: the melt temperature and the glass transition one (T_M and T_g respectively). Melting is a transition occurring in semicrystalline polymers when the polymer chains fall out of their crystal structure and pass to a disordered liquid at a certain temperature (T_M). The glass transition occurs in amorphous materials or in semicrystalline materials which possess amorphous domains and it represents the transition of the polymer from a "glassy" state to a rubbery one.
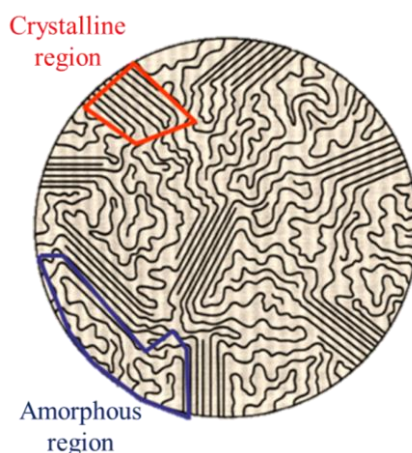
Figure I-4. Crystalline and amorphous regions in a semicrystalline polymer (from [17]).

The amorphous regions can be seen as disordered structures, while the crystalline regions are aggregates of crystallites, folded chains, usually in form of spherulites. The number and size of these last, depending on the macroscopic temperature of the crystallization process, influence the mechanical properties and also the diffusion phenomena. For these polymers the choice of the processing temperature is very critical. The melting temperature have to be reached in order to obtain a viscous state, but it is not very good to exceed this temperature level in order to avoid degradation. The glass transition and melting are the two phenomena which limit the maximum operating temperature for a thermoplastic polymer. In general, we can affirm that a maximal temperature equal to T_g and a maximal temperature equal to T_M can be used for amorphous and semicrystalline matrixes respectively. However these limits are only theoretical because in general the Young modulus E of a semicrystalline polymer already decreases when exceeding the glass transition temperature. In the present work, only semicrystalline matrixes are considered. The great advantage to realize semicrystalline polymers-based composites is the important increase in the tensile modulus E above the T_g. This makes it possible to use the material under high stress at higher temperature. This effect is shown in the figure I-5.
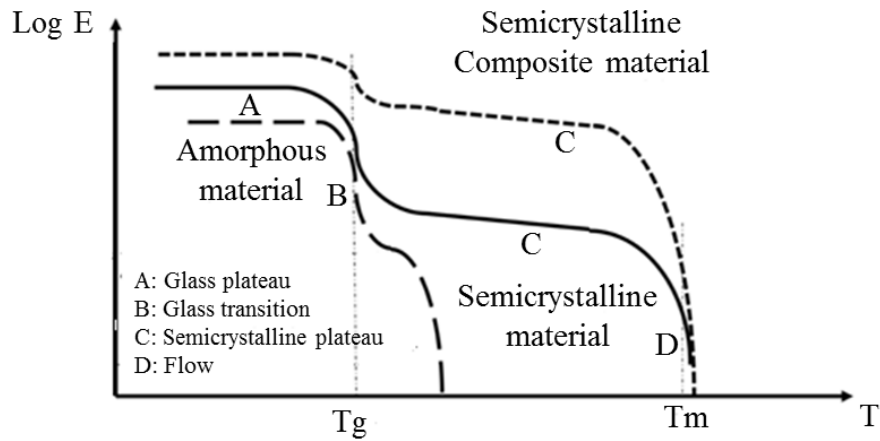
Figure I-5. Log E vs T curves for amorphous, semicrystalline and semicrystalline thermoplastic reinforced with fibers (adapted from [18]).

As previously said, one of the functions of a typical matrix is to bond the fibers together and to transfer loads between them. All these matrixes are often used with glass fiber reinforcement, but they can also be reinforced by plant fibers. This work focuses essentially on this last category whose characteristics will be described more in detail in the next paragraphs.

I-2. THE REINFORCING FIBERS

The main task of fibers used as reinforcement is that to provide strength and stiffness to the final material [19]. According to their origin, fibers can be classified as natural and synthetic. The last ones dominated the composites market until a few years ago, being produced for different application fields, such as textile but also for engineering. Among this category, glass fibers have been largely used due to the possibility to be obtained by continuous process in filaments of undefined length and thanks to their good mechanical resistance at high temperatures. However, their high density and relative low Young modulus, led researchers to find other reinforcing fibers. Carbon and aramid fibers are other fibers largely used in polymeric matrixes. The first ones have good mechanical properties due to the crystalline structure of graphite for instance and the second ones, made up of synthetic polyamide chains, present an excellent specific weight, high mechanical strength and resistance to crack propagation [20]. Despite these good characteristics, the growing attention to environmental issues and specific legislative requirements regarding environmental protection and recycling of materials, has led the researchers to develop new materials from renewable resources [21-25]. More specifically, for what concern the reinforcement of polymer matrixes, the glass fibers were substituted with less invasive reinforcements for the environment such as natural fibers [26, 27]. Actually, other advantages to use a reinforcement derived from a natural source are essentially related

to the minor cost and less density exhibited from this kind of fibers. Compared to the synthetic ones, such as glass or high strength (HS) carbon, certain natural fibers such as bamboo, jute and coir exhibit a minor cost per weight. Figure I-6 shows the relation existing between the tensile modulus and the density, while the figure I-7 that existing between the same modulus and the cost per volume of natural and synthetic fibers and composites respectively [28]. In general synthetic fibers show high tensile moduli but they have high density values and they are not environmentally friendly. Vegetal fibers have competitive values of tensile modulus if compared to synthetic ones and they are less dense [29, 30]. This last criterion in particular is essential in the realization of biocomposites used in the construction field, lightening the weight of the composite due to the difference of density between the two constituents. Natural fiber composites represent a promising class of materials, exhibiting lower cost and density and competitive mechanical properties if compared to synthetic fiber composites.
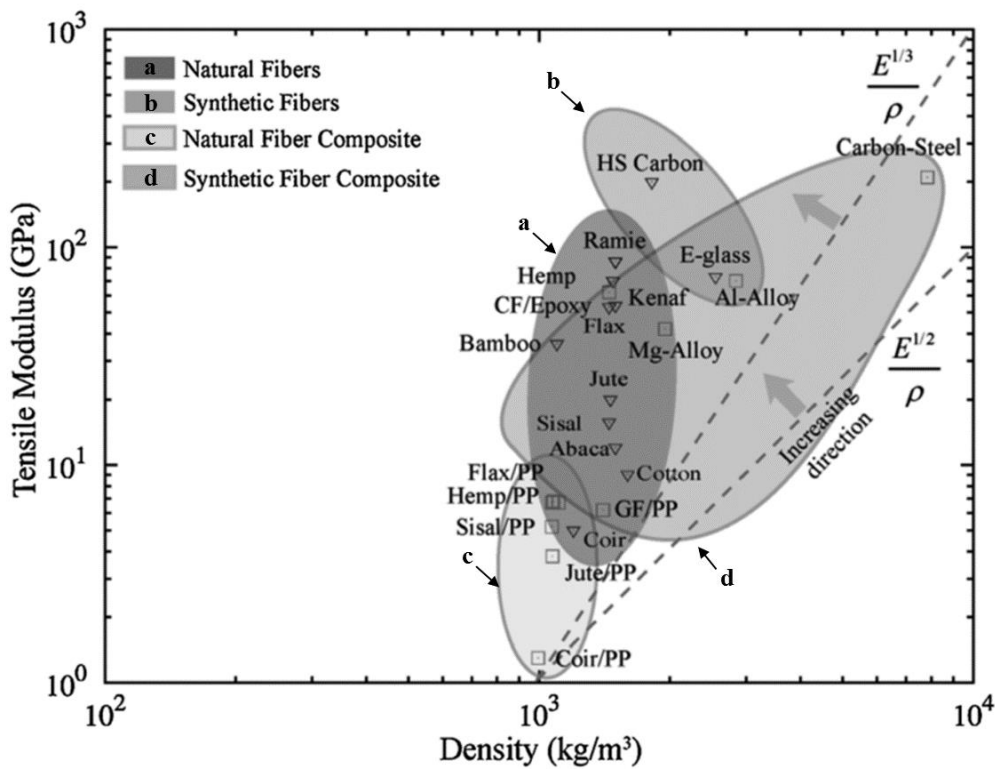
Figure I-6. Tensile Modulus (E) vs Density (ρ) of different fibers and composites (from [28]).
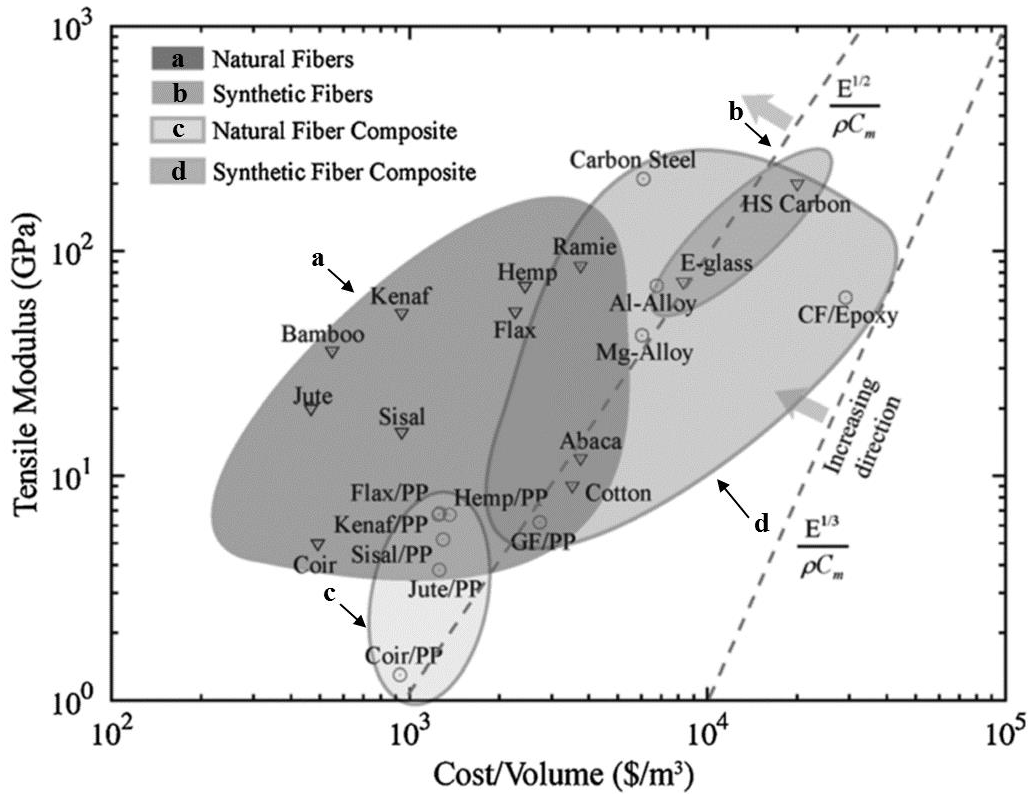
Figure I-7. Tensile Modulus (E) vs Cost (C_m)/Volume of different fibers and composites [28].

I-2.1. NATURAL FIBERS

All fibers that belong to this category can be essentially divided into three great groups, depending on their origin: vegetal, animals and minerals [21, 28]. Among all the existing animal fibers, wool and silk are the most famous and they are widely used in the textile sector. However, for the application in composite materials, plant fibers are the most interesting and popular. They can be produced from different part of the plant, such as steam, leaf or grass. The natural fibers used in composite applications are in general derived from agricultural residues or they can be cultivated specifically for this purpose, such as in the case of textile plants. These fibers have a great number of advantages. They are relatively inexpensive as showed in the previous paragraph and they are immediately available in great quantity. In order to develop a totally green material which is environmental compatible, both matrix and reinforcement must have the ability to undergo biological degradation. Also for this reason natural fibers are preferred to synthetic ones, because of their biodegradability, biocompatibility, recyclability and favorable CO_2 balance. Moreover, their low density and thermal and acoustic insulation, are other common advantages of using vegetal fibers in composite materials and in particular in the construction field [1]. However, the use of this type of fibers in polymer matrix composites has been limited by several factors related to the intrinsic

properties of these fibers. One of the reason is related to the great variability in mechanical properties caused by the harvest, the different extraction techniques, the environmental conditions, the location of the fiber in the plant and in certain cases by its genotype [31-33]. The low resistance to heat is a second negative point of vegetal fibers, which may degrade during the manufacturing process [34, 35]. Finally, one of the fundamental problems of these fibers consists in their hydrophilic nature that causes not only swelling but also incompatibility with most of the matrixes used to realize a composite material which are hydrophobic [36, 37].

I-2.2. PRINCIPAL CHARACTERISTICS OF VEGETAL FIBERS

The physical structure and the chemical composition of vegetal fibers suggest that they can be considered already as advanced composite materials. The conditions of growth, the type of soil, climate and the aging conditions influence the chemical composition of a plant, playing an important role in the final properties of the fibers. Vegetal fibers are constituted of three main constituents, cellulose, hemicellulose and lignin, that are present in all plants but in different proportion as showed in table I-1.

Fibers type	Density [g/cm³]	Cellulose [wt%]	Hemicellulose [wt%]	Lignin [wt%]	Ashes [wt%]	CI* [%]
Jute	1.3-1.4	60	22.1	15.9	1.0	58
Ramie	1.5	80-85	3-4	0.5	-	62.9
Kenaf	1.5	72	20.3	9	4.0	72.1
Flax	1.5	71	18.6-20.6	2.2	-	86.1
Hemp	1.5	72	10	3	2.3	79.9
Sisal	1.5	74-75	10-13.9	7.6-7.9	0.4	72.2
Abaca	1.5	56-63	20-25	7.9	-	68.7
Coir	1.2	42-53	14.7	38-40	-	44
Softwood	-	30-60	20-30	21-37	<1	-
Hardwood	-	31-64	25-40	14-34	<1	71.6
Rice straw	-	43.2	31.7	16.9	9.9	77
Wheat straw	-	43.2	34.1	22	4.99	54.4
Bamboo	0.6-1.1	33-45	30	20-25	-	59.7

*CI: crystallinity index

Table I-1. Chemical composition of some common vegetal fibers (adapted from [38]).

These compounds are very different from each other in terms of physical and chemical properties and for this reason it seems necessary to describe their characteristics more in detail in the next paragraph. Other polysaccharides are present in the vegetal fibers, such as pectins. These last contain a large amount of galacturonic acid residues that can be in general easily extracted using hot acid or chelators [39]. Vegetal fibers are hydrophilic due to the presence of a great number of polar groups, but at the same time they are constituted by other compounds in less content. Among these, we can find phenolic compounds and hydroxyl acids like palmitic acid, stearic and oleic acids. These last form a 3D protective film called the cuticle that is slightly permeable to gases and steam, waterproof, remaining wettable at the same time. Waxes are also present in variable proportions. These last are constituted by fatty acid esters and fatty long-chain alcohol and they are completely hydrophobic, therefore totally impermeable to water and gases, thus reducing plant transpiration. They have different morphologies: sticks, granulation, film or bloom [40]. Table I-2 shows the mechanical properties and the cellulose content of some natural fibers [28, 41].

Fibers type	Density [g/cm^3]	Specific strength [MPa]	Specific Modulus [GPa]	Cellulose [wt %]	Cristallinity [%]	References
Flax	1.5	535-1000	18.4-53	64-71	50-90	[28, 31, 42]
Hemp	1.47	372-608	47.3	70-74	50-90	[28, 31, 42, 43]
Jute	1.3-1.5	269-548	6.8-20.6	61-72	50-80	[28, 31, 42, 43]
Kenaf	1.5-1.6	641	36.55	31-39	-	[28, 31]
Ramie	1.5-1.6	147-625	29.3-85	68.6-76.2	-	[28, 31, 43]
Sisal	1.45	366-441	6.5-15.2	66-78	50-70	[28, 31, 42]
Bamboo	1.1	454	32.6	26-60	40-60	[31]
Coir	1.2	146	3.3-5	32-43	27-33	[28, 42]
Cotton	1.6	179-373	3.4-7.9	82.7-91	-	[28, 42]
Abaca	1.5	267	8	56-63	-	[28, 44]
Pineapple	1.4-1.6	118-446	4-27	70-82	44-60	[42, 43, 45]
Banana	1.35	444	13.2	44-64	45-55	[28, 42]
Miscanthus	1.41	-	6.7	38	-	[46, 47]
Switchgrass	1.40	37.7	6.4	32	-	[46, 48]
E-glass	2.55	1333	28.6	-	-	[28, 44, 45]

Table I-2. Properties of some natural and synthetic fibers [41].

The hydrophilic and hygroscopic nature is responsible of poor adhesion with the polymer matrixes used in composites materials. The same characteristics cause also swelling and may accelerate the

degradation process under certain aging conditions at the interface matrix/fiber. All vegetal fibers are sensible to heat, limiting the maximum operational temperature at which they can be processed in the presence of a matrix. The low melting temperature of certain thermoplastic polyesters, typically < 200°C represents an important advantage for the use of vegetal fibers to realize biocomposites.

At this point, it seems necessary to focus the attention on certain vegetal fibers species and more precisely on those cultivated in France, the country in which this work has been carried out. Among all existing species, the degree of knowledge, research and the use of vegetal fibers is not the same. We can distinguish three categories dependent on these parameters as showed in figure I-8. The first type of fibers are those produced in great quantities at large industrial scale such as hemp and linen. To the second type belong all those fibers whose production at large scale is not perfectly developed but they begin to take place on the market such as cereal straw, flax straw and many others. The last type is probably the most interesting. To this group belong all those potential fibers whose industrial production is not already developed and among these we can find Miscanthus, the plant chosen to realize biocomposites in this work, whose characteristics will be described at paragraph I-2.3.
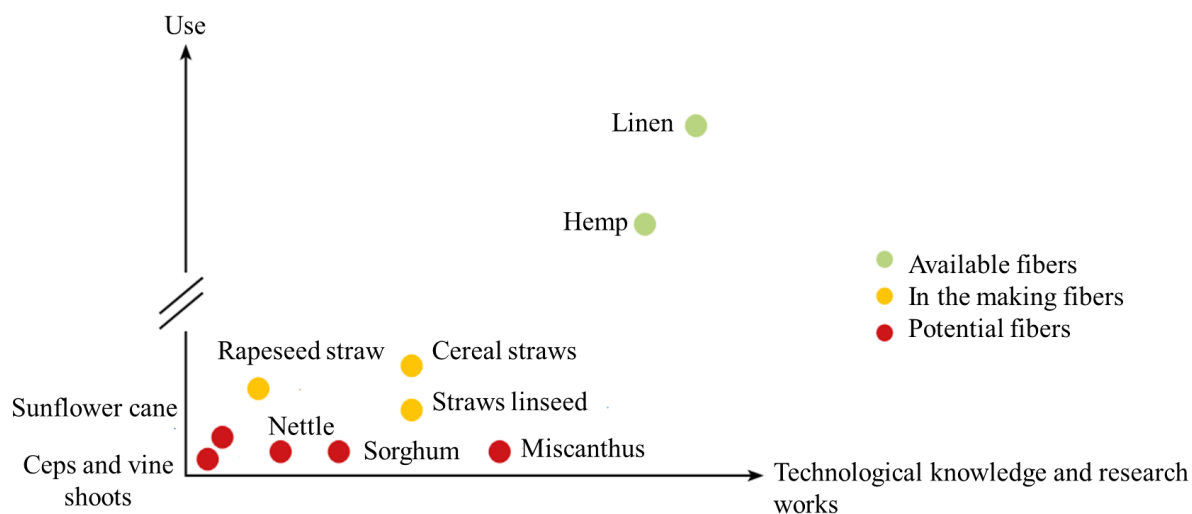
Figure I-8. Fibers used in France in materials field (from [49]).

The potential of a certain type of fibers depends not only on their availability but also on their chemical and mechanical properties. The profound knowledge of these characteristics can led to identify all chemical bonds exploitable for a chemical treatment of fibers surface and to well understand the impact of each constituents in the final resistance of a composite.

I-2.2.1. Cellulose

Cellulose is a common material present in the cell wall of the plants. It was discovered for the first time by the Anselm Payen in 1838 [50] . It is a polysaccharide with the formula $(C_6H_{10}O_5)_n$ constituted by D-glucose units $(C_6H_{12}O_6)$ linked together by β-(1,4) glycosidic bonds in order to form linear chains (see figure I-9). These units have three types of hydroxyl groups: two secondary and one primary.
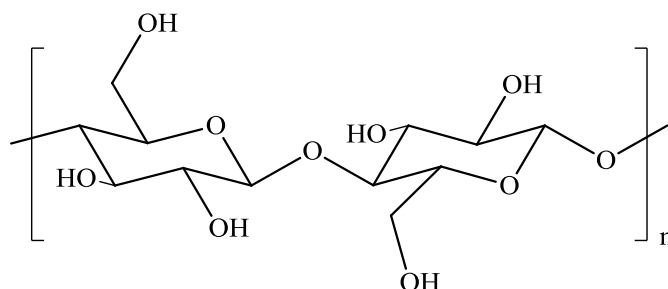
Figure I-9. Chemical structure of cellulose.

Due to its structure, cellulose is considered as a homopolymer with a molar mass ranging from about 10000 to 150000. Cellulose is constituted by six different allomorphs forms. Among these, the cellulose I is the most common crystalline form find in nature. In the cellulose I, the polymeric chains are oriented in a parallel manner and it exist in two different forms, I-α and I-β, depending on the proportion of crystallinity [51]. This form of cellulose is metastable and it can be converted in a more stable form called Cellulose II. This last differ from the cellulose I in unit cell dimensions and in chain polarity [19]. There are also other forms of cellulose crystalline forms identified by III and IV numbers. The passage from one form to another can be made through different chemical treatment as showed in figure I-10. The most famous is undoubtedly the mercerization, a treatment with alkali followed by washing in order to pass from the cellulose I to cellulose II.
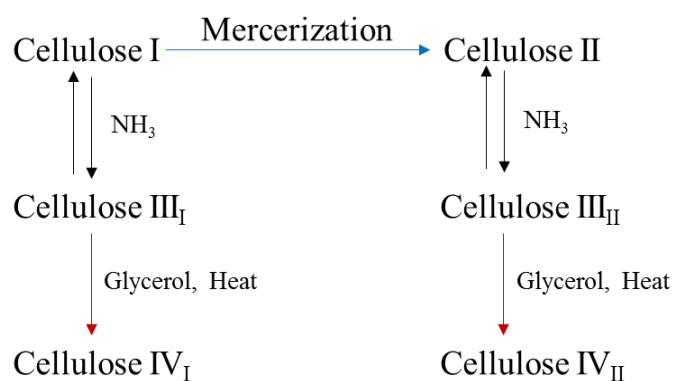
Figure I-10. Formation of cellulose allomorphs (adapted from [52]).

Strong hydrogen bonds between the hydroxyl groups of each glucose unit and the adjacent ones are possible due to their favorable position. These bonds between many cellulose molecules in the parallel direction led to the formation of particular structures, the microfibrils, that interact to form fibrils [19]. These last can be seen as an assembly of microfibrils immerged in an amorphous matrix constituted by hemicellulose, pectins and lignin as showed in figure I-11. The supramolecular architecture due to these hydrogen bonds is responsible for the important crystallinity of fibers. In particular, the composition, the polymerization degree and the crystallinity of cellulose influence the mechanical properties of the vegetal fibers. More precisely higher moduli were found for high content of crystallinity degree. Certain conditions such as temperature and high pressure can favor the increase in crystallinity [53].
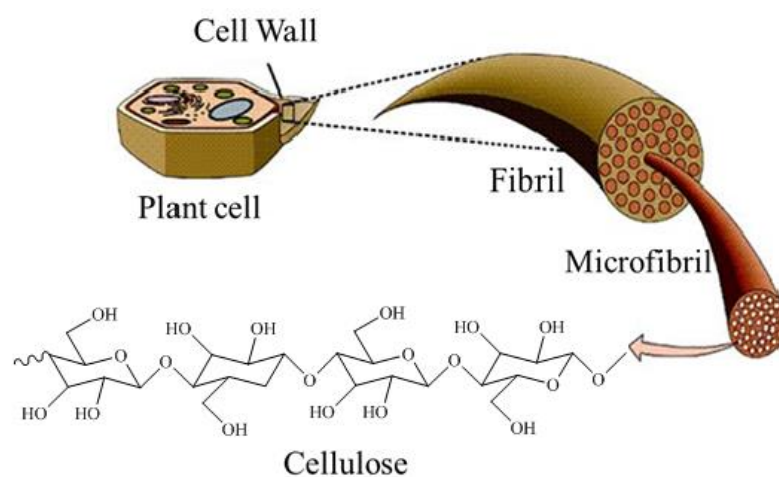
Figure I-11. Arrangement of fibrils, microfibrils and cellulose in cell wall (adapted from [54]).

The possibility to modify certain functional groups using chemical treatment depends on the morphology of the fiber. This last is constituted by three principal layers: the primary wall, the secondary wall and the lumen [19] as showed in figure I-12. The primary wall is constituted by 25 to 30% cellulose, 30 to 65% hemicellulose, 5 to 35% pectin and 0.5 to 5% proteins [55-57]. In this wall fibrils are covered by a layer constituted by pectin, proteins, minerals and waxes called cuticle. The secondary wall constitutes the support for the entire structure. It has the same composition of the primary wall but in different proportions: less hydrated networks, less matrix material and more rigid constituents like cellulose and lignin. In this part fibrils are organized in a parallel way and form a helix along the fiber. Reactive can reach functional groups through a series of void and canal, but in such case fibrils are very close by blocking access to the reactive except when they are swollen. Briefly, the content of cellulose increases from the primary to the secondary wall and that of lignin

decreases in the same way. The reason is that no stress must occur when the content of moisture changes. In this way, layers can contract and swell without problems, assuring the mechanical resistance to the fiber. This structure constitutes a barrier against pathogenic agents and environment [57].
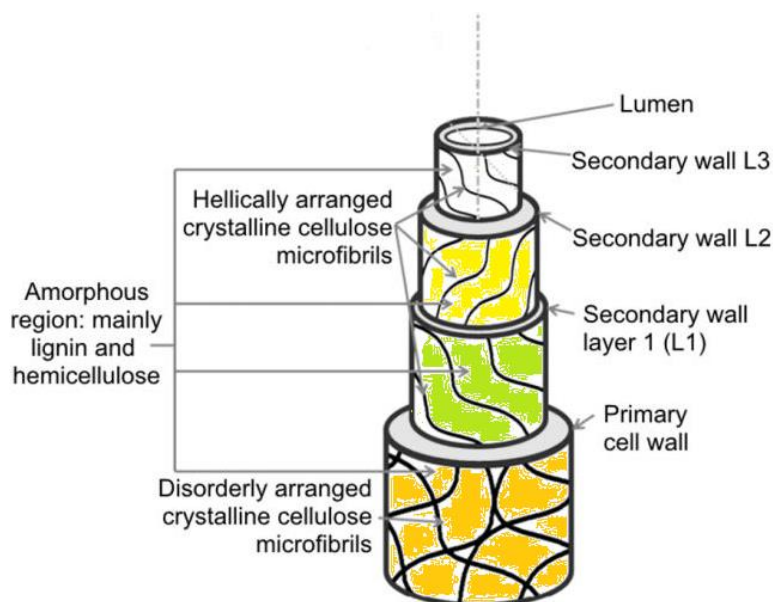
Figure I-12. Internal structure of an elementary natural fiber (from [58]).

For what concern cellulose physical properties, they are strictly dependent from the molecular structure of the same. Cellulose is odorless, hydrophilic, chiral, degradable and crystalline [59]. It was shown to melt at temperature above 300°C [60]. From a mechanical point of view, it is a resistant material and its resistance depends on the geometry of the elementary cell. It is also deformable which gives flexibility and elasticity to the membrane [61].

I-2.2.2. Hemicelluloses

Hemicelluloses includes different organic compounds like xylans, xyloglucans, mannans, glucomannans and β-(1-3,1-4)-glucans showed in figure I-13. They are the second type of polysaccharides after cellulose present in the cell walls of the plants [39]. Hemicellulose is a branched polymer constituted by short chains 500-3000 sugar units, so its polymerization degree (DP) is lower than that of cellulose. Its backbone is in general constituted by one repeating sugar unit linked beta (1-4) with branch points (1-2), (1-3) and/or (1-6). The most important biological role of hemicelluloses is their contribution to strengthening the cell wall by interaction with cellulose and, in some walls, with lignin [62]. Mechanical properties of neat hemicellulose are very difficult to find

in literature and they are not very reproducible. Some works showed an elastic modulus of 8 GPa from xylans fraction extracted while in other case, depending on the compositions of the hemicellulose analyzed, modulus can reach values of 20 GPa [63, 64] .

β1→4 glucan

β1→4 glucomannan

β1→4 xylan

β1→4 mannan
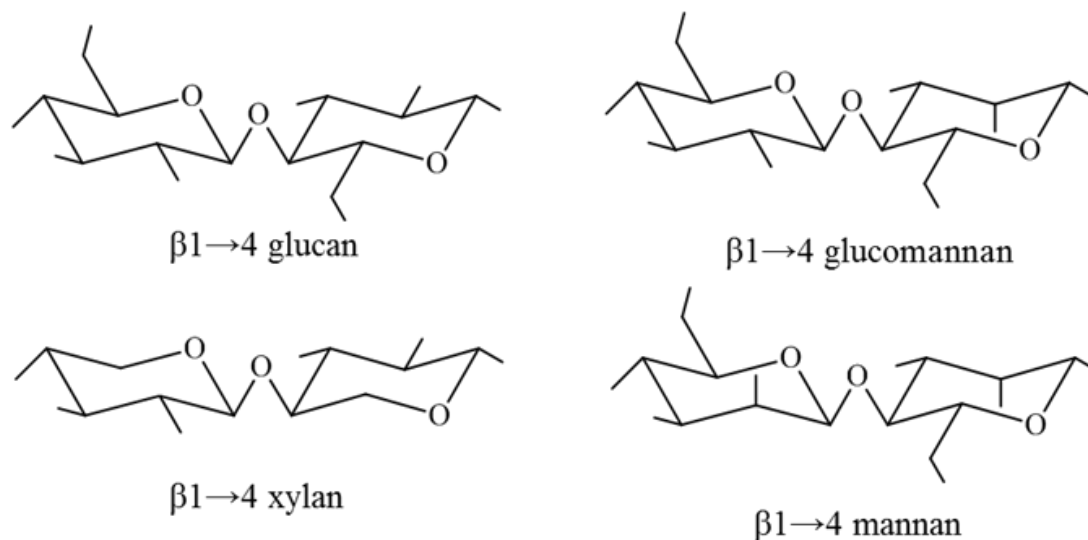
Figure I-13. Principal hemicellulose constituents.

I-2.2.3. Lignin

The research of the lignin structure has been a much discussed topic over the years. Karl Freudenberg in the 50's tried to figure out what really lignin was, if it was a "sort of molecular compost heap" or if it possesses an orderly structure. He preferred this last option [65]. Today lignin is defined as an organic compound with a complex structure composed mainly by polymers of phenyl-propane units. In general three basic building blocks constitute lignin in nature: the p-coumaryl alcohol, the sinapyl alcohol and the coniferyl alcohol whose structures are described in figure I-14 [66]. Each plant species has a different content of these monomers. In softwood there is a predominant presence of coniferyl alcohol, while in hardwood there are both sinapyl and coniferyl alcohols. Lignin from grasses and bamboo contains all three monomers, while lignin from kenaf high amounts of syringyl groups, these last being derived from sinapyl alcohol and containing two aryl-OCH_3 groups [62]. Lignin is produced in vivo through a dehydrogenation polymerization mediated by enzymes, the so called lignification. The final cross-linked material is amorphous and constituted by ether and carbon-carbon bonds [67].
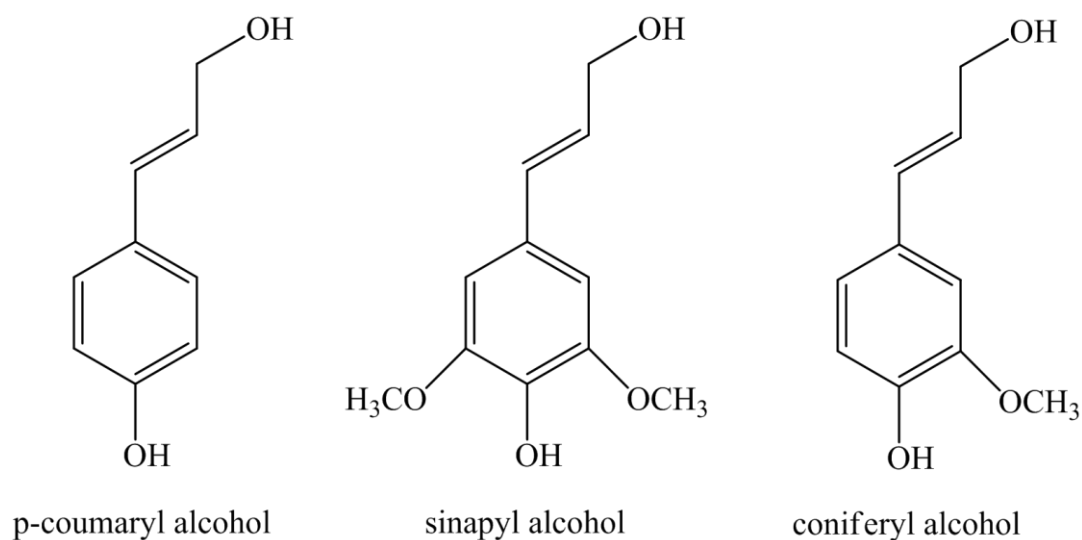
Figure I-14. Three standard monomers of lignin (from [67]).

The truth is that the lignin structure is so complex that still has to be investigated thoroughly. One of the hypothetic structure of lignin is showed in figure I-15.
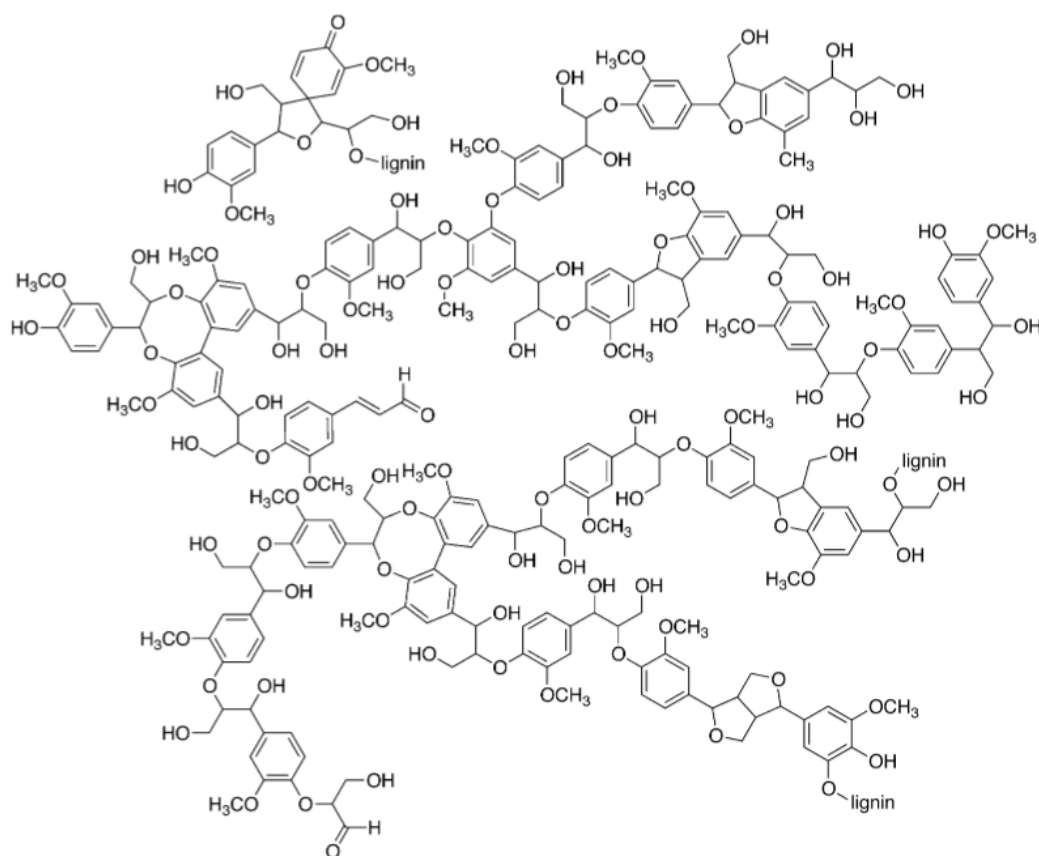
Figure I-15. Structural motif of softwood lignin (from [67]).

Lignin is preferentially distributed in the secondary cell wall of the plant. When lignin is isolated it appears as a brown powder, but it can also appear also as a gummy mixture, this last is constituted by a mixture of lignins having a wide range of molecular weight [19]. Both from mechanical and physical point of view lignin is considered as a very resistant compounds, being responsible for the strength of the plant and having a great resistance to compression. The hydrophobicity is another important characteristic of lignin and this is the reason why plant cells are waterproof. In general lignin is insoluble in acids but soluble in concentrated bases and also very resistant to bacterial degradation. Mechanical properties of lignin are variable and dependent on its location in the plant [68]. Values of elastic modulus can vary from 4 to 7 GPa for an extracted isotropic lignin [64, 69]. Due to its good properties, recently lignin has been used as additive to create composite materials improving mechanical properties of classic thermoplastic matrixes and bioplastics [70, 71].

I-2.3. PRESENTATION OF MISCANTHUS

Miscanthus (M.) can be classified as a lignocellulosic material, being constituted both by cellulose and lignin, the two main constituents of plants [33]. Miscanthus was first introduced in Europe as an ornamental garden grass. It is a genus of woody, perennial, rhizomatous grasses related to sugarcane that originated in Southeast Asia [72]. Among all the existing species, 17 totally, the most important are M. *sinensis* and M. *sacchariflorus* (which originate in East Asia), and also M. *giganteus* (which is common in France), a hybrid species synthesized from the other two [73]. This plant can be cultivated on poor quality soil and needs little amounts of herbicide, nitrogen, and water compared to other energy crops [74].

The productivity is extremely high [75]: in temperate climates, Miscanthus is considered one of the most productive land plants known [76]. It gives also good yield on relatively cold climates [77]. It has been estimated that the yield of production can go up to 35 dry tons per hectare. In Europe in particular, Miscanthus plantations are located in the United Kingdom (15 000 hectares), Germany and France (2000 hectares). This plant is also a particularly suitable candidate for the production of biofuels and chemicals on large scales [78, 79] because of some valuable advantages including good yield and high calorific value (20 kJ/ kg if dry matter) [80]. Traditionally, in terms of the ratio of energy content to volume, combustion and pyrolysis are efficient methods for controlling the energy efficiency of Miscanthus [81]. Few studies have been performed on the use of Miscanthus as a source of bioenergy for fuel [82-85]. It is currently being grown in the British Isles for use as a biomass fuel to reducing greenhouse gas emissions that is a fundamental point of the Kyoto Accord [86]. It has been estimated that undried straw of Miscanthus, which is 70-80% of the total mass, contains very little amount of water and this gives it a calorific value of 4700 kWh/t. This value is higher than that of the woodchips (3300 kWh/t). This fact means that Miscanthus could replace up to 50% of wood in a power plant and that it could be also used for the domestic heating. In France, as in other countries, the main outlet for Miscanthus crops is energy recovery.

However, many other outlets are receiving a growing attention from the R&D sector and this is the case of manufacture of second-generation biofuels, litter, horticultural mulch, plastics and agro-materials for construction [87]. In this fields, Miscanthus has been already used for the realization of various construction materials including insulation panels and bio-concretes. Some of the final applications of Miscanthus are showed in the figure I-16. Actually, it is preferred to other straws due to its resistance to putrefaction and to its ease and rapidity of implementation. Other potential applications include its use as an emulsifier for oils. This means that Miscanthus powder could be

useful used for oil spilled during environmental disasters [88]. Undoubtedly one of the most attractive application field is that of biocomposites, in which Miscanthus fibers can be used to reinforce traditional plastics or bioplastics in order to create materials with improved mechanical properties [47, 89].
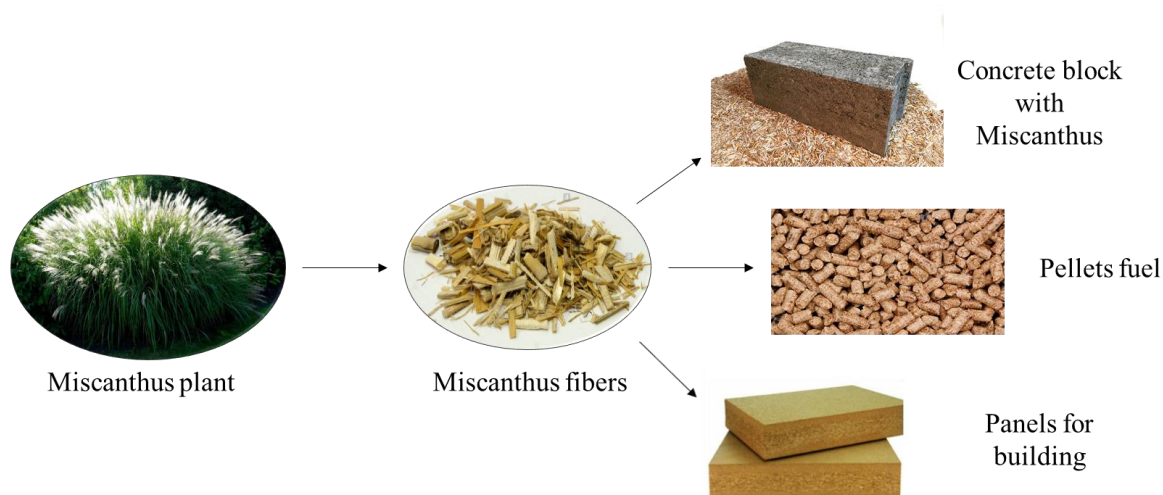
Figure I-16. Miscanthus: from plant to common applications.

The mechanical properties of reed fibers were studied by Kaack et al. [33]. The influence of structure and chemistry of stems on the flexural modulus of Miscanthus fibers was investigated. They revealed a proportional relation between the content of cellulose and lignin and the improvement of the elastic modulus. The values of elastic modulus were found between 0.5 and 6 GPa. More precisely, Young Modulus is higher for high content of cellulose and lignin and for specific plant conformation (high internode length, number of internodes etc.). In another work, Kaack et al. [90] showed that the variation in elastic modulus is also related to the position on the stem from which the sample was recovered. They indicated that the average modulus was higher for the nodes than for the internodes and that the modulus decreases significantly and linearly from the lower to the upper part of the stem. The average modulus of the nodes was 5.8 and 4.5 GPa for the internodes. In a recent work, Lundquist et al. [91] found a Young modulus and a tensile strength equal to 59.5 ± 0.2 GPa and 913 ± 79 MPa, respectively. The latter values seem very high and should be confirmed. These values can be compared to other vegetal fibers whose values are listed in Table I-3.

Fibers	Young Modulus [GPa]	Tensile strength [MPa]	Reference
Miscanthus	59.5	913	[91]
Flax	58	1339	[92]
Hemp	35	389–900	[22]
Sisal	9–22	347–700	[24]

Table I-3. Young Modulus and tensile strength for different natural fibers.

Miscanthus fibers were processed with different matrixes using industrial techniques at high temperatures. The knowledge of the degradation behavior of this plant seems necessary in order to appropriately determine processing parameters. The thermal degradation of Miscanthus sisal was studied by Szabo et al. [93]. They highlighted the beginning of degradation close to 210 °C and an improvement in thermal resistance for HCl washing fibers. Lundquist et al. [91] indicated that the temperature of 1% weight loss of the china reed (Miscanthus *giganteus*) was equal to 203 ± 4 °C which is in the range of processing temperatures of many thermoplastics polymers. They also studied the influence of chemical treatments on reed fibers. Optimal mechanical properties were obtained for methanol (10 vol %) and alkali (15 vol %) treated fibers with a pulping time of 25 min and a pulping temperature of 170 °C. Few authors studied the incorporation of reed as reinforcement in a polymer matrix. Johnson et al. investigated the impact performance of Mater-Bi reed composites and showed that the addition of Miscanthus fibers to Mater-Bi increases the impact load by, on average, up to 30% over that of the pure biopolymer [94]. Temperature is the main influent factor on the impact properties of these composites [86]; as the temperature of processing increases so does the load and impact energy absorbed by the biocomposite. On the other hand, the fiber loading does not significantly influence the results [47]. For all the reasons largely discussed in this paragraph and for its growing potential in France due to its availability, low cost and good mechanical properties, Miscanthus seems to be a good candidate for the realization of biocomposites. Moreover, the absence in literature of a totally green chemical modification applied to this kind of fibers constitutes an attractive opportunity to be exploited in order to improve the mechanical properties of future biocomposites.

I-3. ALIPHATIC BIODEGRADABLE POLYESTERS

In order to realize a totally green composite, the use of a matrix environmentally friendly that could replace all those plastics derived from oil resources is necessary. Among all properties that a matrix should possess, the biodegradability is certainly one of the principal that we have taken into account in this work to limit the disposal problems with environmental impact caused by non-biodegradable plastics [95]. The possibility for a polymer to be degraded into simple and natural molecules such as carbon dioxide, methane and water under the action of enzymes or living organisms such as bacteria or fungi [96] has a fundamental impact on the wastes management.

Previsions about the capacities of the global biodegradable polymer market presented in figure I-17, show that this market is expected to reach around USD 5.18 billion in 2020. In this context, Europe accounted for majority of the market share for biodegradable polymers market in 2014 and this fact is mainly due to strong focus on green technology.
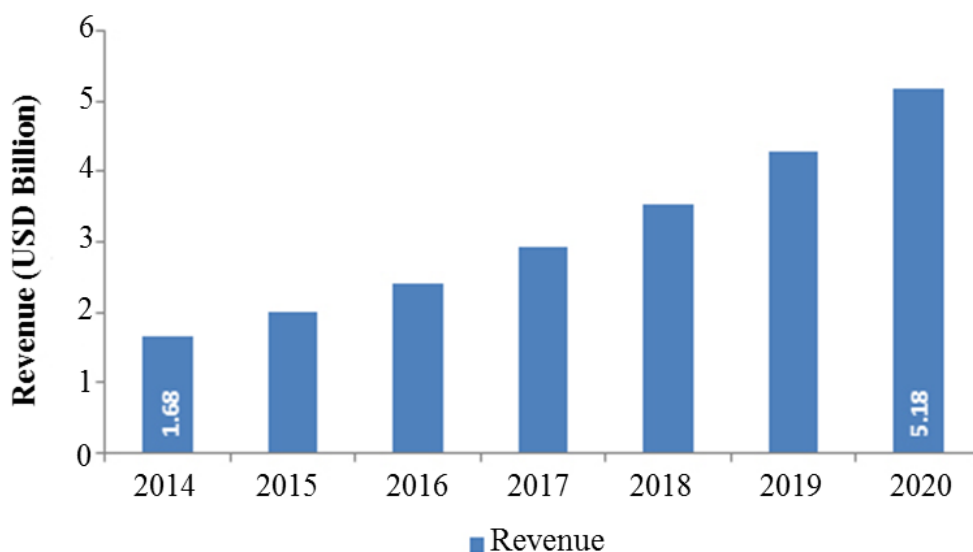
Figure I-17. Global biodegradable polymer market, 2014-2020 (from [97]).

Biodegradable polymers are in general divided in two categories based on their origin and we can distinguish natural and synthetic ones. To the first group belong starch, cellulose and many other polysaccharides and proteins, while to the second group belongs a great number of polyesters and polyurethanes. Moreover, in recent years microbial polymers were produced and they can considered as a third category of biodegradable polymers, due to their natural origin and their interesting properties [98, 99]. In this context, the term "biopolymer" is more appropriate and it refers to a bio-based plastic [100] derived from living organisms or from a natural source.

The high cost and the low performances of certain bioplastics, concerning in particular their low mechanical resistance and high permeability to water vapor compared to traditional ones [101] constitute two fundamental problems for which these polymers are unable to take over the market [102]. Moreover, biopolymers are extremely sensitive to moisture and high temperature during the processing steps [103]. For this reason aliphatic biodegradable polyesters and among these some bio-based polymers constitutes an attractive solution due to their excellent biocompatibility and thanks to their large spectrum of properties that can be modulated in order to obtain products for specific applications according to the need.

For these last reasons, this section focuses the attention on biodegradable synthetic and microbial polymers. Among all the existing matrixes belonging to these groups, we have chosen aliphatic polyesters and in particular poly(lactic acid) (PLA), poly(ε-caprolactone) (PCL), and poly(3-hydroxybutyrate-*co*-3-hydroxyvalerate) (PHBHV) whose structures are presented in figure I-18.

PLA

PCL
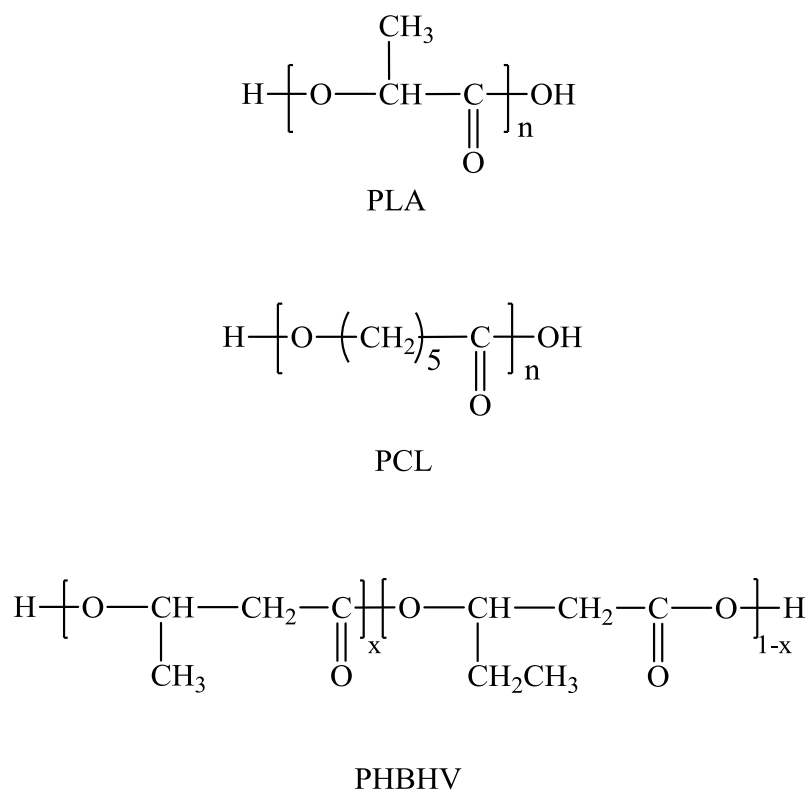
PHBHV

Figure I-18. Molecular structures of PLA, PCL and PHBHV polymers.

The thermoplastic character is one of the main characteristics of these three matrixes, however their origin is not the same and as consequence also their properties are different.

Poly(lactic acid) is produced both from fossil oil resources and from renewable natural ones. This polymer has a biodegradable and biocompatible character [104]. The economical production of high molar mass poly(lactic acid) constitutes the fundamental driver for the expansion in the PLA production and use [105] . Concerning this point, a strong reduction of the production cost of PLA began with the first PLA produced from renewable resource by the Cargill Dow LLC, the so called NatureWorks[TM] PLA. This reduction caused an expansion in the use of this polymer beyond biomedical applications and more precisely in the field of packaging and fiber applications with particular attention to the environmental sustainability. Moreover, PLA is an excellent candidate for the realization of totally green composites [106] thanks to its natural origin, its variegate properties and its high productivity (140,000 tons per year) [107, 108]. Actually it is one of the major bioplastics produced in the world after starch-derived plastics [109]. For what concerns poly(ε-caprolactone), this polymer is not bio-based, being produced from petrochemical resources. However it is biodegradable and biocompatible. In particular, thanks to this last characteristic, PCL has been largely used in biomedical and biomaterial applications [110-112]. Poly(3-hydroxybutyrate-*co*-3-hydroxyvalerate) belongs to the poly(3-hydroxyalkanoate)s or P(3-HA)s family, which are aliphatic polyesters produced by bacteria after fermentation of natural raw material and accumulated as intracytoplasmic inclusions. Their natural origin, their biodegradability and biocompatibility makes these polymers particularly attractive. However, this polymer has a higher cost if compared to traditional polyolefin [113] and this fact is essentially due to all those purification steps (solvent extraction for example) that represents from 60 to 80% of the total cost. Moreover the use of solvent is strictly related to toxicity problems and high price, especially when large amount of solvent is needed [114]. The addition of natural fibers and the improvement of processing methods, preferring for example blending to the synthesis of high-cost new biopolymers, can reduce the total cost of the material [115]. In this regard, numerous studies have been performed concerning the development of biocomposites with natural fibers and biodegradable polyesters such as PLA, PCL and PHBHV [116-120]. The characteristics and the applications in the biocomposites field of these three promising biodegradable polymers will be the focus of the next paragraphs.

I-3.1. SYNTHESIS OF BIODEGRADABLE ALIPHATIC POLYESTERS

I-3.1.1. Synthesis of poly(lactic acid) (PLA)

The poly(lactic acid) is commonly made from α-hydroxy acids and we can consider that lactic acid (2-hydroxy-propionic acid) is the basic building block of this polymer. Lactic acid was produced by petrochemical route and since 1990 by polysaccharides and sugar fermentation, this last being a

more eco-friendly approach [121]. Lactic acid exists in two optical isomers, defined as L and D-lactic acid. Actually, by the petrochemical synthesis, the produced lactic acid is a 50/50 mixture of the two isomers, while by the fermentation route, the content of L-isomer is predominant (99.5% of L-isomer and 0.5% of D-isomer) [122]. There are two main ways to produce high molar mass PLA as shown in scheme I-1.
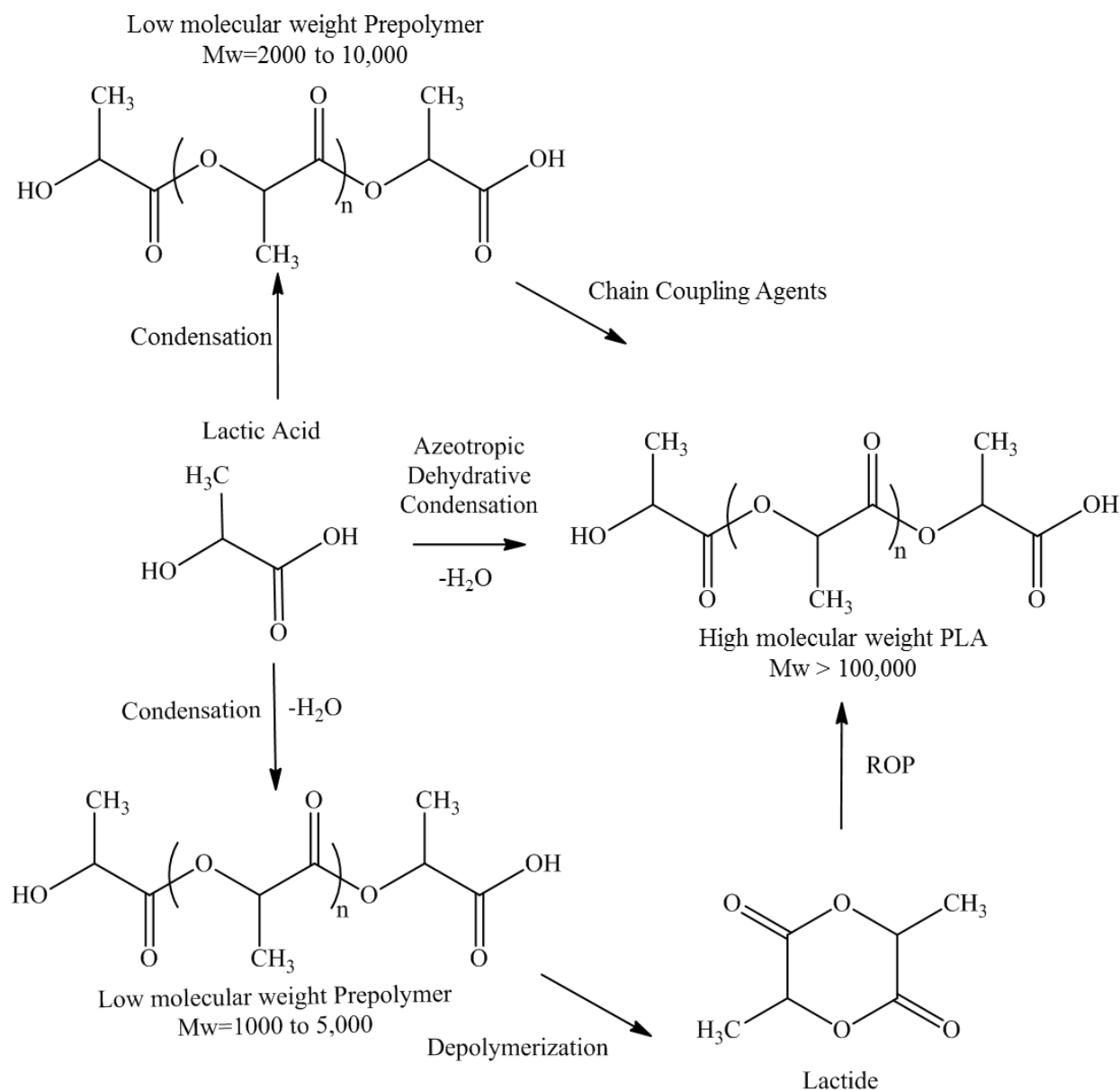
Scheme I-1. Synthesis methods for high molecular weight PLA: condensation/coupling, azeotropic dehydrative condensation and ring-opening polymerization of lactide (adapted from [121]).

Starting from lactic acid, PLA can be produced by condensation resulting in low molar mass. This last can be improved only by the use of coupling agents, esterification-promoting adjuvants or

chain-extending agents, these last increasing the cost and the complexity of the process. The azeotropic dehydrative condensation is a second route producing a PLA with high molar mass without the use of adjuvants or coupling agents. However, this way requires the use of high quantities of catalysts to favor the reaction rate, whose residues can cause many problems in further processing such as undesired degradation or uncontrolled hydrolysis. For all these reasons the ring opening polymerization of lactides, demonstrated for the first time by Carothers in 1932 [123], is considered as the best way to produce high molar mass and pure PLA. The process starts from lactide which is obtained by depolymerization of low molar mass PLA and which results in a mixture of L-lactide, D-lactide and *meso*-lactide. The ring opening polymerization can be cationic or it can be anionic [121]. Actually, the commercial PLA is a combination of various copolymers, such as the poly (L-lactic acid) (PLLA), the poly(D-lactic acid) (PDLA) and the poly(DL-lactic acid) (PDLLA), synthesized from L, D and DL-lactic acid monomers respectively whose stereoforms are showed in figure I-19 [124, 125].
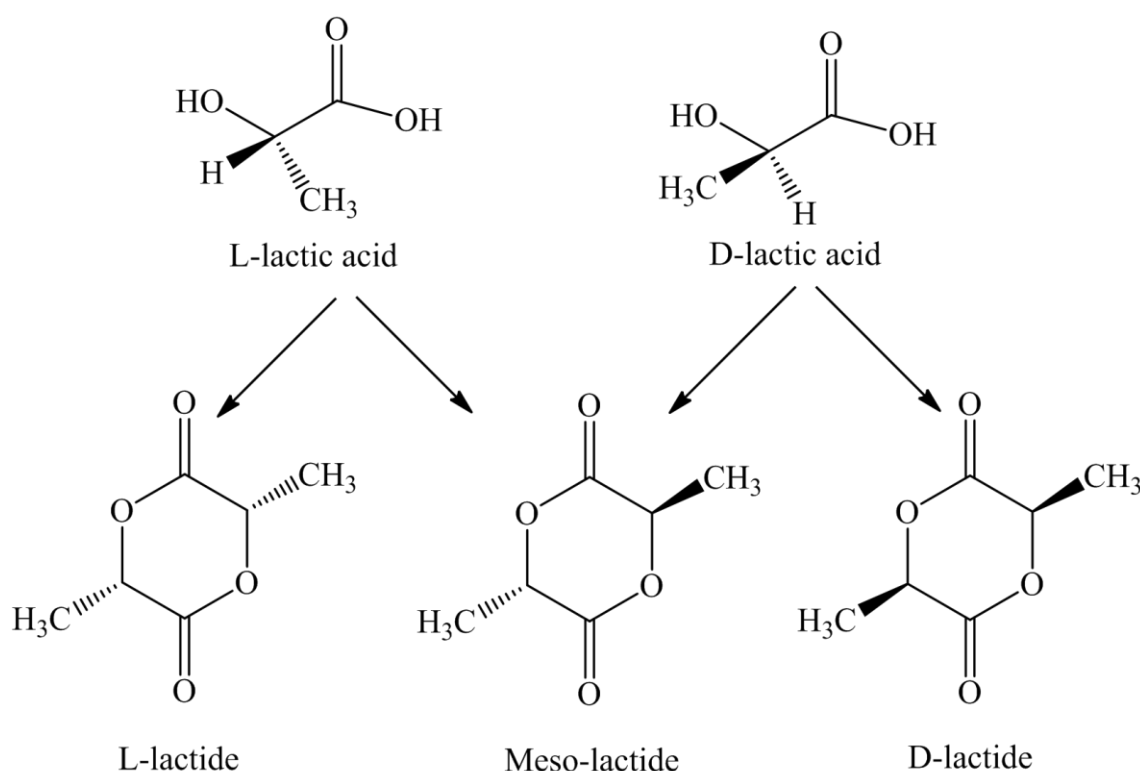
Figure I-19. Stereoforms of lactides ([125]).

I-3.1.2. Synthesis of poly(ε-caprolactone) (PCL)

Poly(ε-caprolactone) is constituted by hexanoate repeat units. Similarly to poly(lactic acid), PCL can be synthesized by different routes: the condensation of the 6-hydroxyhexanoic acid and the ring opening polymerization of lactones (ROP) [126]. The second route to synthesize PCL, *via* ring opening polymerization of lactones is undoubtedly the most used. The possibility to work under mild conditions results in polyesters with high molar mass obtained in a shorter time than polycondensation. The ring-opening polymerization can be performed in bulk, in solution, in emulsion or dispersion and to start the process the use of an initiator is necessary, an active species that react with the monomer to give the polymer. This kind of reaction is classified depending on the catalyst used: metal-based, organic and enzymatic. We can distinguish anionic, cationic, monomer-activated and coordination-insertion ROP. Among these four categories, the coordination-insertion showed in scheme I-2 is the most common. In this process, the propagation proceeds through the coordination of the monomer to the catalyst with the subsequent insertion of the monomer into the metal-oxygen bond of the catalyst [127].
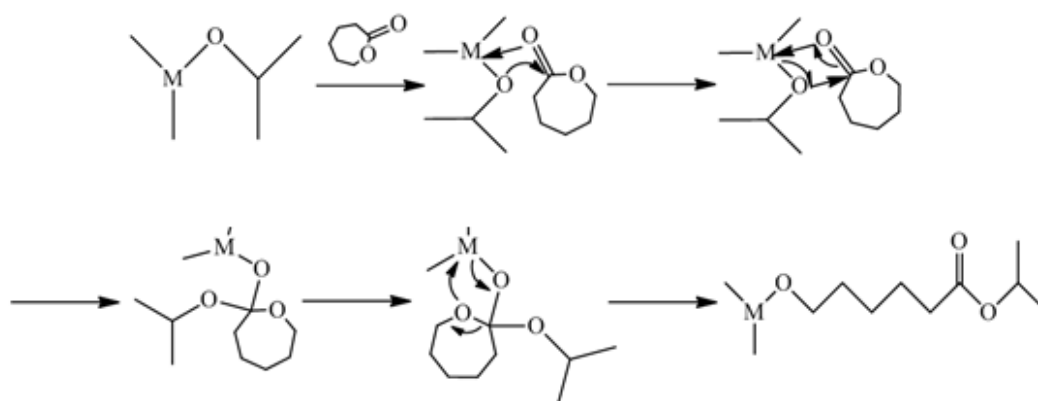
Scheme I-2. Initiation step for coordination-insertion ROP (adapted from [126]).

Another way to synthesize PCL is the use of enzymes under mild conditions. This route can be considered as a green way to synthesize these biodegradable polymers because of the absence of toxic reagents and it includes also the possibility to recycle the catalyst [126, 128, 129]. One of this mechanism is proposed in the scheme I-3 and it concerns a ROP using lipase, in which a lipase-activated monomer complex, formed after the reaction between the lipase and the lactone, reacts with an alcohol to form the polymer [126, 130, 131].
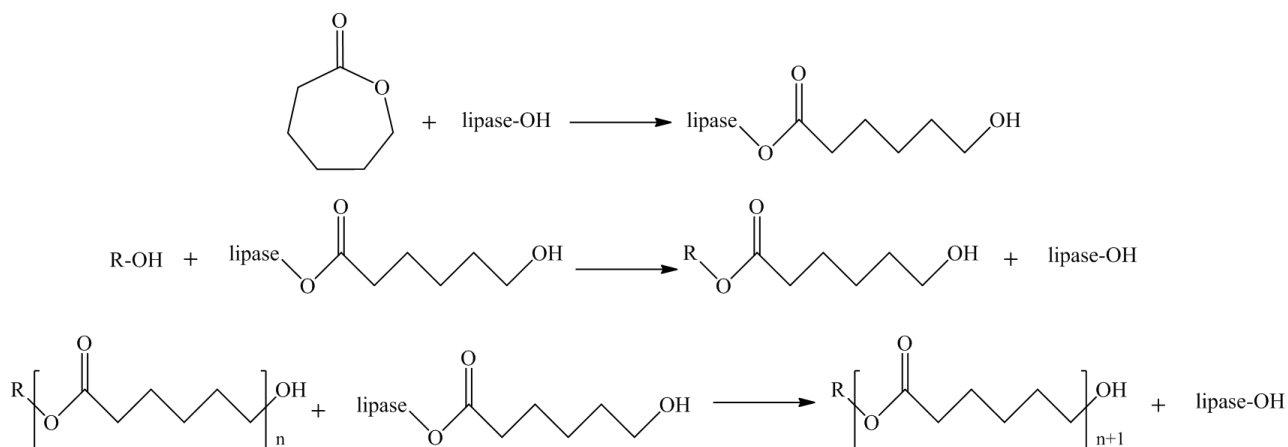
Scheme I-3. Mechanism of ROP using lipase (adapted from [126]).

I-3.1.3. Synthesis of poly(3-hydroxybutyrate-*co*-3-hydroxyvalerate) (PHBHV)

The synthesis and the properties of the poly(3-hydroxybutyrate-*co*-3-hydroxyvalerate) are strictly related to those of poly(3-hydroxyalkanoates), the family of polymers to which PHBHV belongs. The PHAs possess many linear carbon side chains (renamed here R) with different lengths depending from the carbon source and the nature of the bacteria (see figure I-20).
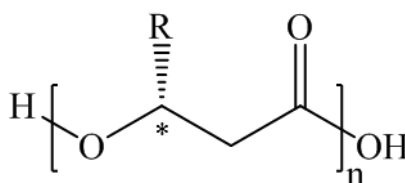
Figure I-20. General formula of (PHA)s.

In this context, three types of PHAs can be differentiated: short-, medium- and long-chain. The first type of PHA, the so-called PHA scl (short chain length) has a lateral chain constituted by 1 to 3 carbon atoms ($R=CH_3$ to C_3H_7), the PHA mcl (medium chain length) has a number of carbons atoms in the lateral chain from 4 to 9 ($R=C_4H_9$ to C_9H_{19}) and at last the PHA lcl from 10 to 14 ($C_{10}H_{21}$ to $C_{14}H_{29}$). The poly (3-hydroxybutyrate) (PHB) and poly (3-hydroxybutyrate-*co*-3-hydroxyvalerate) (PHBHV), whose properties will be also investigated in the experimental part, belong to the P(3-HA)s group [132].

The synthesis of the PHBHV showed in scheme I-4 consists in three fundamental steps based on the chemistry of the acetyl-CoA as precursor, this last being produced by the oxidation of fatty acids and sugars. This route is the most common metabolic way to produce this copolymer. At first

the enzymatic activity of the β-ketothiolase allows to the condensation of two molecules of acetyl-CoA to form acetoacetyl-CoA and the condensation of acetyl-CoA with propionyl-CoA to form β-ketovaleryl-CoA. In a second moment, the formed products are converted into the polymer by the activities of the (acetoacetyl-CoA) reductase and of the PHB synthase. The quantity of HV units are dependent from the carbon source; for example, the addition of glucose to the propionic acid results in a great variability of HV units from 0 to 57%.
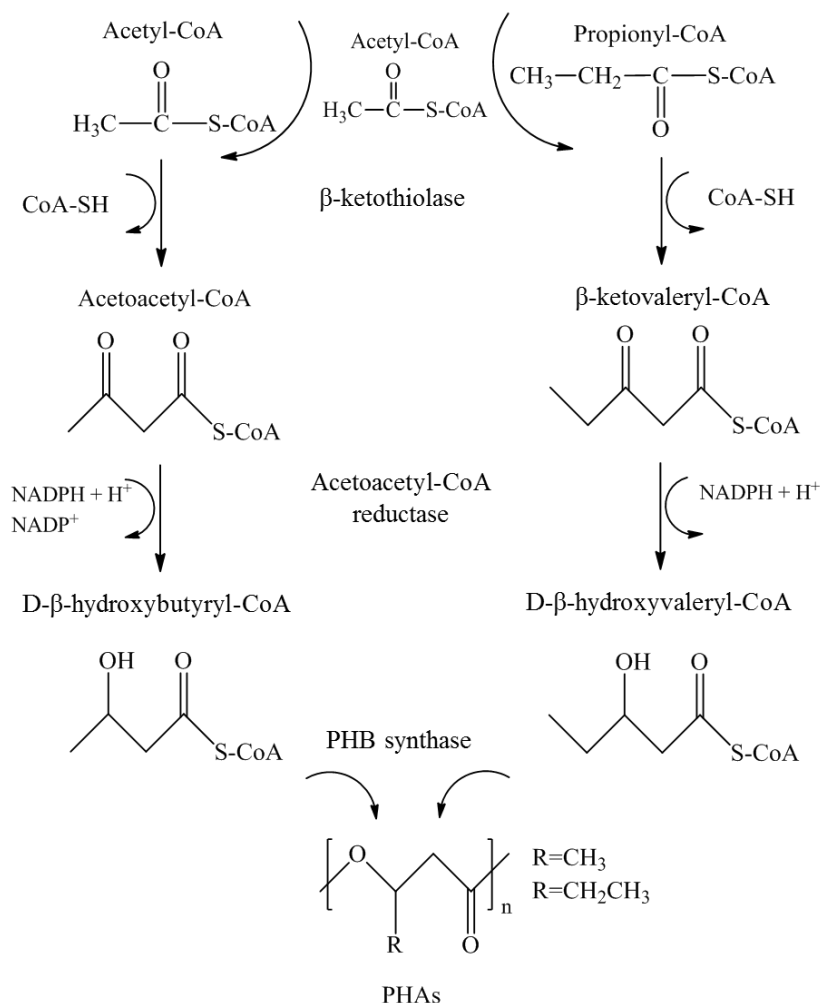
Scheme I-4. Pathway for the production of PHBHV from acetyl-CoA and from propionyl-CoA (adapted from [133]).

I-3.2. THERMAL AND MECHANICAL PROPERTIES OF ALIPHATIC BIODEGRADABLE POLYESTERS

Polyesters previously described can be considered as thermoplastic polymers with a semicrystalline behavior. This means that a glass transition and a melt temperature characterize them.

Although PLA, PCL and PHBHV have these common characteristics, the range of temperatures at which these polymers can be used and processed is not the same as showed in figure I-21. Properties of PLA change with the content of L-isomer and in the case of PHBHV the variability in the content of the HV units caused different mechanical and thermal properties.
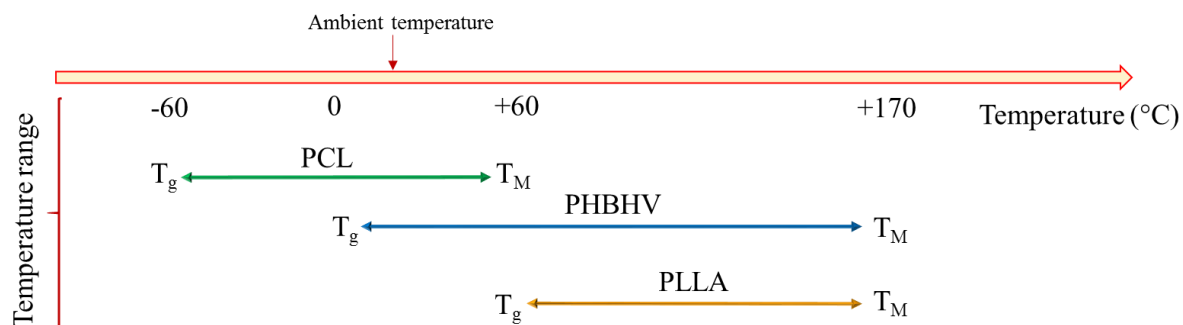
Figure I-21. Principal temperature ranges for PLA, PCL and PHBHV polymers.

The way of synthesis of PLA and PCL influences their mechanical and thermal properties. In the case of poly(lactic acid), the content of L-isomer that characterize PLA produced from renewable source influences preferentially the crystallinity. More precisely, high content of L-isomer induces crystallinity while low content results in an amorphous PLA, decreasing also the melting and the glass transition temperatures [105, 134, 135]. While, the melting temperature of the polymer is mainly dependent on the optical purity of PLA and it can vary from a maximum of 180°C to 120°C depending on the amount of D-lactide incorporated, the glass transition one is dependent also from the thermal history of the polymer. The mechanical properties of PLA are variable and strictly related to the crystallinity behavior of the polymer. Semicrystalline PLA has an elastic modulus of around 3 GPa, a tensile strength that varies from 50 to 70 MPa and an elongation at break of about 4% [136, 137]. Due to these properties it is considered as a brittle material. For high mechanical performances, semicrystalline PLA is preferred to an amorphous one. Mechanical properties of PLA are related to the molecular weight, to the presence of the L or D isomers and also to thermal treatment such as annealing as showed in previous works [138, 139].

Similarly to PLA, high molar mass poly(ε-caprolactone) can be obtained by ring opening polymerization of lactones and also in this case thermal and mechanical properties of this polymer are dependent from its molar mass and its crystallinity. PCL cannot be considered as a brittle material, exhibiting a low tensile strength (approximately 23 MPa) and high elongation at break (>770%). It has the great advantage to possess lower density than the others, to be miscible with a lot of other

polymers and to be mechanically compatible with polyethylene, polypropylene and rubber [117, 126, 140]. It is characterized by a melting temperature around 60°C and a glass transition temperature of around -60°C [141, 142].

Failure stress and Young Modulus of the homopolymer PHB are similar to those of polypropylene but the elongation at break of this last is higher (400%) [143, 144]. The introduction of a co-monomer into the polymer backbone like 3-HV causes a change in thermal properties and a consequent change in mechanical properties. In particular, the final copolymer exhibits an increase in flexibility and toughness, but at the same time a reduction in polymer stiffness. Compared to its equivalent homopolymer, the PHB, that is highly crystalline and brittle, the introduction of 3-HV units allows a decrease in glass transition temperature (T_g) and melting temperature (T_M) without significant changes in the crystallinity [114, 143, 145-148]. This weak change is due to a phenomenon of co-crystallization of the two-monomer units (HV and HB) that rearrange creating an intermediary structure and preserving the crystalline character. One of the problems of PHBHV is the presence of a secondary crystallization of the amorphous phase, which occurs during storage time at room temperature. Several authors studied this phenomenon, so a sample stored at room temperature for 60 days have lower values for elongation at break than samples stored for 30 days [149-151]. The range of principal thermal and mechanical properties of PLA, PHBHV at different compositions and PCL are listed in the table I-4.

Properties	PLLA	PDLLA	PCL	PHB	PHB$_{86}$HV$_{14}$
Density [g/cm^3]	1.26	1.27	1.20	1.25	1.25
Melting point [°C]	170-183	-	56-65	177	150
Glass transition [°C]	55-65	59	-60	4	4
Tensile Modulus [GPa]	2.7-3.5	1.9	0.2-0.	3.5	1.5
Tensile strength [MPa]	50-70	49-53	4-28	40	35
Failure strain [%]	4	-	700-1000	4	12
Crystallinity [%]	35-40	-	59-64	60	57

Table I-4. Thermal and mechanical properties of PLLA, PDLLA, PCL, PHB and PHB$_{86}$HV$_{14}$ [125, 126, 152, 153].

I-3.3. BIODEGRADABILITY OF ALIPHATIC POLYESTERS

Biodegradation is considered as a form of degradation due to the action of many microorganisms such as bacteria, fungi and algae. These living organisms assimilate biodegradable polymers, producing degradation products like biomass, carbon dioxide, methane and water. Many environmental factors influence the biodegradation like temperature, this last affecting the microorganisms growth and also the pH and the source of carbon and nitrogen. However, the type of living organism and the environmental characteristics are not the only requirements for a total degradation of a polymer. The chemical structure and the physico-chemical properties of a plastic are two fundamental parameters for a complete biodegradation. In this context, we will focus the attention on the biodegradability of aliphatic polyesters previously described. These last are constituted by ester bonds that can be degraded by many enzymes present in various living organisms.

Actually PLLA needs more than 2 years to reach the 50% of its initial mass and PDLLA needs just 12-16 months [152]. Enzymes present in living organism can hydrolyze the ester linkage in different biotic environments releasing carbon dioxide as showed in the lifecycle of PLA in scheme I-5. PLA degradation is influenced by different factors that are dependent on the polymer properties such as its crystallinity, molar mass and purity, but also from environmental parameters such as temperature, pH, humidity, salinity, the presence or absence of oxygen etc. [125, 154]. It can undergo hydrolytic degradation of the esters group preferentially present in the amorphous phase. The hydrolytic process is a function of different factors such as aging time and conditions, molar mass, the degree of swelling of the matrix, macromolecular conformation, chain mobility and crystallinity [155]. Different hydrolytic mechanism have been proposed in these years. One of this suggests that the polymer with high molar mass degrade *via* a heterogeneous mechanism, proceeding more rapidly in the center than at the surface due to the autocatalytic action of the carboxylic acid end groups of the degraded products entrapped in the matrix. These last are in general oligomers and monomers that are water-soluble and that can move on the surface of polymer or remain entrapped inside [138, 156].
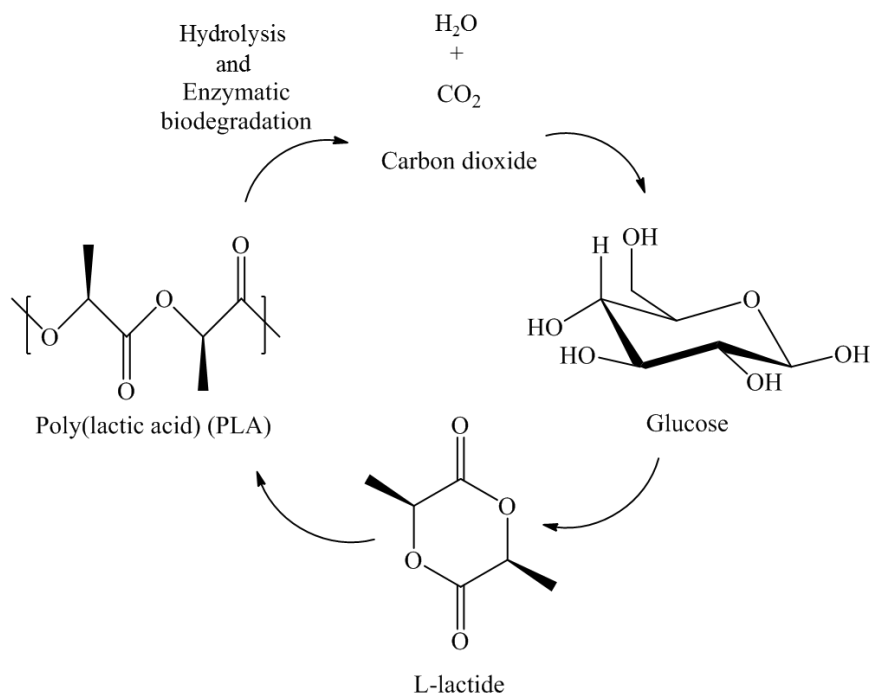
Scheme I-5. Lifecycle of poly(lactic acid) (PLA) (adapted from [154]).

As in the case of PLA, the PCL totally biodegrades under the action of microbes in nature [157] that are located in marine, sewage sludge, soil and compost ecosystem [98]. Compared to conventional plastics which fully degradation require hundreds or thousands years, the biodegradation of poly(ε-caprolactone) occurs in a few years, with a relatively slow degradation rate (2–3 years) that led to its use in long-term drug/vaccine delivery vehicle and allows to classify it as an excellent candidate for the realization of eco-friendly materials [158, 159]. Many studies reported that increasing the molecular weight of PCL, the degradability is reduced. This is also affected by the microorganism's type and by the enzymes produced. For example, PCL is easily hydrolyzed by esterase and lipase [98]. The degradation starts at the amorphous domain causing an increase in crystallinity degree while the molecular weight remain constant [160]. In a second step, the molar mass loss occurs due to the diffusion of formed oligomers from the bulk [98, 161, 162]. The process starts by the hydrolysis of the polymer chain and the formation of an intermediate of ω-oxidation and it proceeds by the β-oxidation to the acetyl-CoA which can further degrade in carbon dioxide and water as illustrated in scheme I-6. PCL degradation is autocatalyzed by carbon end groups of the polymer chain during the first step of hydrolytic degradation [161] but it can also be catalyzed by enzymes, resulting in faster decomposition [163]. While PCL can be enzymatically degraded in the environment, it cannot be degraded enzymatically in the body [126, 152] .
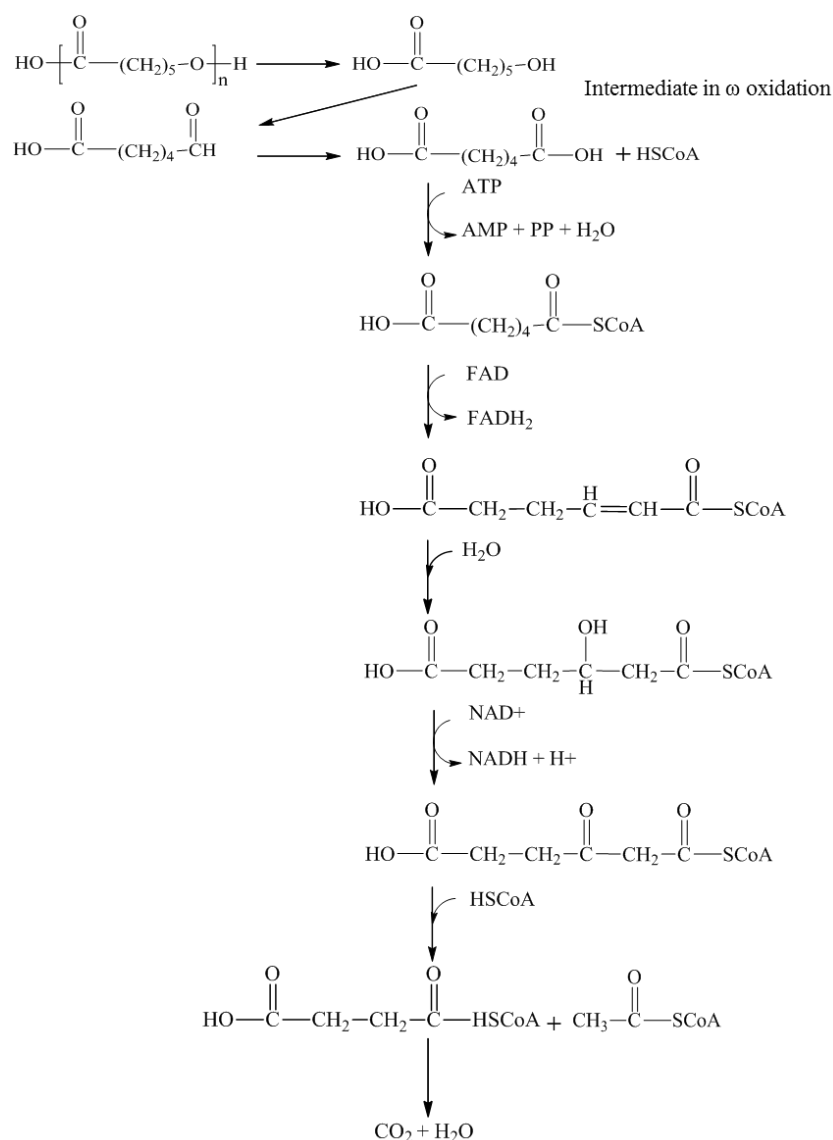
Scheme I-6. Degradation pathway for poly(ε-caprolactone) (PCL) (adapted from [164]).

Compared to PLA and PCL, microbial polymers are relative resistant to the hydrolytic degradation and they can be totally biodegraded by many microorganisms releasing carbon dioxide and water. The degradation rate of PHAs is lower than PLA and PCL. It has been estimated that after 28 days in river water, polymers are totally degraded and that PHBHV in the composition range of 12-21 mol% HV degrades rapidly than its homopolymer [165]. The reaction leading to the formation of PHAs is a reversible polymerization carried out by enzymes known as polymerases. The presence of the reverse enzyme, the so called depolymerase, allows the degradation of these polymers. The biodegradation process can be divided in two macro-categories: the intra and extracellular biodegradation. In the case of intracellular processes, bacteria can hydrolyze PHA$_S$ previously formed

thanks to the enzyme situated in the cytoplasm and more precisely on the surface of PHAs granules [166]. To give an example, this degradation process is showed in scheme I-7 for PHB polymer.
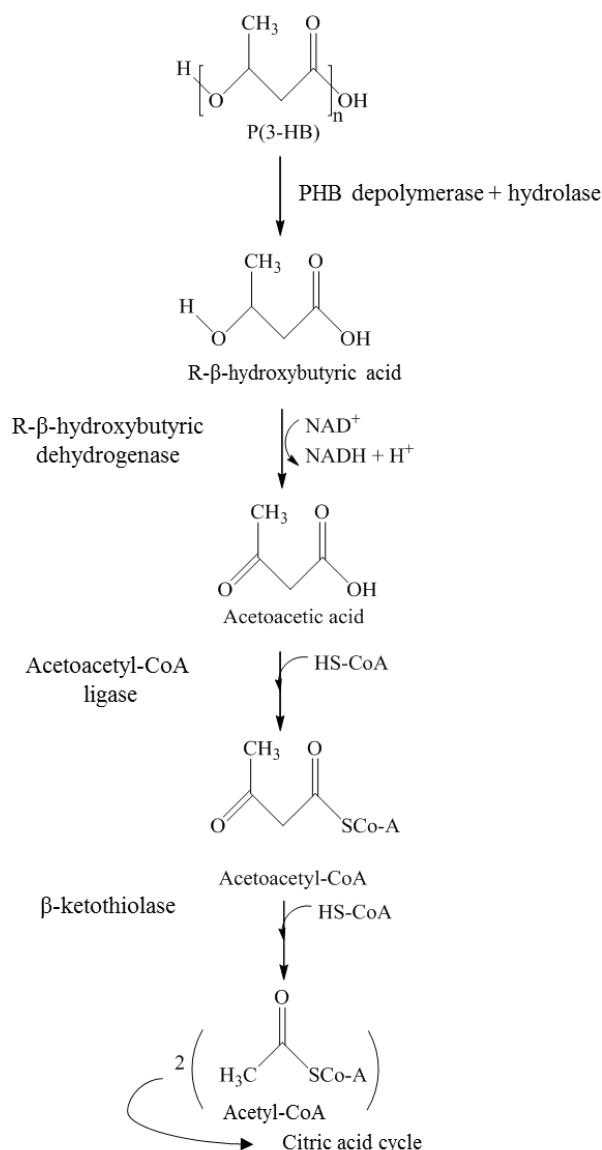
Scheme I-7. Intracellular degradation pathway for PHB polymer (adapted from [167]).

For what concern the extracellular degradation, this last is clearly dependent on different factors like the type of environment [168, 169], the type of water [170-172] but also temperature and pH. During this process bacteria produce extracellular enzymes that can hydrolyze PHAs forming oligomers soluble in water. These last can easily converted in molecules such as CO_2 or H_2O necessary to life of the bacteria. It was proved that the weight loss reached in the case of PHBHV copolymer is higher than that obtained in the case of the homopolymer. This fact can be explained by

the presence of HV units that cause less crystallinity of PHBHV [173].

I-3.4. THERMAL DEGRADATION OF ALIPHATIC POLYESTERS

All thermoplastic polymers are known to undergo thermal degradation during conventional processing such as extrusion or injection molding. In this case of PLA, degradation is caused by high process temperature, long residence time in the compounding machines and extrusion screw torque [174]. The presence of residual water in the polymer and the use of too much high temperature are two of the main factors favoring the thermal degradation of this polymer. Various reactions may occurs during this process such as random and oxidative chain scission, inter and intramolecular transesterification and were largely described in literature [136, 175, 176].

The thermal degradation mechanism of PCL occurs a two-steps degradation mechanism [177], the first consisting in a cleavage of the polymer chain via cis-elimination and the second in an unzipping depolymerization from hydroxyl end of the polymer chain. The thermal degradation of PCL produces small molecules with low boiling point that volatilize immediately. The final mechanism is described in the scheme I-8 [178].
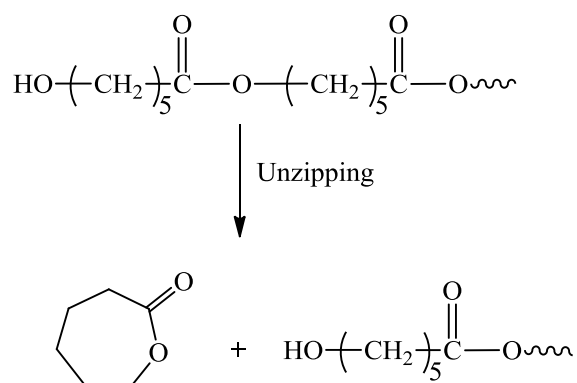
Scheme I-8. Unzipping depolymerization step of PCL (adapted from [178]).

Temperatures can influence the chain scission type: the polymer degrades by end chain scission at higher temperatures while it can degrade by random chain scission at lower temperatures as showed in figure I-22 [179].
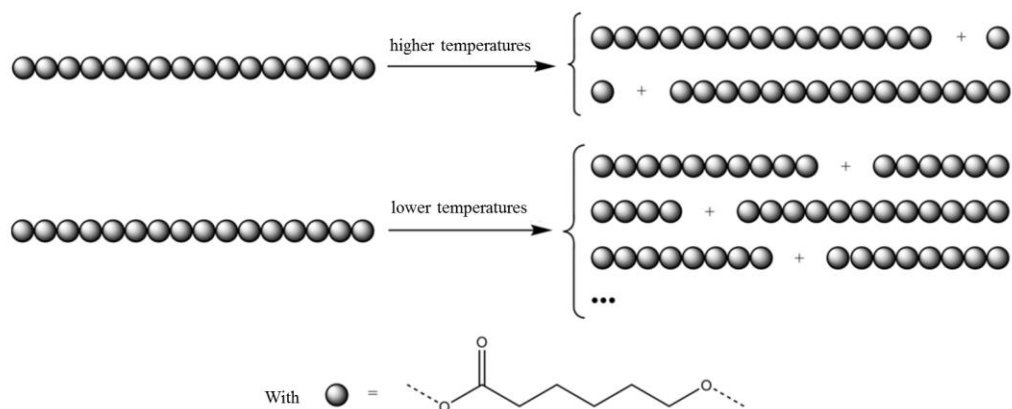
Figure I-22. Cleavage of the polymeric chain during the degradation of PCL (adapted from [126]).

For what concerns the thermal degradation of PHAs, a prolonged exposure to high temperatures just above their melting point (for example 180°C) could induce random chain scission reactions with subsequent degradation and production of degraded products like crotonic acid and different oligomers [180-182]. These reactions involving chain scission results in a polymer with low molecular weight [183]. The mechanism of thermal degradation of PHB is showed in the scheme I-9.
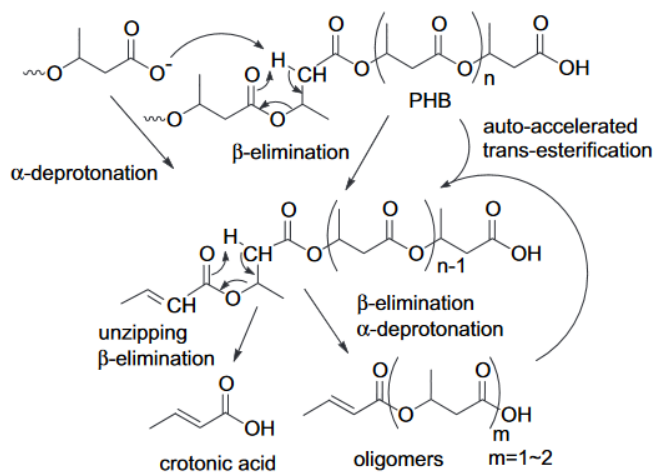
Scheme I-9. Thermal degradation mechanism for PHB.

The higher ductility of PHBHV compared to PHB led to an easy processability. The lower temperature used during the processing reduces the thermal degradation problem typical of PHB [181, 182]. A similar degradation mechanism for PHBHV was proposed by other researchers [184].

I-4. TOWARD BIOCOMPOSITES

The nature of the reinforcement and that of the matrix are the principal factors affecting the mechanical performances of biocomposites. However, there are other factors such as fibers dispersion, shapes, orientation and composite manufacturing that can affect the global properties of the final material [36]. Many of these factors such as fibers dispersion and orientation depend on the fiber/matrix interfacial adhesion and on the choice of processing parameters. Among all the existing factors affecting the properties of a biocomposite, the compatibilization between the reinforcement and the matrix has a fundamental role. In the next paragraphs, the existing treatments used to improve the compatibility of fibers with the matrix and to the processing methods used today to realize biocomposites are presented.

I-4.1. TREATMENT OF VEGETAL FIBERS

The fiber/matrix interface plays a fundamental role in the stress transmission. For biopolymers reinforced with vegetal fibers, there is a limited interaction between the hydrophilic reinforcement and the hydrophobic continuous phase, leading to poor interfacial bonding decreasing the mechanical performances as well as low moisture resistance affecting long term properties [36].

In the specific case of natural fibers used as reinforcement for a composite material, their hydrophilic nature, poor resistance to moisture, poor dimensional stability and their limited maximum processing temperature, constitute important limitations to the realization and final application of a biocomposite. In order to have a good adhesion between the matrix and the reinforcement, the fibers must present sufficient wettability. To achieve this goal, special treatments to modify the surface of vegetal fibers are generally proposed [185-188]. Among these techniques, physical and chemical modifications are largely used [3, 36]. Physical modification of fibers means that only the structure and the surface of the fibers are modified by this treatment, but the chemical composition is preserved. One of the traditional methods is the thermo-treatment, during which different phenomena can occur. For example, the migration of softened lignin to the surface of the fibers was postulated, when the treatment is conducted at temperatures much above its glass transition or the depolymerization of hemicellulose and lignin into aldehyde and phenolic compounds that form resins after curing [189-191]. Other physical techniques are the low-temperature plasma, the corona discharge and the sputtering [192, 193]. The first one causes a great number of chemical modification due to the possibility to use different gases, typically formation of radicals or surface functional groups, changes

in crystallinity, polymerization and cross-linking. The corona discharge and the sputtering cause mainly changes to the surface of fibers, like surface roughness [194, 195].

For what concern the chemical modification techniques, the basic principle is the use of a reactive agent to modify the chemical structure of the fibers. In this context one of the most famous technique is the mercerization. This process was used for the first time in 1844 to treat cotton fibers with sodium hydroxide (NaOH). During these treatment fibers swell and hydrogen bonds were broken and re-bond during swelling and drying respectively, causing a decrease in fiber diameter, an increase in the aspect ratio and an increase in exterior roughness. The significant improvement of the fibers wettability reached by this technique causes an increase in final strength and in the Young Modulus of composites realized by alkali-treated fibers, probably favored also by a change in the crystalline structure of fibers. Substances like lignin and hemicellulose are removed during this treatment and amorphous cellulose is hydrolyzed, leaving place to crystalline cellulose [196, 197]. In general, the majority of surface chemical modification focuses on cellulose. They can be divided in three macro-categories: the substitution of hydroxyl groups with small molecules, the polymer grafting based on the technique of the grafting "from" in which reactions such as ROP may occur and the grafting "onto" in which coupling agents are used [198]. Some of these techniques are showed in figure I-23. The oxidation is probably the simplest process and it refers to the oxidation of primary or secondary hydroxyl groups in the cellulose chain initiated by oxidants or nitroxyls radicals such as the 2,6,6-tetramethylpiperidine-1-oxyl radical, this last resulting in the TEMPO-oxidized cellulose. The advantages of this kind of reaction are that it can be conducted under mild conditions, in aqueous solution and it can be efficiently used to convert the alcoholic hydroxyl groups to aldehydes, ketones and carboxyl groups [201]. Chemical coupling is the most used method to improve the adhesion fiber/matrix in composite materials. A coupling agent is a compound, a bonding agents or a surfactant, used in very low quantity to treat a surface and to bond this one with that of the second constituent of a composite [202, 203]. The most used are silanes and isocyanates [204-206].
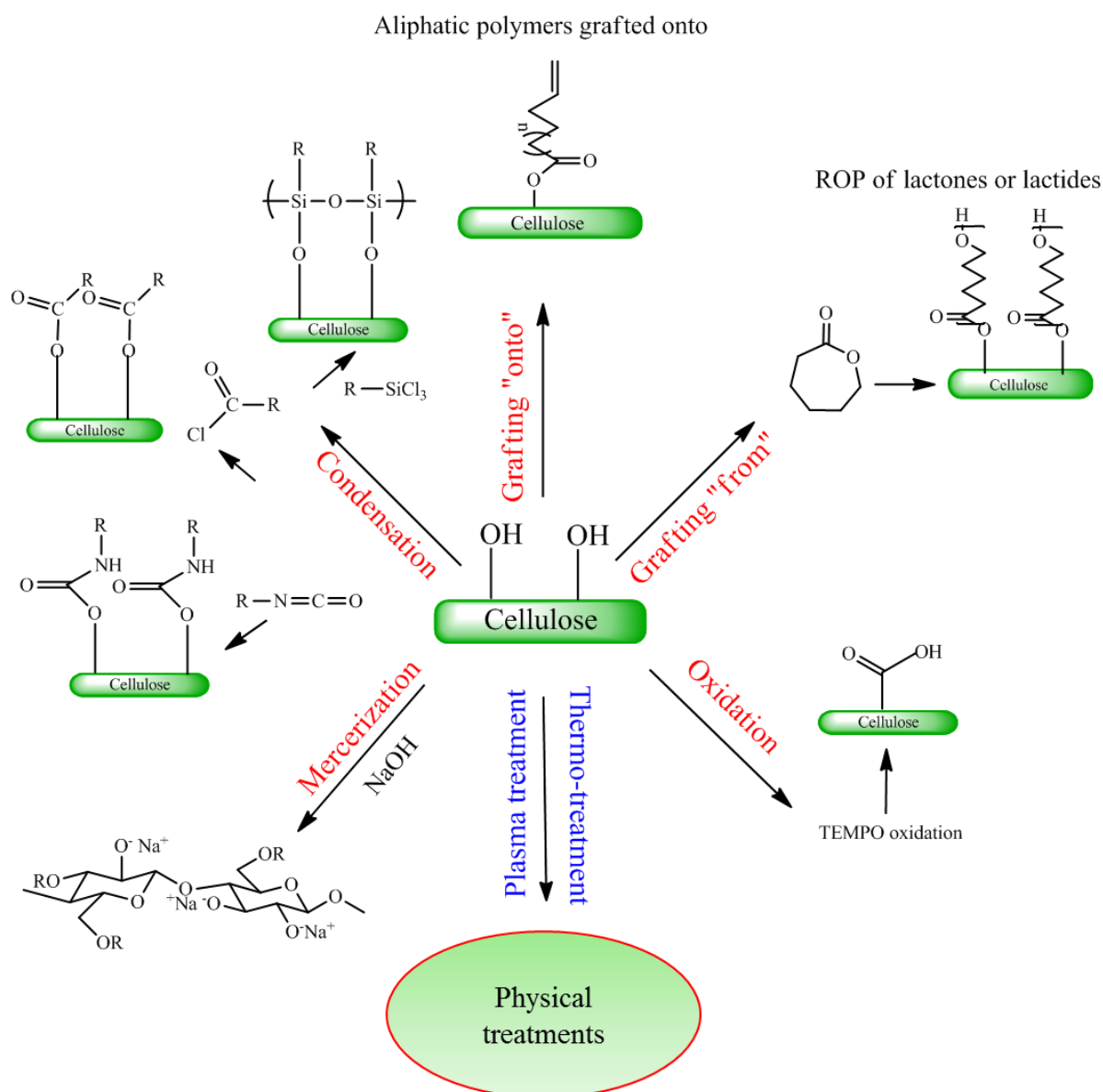
Figure I-23. Physical and chemical treatments of cellulose (adapted from [198-200]).

The term grafting can be referred to a grafting "onto" in which aliphatic polymers and oligomers with reactive ending groups are attached to the cellulose surface, or to a grafting "from" in which the monomer reacts directly with the hydroxyl groups of cellulose. The first method has different advantages such as the possibility to control the length of the grafted oligomer and the great variability of this last. Actually, many polyesters and their oligomers such as PHB, PHBHV, PCL and many others can be used [207]. However, this method has also many disadvantages such as the fact that oligomers have to be synthesized in a previous step and that they have to be functionalized in order to react with the hydroxyls of cellulose. In this case, hydroxyl groups of cellulose act as initiator for polymerization reactions like the ROP of lactide and lactones. This technique has the great advantage

to use native cellulose without previous chemical treatment of the same and to use directly a monomer [200]. In such cases the graft co-polymerization of monomers compatible with the matrix in order to improve the compatibility fiber/matrix has been considered as another possible route to modify cellulose and its derivatives. Vinyl monomers such as methyl methacrylate, acrylamide, and acrylonitrile have been largely used [22]. The fibers are generally exposed to high-energy ionizing radiation in order to create free radicals in the cellulose molecules [25, 208-210].

The most part of chemical modification previously described acts on cellulose structure. The ambitious aim of this study is to use the thiol-ene click chemistry, successfully applied on cellulose surface in a previous work [211], on the double bonds presents in the structure of Miscanthus fibers in order to realize a totally green composite by photo-activation. The originality of this work resides in the possibility to apply this chemistry on the unsaturated bonds of lignin and to use raw fibers without previous chemical treatment of these last. Click-chemistry is a very efficient way to modify surface fibers due to the mild reaction conditions, the high yields, the low quantity of sub-products released during the process, the regio-specificity and the stereo-specificity [212].

I-4.2. PROCESSING METHODS

The chemical treatment of fibers and the appropriate choice of a matrix are undoubtedly two fundamental steps in the realization of a composite material, but they are not the only requirements to realize a material with good properties for a specific application. Temperature, pressure and speed adopted during the processing have an impact on the degradation of fibers and matrix, on fibers dispersion and orientation. For this reason, this paragraph focuses on the principal processing methods used to realize composites and more precisely on the compounding methods followed by the molding step. The term "processing" deals with the transformation of raw materials into finished product using compounding, chemical reaction and final molding techniques. Tadmor and Gogos [213] give a more precise definition of polymer processing, this last concerning 'operations carried out on polymeric materials or systems to increase their utility'. By this last definition, it's clear that the principal goal of polymer processing is to increase the value of the polymer or of a certain formulation. The final performances of a material are correlated to the processing used to realize it and they are responsible of the final value of a certain object and of its applicability. Specific performances can be achieved by the appropriate combination of materials and processing techniques. The choice of the appropriate operational temperature is a function of the crystalline nature of the polymer. If this last is amorphous (case 1), the operational temperature (T_o) needs to be higher than the glass transition temperature (T_g), while if it is semicrystalline (case 2), T_o needs to be higher than the melt temperature (T_M). Processing can be continuous or discontinuous. In the first case the most important parameter is the flow, while in the second case is the number of pieces produced that is correlated to the number of cycles.

I-4.2.1. The compounding processes

Mixing, blending and compounding are three terms largely used in the field of polymer processing. The term mixing refers to the physical act of homogenization, during which all constituents are distributed in a uniform manner in the total volume by applying a shear force. Blending refers to the preparation of polymer alloys and compounding to the incorporation of fillers (of different nature) in the raw polymer matrix using a specific formulation recipe [214]. The design of new synthetic materials with specific properties for demanding applications is an expensive way compared to the simple compounding of existing polymers. The minor cost of the mixing process is the fundamental reason that led researchers to use this technique in order to create composites for specific applications instead of synthesizing new polymeric materials. Optimal properties can be achieved by controlling the ratio between the different constituents of a polymer blend and also by

controlling the reaction time in the case of reactive blends. The absence of solvent, the good processability and the uniformity of the product are three important points that could lead to choice compounding methods. Moreover, this technique offers the possibility to change quickly the formulation and to have high productivity [214, 215]. Polymer compounding includes different steps. First of all raw materials (matrix and filler) have to be prepared. One common preparation step is drying that is essential in the specific case for vegetal fibers and for certain matrixes sensible to hydrolysis at high temperature, such as PLA [121]. The preparation can be followed by a pre-mixing step in which eventual agglomerates are break and well dispersed and then the mixing and molding operations can be carried out. Mixing processing is carried out in different type of equipment such as single or twin extruders or internal mixers. These last can have great or small size depending on other equipment associated such as those for mix discharge (blades) or power input (large or little motors) and depending also on batch weight and speed of mixing. The constituents in a fluid state are compressed, folded it over and then compressed again. High shear stresses existing between the moving (rotating blades) and stationary (chamber) elements are applied to the material that is torn apart [216]. One of the most famous compounding methods is the extrusion thanks to its versatility and large use. The versatility of this method is due to the possibility to produce different artifacts with symmetrical or not sections, such as hollows, pipes, sheet, film and beams. A typical extruder can be considered as a pump used for melt or more precisely for plasticize and carry high viscosity fluids (See Figure I-24). The process converting the solid polymer into the plastic state is induced not only by heating but also by compression and high shear applied during extrusion. The molten is pushed and forced through a die that impart the desired shape. In general the polymer melts due to the heating system and also to the heating released during the screw rotation. An extruder can have a single screw or a twin, these last being co-rotating or counter-rotating. The rotation type depends on the final purpose. More precisely, a counter-rotating twin screw extruder is preferred to optimize the mixing of different constituents, while a co-rotating is preferred in the case of high pressures required. [12, 217, 218]. Extrusion can be also used also to perform a series of reactions such as bulk polymerization, graft reaction, interchain copolymer formation, coupling/crosslinking reactions and functionalization. This is the reason why in this case extrusion is called more properly with the name of reactive extrusion [219]. Grafting reactions have been already described in paragraph I-4.1. They are associated to other side reactions such as radical combination [220], induced-crosslinking [221, 222], and degradation caused by beta-scission [223]. In order to limit these side reactions favoring the grafting, it's not sufficient to control only the monomer and initiator concentration, but also some extruder's parameters, such as residence time, screw speed and temperature [224-226].
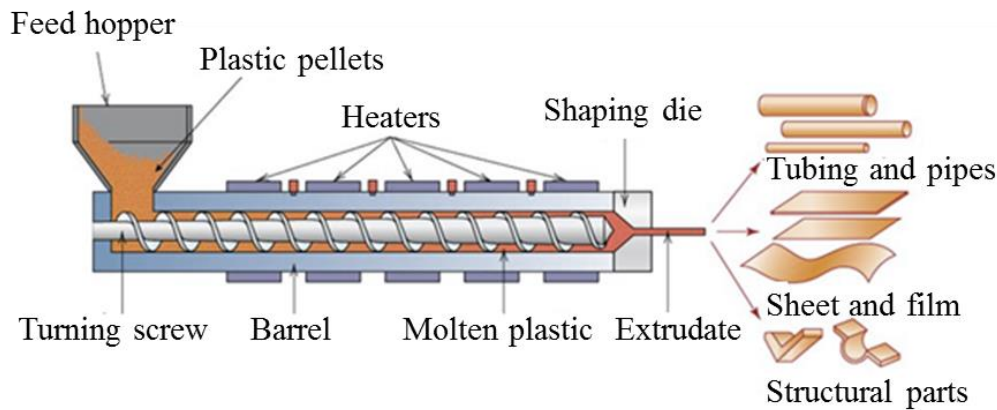
Figure I-24. Typical extrusion process [9].

I-4.2.2. The molding processes

Mold processes refers in a more general sense to all processes in which polymers or blends are transferred into a cavity having the shape of the work piece. They can be classified in two principal categories depending on the used mold. We can distinguish open mold processes and closed mold processes. In the first group, one can find processes such as the hand lay-up and the spray lay-up, while in the second group there are processes such as compression and injection molding. Hand lay-up and spray lay-up consist in creating a first layer of polymer and reinforcement in to a mold, adding other layers until the desired thickness. These two techniques can be distinguished by the deposition method of the polymer and the fibers (trough spray or roller) and are used to create component parts or more in general large pieces. Several disadvantages here are associated to the open-mold processes such as low productivity, health problems for operators due to the contact with the materials and low surface smooth due to the absence of a counter mold. In the more specific case of the spray lay-up the impossibility to orient fibers, limiting the process to the production of isotropic materials [227]. In this work more attention will be dedicated to the closed mold processes and in particular to compression and injection molding. Compression molding (Figure I-25) is used for high production volume per unit of time. At first a controlled volume of material (blend or polymer granules) is deposited inside the mold cavity heated sufficiently to allow the fusion of polymer. A pressure is mechanically applied through a male mold to the charge deposited in a female mold in order to achieve the desired shape. At the end of the procedure the final piece can be extracted, this last in general having a sheet molding shape.
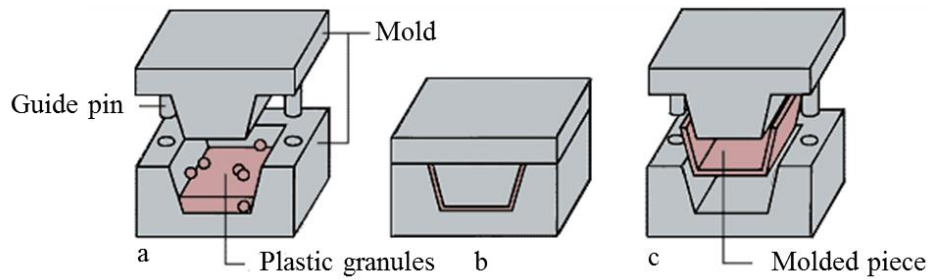
Figure I-25. Compression molding process (adapted from [228]).

Injection molding is widely used for thermoplastic polymers manufacturing. During this process the constituents mixed previously in a tank with rotating screws is pushed inside a cylinder heated at a temperature that allow the material to remain in a molten state and to flow into the cavity of the mold through a gate. It is kept at a temperature lower than the glass transition one in order to allow the solidification of material one it is filled completely (See Figure I-26).
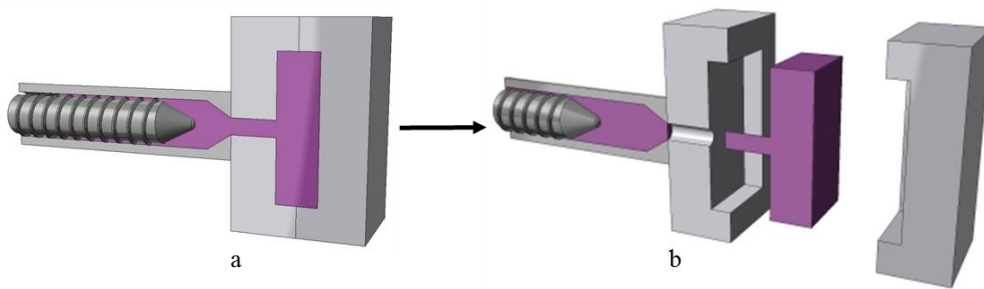
Figure I-26. Injection molding process (adapted from [229]).

During this process, the applied pressure plays a fundamental role. Indeed, one filled the cavity, it starts the maintenance phase during which a pressure is applied to force in the cavity other material to compensate the increase in density and the withdrawal of the molded piece due to decrease in temperature and solidification, which take place both during the maintenance phase and subsequently. The dimension of the gate has a great impact on the cooling step. This last is more rapid if the gate is thin. Then, the polymer became solid in the gate and less polymer fills the cavity with a consequent impact on the residual pressure in the cavity (pressure at the opening of the mold). Another parameter of great importance in this process is the pressure. This last tends to separate the two parts of the mold once applied. An incomplete fill of the mold can happen. During the fill of the cavity, polymer tends to become solid in contact with the mold walls, reducing the section available for the flux. In these conditions the polymer doesn't flow and flux is stopped when the pressure reaches the maximum value possible for the machine. This effect can be reduced by increasing the injection temperature

(T_I) and the mold temperature (T_m). Compared to the compression molding in which there is no a particular orientation of the material in the mold, the injection molding is known to create pieces with a certain orientation of both polymer chains and reinforcement. The orientation and the morphology of a polymer during the injection is essentially due to the cooling rate and to the orientation accumulated in the previous step. In general injected pieces are not homogeneous, with variable orientation and morphology from the mold walls to the center. All these effects suggest that the mechanical properties of polymers injected are very different from those compressed and they are related to the internal stresses applied. As said previously, macromolecules can be oriented along the flow direction and after the end of this driving force they should return to the original conformation. In the reality, the rapid cooling of the molten in the mold causes a shift of the relaxation time to higher temperature than that of the process, causing residual deformations [11, 12, 217].

I-4.3. PLA-BASED COMPOSITES

The high productivity, the biodegradable and bio-based character of PLA are not the only requirements for the realization of biocomposites. The low melting temperature at which PLA can be processed constitutes an important advantage in the realization of composites reinforced with vegetal fibers, these last being not degraded after processing. PLA can substitute the oil-derived plastics in many sectors such as automobiles or packaging [230]. A comparison between PP and PLA reinforced with 30-40% of flax fibers showed that the tensile strength was better in the case of PLA as matrix of about 50%, with no decrease in PLA properties after compounding and an improvement of the final stiffness [120]. This result suggests that a possible strategy to modify thermal and mechanical properties of PLA, reducing the total cost of the final material is to reinforce the matrix with various natural fibers.

Many PLA-based composites have thus been realized using kenaf, flax, jute, abaca, miscanthus, cellulose and wood [47, 120, 231-235]. The comparison between different samples showed that in general the addition of fibers caused an increase in tensile modulus and a decrease in elongation at break and in tensile strength when they are used in the absence of a compatibilizing agent. Moreover these results are independent from the realization method. The composites exhibit classical problems related to the incompatibility between matrix and fibers such as the presence of void at the interface [232, 236]. For this reason, many efforts have been made in the field of chemical treatment of fibers in order to improve the mechanical performances of PLA-based biocomposites. Hemp and ramie fibers treated with alkali and added to PLA showed much higher values in tensile strength and elastic modulus than neat matrix [237, 238]. A similar trend for the tensile strength was found in the case of

ramie fibers treated with silane [238] although the maximum strength was obtained in the case of fibers treated with NaOH due to the bonding at the interface between the ramie fiber and PLA matrix. In other works, a silane treatment on wood fibers induced an increase in tensile strength and in elastic modulus, reflecting the improvement of the interfacial adhesion fibers/matrix [239]. The mechanical discussed above are summarized in table I-5 and compared to the properties of the neat matrix. PLA/kenaf composites are used for spare tire covers or circuit boards [230], PLA/cordenka composites are used in automotive and electronic fields [240] and many PLA reinforced with man-made cellulose suggested different fields of application like furniture, car parts, grinding discs and safety helmets [241].

Sample	Chemical treatment	fibers [wt%]	E [GPa]	σ [MPa]	ε [%]	Reference
PLA	-	-	3.4 ± 1.0	60.4 ± 0.8	4.1 ± 1.3	[47]
PLA/flax	-	40	7.3 ± 0.5	44.0 ± 7.2	0.9 ± 0.2	[120]
PLA/jute	-	40	8.1 ± 0.4	72.7 ± 2.3*	1.5 ± 0.0	[232]
PLA/miscanthus	-	40	6.6 ± 1.9	41.2 ± 1.5	0.9 ± 0.2	[47]
PLA/wood flour	-	40	3.7 ± 2.5	36.2 ± 2.0	1.1 ± 0.2	[239]
PLA/hemp	-	40	7.4	44.6	nd	[237]
PLA/hemp-NaOH	NaOH	40	8.5	54.6	nd	
PLA/ramie	-	30	nd	52.5 ± 8.0	3.2 ± 0.2	[238]
PLA/ramie-NaOH	NaOH	30	nd	66.8 ± 1.7	4.8 ± 0.2	
PLA/ramie-silane	silane	30	nd	64.2 ± 0.7	3.6 ± 0.1	
PLA/wf [(**)]	-	40	3.7 ± 2.5	37.2 ± 2.0	1.1 ± 0.2	[239]
PLA/wf-silane	silane	40	4.3 ± 4.2	48 ± 4.7	1.3 ± 0.2	

*Maximum strength at yield

** wf: wood flour

Table I-5. Tensile properties of PLA-based composites with fibers untreated and treated with NaOH and silane. E: tensile modulus; σ: strength at yield; ε: elongation at break; nd: not determined.

I-4.4. PCL-BASED BIOCOMPOSITES

In order to keep intact the biodegradability of the starting material, improving at the same time the mechanical properties of the final composite, PCL can be combined with various natural fibers by adjusting the ratio matrix/fiber [242, 243]. For different application areas, the use of lignocellulosic filler (cellulose, sisal, flax fibers) in PCL matrix was investigated [244, 245]. PCL is generally blended [115, 246, 247], but it can be also extruded [248] and in this case the influence of extrusion parameters like rotation speed, throughput, and screw configuration on the residence time have to be taken into account. One of the advantage of PCL-based biocomposites is that they require low energy for thermal recycling and they can be used as eco-friendly materials for energy recovery. The low melt temperature of PCL is a great problem not only for the manufacturing the biocomposites, but also for the final applications of the materials that cannot be exposed to slightly elevated temperatures. In order to avoid the problem related to low melt temperature and degradation of matrix and lignocellulosic fibers, biocomposites were realized by impregnation baths for fibrous mats. In this case, thermal properties of PCL were maintained and mechanical ones were improved thanks to this technique and to the refining treatment of alfa fibers [249]. Composites with various types of lignocellulosic fibers, such as cotton, cellulose obtained from the same and hydrolyzed cellulose were realized [250]. In this case, best performances were obtained for a composite with 15% of simple cellulose, in which mechanical properties were improved and the barrier properties of the pure matrix were not affected by the presence of the filler. The results demonstrated also that the effort and costs involved in the chemical treatments to prepare the hydrolyzed cellulose were not justified. In such case, other biocomposites properties such as water-resistance were improved acting on the modification of the polymer, as demonstrated by PCL modified with acrylic acid or cross-linked PCL, exhibiting lower swelling, higher water resistance but at the same time lower degradation rate [251, 252].

I-4.5. PHBHV-BASED BIOCOMPOSITES

A lot of fibers have been used these last years to improve the mechanical properties of PHBHV, such as flax [253], jute [119], cellulose [118], wood [254] and bamboo [255]. The elastic properties of some of these composites are showed in table I-6.

Sample	% fibers [wt%]	E [GPa]	σ [MPa]	References
PHB$_{97}$HV$_3$	-	2.1 ± 0.07	27.3 ± 0.3	
PHB$_{97}$HV$_3$/man made cellulose	30	4.4 ± 0.34	41.7 ± 3.8	[119]
PHB$_{97}$HV$_3$/abaca	30	4.4 ± 0.06	28.0 ± 1.3	
PHB$_{97}$HV$_3$/jute	30	7.0 ± 0.26	35.2 ± 1.3	
Biopol	-	1.0 ± 0.09	21.4 ± 1.5	[254]
Biopol/wood	30	1.9 ± 0.33	18.0 ± 2.04	
Biopol/bamboo	30	1.71	18.9	[255]

Table I-6. Tensile properties of PHBHV-based composites with different vegetal fibers. E: tensile modulus; σ: strength at yield.

In general these composites show an increase in mechanical properties and various changes in thermal properties with increasing the filler content. For example, the elastic modulus of neat PHBHV can be improved by around 167% by adding 40 % by weight of wood flour. In contrast tensile strength decreases with increasing wood flour content [254]. A similar trend can be found changing reinforcement type, using for example 40 wt% of recycled cellulose as filler for PHBHV. In this case tensile modulus was improved by 220% and at higher cellulose content (over 20%) tensile strength increases [118]. Exception to this case, in general when fibers are not modified by a chemical or a physical treatment, a decrease in final strength can be observed. The incompatibility between the hydrophilic fibers and the hydrophobic matrix led to lack adhesion fiber/matrix with poor dispersion of the reinforcement in the matrix. These results are often confirmed by SEM images in which fibers pull out from the matrix or with formation of fibers aggregates at high content of reinforcement. The crystal morphology of PHBHV-based biocomposites is another parameter that can be affected by the presence of natural filler and that can influence the mechanical properties of the final composite. Fibers or flour can act as nucleation points increasing crystallinity and changing the crystallization rate [255]. Similar results were reported in literature on wood fiber and wheat straw fiber filled

PHBHV composites [256, 257]. However there are also many case reported in literature in which no change in crystallinity of PHBHV or its crystallization kinetics are detected [258-260]. A great amount of investigations done with PHBHV biocomposites focuses on processing techniques and in particular on compression molding of thin layers or films [261-263]. The use of lab-scale equipment such as mini-molders or mini-processing machines [118, 255] constitutes a limitation for a large scale application of these materials. In most cases, the up-scaling procedure is not applicable [119]. However many studies [264, 265] were carried out using semi-scale processing equipment, resulting in excellent fibers dispersion. These results are encouraging for an industrial application of these materials. In order to show the advantages of PHBHV-based biocomposites, polypropylene (PP) was used as matrix and reinforced with vegetal fibers. The comparison between the two matrixes was possible because processing parameters and fibers type were the same in the two cases. The addition of 30% of wheat straw in PP and PHBHV causes a much higher increase in Young Modulus for this last matrix. This fact can be explained by the better compatibility of wheat straw with the PHBHV matrix as compared to PP matrix. Moreover, scanning electron microscopy (SEM) images reveal more deformation of PP matrix than PHBHV in all biomass reinforced composites, with a significant gap between the fibers and PP, while no gap was detected for biomass fiber-reinforced PHBHV [266]. The results described proved that these green composites can surely provide a sustainable alternative to oil-derived composites.

I-5. MICROMECHANICS OF HETEROGENEOUS MATERIALS

The constitution of a material intended as its chemical composition, the arrangement of the different constituents and their volumetric fraction, constitute important requirements to realize a composite with desired properties. The possibility to evaluate and predict the overall characteristics of a composite has a fundamental role.

Thus, a multiscale procedure consists in evaluating the effective properties of a hierarchically structured material at a scale of observation from considerations of the phenomena occurring at the lowers scales. As presented in figure I-27, the methods that have to be carried out to obtain this effective behavior depend on the considered scales, from stochastic approaches for very large systems to classical multiscale methods of continuum mechanics and even atomistic approaches necessary to describe nanometric media.
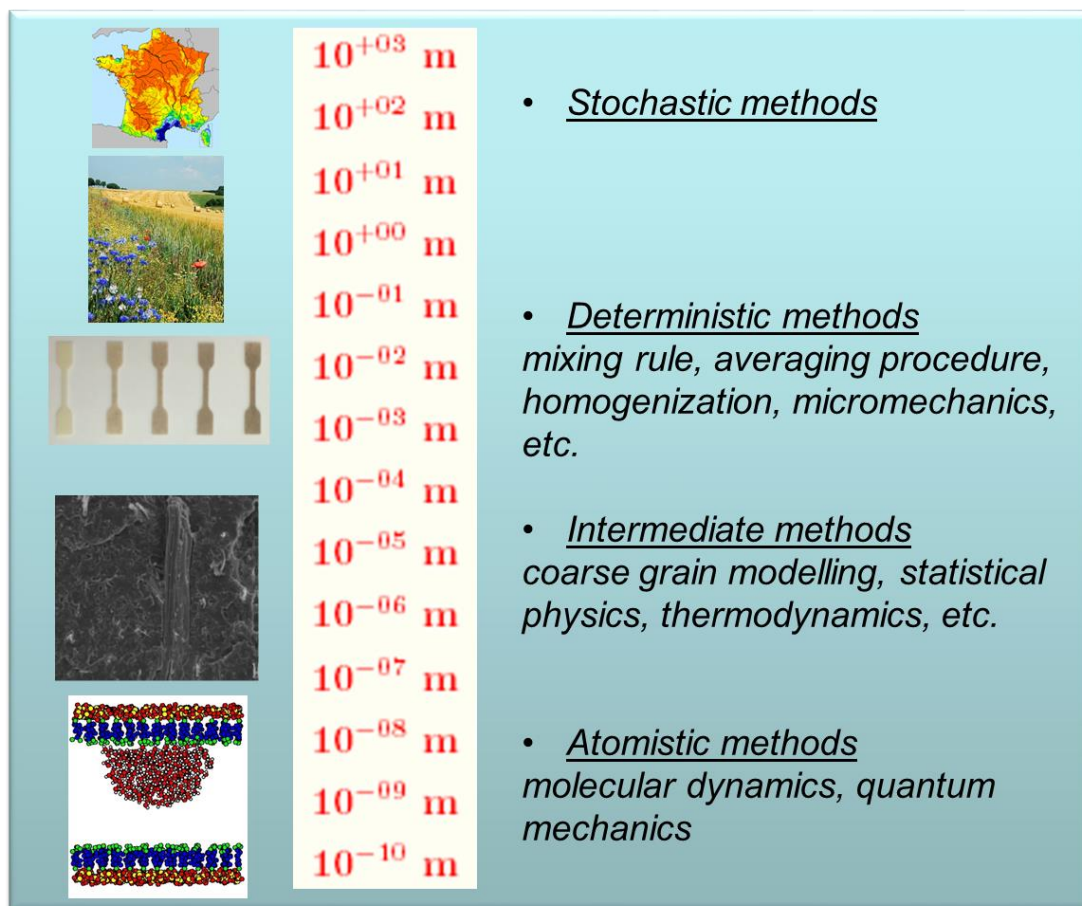
Figure I-27. Multiscale methods for different length scale levels.

At the laboratory scale, all the observable material properties are only the macroscopic manifestation of very many complex interaction mechanisms involving structural components on numerous scales smaller than those we perceive with the naked eye. Among these last, some of interest are the mechanical performance (elastic modulus, hardness, toughness and ductility, or its fracture resistance) and also the acoustic (i.e., its ability to propagate or attenuate acoustic waves), electric (e.g., the electrical conductivity or the magnetic permeability) and optical properties. Therefore, it's necessary to investigate the multiscale nature of the materials in order to well understand, describe and control the mechanics and physics of solids. In this context, composites materials perfectly describe the differences between scales, being constituted by different phases and they are a perfect example of how the microscopic structure can influence qualitatively and quantitatively the macroscopic properties of the final material.

To illustrate how multiscale phenomena can influence the overall properties of a given material, we can refers to a crystalline material. As already discussed, the crystallinity (for example of a polymer) is linked to the chemical structure and influence the mechanical behavior of a material. At the macroscale, which ranges above a few millimeters, it's possible to observe the general organization of a material. When zooming in, it is then possible to observe a large number of grains with different properties of orientation. At this scale, often called mesoscale, the local particularities and heterogeneities of the material appear. The next length scale, the microscale with typical submicronic dimensions, requires imaging tools such as microscopy or tomography. At this scale, within each grain, complex configurations of defects in the regular atomic lattice (most importantly, the so-called dislocations) become visible, forming a complicated network. Together with all other crystal defects, the dislocation network forms the microstructure.

I-5.1. MICROMECHANICAL FRAMEWORK

When studying matrix-fiber composites, the microscale typically refers to the inclusion size whereas the macroscale is linked to the size of the composite product. According to figure I-27, this situation typically corresponds to the use of deterministic methods such as micromechanics. Aiming describing heterogeneous materials by considering the properties of the matrix, the inclusions and the interfacial phenomena, this approach involves classical tools of continuum mechanics. At the macroscale, the notion of material particle is however replaced by the concept of Representative Volume Element (RVE) [267]. This last can be seen as a sub-volume of a heterogeneous medium that perfectly represents from a statistical point of view the composite, including all the micro-elements (fibers, voids etc.) that constitutes the total material. It has thus to be large enough in comparison with

the size of the microstructural constituents. Moreover, the RVE also has to be small enough when compared to the characteristic size of the macroscopic medium in order to be able to introduce the concept of material particle during a structural calculation [268].

The Russian dolls configuration of our types of composite materials are showed in figure I-28 [269].

Figure I-28. Principal scales in micromechanics approach.

Focusing the attention on the mechanical response, micromechanics tools make it possible to determine the elastic moduli of a composite material starting from those of its constituents [270, 271]. The problem of the determination of elastic moduli in heterogeneous materials has been largely investigated in past years [272-274] The transformation of a heterogeneous material into a constitutively equivalent body of a homogeneous continuum constitutes the basic principle for various composite homogenization models whose characteristics will be described in the next paragraph.

I-5.2. FIRST SIMPLE ANALYTICAL METHODS

We consider hereafter that the scales separation that is necessary to derive the concept of RVE is valid. This RVE is made by the union of two phases (typically the matrix and the fibers indexed "*M*" and "*F*").

The volume of this representative element is noted V (V_F and V_M being the subvolumes occupied by the fibers and the matrix) and the averaging over this domain of a quantity $ is noted

$$\langle \$ \rangle = \frac{1}{V}\int_V \$ dV = \frac{1}{V}\left[\int_{V_F} \$ dV + \int_{V_M} \$ dV\right] \qquad (\text{I-1})$$

To illustrate how this averaging procedure can be performed, let us consider the Young E modulus as the quantity $\$$. It is then possible to derive the rule of mixtures (ROM) providing an estimation of the effective Young modulus E_{eff} from the constant moduli of the two phases:

$$E_{eff} = \frac{1}{V}\left[\int_{V_F} E_F dV + \int_{V_M} E_M dV\right] = \Phi_F E_F + (1-\Phi_F)E_M \qquad (\text{I-2})$$

where $\Phi_F = V_F/V$ is the fibers volume fraction.

More generally, the development of a micromechanical model requires to provide the behavior of each constituent of the heterogeneous medium. For instance, if x represents a location inside the RVE and if each phase is considered as an elastic material, the local Hooke's law in a Cartesian frame reads:

$$\sigma_{ij}(x) = C_{ijkl}(x)\varepsilon_{kl}(x) \qquad (\text{I-3})$$

or

$$\varepsilon_{ij}(x) = S_{ijkl}(x)\sigma_{kl}(x) \qquad (\text{I-4})$$

Here, σ_{ij} and ε_{kl} represent the local stress and strain tensors and $C = S^{-1}$ are the two fourth-order elastic tensors (stiffness and compliance tensors). The aim of micromechanics being to provide effective values of these latter properties tensors, the first two simple ideas consist in considering homogeneous strain (Voigt approach), respectively homogeneous stress (Reuss approach), by applying average values of the strain $\langle \varepsilon \rangle$, respectively of the stress $\langle \sigma \rangle$ at the boundaries of the RVE.

Thus, the effective stiffness tensor C_{eff} linking the average stress and strain through the effective Hooke's law

$$\langle \sigma \rangle = C_{eff}\langle \varepsilon \rangle \qquad (\text{I-5})$$

can be derived as follows

$$C_{eff} = \langle C \rangle \qquad (\text{I-6})$$

in the case of the Voigt approximation and

$$C_{eff} = \langle S \rangle^{-1} \tag{I-7}$$

in the case of the Reuss approximation.

Being quite simple, these two approximations do not generally provide a satisfactory description of the effective behavior of the heterogeneous material. Indeed, the Voigt method tends to overestimate the stiffness of the equivalent homogeneous material, whereas the Reuss one leads to an underestimation. That is why other approaches have been proposed in order to obtain more realistic descriptions of the effective behavior of heterogeneous materials.

I-5.3. ESHELBY APPROXIMATION

Seeded in the works of Hill [273] introducing the fiber strain concentration tensor A_F, it can be demonstrated that the average composite stiffness C_{eff} can be expressed as a function of this tensor and the stiffness tensors of fibers (indexed "F") and matrix (indexed "M"):

$$C_{eff} = C_M + \Phi_F (C_F - C_M) A_F \tag{I-8}$$

The fiber strain concentration tensor A_f corresponds to the ratio between the average strain in the fiber and that of the composite. Note that the previous Voigt and Reuss approximations can be easily recovered from this equation considering homogeneous strain or stress conditions.

However, the determination of C_{eff} remains very complex since the stress and strain fields in the heterogeneous medium have to be determined. An analytical possibility to achieve such a determination is based on the inclusion theory of Eshelby, developed in 1957 [275], concerning the problem of an elastic inclusion in an infinite elastic homogenous medium. Eshelby considered the matrix as a linear elastic solid containing an inclusion constituted by the same material of the matrix, of a certain volume V_i and boundary S_i which undergoes a change in shape and size caused by the surrounding matrix. In order to determine the exact elastic state of the inclusion and the matrix, Eshelby started to remove the inclusion from the matrix. This caused the so called "eigenstrain" [276, 277], a uniform strain with zero stress indicated with ε^T. After this removing step, by applying a surface force on S_i, he restored the cut inclusion to its original shape causing this time a stress in the region of the inclusion with zero stress in the matrix. The whole body developed a complicated strain field ε^C. At the end of this procedure, Eshelby calculated the stress and strain fields in the inclusion,

allowing to determine the effective elastic tensor C_{eff}. More precisely he defined the stress in the inclusion σ_I as:

$$\sigma_I = C_M(\varepsilon^C - \varepsilon^T) \qquad \text{(I-9)}$$

where C_M is the stiffness of the matrix. For an ellipsoidal inclusion, Eshelpy showed that the strain field ε^C was uniform and related to the eigeinstrain ε^T by the following relation:

$$\varepsilon^C = E\varepsilon^T \qquad \text{(I-10)}$$

Where E is the Eshelby tensor and is dependent on inclusion aspect ratio and the matrix elastic constants [278]. The second step in Eshelby's approach consists in demonstrating an equivalence between the homogeneous inclusion problem and an inhomogeneous inclusion of the same shape. He showed that the stress field in the inhomogeneous inclusion can be expressed as follows:

$$\sigma_I = C_M(E-I)[(C_I - C_M)E + C_M]^{-1}C_I \varepsilon^{T*} \qquad \text{(I-11)}$$

where I is the identity tensor, ε^{T*} is the eigenstrain in the inhomogeneity and C refers to the stiffness tensor of matrix (indexed "M") and inclusion (index "I"). The Eshelby theory is considered as the background for all the homogenization methods developed. However, this method is restricting because it was formulated for a single particle surrounded by an infinite medium. Moreover, Eshelby solution treated only ellipsoidal fibers and can be used to evaluate the stiffness of a certain composite with good accuracy for low volume fractions of fibers. This approximation is often called very dilute inclusion approximation.

I-5.4. HALPIN-TSAI EQUATIONS

Other analytical techniques can be used to predict and better characterize the behavior of these composites [279]. Again, these methods make simplifying assumptions about the microstructure to solve the problem [280-282]. The perfect interface between the constituents and the elastic behavior of fibers and matrix during the mechanical response are two of the most used assumptions in the modelling of mechanical behavior of fibers-reinforced composites.

When focusing on the Young modulus, experimental observations have shown that the values obtained with the rule of mixtures (equation I-2) do not predict the real values [283]. This remark is particularly true when considering anisotropic materials. For instance in figure I-29, the fibers are

mainly oriented in the longitudinal direction and it is obvious that the mechanical properties in this direction strongly differs from the one in the transverse one.

Figure I-29. Scheme of a composite with fiber aligned in the stress direction

In such a configuration, the Halpin-Tsai model [284], largely used in the case of polymeric blends [285] but also in the case of biopolymers reinforced with natural fillers [118, 254], is rather efficient. Halpin-Tsai equations predicts the longitudinal (E_1) and transversal (E_2) moduli of an aligned short fiber composite [286]:

$$E_1 = E_F \Phi_F + E_M (1 - \Phi_F) \tag{I-12}$$

$$\frac{E_2}{E_M} = \left[\frac{1 + \xi \eta \Phi_F}{1 - \eta \Phi_F} \right] \eta \tag{I-13}$$

where ξ is the "reinforcing factor" depending on the fibers geometry, their "packing", the loading condition and where η is given by the following expression:

$$\eta = \left[\frac{\left(\frac{E_F}{E_M}\right) - 1}{\left(\frac{E_F}{E_M}\right) + \xi} \right] \tag{I-14}$$
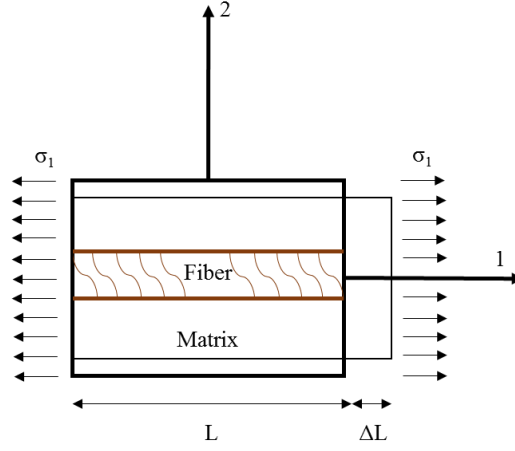
I-5.5. MORI-TANAKA-BENVENISTE MODEL

Another model largely used in the domain of composite materials is the Mori-Tanaka model [287] developed in 1973 and then reformulated by Benveniste in 1987 [288]. In their work, Mori and Tanaka, starting from Eshelby's theory, proposed a method to correlate the average stresses and

strains of the inclusion with those of the matrix in a composite [289]. This approach is based on some assumptions:

- The matrix is considered as a linear elastic and isotropic material;
- Fibers are considered as linearly elastic and they can be isotropic or transversely isotropic;
- Fibers can be characterized by a certain aspect ratio between their length "*l*" and their diameter "*d*";
- There is a perfect contact at the interface between fibers and matrix; no interfacial slip, or fiber/matrix debonding, or matrix crack is considered.
- The average strain in fiber is related to the average strain in the matrix by a fourth order tensor expressing the relation between the uniform strain in the inclusion embedded in a matrix material subjected to uniform strain at infinity.

Such approaches have been used in the laboratory to study bone properties [290] and these implemented methods will thus be used to characterize our composites.

I-5.6. NUMERICAL METHODS: A FOCUS ON FINITE ELEMENT METHOD

If many theoretical models are present in literature [291-294], they are appropriate for the case of unidirectional short-fiber composites but from an experimental point of view, it's very difficult to manufacture a material with short fibers perfectly aligned in a direction. In general, partial alignment can be obtained using processing methods such as those described in the previous paragraph (injection for instance). As visible in figure I-30, advanced imaging techniques such as micro-tomography shows that the intimate structure of the composite presents a level of disorder that increases the accuracy of the theoretical estimations of the effective mechanical parameters.

The idea can then to simulate a tensile test on a sample to derive a numerical estimation of the effective properties.

To do that, the most classical approach consist in using a Finite Element Method (FEM). This numerical procedure is very well adapted to solve elliptic problems such as elasticity problem. Basically, its idea consists in transforming the problem in its strong sense (the set of the partial differential equations and the convenient boundary conditions defined over an open material domain V and its boundaries ∂V) into a problem in the weak sense by using the scalar product by a test function belonging to a convenient vector space of functions W. Using Green formulae, it is then possible to explicitly incorporate the boundary condition into the formulation. Then, the solution to

the problem is searched from this weak problem. To overcome the infinite dimension of the vector space W, an approximation of the solution is searched on a discrete sub-vector-space (for instance polynomial functions of a given degree with prescripted values over identified nodes of the domain and its boundary) with a finite dimension, the problem often becoming the resolution of a quite simple linear problem. These nodes form a mesh of the material domain.

This analysis is useful in the case of complex geometries and different properties of the inclusions compared to those of matrix. The division of the problem in subdomains allows to detect also local effects.

In the finite element analysis, the mesh generation is a fundamental part of the analysis because it guarantees the geometric accuracies and participates to the numerical precision. In fact, in such cases classical mesh generation led to poor accuracies and fail to characterize the material heterogeneities, while ultra-fine meshes assure good accuracies but they may affect the computational efficiency [295].

In our situation, the FEM models can be built from geometrical representations of the composite (see chapter IV for instance) or from advanced imaging techniques such as micro-tomography to predict the elastic properties of materials [296] and in order to have realistic information about the geometry of the inclusions [297].

Micro-CT reconstruction

RVE for FE analysis
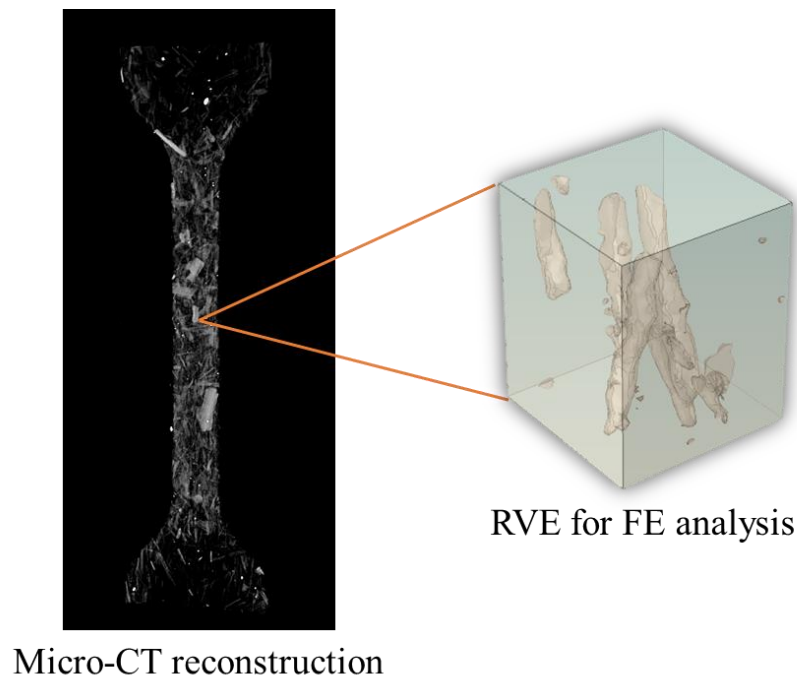
Figure I-30. Micro-CT reconstruction of a polymer/fibers composite and determination of a realistic RVE volume.

I-6. CONCLUSIONS

In this chapter the characteristics of different matrixes and reinforcements, the principal processing methods, the current chemical treatments of cellulose and some numerical and analytical approaches were described. Thanks to the information provided by this study, only three matrixes were retained for the next part of this thesis. We decided to reinforce poly(ε-caprolactone), poly(lactic acid) and poly(3-hydroxybutyrate-*co*-3-hydroxyvalerate), all belonging to the group of biodegradable aliphatic polyesters, with vegetal fibers of Miscanthus *giganteus*.

The description of all possible chemical treatments on the reinforcement suggested that the majority of these methods are applied to the hydroxyl groups of cellulose and some of these are very aggressive in terms of reaction conditions. In the following part, we have tried to identify an eco-friendly chemical treatment that could maintain the green character of the biocomposites, improving at the same time the mechanical properties of the final material. The method that we have chosen is not based on the chemical modification of the hydroxyl groups of cellulose (largely described in literature), but it is based on the reactivity of the double bonds present in the lignin structure of vegetal fibers. To this innovative technique we have associated a grafting initiated by peroxides which can improve the adhesion matrix/fibers, acting also on the cross-linking of the matrix.

The study about the processing methods suggested that in order to realize a biocomposite with competitive mechanical properties, a good dispersion and a good alignment of the reinforcement into the matrix are two fundamental requirements to be achieved. To this aim, we have retained for the next part extrusion and mixing as two compounding methods and injection and compression molding as final steps to give a shape to biocomposites.

The descriprion of the basics of micromechanics revealed that different methods (analytical and numerical) can be used in order to describe the elastic behaviour of the final biocomposite. Among all the possible models, we have retained the Mori-Tanaka model and the finite element methods to describe the effect of fibers content, size, arrangment and adhesion to the matrix on the mechanical behaviour of the biocomposite.

I-7. REFERENCES

1. Pandey, J.K. et al., Commercial potential and competitiveness of natural fiber composites, in *Biocomposites: Design and Mechanical Performance*, M. Misra, J.K. Pandey, and A.K. Mohanty, Editors. Woodhead Publishing (**2015**).
2. Wang, R.M. et al., Polymer Matrix Composites and Technology. Woodhead Publishing Limited and Science Press Limited (**2011**).
3. Available from: http://compositeslab.com/composites-101/history-of-composites /. June 26, 2017.
4. Jones, R.M., Mechanics of Composite Materials. Second ed.: Taylor and Francis Group (**1999**).
5. Matthews, F.L. et al., Composite Materials: Engineering and Science. Woodhead Publishing Limited and CRC Press LLC (**1999**).
6. Kaw, A.K., Mechanics of Composite Materials. Second ed.: CRC Press (**2005**).
7. United, S., Advanced materials by design. Washington, DC: Congress of the U.S., Office of Technology Assessment : For sale by the Supt. of Docs., U.S. G.P.O. (**1988**).
8. Shalin, R.E., Polymer Matrix Composites. First ed.: Springer Netherlands (**1995**).
9. Callister, W.D. et al., Scienza e ingegneria dei materiali. Third ed.: Edises, Napoli (**2012**).
10. Peng, W. et al., Thermosetting Resins. *Journal of Chemical Education* 72(7), p. 587 (**1995**).
11. Marchetti, M. et al., Tecnologie dei materiali compositi. Editoriale ESA, Milano (**1991**).
12. Brukner, S. et al., Scienza e Tecnologia dei Materiali Polimerici. I ed, ed. N. Edises. (**2001**).
13. Vázquez, A. et al., Bagasse Fiber-Polypropylene Based Composites. *Journal of Thermoplastic Composite Materials* 12(6), p. 477-497 (**1999**).
14. Berglund, L.A., Thermoplastic resins, in *Handbook of Composites*, S.T. Peters, Editor. Chapman & Hall, London (**1998**).
15. Baker, A.-M. et al., Thermoplastics, in *Handbook of Plastics, Elastomers & Composites*, C.A. Harper, Editor. McGraw Hill, New York (**2002**).
16. Strong, A.B., Fundamentals of composites manufacturing: materials, methods and applications. Second ed.: SME, Dearborn (**1989**).
17. Wayne Hayden, H. et al., Mechanical behavior, in *Structure and properties of materials*. John Wiley and Sons, Inc. (**1965**).
18. Available from: http://www.pluscomposites.eu/sites/default/files/technical-articles-chapter6-English_0.pdf./ June 26, 2017.
19. Biagiotti, J. et al., A Review on Natural Fibre-Based Composites-Part I. *Journal of Natural Fibers* 1(2), p. 37-68 (**2004**).
20. Mallick, P.K., Fiber-reinforced composites: materials, manufacturing and design. CRC Press, Boca Raton (**2007**).
21. Bledzki, A.K. et al., Composites reinforced with cellulose based fibres. *Progress in Polymer Science* 24(2), p. 221-274 (**1999**).
22. Saheb, D.N. et al., Natural fiber polymer composites: A review. *Advances in Polymer Technology* 18(4), p. 351-363 (**1999**).
23. Glasser, W.G. et al., Fiber-reinforced cellulosic thermoplastic composites. *Journal of Applied Polymer Science* 73(7), p. 1329-1340 (**1999**).
24. Li, Y. et al., Sisal fibre and its composites: a review of recent developments. *Composites Science and Technology* 60(11), p. 2037-2055 (**2000**).
25. Eichhorn, S.J. et al., Review: Current international research into cellulosic fibres and composites. *Journal of Materials Science* 36(9), p. 2107-2131 (**2001**).
26. Corbière-Nicollier, T. et al., Life cycle assessment of biofibres replacing glass fibres as reinforcement in plastics. *Resources, Conservation and Recycling* 33(4), p. 267-287 (**2001**).
27. Joshi, S.V. et al., Are natural fiber composites environmentally superior to glass fiber reinforced composites? *Composites Part A: Applied Science and Manufacturing* 35(3), p. 371-376 (**2004**).
28. Ahmad, F. et al., A Review: Natural Fiber Composites Selection in View of Mechanical, Light Weight, and Economic Properties. *Macromolecular Materials and Engineering* 300(1), p. 10-24 (**2015**).
29. Ray, A.K. et al., Bamboo—A functionally graded composite-correlation between microstructure and mechanical strength. *Journal of Materials Science* 40(19), p. 5249-5253 (**2005**).

30. Dittenber, D.B. et al., Critical review of recent publications on use of natural composites in infrastructure. *Composites Part A: Applied Science and Manufacturing* 43(8), p. 1419-1429 (**2012**).

31. Dicker, M.P.M. et al., Green composites: A review of material attributes and complementary applications. *Composites Part A: Applied Science and Manufacturing* 56, p. 280-289 (**2014**).

32. Charlet, K. et al., Characteristics of Hermès flax fibres as a function of their location in the stem and properties of the derived unidirectional composites. *Composites Part A: Applied Science and Manufacturing* 38(8), p. 1912-1921 (**2007**).

33. Kaack, K. et al., Variation in morphology, anatomy and chemistry of stems of Miscanthus genotypes differing in mechanical properties. *Industrial Crops and Products* 17(2), p. 131-142 (**2003**).

34. De Rosa, I.M. et al., Morphological, thermal and mechanical characterization of okra (Abelmoschus esculentus) fibres as potential reinforcement in polymer composites. *Composites Science and Technology* 70(1), p. 116-122 (**2010**).

35. Wielage, B. et al., Thermogravimetric and differential scanning calorimetric analysis of natural fibres and polypropylene. *Thermochimica Acta* 337(1), p. 169-177 (**1999**).

36. Pickering, K.L. et al., A review of recent developments in natural fibre composites and their mechanical performance. *Composites Part A: Applied Science and Manufacturing* 83, p. 98-112 (**2016**).

37. Célino, A. et al., The hygroscopic behavior of plant fibers: a review. *Frontiers in Chemistry* 1, p. 43 (**2013**).

38. Pereira, P.H.F. et al., Vegetal fibers in polymeric composites: a review. *Polímeros* 25, p. 9-22 (**2015**).

39. Scheller, H.V. et al., Hemicelluloses, in *Annual Review of Plant Biology, Vol 61*, S. Merchant, W.R. Briggs, and D. Ort, Editors. (**2010**).

40. Available from: http://www.cours-pharmacie.com/biologie-vegetale/les-parois-vegetales.html. June 26, 2017.

41. Muthuraj, R. et al., 5 - Studies on mechanical, thermal, and morphological characteristics of biocomposites from biodegradable polymer blends and natural fibers, in *Biocomposites*. Woodhead Publishing. (**2015**).

42. Shah, D.U., Developing plant fibre composites for structural applications by optimising composite parameters: a critical review. *Journal of Materials Science* 48(18), p. 6083-6107 (**2013**).

43. Mohanty, A.K. et al., Biofibres, biodegradable polymers and biocomposites: An overview. *Macromolecular Materials and Engineering* 276-277(1), p. 1-24 (**2000**).

44. Koronis, G. et al., Green composites: A review of adequate materials for automotive applications. *Composites Part B: Engineering* 44(1), p. 120-127 (**2013**).

45. Akil, H.M. et al., Kenaf fiber reinforced composites: A review. *Materials & Design* 32(8), p. 4107-4121 (**2011**).

46. Nanda, M.R. et al., Performance Evaluation of Biofibers and Their Hybrids as Reinforcements in Bioplastic Composites. *Macromolecular Materials and Engineering* 298(7), p. 779-788 (**2013**).

47. Bourmaud, A. et al., Investigations on mechanical properties of poly(propylene) and poly(lactic acid) reinforced by miscanthus fibers. *Composites Part a-Applied Science and Manufacturing* 39(9), p. 1444-1454 (**2008**).

48. Nagarajan, V. et al., New engineered biocomposites from poly(3-hydroxybutyrate-co-3-hydroxyvalerate) (PHBV)/poly(butylene adipate-co-terephthalate) (PBAT) blends and switchgrass: Fabrication and performance evaluation. *Industrial Crops and Products* 42, p. 461-468 (**2013**).

49. Available from: http://www.agrobiobase.com/sites/default/files/dossiers/fichiers/memento_2016_-_panorama_des_marches_fibres_vegetales_techniques_materiaux_hors_bois.pdf. 26 June, 2017.

50. Woodings, C., A brief history of regenerated cellulosic fibers in *Regenerated cellulose fibres*, C. Woodings, Editor. Woodhead Publishing Ltd. (**2001**).

51. Atalla, R.H. et al., Native Cellulose: A Composite of Two Distinct Crystalline Forms. *Science* 223(4633), p. 283 (**1984**).

52. Rojas, J., Effect of Polymorphism on the Particle and Compaction Properties of Microcrystalline Cellulose, in *Cellulose - Medical, Pharmaceutical and Electronic Applications*, T.v.d. Ven and L. Godbout, Editors. InTech: Rijeka. (**2013**).

53. Deguchi, S. et al., Cooking cellulose in hot and compressed water. *Chemical Communications* 21(31), p. 3293-3295 (**2006**).

54. Moore, R. et al., Botany Visual Resource Library the McGraw-Hill Companies, Inc. (**1998**).

55. Brett, C. et al., Physiology and Biochemistry of Plant Cell Walls. First ed.: Chapman and Hall, London (**1990**).
56. Darvill, J.E. et al., Structure of Plant Cell Walls. *Plant Physiology* 66, p. 1135-1139 (**1980**).
57. Available from: https://employees.csbsju.edu/ssaupe/biol327/Lecture/cell-wall.htm. June 26, 2017.
58. Cordeiro, R., Plasma Treatment of Natural Fibers to Improve Fiber-Matrix Compatibility. (**2016**).
59. Klemm, D. et al., Cellulose: Fascinating Biopolymer and Sustainable Raw Material. *Angewandte Chemie International Edition* 44(22), p. 3358-3393 (**2005**).
60. Krumm, C. et al., Millisecond Pulsed Films Unify the Mechanisms of Cellulose Fragmentation. *Chemistry of Materials* 28(9), p. 3108-3114 (**2016**).
61. Available from: http://www.cours-pharmacie.com/biologie-vegetale/les-parois-vegetales.html. June 26, 2017.
62. Rowell, R.M. et al., Paper and Composites from Agro-Based Resources. CRC Press, Inc, US (**1997**).
63. Salmén, L., Micromechanical understanding of the cell-wall structure. *Comptes Rendus Biologies* 327(9–10), p. 873-880 (**2004**).
64. Cousins, W.J., Young's modulus of hemicellulose as related to moisture content. *Wood Science and Technology* 12(3), p. 161-167 (**1978**).
65. Freudenberg, K., Biosynthesis and Constitution of Lignin. *Nature* 183(4669), p. 1152-1155 (**1959**).
66. Heitner, C. et al., Lignin and Lignans: Advances in Chemistry. CRC Press, Boca Raton, FL (**2010**).
67. Upton, B.M. et al., Strategies for the conversion of lignin to high-value polymeric materials: Review and perspective. *Chemical reviews* 116(4), p. 2275-2306 (**2015**).
68. Monties, B., *Biological variability of lignification and mechanical behaviour of woody plants*, in *International Conference of the European Society for Wood Mechanics*. 2004: Stockholm, SWE. p. 3-14.
69. Cousins, W.J. et al., Young's modulus of lignin from a continuous indentation test. *Journal of Materials Science* 10(10), p. 1655-1658 (**1975**).
70. Faruk, O. et al., 6 - Lignin Reinforcement in Thermoplastic Composites, in *Lignin in Polymer Composites*. William Andrew Publishing. (**2016**).
71. Al Mamun, A. et al., 8 - Lignin Reinforcement in Bioplastic Composites, in *Lignin in Polymer Composites*. William Andrew Publishing. (**2016**).
72. EL Bassam, N., Energy Plant Species: Their Use and Impact on Environment and Development. James & James (Science Publishers) Ltd. (**1998**).
73. Moon, Y.-H. et al., Development of "Miscanthus" the Promising Bioenergy Crop. *Korean Journal of Weed Science* 30(4), p. 330-339 (**2010**).
74. Murnen, H.K. et al., Optimization of Ammonia Fiber Expansion (AFEX) Pretreatment and Enzymatic Hydrolysis of Miscanthus x giganteus to Fermentable Sugars. *Biotechnology Progress* 23(4), p. 846-850 (**2007**).
75. Dohleman, F.G. et al., More Productive Than Maize in the Midwest: How Does Miscanthus Do It? *Plant Physiology* 150(4), p. 2104-2115 (**2009**).
76. Heaton, E.A. et al., Miscanthus. *Advances in Botanical Research* 56, p. 75-137 (**2010**).
77. Beale, C.V. et al., Can perennial C4 grasses attain high efficiencies of radiant energy conversion in cool climates? *Plant, Cell & Environment* 18(6), p. 641-650 (**1995**).
78. Botto, L. et al., Physical characterisation and yield stress of a concentrated Miscanthus suspension. *Rheologica Acta* 53(10), p. 805-815 (**2014**).
79. Heaton, E.A. et al., Meeting US biofuel goals with less land: the potential of Miscanthus. *Global Change Biology* 14(9), p. 2000-2014 (**2008**).
80. Fischer, G. et al., Biomass potentials of miscanthus, willow and poplar: results and policy implications for Eastern Europe, Northern and Central Asia. *Biomass and Bioenergy* 28(2), p. 119-132 (**2005**).
81. Dorge, S. et al., Thermal degradation of Miscanthus pellets: kinetics and aerosols characterization. *Waste and Biomass Valorization* 2(2), p. 149-155 (**2011**).
82. Michel, R. et al., Miscanthus × Giganteus straw and pellets as sustainable fuels and raw material for activated carbon. *Environmental Chemistry Letters* 4(4), p. 185-189 (**2006**).
83. De Jong, W., Prolysis of Miscanthus giganteus and wood pellets : TG-FITIR analysis and reaction kinetics. *Fuel* 82, p. 1139-1147 (**2003**).
84. Collura, S. et al., Thermal behaviour of Miscanthus grasses, an alternative biological fuel. *Environmental Chemistry Letters* 5(1), p. 49-49 (**2007**).

85. Collura, S. et al., Miscanthus giganteus straw and pellets as sustainable fuels combustion and emission tests. *Environmental Chemistry Letters* 4, p. 75-78 (**2006**).

86. Johnson, M. et al., Improvement of the impact performance of a starch based biopolymer via the incorporation of Miscanthus giganteus fibres. *Industrial Crops and Products* 22(3), p. 175-186 (**2005**).

87. Ly, A. et al., *Fibres de miscanthus et matériaux composites*, in *Cerig/Grenoble INP-Pagora*. 2015.

88. Available from: http://www.valbiom.be/files/library/Docs/Chanvre/etudecomparativedesapplicationsnonenergetiques duchanvreetdumiscanthus1302508542.pdf. June 26, 2017.

89. Zhang, K. et al., Co-Injection Molded New Green Composites from Biodegradable Polyesters and Miscanthus Fibers. *Macromolecular Materials and Engineering* 299(4), p. 436-446 (**2014**).

90. Kaack, K. et al., Morphological and mechanical properties of Miscanthus in relation to harvesting, lodging, and growth conditions. *Industrial Crops and Products* 14(2), p. 145-154 (**2001**).

91. Lundquist, L. et al., Alkali–methanol–anthraquinone pulping of Miscanthus x giganteus for thermoplastic composite reinforcement. *Journal of Applied Polymer Science* 92(4), p. 2132-2143 (**2004**).

92. Baley, C., Analysis of the flax fibres tensile behaviour and analysis of the tensile stiffness increase. *Composites Part A: Applied Science and Manufacturing* 33(7), p. 939-948 (**2002**).

93. Szabó, P. et al., Thermogravimetric/mass spectrometric characterization of two energy crops, Arundo donax and Miscanthus sinensis. *Journal of Analytical and Applied Pyrolysis* 36(2), p. 179-190 (**1996**).

94. Johnson, R.M. et al., Impact performance of Miscanthus/Novamont Mater-Bi® biocomposites. *Polymer Testing* 22(2), p. 209-215 (**2003**).

95. Chanprateep, S., Current trends in biodegradable polyhydroxyalkanoates. *Journal of Bioscience and Bioengineering* 110(6), p. 621-632 (**2010**).

96. Albertsson, A.-c. et al., Macromolecular Architecture-Nature as a Model for Degradable Polymers. *Journal of Macromolecular Science, Part A* 33(10), p. 1565-1570 (**1996**).

97. Research, Z., *Biodegradable Polymer (Polymers with Carbon Backbones, Polymers with Hydrolyzable Backbones, Natural Polymers) Market For Packaging, Agricultural, Medical and Other Applications: Global Industry Perspective, Comprehensive Analysis, Size, Share, Growth, Segment, Trends and Forecast 2014 – 2020*, p. 110 (**2016**).

98. Leja, K. et al., Polymer Biodegradation and Biodegradable Polymers – a Review *Polish Journal of Environmental Studies* 19(2), p. 255-266 (**2010**).

99. Doppalapudi, S. et al., Biodegradable polymers—an overview. *Polymers for Advanced Technologies* 25(5), p. 427-435 (**2014**).

100. Armentano, I. et al., Multifunctional nanostructured PLA materials for packaging and tissue engineering. *Progress in Polymer Science* 38(10), p. 1720-1747 (**2013**).

101. Sadegh-Hassani, F. et al., Preparation and characterization of bionanocomposite films based on potato starch/halloysite nanoclay. *International Journal of Biological Macromolecules* 67, p. 458-462 (**2014**).

102. Mensitieri, G. et al., Processing and shelf life issues of selected food packaging materials and structures from renewable resources. *Trends in Food Science & Technology* 22(2–3), p. 72-80 (**2011**).

103. Sarasini, F., 4 - Thermoplastic biopolymer matrices for biocomposites A2 - Ray, Dipa, in *Biocomposites for High-Performance Applications*. Woodhead Publishing. (**2017**).

104. Murariu, M. et al., PLA composites: From production to properties. *Advanced Drug Delivery Reviews* 107, p. 17-46 (**2016**).

105. Lim, L.T. et al., Processing technologies for poly(lactic acid). *Progress in Polymer Science* 33(8), p. 820-852 (**2008**).

106. Plackett, D. et al., Polylactide-based biocomposites, in *Natural fibers, biopolymers and biocomposites*, A.K. Mohanty, M. M., and L.T. Drzal, Editors. Boca Raton, FL: CRC Press. (**2005**).

107. Mukherjee, T. et al., PLA Based Biopolymer Reinforced with Natural Fibre: A Review. *Journal of Polymers and the Environment* 19(3), p. 714-725 (**2011**).

108. Plackett, D. et al., Natural polymer sources, in *Green composites: polymer composites and the environment*, C. Baillie, Editor. Woodhead Publishing Ltd and CRC Press LLC: Cambridge, UK. (**2004**).

109. Shen, L. et al., Present and future development in plastics from biomass. *Biofuels, Bioproducts and Biorefining* 4(1), p. 25-40 (**2010**).

110. Eshraghi, S. et al., Mechanical and microstructural properties of polycaprolactone scaffolds with one-dimensional, two-dimensional, and three-dimensional orthogonally oriented porous architectures produced by selective laser sintering. *Acta Biomaterialia* 6(7), p. 2467-2476 (**2010**).

111. Serrano, M.C. et al., In vitro biocompatibility assessment of poly(ε-caprolactone) films using L929 mouse fibroblasts. *Biomaterials* 25(25), p. 5603-5611 (**2004**).

112. Lahiri, D. et al., Boron nitride nanotube reinforced polylactide–polycaprolactone copolymer composite: Mechanical properties and cytocompatibility with osteoblasts and macrophages in vitro. *Acta Biomaterialia* 6(9), p. 3524-3533 (**2010**).

113. Choi, J.-i. et al., Process analysis and economic evaluation for Poly(3-hydroxybutyrate) production by fermentation. *Bioprocess Engineering* 17(6), p. 335-342 (**1997**).

114. Jacquel, N. et al., Solubility of polyhydroxyalkanoates by experiment and thermodynamic correlations. *AIChE Journal* 53(10), p. 2704-2714 (**2007**).

115. Yu, L. et al., Polymer blends and composites from renewable resources. *Progress in Polymer Science* 31(6), p. 576-602 (**2006**).

116. Satyanarayana, K.G. et al., Biodegradable composites based on lignocellulosic fibers—An overview. *Progress in Polymer Science* 34(9), p. 982-1021 (**2009**).

117. Arbelaiz, A. et al., Mechanical properties of short flax fibre bundle/poly(ε-caprolactone) composites: Influence of matrix modification and fibre content. *Carbohydrate Polymers* 64(2), p. 224-232 (**2006**).

118. Bhardwaj, R. et al., Renewable Resource-Based Green Composites from Recycled Cellulose Fiber and Poly(3-hydroxybutyrate-co-3-hydroxyvalerate) Bioplastic. *Biomacromolecules* 7(6), p. 2044-2051 (**2006**).

119. Bledzki, A. et al., Mechanical performance of biocomposites based on PLA and PHBV reinforced with natural fibres–A comparative study to PP. *Composites science and technology* 70(12), p. 1687-1696 (**2010**).

120. Oksman, K. et al., Natural fibres as reinforcement in polylactic acid (PLA) composites. *Composites Science and Technology* 63(9), p. 1317-1324 (**2003**).

121. Garlotta, D., A Literature Review of Poly(Lactic Acid). *Journal of Polymers and the Environment* 9(2), p. 63-84 (**2001**).

122. Rasal, R.M. et al., Poly(lactic acid) modifications. *Progress in Polymer Science* 35(3), p. 338-356 (**2010**).

123. Carothers, W.H. et al., Studies of polymerization and ring formation. X. The reversible polymerization of six-membered cyclic esters *Journal of the American Chemical Society* 54(2), p. 761-772 (**1932**).

124. Auras, R. et al., An Overview of Polylactides as Packaging Materials. *Macromolecular Bioscience* 4(9), p. 835-864 (**2004**).

125. Madhavan Nampoothiri, K. et al., An overview of the recent developments in polylactide (PLA) research. *Bioresource Technology* 101(22), p. 8493-8501 (**2010**).

126. Labet, M. et al., Synthesis of polycaprolactone: a review. *Chemical Society Reviews* 38, p. 3484–3504 (**2009**).

127. Stridsberg, K.M. et al., Controlled Ring-Opening Polymerization: Polymers with designed Macromolecular Architecture, in *Degradable Aliphatic Polyesters*. Springer Berlin Heidelberg: Berlin, Heidelberg. (**2002**).

128. Okada, M., Chemical syntheses of biodegradable polymers. *Progress in Polymer Science* 27(1), p. 87-133 (**2002**).

129. Seyednejad, H. et al., Functional aliphatic polyesters for biomedical and pharmaceutical applications. *Journal of Controlled Release* 152(1), p. 168-176 (**2011**).

130. Kobayashi, S., Enzymatic polymerization: A new method of polymer synthesis. *Journal of Polymer Science Part A: Polymer Chemistry* 37(16), p. 3041-3056 (**1999**).

131. MacDonald, R.T. et al., Enzyme-Catalyzed .epsilon.-Caprolactone Ring-Opening Polymerization. *Macromolecules* 28(1), p. 73-78 (**1995**).

132. Anjum, A. et al., Microbial production of polyhydroxyalkanoates (PHAs) and its copolymers: A review of recent advancements. *International Journal of Biological Macromolecules* 89, p. 161-174 (**2016**).

133. Slater, S. et al., Multiple β-ketothiolases mediate poly (β-hydroxyalkanoate) copolymer synthesis in Ralstonia eutropha. *Journal of bacteriology* 180(8), p. 1979-1987 (**1998**).

134. Urayama, H. et al., Microstructure and Thermal Properties of Polylactides with Different L- and D-Unit Sequences: Importance of the Helical Nature of the L-Sequenced Segments. *Macromolecular Materials and Engineering* 288(2), p. 137-143 (**2003**).

135. Tsuji, H. et al., Crystallization from the melt of poly(lactide)s with different optical purities and their blends. *Macromolecular Chemistry and Physics* 197(10), p. 3483-3499 (**1996**).

136. Södergård, A. et al., Properties of lactic acid based polymers and their correlation with composition. *Progress in Polymer Science* 27(6), p. 1123-1163 (**2002**).

137. Jacobsen, S. et al., Plasticizing polylactide—the effect of different plasticizers on the mechanical properties. *Polymer Engineering & Science* 39(7), p. 1303-1310 (**1999**).

138. Gupta, A.P. et al., New emerging trends in synthetic biodegradable polymers – Polylactide: A critique. *European Polymer Journal* 43(10), p. 4053-4074 (**2007**).

139. Perego, G. et al., Effect of molecular weight and crystallinity on poly(lactic acid) mechanical properties. *Journal of Applied Polymer Science* 59(1), p. 37-43 (**1996**).

140. Karakus, K., Polycaprolactone (PCL) based polymer composites filled wheat straw flour. *Kastamonu University Journal of Forestry Faculty* 16(1) (**2016**).

141. Koleske, J.V., Blends containing poly-caprolactone and related polymers, in *Polymer Blends*, D.R. Paul and S. Neuman, Editors. Academic Press New York. (**1978**).

142. Armani, D.K. et al., Microfabrication technology for polycaprolactone, a biodegradable polymer. *Journal of Micromechanics and Microengineering* 10, p. 80-84 (**2000**).

143. Sudesh, K. et al., Synthesis, structure and properties of polyhydroxyalkanoates: biological polyesters. *Progress in Polymer Science* 25(10), p. 1503-1555 (**2000**).

144. Anderson, A.J. et al., Occurrence, metabolism, metabolic role, and industrial uses of bacterial polyhydroxyalkanoates. *Microbiological Reviews* 54(4), p. 450-472 (**1990**).

145. Brandl, H. et al., Plastics from bacteria and for bacteria: Poly(β-hydroxyalkanoates) as natural, biocompatible, and biodegradable polyesters, in *Microbial Bioproducts*. Springer Berlin Heidelberg: Berlin, Heidelberg. (**1990**).

146. Asrar, J. et al., Biosynthesis and properties of poly (3-hydroxybutyrate-co-3-hydroxyhexanoate) polymers. *Biomacromolecules* 3(5), p. 1006-1012 (**2002**).

147. Doi, Y., Microbial polyesters. VCH, Weinheim (**1990**).

148. Lee, S.Y., Bacterial polyhydroxyalkanoates. *Biotechnology and Bioengineering* 49(1), p. 1-14 (**1996**).

149. Kai, W. et al., Fast crystallization of poly(3-hydroxybutyrate) and poly(3-hydroxybutyrate-co-3-hydroxyvalerate) with talc and boron nitride as nucleating agents. *Polymer International* 54(5), p. 780-789 (**2005**).

150. Bugnicourt, E. et al., The main Characteristics, Properties, Improvements, and Market Data of Polyhydroxyalkanoates, in *Handbook of Sustainable Polymers: Processing and Applications*, V.K. Thakur and M.K. Thakur, Editors. Pan Stanford Publishing Pte. Ltd. (**2016**).

151. El-Hadi, A. et al., Correlation between degree of crystallinity, morphology, glass temperature, mechanical properties and biodegradation of poly (3-hydroxyalkanoate) PHAs and their blends. *Polymer Testing* 21(6), p. 665-674 (**2002**).

152. Ikada, Y. et al., Biodegradable polyesters for medical and ecological applications. *Macromolecular Rapid Communications* 21(3), p. 117-132 (**2000**).

153. Luckachan, G.E. et al., Biodegradable Polymers- A Review on Recent Trends and Emerging Perspectives. *Journal of Polymers and the Environment* 19(3), p. 637-676 (**2011**).

154. Martin, R.T. et al., Marine-degradable polylactic acid. *Green Chemistry* 16(4), p. 1768-1773 (**2014**).

155. Celli, A. et al., Thermal properties and physical ageing of poly (l-lactic acid). *Polymer* 33(13), p. 2699-2703 (**1992**).

156. Middleton, J.C. et al., Synthetic biodegradable polymers as orthopedic devices. *Biomaterials* 21(23), p. 2335-2346 (**2000**).

157. Gross, R.A. et al., Biodegradable Polymers for the Environment. *Science* 297(5582), p. 803-807 (**2002**).

158. Zhu, Y. et al., Surface Modification of Polycaprolactone Membrane via Aminolysis and Biomacromolecule Immobilization for Promoting Cytocompatibility of Human Endothelial Cells. *Biomacromolecules* 3(6), p. 1312-1319 (**2002**).

159. Bosworth, L.A. et al., Physicochemical characterisation of degrading polycaprolactone scaffolds. *Polymer Degradation and Stability* 95(12), p. 2269-2276 (**2010**).

160. Lam, C.X.F. et al., Comparison of the degradation of polycaprolactone and polycaprolactone–(β-tricalcium phosphate) scaffolds in alkaline medium. *Polymer International* 56(6), p. 718-728 (**2007**).

161. Sinha, V.R. et al., Poly-ϵ-caprolactone microspheres and nanospheres: an overview. *International Journal of Pharmaceutics* 278(1), p. 1-23 (**2004**).

162. Pena, J. et al., Long term degradation of poly (ε-caprolactone) films in biologically related fluids. *Polymer Degradation and Stability* 91(7), p. 1424-1432 (**2006**).

163. Chen, D. et al., Polycaprolactone microparticles and their biodegradation. *Polymer Degradation and Stability* 67(3), p. 455-459 (**2000**).

164. Goldberg, D., A review of the biodegradability and utility of poly (caprolactone). *Journal of Polymers and the Environment* 3(2), p. 61-67 (**1995**).

165. Numata, K. et al., Biodegradability of poly (hydroxyalkanoate) materials. *Materials* 2(3), p. 1104-1126 (**2009**).

166. J Moskowitz, G. et al., Metabolism of Poly-β-hydroxybutyrate. II. Enzymatic Synthesis of D-(-)-β-Hydroxybutyryl Coenzyme A by an Enoyl Hydrase from Rhodospirillum rubrum.Vol. 8. (**1969**).

167. Hocking, P. et al., Poly(hydroxyalkanoates), in *Biopolymers from renewable resources*, D.L. Kaplan, Editor. Springer-Verlag Berlin Heidelberg. (**1998**).

168. Mergaert, J. et al., Microbial degradation of poly(3-hydroxybutyrate) and poly(3-hydroxybutyrate-co-3-hydroxyvalerate) in soils. *Applied and Environmental Microbiology* 59(10), p. 3233-3238 (**1993**).

169. Mergaert, J. et al., Biodiversity of microorganisms that degrade bacterial and synthetic polyesters. *Journal of Industrial Microbiology* 17(5), p. 463-469 (**1996**).

170. Doi, Y. et al., Biodegradation of microbial polyesters in the marine environment. *Polymer degradation and stability* 36(2), p. 173-177 (**1992**).

171. Volova, T. et al., Degradation of polyhydroxyalkanoates in eutrophic reservoir. *Polymer Degradation and Stability* 92(4), p. 580-586 (**2007**).

172. Volova, T. et al., Biodegradation of polyhydroxyalkanoates (PHAs) in the South China Sea and identification of PHA-degrading bacteria. *Microbiology* 80(2), p. 252-260 (**2011**).

173. Weng, Y.-X. et al., Biodegradation behavior of PHAs with different chemical structures under controlled composting conditions. *Polymer Testing* 30(4), p. 372-380 (**2011**).

174. Taubner, V. et al., Influence of processing parameters on the degradation of poly(L-lactide) during extrusion. *Journal of Applied Polymer Science* 79(12), p. 2128–2135 (**2001**).

175. Kopinke, F.D. et al., Thermal decomposition of biodegradable polyesters—II. Poly(lactic acid). *Polymer Degradation and Stability* 53(3), p. 329-342 (**1996**).

176. McNeill, I.C. et al., Degradation studies of some polyesters and polycarbonates—2. Polylactide: Degradation under isothermal conditions, thermal degradation mechanism and photolysis of the polymer. *Polymer Degradation and Stability* 11(4), p. 309-326 (**1985**).

177. Persenaire, O. et al., Mechanisms and kinetics of thermal degradation of poly(epsilon-caprolactone). *Biomacromolecules* 2(1), p. 288-294 (**2001**).

178. Aoyagi, Y. et al., Thermal degradation of poly[(R)-3-hydroxybutyrate], poly[ε-caprolactone], and poly[(S)-lactide]. *Polymer Degradation and Stability* 76(1), p. 53-59 (**2002**).

179. Joshi, P. et al., Degradation of polycaprolactone in supercritical fluids. *Polymer Degradation and Stability* 93(10), p. 1901-1908 (**2008**).

180. Doi, Y. et al., Biodegradation of Biosynthetic and Chemosynthetic Polyhydroxyalkanoates. *Studies in Polymer Science* 12, p. 39-51 (**1994**).

181. Grassie, N. et al., The thermal degradation of poly (-(D)-beta-hydroxybutyric acid): Part I-Identification and quantitative analysis of products. *Polymer Degradation and Stability* 6(1), p. 47-61 (**1984**).

182. Grassie, N. et al., The thermal degradation of poly (-(D)-beta-hydroxybutyric acid): Part II-Changes in molecular weight. *Polymer Degradation and Stability* 6(2), p. 95-103 (**1984**).

183. Mohanty, A.K. et al., Sustainable Bio-Composites from Renewable Resources: Opportunities and Challenges in the Green Materials World. *Journal of Polymers and the Environment* 10(1), p. 19-26 (**2002**).

184. Xiang, H. et al., Thermal depolymerization mechanisms of poly(3-hydroxybutyrate-co-3-hydroxyvalerate). *Progress in Natural Science: Materials International* 26(1), p. 58-64 (**2016**).

185. Le Troedec, M. et al., Influence of various chemical treatments on the composition and structure of hemp fibres. *Composites Part A: Applied Science and Manufacturing* 39(3), p. 514-522 (**2008**).

186. Sgriccia, N. et al., Characterization of natural fiber surfaces and natural fiber composites. *Composites Part A: Applied Science and Manufacturing* 39(10), p. 1632-1637 (**2008**).

187. Kalia, S. et al., Pretreatments of natural fibers and their application as reinforcing material in polymer composites—A review. *Polymer Engineering & Science* 49(7), p. 1253-1272 (**2009**).

188. John, M.J. et al., Effect of chemical modification on properties of hybrid fiber biocomposites. *Composites Part A: Applied Science and Manufacturing* 39(2), p. 352-363 (**2008**).

189. Ray, P.K. et al., Fine structure and mechanical properties of jute differently dried after retting. *Journal of Applied Polymer Science* 20(7), p. 1765-1767 (**1976**).

190. Da Cunha, C. et al., Synthesis and polymerization of lignin-based macromonomers. III. Radical copolymerization of lignin-based macromonomers with methyl methacrylate. *Journal of Applied Polymer Science* 48(5), p. 819-831 (**1993**).

191. Stamboulis, A. et al., Environmental Durability of Flax Fibres and their Composites based on Polypropylene Matrix. *Applied Composite Materials* 7(5), p. 273-294 (**2000**).

192. Yuan, X. et al., Effects of plasma treatment in enhancing the performance of woodfibre-polypropylene composites. *Composites Part A: Applied Science and Manufacturing* 35(12), p. 1363-1374 (**2004**).

193. Gouanvé, F. et al., Study of water sorption in modified flax fibers. *Journal of Applied Polymer Science* 101(6), p. 4281-4289 (**2006**).

194. Wong, K.K. et al., Topographical Study of Low Temperature Plasma Treated Flax Fibers. *Textile Research Journal* 70(10), p. 886-893 (**2000**).

195. Lee, S.G. et al., Characterization of surface modified flax fibers and their biocomposites with PHB. *Macromolecular Symposia* 197(1), p. 089-100 (**2003**).

196. Aziz, S.H. et al., The effect of alkalization and fibre alignment on the mechanical and thermal properties of kenaf and hemp bast fibre composites: Part 1 – polyester resin matrix. *Composites Science and Technology* 64(9), p. 1219-1230 (**2004**).

197. Rodriguez, E.S. et al., Effects of Fibers' Alkali Treatment on the Resin Transfer Molding Processing and Mechanical Properties of Jute—Vinylester Composites. *Journal of Composite Materials* 41(14), p. 1729-1741 (**2007**).

198. Dufresne, A., Nanocellulose: a new ageless bionanomaterial. *Materials Today* 16(6), p. 220-227 (**2013**).

199. Moon, R.J. et al., Cellulose nanomaterials review: structure, properties and nanocomposites. *Chemical Society Reviews* 40(7), p. 3941-3994 (**2011**).

200. Carlmark, A. et al., Grafting of cellulose by ring-opening polymerisation–A review. *European Polymer Journal* 48(10), p. 1646-1659 (**2012**).

201. Isogai, A. et al., TEMPO-oxidized cellulose nanofibers. *Nanoscale* 3(1), p. 71-85 (**2011**).

202. Park, S.-J. et al., Effect of Silane Coupling Agent on Interphase and Performance of Glass Fibers/Unsaturated Polyester Composites. *Journal of Colloid and Interface Science* 242(1), p. 174-179 (**2001**).

203. Hu, L. et al., Effect of coupling treatment on mechanical properties of bacterial cellulose nanofibre-reinforced UPR ecocomposites. *Materials Letters* 63(22), p. 1952-1954 (**2009**).

204. Valadez-Gonzalez, A. et al., Effect of fiber surface treatment on the fiber–matrix bond strength of natural fiber reinforced composites. *Composites Part B: Engineering* 30(3), p. 309-320 (**1999**).

205. Raj, R.G. et al., Effect of chemical treatment of fibers on the mechanical properties of polyethylene-wood fiber composites. *Journal of Adhesion Science and Technology* 3(1), p. 55-64 (**1989**).

206. Kokta, B.V. et al., Composites of Polyvinyl Chloride-Wood Fibers. I. Effect of Isocyanate as a Bonding Agent. *Polymer-Plastics Technology and Engineering* 29(1-2), p. 87-118 (**1990**).

207. Samain, X. et al., Grafting biodegradable polyesters onto cellulose. *Journal of Applied Polymer Science* 121(2), p. 1183-1192 (**2011**).

208. Canché-Escamilla, G. et al., Mechanical properties of acrylate-grafted henequen cellulose fibers and their application in composites. *Composites Part A: Applied Science and Manufacturing* 30(3), p. 349-359 (**1999**).

209. Gupta, K.C. et al., Graft Copolymerization of Ethyl Acrylate onto Cellulose Using Ceric Ammonium Nitrate as Initiator in Aqueous Medium. *Biomacromolecules* 3(5), p. 1087-1094 (**2002**).

210. Nayak, P.L. et al., Grafting vinyl monomers onto silk fibers. II. Graft copolymerization of methyl methacrylate onto silk by hexavalent chromium ion. *Journal of Applied Polymer Science* 23(5), p. 1345-1354 (**1979**).

211. Tingaut, P. et al., Highly efficient and straightforward functionalization of cellulose films with thiol-ene click chemistry. *Journal of Materials Chemistry* 21(40), p. 16066-16076 (**2011**).

212. Hoyle, C.E. et al., Thiol–Ene Click Chemistry. *Angewandte Chemie International Edition* 49(9), p. 1540-1573 (**2010**).

213. Tadmor, Z. et al., Principles of Polymer Processing 2nd Edition. John Wiley & Sons, Inc. (**2006**).

214. Sunny, A.T. et al., 1 - Recent advances in polymer processing: the state of the art, new challenges and opportunities, in *Advances in Polymer Processing*. Woodhead Publishing. (**2009**).

215. Utracki, L.A., Polymer Blends Handbook, ed. T.N. Kluwer Academic Publishers.Vol. 1. (**2002**).

216. Silviya, E.K. et al., 4 - Compounding and mixing of polymers, in *Advances in Polymer Processing*. Woodhead Publishing. (**2009**).

217. Guaita, M. et al., Fondamenti di scienza dei polimeri, ed. Pacini. (**2003**).

218. Sikora, J.W., 5 - Screw extrusion, in *Advances in Polymer Processing*. Woodhead Publishing. (**2009**).

219. JeziÓrska, R.M., 6 - Reactive extrusion of polymers, in *Advances in Polymer Processing*. Woodhead Publishing. (**2009**).

220. Bremner, T. et al., Peroxide modification of linear low-density polyethylene: A comparison of dialkyl peroxides. *Journal of Applied Polymer Science* 49(5), p. 785-798 (**1993**).

221. Rengarajan, R. et al., Solid phase graft copolymerization. I. Effect of initiator and catalyst. *Journal of Applied Polymer Science* 39(8), p. 1783-1791 (**1990**).

222. Ghahari, S.M. et al., Study on Functionalization of Isotactic PP with Maleic Anhydride in an Internal Mixer and a Twin-screw Extruder. *International Polymer Processing* 18(3), p. 285-290 (**2003**).

223. Ruggeri, G. et al., Some aspects of polypropylene functionalization by free radical reactions. *European Polymer Journal* 19(10), p. 863-866 (**1983**).

224. Bettini, S.H.P. et al., Grafting of maleic anhydride onto polypropylene by reactive processing. Part II. Effect of rotor speed and reaction time. *Journal of Applied Polymer Science* 74, p. 256-263 (**1999**).

225. Moad, G., The synthesis of polyolefin graft copolymers by reactive extrusion. *Progress in Polymer Science* 24(1), p. 81-142 (**1999**).

226. Jeziórska, R., Functionalization of Low Density Polyethylene with Ricinol-2-oxazoline Methyl Maleate in a Twin-screw Extruder. *International Polymer Processing* 22(2), p. 122-131 (**2007**).

227. Kaynak, C. et al., Open Mould Processes, in *Handbook of Composite Fabrication*, G. Akovali, Editor. Rapra Technology Ltd. (**2001**).

228. Available from: http://kids.britannica.com/students/assembly/view/53835 June 26, 2017.

229. Available from: http://injectionmoldingprocess.net/how-to-mold-polymer-clay. June 26, 2017.

230. Bajpai, P.K. et al., Development and characterization of PLA-based green composites: A review. *Journal of Thermoplastic Composite Materials* 27(1), p. 52-81 (**2014**).

231. Nishino, T. et al., Kenaf reinforced biodegradable composite. *Composites Science and Technology* 63(9), p. 1281-1286 (**2003**).

232. Plackett, D. et al., Biodegradable composites based on l-polylactide and jute fibres. *Composites Science and Technology* 63(9), p. 1287-1296 (**2003**).

233. Shibata, M. et al., Biocomposites Made from Short Abaca Fiber and Biodegradable Polyesters. *Macromolecular Materials and Engineering* 288(1), p. 35-43 (**2003**).

234. Awal, A. et al., Thermorheological and mechanical properties of cellulose reinforced PLA bio-composites. *Mechanics of Materials* 80, Part A, p. 87-95 (**2015**).

235. Csikós, Á. et al., Modification of interfacial adhesion with a functionalized polymer in PLA/wood composites. *European Polymer Journal* 68, p. 592-600 (**2015**).

236. Yu, T. et al., Preparation and properties of short natural fiber reinforced poly(lactic acid) composites. *Transactions of Nonferrous Metals Society of China* 19, p. s651-s655 (**2009**).

237. Hu, R. et al., Fabrication and mechanical properties of completely biodegradable hemp fiber reinforced polylactic acid composites. *Journal of Composite Materials* 41(13), p. 1655–1669 (**2007**).

238. Yu, T. et al., Effect of fiber surface-treatments on the properties of poly(lactic acid)/ramie composites. *Composites Part A: Applied Science and Manufacturing* 41(4), p. 499-505 (**2010**).

239. Gregorova, A. et al., Surface modification of spruce wood flour and effects on the dynamic fragility of PLA/wood composites. *Polymer Engineering & Science* 51(1), p. 143-150 (**2011**).

240.   Bax, B. et al., Impact and tensile properties of PLA/Cordenka and PLA/flax composites. *Composites Science and Technology* 68(7–8), p. 1601-1607 (**2008**).

241.   Graupner, N. et al., Natural and man-made cellulose fibre-reinforced poly(lactic acid) (PLA) composites: An overview about mechanical characteristics and application areas. *Composites Part A: Applied Science and Manufacturing* 40(6–7), p. 810-821 (**2009**).

242.   Song, F. et al., Biodegradable Soy Protein Isolate-Based Materials: A Review. *Biomacromolecules* 12(10), p. 3369-3380 (**2011**).

243.   Wu, C.-S. et al., Polycaprolactone-Based Green Renewable Ecocomposites Made from Rice Straw Fiber: Characterization and Assessment of Mechanical and Thermal Properties. *Industrial & Engineering Chemistry Research* 51(8), p. 3329-3337 (**2012**).

244.   Ruseckaite, R.A. et al., Thermal degradation of mixtures of polycaprolactone with cellulose derivatives. *Polymer Degradation and Stability* 81(2), p. 353-358 (**2003**).

245.   Van de Velde, K. et al., Biopolymers: overview of several properties and consequences on their applications. *Polymer Testing* 21(4), p. 433-442 (**2002**).

246.   Ludueña, L.N. et al., Processing and microstructure of PCL/clay nanocomposites. *Materials Science and Engineering: A* 460–461, p. 121-129 (**2007**).

247.   Swapna, J.C. et al., Optimum Blend of Chitosan and Poly-(ε-caprolactone) for Fabrication of Films for Food Packaging Applications. *Food and Bioprocess Technology* 4(7), p. 1179-1185 (**2011**).

248.   Villmow, T. et al., Influence of screw configuration, residence time, and specific mechanical energy in twin-screw extrusion of polycaprolactone/multi-walled carbon nanotube composites. *Composites Science and Technology* 70(14), p. 2045-2055 (**2010**).

249.   Marrakchi, Z. et al., Biocomposites based on polycaprolactone reinforced with alfa fibre mats. *Composites Part A: Applied Science and Manufacturing* 43(4), p. 742-747 (**2012**).

250.   Ludueña, L. et al., Effect of lignocellulosic filler type and content on the behavior of polycaprolactone based eco-composites for packaging applications. *Carbohydrate Polymers* 87(1), p. 411-421 (**2012**).

251.   Wu, C.-S., Preparation and characterizations of polycaprolactone/green coconut fiber composites. *Journal of Applied Polymer Science* 115(2), p. 948-956 (**2010**).

252.   Koenig, M.F. et al., Evaluation of crosslinked poly(caprolactone) as a biodegradable, hydrophobic coating. *Polymer Degradation and Stability* 45(1), p. 139-144 (**1994**).

253.   Yan, L. et al., Flax fibre and its composites – A review. *Composites Part B: Engineering* 56, p. 296-317 (**2014**).

254.   Singh, S. et al., Wood fiber reinforced bacterial bioplastic composites: Fabrication and performance evaluation. *Composites Science and Technology* 67(9), p. 1753-1763 (**2007**).

255.   Singh, S. et al., Renewable resource based biocomposites from natural fiber and polyhydroxybutyrate-co-valerate (PHBV) bioplastic. *Composites Part A: Applied Science and Manufacturing* 39(5), p. 875-886 (**2008**).

256.   Reinsch, V.E. et al., Crystallization of poly(hydroxybutrate-co-hydroxyvalerate) in wood fiber-reinforced composites. *Journal of Applied Polymer Science* 64(9), p. 1785-1796 (**1997**).

257.   Dufresne, A. et al., Lignocellulosic flour-reinforced poly(hydroxybutyrate-co-valerate) composites. *Journal of Applied Polymer Science* 87(8), p. 1302-1315 (**2003**).

258.   Luo, S. et al., Mechanical and thermal properties of environment-friendly "green" composites made from pineapple leaf fibers and poly(hydroxybutyrate-co-valerate) resin. *Polymer Composites* 20(3), p. 367-378 (**1999**).

259.   Gatenholm, P. et al., Cellulose-Polymer Composites with Improved Properties, in *Advances in New Materials*, J.C. Salamone and J.S. Riffle, Editors. Springer US: Boston, MA. (**1992**).

260.   Buzarovska, A. et al., Crystallization behavior of poly(hydroxybytyrate-co-valerate) in model and bulk PHBV/kenaf fiber composites. *Journal of Materials Science* 42(16), p. 6501-6509 (**2007**).

261.   Zini, E. et al., Bio-composite of bacterial poly(3-hydroxybutyrate-co-3-hydroxyhexanoate) reinforced with vegetable fibers. *Composites Science and Technology* 67(10), p. 2085-2094 (**2007**).

262.   Avella, M. et al., Poly(3-hydroxybutyrate-co-3-hydroxyvalerate) and wheat straw fibre composites: thermal, mechanical properties and biodegradation behaviour. *Journal of Materials Science* 35(4), p. 829-836 (**2000**).

263.   Luo, S. et al., Interfacial and mechanical properties of environment-friendly "green" composites made from pineapple fibers and poly(hydroxybutyrate-co-valerate) resin. *Journal of Materials Science* 34(15), p. 3709-3719 (**1999**).

264. Gatenholm, P. et al., Biodegradable natural composites. I. Processing and properties. *Journal of Applied Polymer Science* 45(9), p. 1667-1677 (**1992**).

265. Gatenholm, P. et al., Biodegradable natural composites. II. Synergistic effects of processing cellulose with PHB. *Journal of Applied Polymer Science* 51(7), p. 1231-1237 (**1994**).

266. Ahankari, S.S. et al., Mechanical behaviour of agro-residue reinforced poly(3-hydroxybutyrate-co-3-hydroxyvalerate), (PHBV) green composites: A comparison with traditional polypropylene composites. *Composites Science and Technology* 71(5), p. 653-657 (**2011**).

267. Nemat Nasser, S. et al., Micromechanics: overall properties of heterogeneous materials. Second ed.: North Holland (**1999**).

268. Kanit, T. et al., Determination of the size of the representative volume element for random composites: statistical and numerical approach. *International Journal of Solids and Structures* 40(13), p. 3647-3679 (**2003**).

269. Aboudi, J. et al., Chapter 7 - Multiscale Modeling of Composites, in *Micromechanics of Composite Materials*. Butterworth-Heinemann: Oxford. (**2013**).

270. Vasiliev, V.V. et al., Mechanics and Analysis of Composite Materials Elservier Science Ltd (**2001**).

271. Kollar, L.P. et al., Micromechanics, in *Mechanics of composites structures* Cambridge University Press (**2003**).

272. Hashin, Z., The Elastic Moduli of Heterogeneous Materials. *Journal of Applied Mechanics* 29(1), p. 143-150 (**1962**).

273. Hill, R., Elastic properties of reinforced solids: Some theoretical principles. *Journal of the Mechanics and Physics of Solids* 11(5), p. 357-372 (**1963**).

274. Dvorak, G., Micromechanics of Composite Materials. First ed. Solid Mechanics and Its Applications. Springer Netherlands (**2013**).

275. Eshelby, J.D., The Determination of the Elastic Field of an Ellipsoidal Inclusion, and Related Problems. *Proceedings of the Royal Society of London. Series A. Mathematical and Physical Sciences* 241(1226), p. 376 (**1957**).

276. Jun, T.-S. et al., Evaluation of residual stresses and strains using the Eigenstrain Reconstruction Method. *International Journal of Solids and Structures* 47(13), p. 1678-1686 (**2010**).

277. Mura, T., General theory of eigenstrains, in *Micromechanics of defects in solids*. Springer Netherlands: Dordrecht. (**1987**).

278. Tucker Iii, C.L. et al., Stiffness predictions for unidirectional short-fiber composites: Review and evaluation. *Composites Science and Technology* 59(5), p. 655-671 (**1999**).

279. Aboudi, J. et al., Chapter 1 - Introduction, in *Micromechanics of Composite Materials*. Butterworth-Heinemann: Oxford. (**2013**).

280. Houshyar, S. et al., Modelling of polypropylene fibre-matrix composites using finite element analysis *Express Polymer Letters* 3(1), p. 2-12 (**2009**).

281. Houshyar, S. et al., The effect of fiber concentration on mechanical and thermal properties of fiber-reinforced polypropylene composites. *Journal of Applied Polymer Science* 96(6), p. 2260-2272 (**2005**).

282. Kalaprasad, G. et al., Theoretical modelling of tensile properties of short sisal fibre-reinforced low-density polyethylene composites. *Journal of Materials Science* 32(16), p. 4261-4267 (**1997**).

283. Facca, A.G. et al., Predicting the elastic modulus of natural fibre reinforced thermoplastics. *Composites Part A: Applied Science and Manufacturing* 37(10), p. 1660-1671 (**2006**).

284. Affdl, J.C.H. et al., The Halpin-Tsai equations: A review. *Polymer Engineering & Science* 16(5), p. 344-352 (**1976**).

285. Kumar, C.R. et al., Morphology and mechanical properties of thermoplastic elastomers from nylon-nitrile rubber blends. *Journal of Applied Polymer Science* 61(13), p. 2383-2396 (**1996**).

286. Pal, B. et al., Analytical Estimation of Elastic Properties of Polypropylene Fiber Matrix Composite by Finite Element Analysis. *Advances in Materials Physics and Chemistry* 2(1), p. 23-30 (**2012**).

287. Mori, T. et al., Average stress in matrix and average elastic energy of materials with misfitting inclusions. *Acta Metallurgica* 21(5), p. 571-574 (**1973**).

288. Benveniste, Y., A new approach to the application of Mori-Tanaka's theory in composite materials. *Mechanics of Materials* 6(2), p. 147-157 (**1987**).

289. Liu, L. et al., A Note on mori-tanaka's method. *Acta Mechanica Solida Sinica* 27(3), p. 234-244 (**2014**).

290. Sansalone, V. et al., Determination of the heterogeneous anisotropic elastic properties of human femoral bone: from nanoscopic to organ scale. *Journal of Biomechanics* 43(10), p. 1857-1863 (**2010**).

291. Hashin, Z. et al., The Elastic Moduli of Fiber-Reinforced Materials. *Journal of Applied Mechanics* 31(2), p. 223-232 (**1964**).

292. Lielens, G. et al., Prediction of thermo-mechanical properties for compression moulded composites. *Composites Part A: Applied Science and Manufacturing* 29(1), p. 63-70 (**1998**).

293. Laws, N. et al., The effect of fibre length on the overall moduli of composite materials. *Journal of the Mechanics and Physics of Solids* 27(1), p. 1-13 (**1979**).

294. Chou, T.-W. et al., A Self-Consistent Approach to the Elastic Stiffness of Short-Fiber Composites. *Journal of Composite Materials* 14(3), p. 178-188 (**1980**).

295. You, Y.H. et al., Adaptive meshing for finite element analysis of heterogeneous materials. *Computer-Aided Design* 62, p. 176-189 (**2015**).

296. Arns, C.H. et al., Computation of linear elastic properties from microtomographic images: Methodology and agreement between theory and experiment. *Geophysics* 67(5), p. 1396 (**2002**).

297. Alemdar, A. et al., Determination of Fiber Size Distributions of Injection Moulded Polypropylene/Natural Fibers Using X-ray Microtomography. *Advanced Engineering Materials* 10(1-2), p. 126-130 (**2008**).

Chapter II

"Science is but a perversion of itself
unless it has as its ultimate goal
the betterment of humanity"

(Nikola Tesla)

FUNCTIONALIZATION OF MISCANTHUS BY PHOTO-ACTIVATED THIOL-ENE ADDITION TO IMPROVE INTERFACIAL ADHESION WITH POLYCAPROLACTONE

In this chapter totally green biocomposites were realized using poly(ε-caprolactone) (PCL) as matrix, thanks to its biodegradable character and its good elasticity and Miscanthus giganteus (MIS) fibers as reinforcement. The main goal of this work was to find a totally green chemical treatment of fibers able to improve the adhesion matrix/reinforcement. To this aim, a fast thiol-ene reaction between the unsaturated groups of the Miscanthus fibers and poly(mercaptopropyl)methylsiloxane (PMMS) activated by a photo-initiator was adopted in order to improve the interfacial bonding matrix/fibers. To this aim PCL-based biocomposites with 20 % by weight of raw, coated and grafted MIS fibers were realized by a lab-scale extruder and injector molding in the presence of benzoyle peroxide (BPO) as radical initiator for the in-situ grafting reaction. Specimens realized were then characterized by tensile tests (Figure II-1) and the evidence of the grafting was studied by energy-dispersive X-ray (EDX), X-ray photoelectron spectrometry (XPS) and FTIR-ATR spectroscopy. PCL grafting was found to have a significant influence on the mechanical properties of biocomposites with an important increase in final strength, revealing that this in situ reactive extrusion grafting offers not only an effective approach to functionalize MIS fibers but it constitutes also an attractive solution suitable for any type of polyesters used.
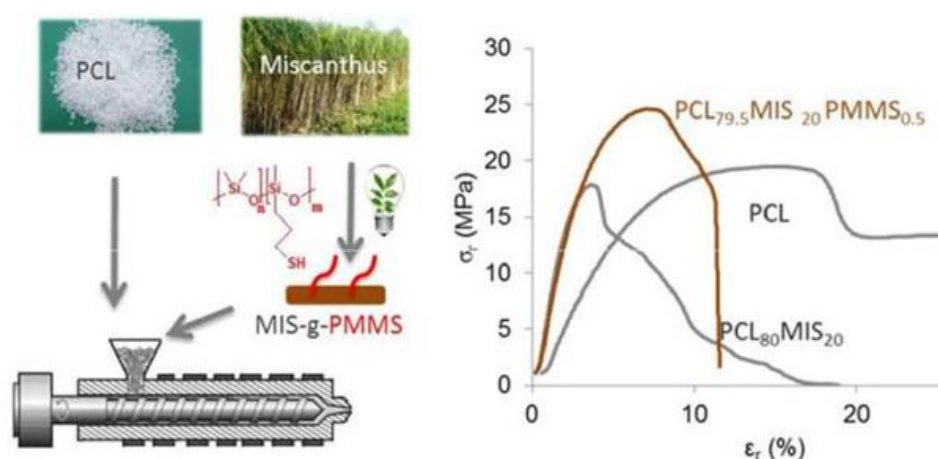
Figure II-1. Realization and mechanical characterization of PCL/MIS biocomposites.

II-1. INTRODUCTION

Growing environmental consciousness and changes in public legislations have led to an important demand for environmental eco-friendly materials, especially for bio-composites resulting from the combination of vegetal fibers and biodegradable and/or bio-based polyesters [1-12]. Low cost, low density and biodegradability are some of the main reasons that lead to use these fibers as a promising substitute for reinforcing polyesters. Among the different vegetable fibers, Miscanthus (Miscanthus *giganteus*) present some valuable advantages concerning simple cultivation and harvesting [13, 14]. Biocomposites based on hydrophilic natural fibers and hydrophobic polyesters present an important drawback due to the low adhesion between the two components.

Different methods have already been developed to improve interfacial adhesion, by using coupling agents [12, 15, 16], phenols [17], silane [18], modifications of fibers [19-22], plasticizers [23], chemical modifications of polyesters [20, 24, 25] or graft polymerization of polyesters on cellulose [26-28]. In all cases, the chemical modifications of fibers are only based on the reactivity of the hydroxyl groups of the cellulose structure. In this context, we proposed an innovating approach to improve adhesion between fibers and poly(ε-caprolactone), a biodegradable polyester, by using the reactivity of the unsaturated groups of the lignin. Lignin contains a number of double bonds as stilbene groups, cinnamyl, cinnamaldehyde groups [29-33].

We reported here a novel route to functionalize Miscanthus fibers *via* a fast photo-activated thiol-ene addition of a derivative of silicone, the poly(mercaptopropyl)methylsiloxane, PMMS, onto the unsaturated bonds of the Miscanthus fibers, MIS-g-PMMS (table II-1). As the content of stilbene units in the lignin of the Miscanthus is low, it is necessary to use a polymer containing an important ratio of thiol groups to enhance the efficiency of the thiol-ene reaction. Moreover, silicones are extensively used in different applications because of their thermal and oxidative stability, flexibility and moldability. Among the different derivatives of silicones, poly(mercaptopropyl) methylsiloxane (PMMS) with multifunctional thiol pendant groups is suitable for the thiol-ene reaction [34, 35]. Because of its efficiency and simplicity, the thiol-ene method appears to be an ideal reaction for quantitative functionalization of the Miscanthus.

Biocomposites were then prepared by blending MIS coated with PMMS (scheme II-1, A) or MIS grafted with PMMS (scheme II-1, B) with PCL as matrix. This study is expected to provide information to support the development and application of cost-effective and eco-friendly bio-composites through a comprehensive evaluation and understanding of their chemical and mechanical

characteristics. This work aims at demonstrating that the functionalization of fibers promotes an increase in toughness without significant loss in modulus and thermal properties.
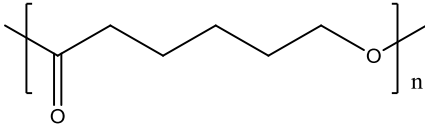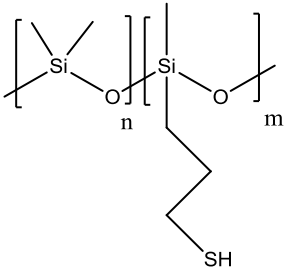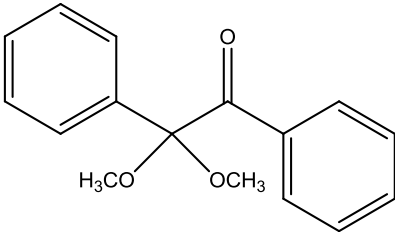
Compound	Structure
Poly(ε-caprolactone) (PCL)	
Poly(mercaptopropyl)methylsiloxane (PMMS)	
2,2-Dimethoxy-1,2-diphenylethan-1-one (DMPA)	

Table II-1. Structure of the polymer, the grafting agent and photo-initiator used in this study.

II-2. EXPERIMENTAL

II-2.1. MATERIALS

The PCL (Capa6400, molar mass $M_w = 37000$ g*mol^{-1}) was purchased from Solvay Caprolactones, Solvay Interox Ltd. in granular form. Miscanthus *giganteus* was provided from Miscanplus (France). It came from a 2014 spring crop roughly chopped and subsequently milled to obtain fibers about 1 mm long. Poly(mercaptopropyl)methylsiloxane (PMMS) was purchased from abcr GmbH & Co. (Germany). Benzoyl peroxide (BPO) and 2,2-Dimethoxy-1,2-diphenylethan-1-one (DMPA) were provided from Acros Organics and BASF company respectively.

II-2.2. PMMS GRAFTING ONTO MISCANTHUS GIGANTEUS FIBERS

The Miscanthus *giganteus* powder was treated with two different methods in order to obtain fibers coated with PMMS. In the first method (scheme II-1, A) the fibers were impregnated for 1 hour in a PMMS solution (200 g/l or 40 g/l in chloroform). The fibers were then filtered. In the second method (scheme II-1, B) the fibers were impregnated in a PMMS solution diluted in chloroform (40 g/l) containing 0.76 g of DMPA followed by a photo-grafting step. Fibers were filtrated and then irradiated for 5 minutes at room temperature with a Hamamatsu Lightning LC8 (L8251) instrument. This lamp was equipped with a mercury-xenon lamp (200 W) coupled with a flexible light guide. The end of the guide has been placed at 11 cm from the sample, which corresponds to a maximum UV light intensity of 180 mW cm^{-2} and 250-450 nm. This intensity was measured by radiometry (International Light Technologies ILT 393). After photo-grafting, the collected fibers were extracted 3 times in dichloromethane at 50 °C under pressure in order to remove the non-grafted PMMS.
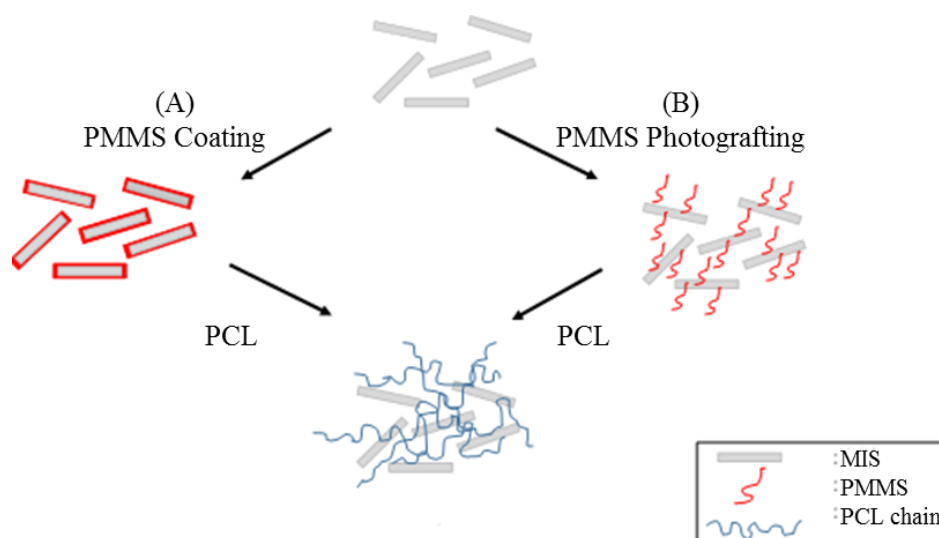
Scheme II-1. Different methods to elaborate PCL$_x$MIS$_y$ composites by using PMMS coating (A) or PMMS photo-grafting (B).

II-2.3. COMPOSITES MANUFACTURING, PCL$_x$MIS$_Y$

Before the realization of PCL-based composites with improved interface between fibers and matrix, an optimization procedure was carried out in order to find the optimum ratio fibers/matrix and the best processing parameters. To this aim, biocomposites with 0, 5, 10 and 20 wt % of fibers were realized changing processing parameters (table II-A1 and II-A2 in appendix II-A). The results of this procedure suggested to retain 20 wt % as the good content of fibers for the realization of biocomposites with modified fibers. Once found the good composition and processing parameters, PCL and modified MIS were mixed together in a lab-scale twin-screw extruder (Minilab Thermo Scientific Haake) with or without the thermal initiator BPO (5%). The experiments were performed at 140°C (T$_E$) with a screw speeds of 60 rpm. The retention time for the pure matrix was of 1 minute; this time was increased to 2 minutes in order to well disperse fibers into matrix. After recirculation, the extruded molten material was transferred by means of a preheated piston-cylinder assembly and was shot in the micro-injection unit (MiniJet Thermo Scientific Haake) at a certain injection pressure (P$_I$) for 30 seconds. A maintenance pressure (P$_M$), lower than that during the phase of injection, was applied for other 30 seconds. All composites were realized with a weight ratio 80/20 between matrix and fibers and the amount of BPO was fixed at 5 % of the total mass.

II-2.4. ANALYTICAL TECHNIQUES

The mechanical properties of the PCL/MIS composites were studied using an Instron 5965 Universal Testing Machine equipped of a cell load of 2kN.

All specimens with standard dimensions according to ASTM638 were tested at a crosshead displacement rate of 50 mm/min at room temperature (23°C). The FTIR spectra of the Miscanthus fibers were recorded using a Bruker Tensor 27 spectrometer equipped with an attenuated internal reflection accessory using a diamond crystal. Infrared spectra were collected with an accumulation of 32 scans. The morphological appearance of tensile fractured surfaces of specimens was investigated using a Merlin Zeiss scanning electron microscopy. Images were recorded with an acceleration voltage of 5keV. Prior to analyses, the samples were sputter-coated with a nanometric layer of Pt/Pd in a Cressington 208 HR sputter-coater. The thickness of the metallic layer was monitored by a MTM-20 Cressington quartz balance. Thermogravimetric analyses were carried out using a Setaram Setsys Evolution 16 thermobalance. A total of 10 mg of composites and Miscanthus samples were heated from the ambient temperature to 600°C at a heating rate of $10°C \ min^{-1}$ in air flow. Structural characterizations of Miscanthus powder and PCL/MIS composites were determined by X-Ray diffraction (XRD) using a D8 advance Bruker diffractometer operating at 30kV and 40 mA with a CuKα radiation. The crystallinity of composites was determined as the ratio of the areas of crystalline reflections to the whole area in the range $2\theta \approx 10\text{-}50°$. The X-ray photoelectron spectra were recorded using a Thermo Fischer K-alpha spectrometer with a monochromatic Al Kα X-ray source as the X-Ray source. XPS spectra were obtained with an energy step of 0.05 eV with a dwell time of 200 ms. Data acquisition mainly focused on the C1s, O1s, N1s, S2p and Si2p core level lines. The elemental composition and element chemical bonding were deduced from peaks shapes. Analysis of the elements was carried out by EDX analysis using an OXFORD INCA 300 system. To determine their distribution, Smart Map acquisition was used. Smart Map performs the simultaneous acquisition of X-ray data from each pixel on the image area.

II-3. RESULTS AND DISCUSSION

II-3.1. PMMS PHOTO-GRAFTING ON THE MISCANTHUS FIBERS

In most of the studies dealing with chemical modifications of fibers, hydroxyl groups have been used as reactive groups for grafting monomers or polymers. The originality of this method is to graft poly(mercaptopropyl)methylsiloxane (PMMS) onto the MIS, by using unsaturated groups present on the stilbene units of the lignin in the presence of DMPA, a photo-initiator. As the content of stilbene units is low, we used a polymer containing an important ratio of thiol groups to enhance the efficiency of the reactions. First, to confirm the reactivity of the double bonds of the lignin, a solution of dibromine was added to the MIS. The discoloration of the orange-yellow bromine solution indicates that the unsaturated groups of MIS have reacted with Br_2. As a further demonstration, the EDX spectrum (figure II-2) exhibited a well-defined peak for Br atoms at 105 keV, proving that bromide is covalently linked onto the MIS. This initial result indicated effectiveness of the reactivity of double bonds at the MIS surface.

PMMS was then grafted under photo-activation in presence of DMPA onto the MIS. In order to testify the occurrence of PMMS grafting onto MIS, extraction with dichloromethane as solvent was carried out. As shown in figure II-3, PMMS presents absorbance peaks at 760, 1000-1100, 1258 and 2540 cm^{-1} corresponding respectively to the Si-CH$_3$ symmetric deformation, Si-O-Si asymmetric stretching, Si-CH$_3$ stretching vibration and SH groups. The presence of the peaks at 760 and 1258 cm^{-1} on the MIS-g-PMMS spectrum confirms that PMMS has been successfully grafted to MIS. The ratio R_1 between the peak at 1258 cm^{-1} relative to Si-CH$_3$ bond of PMMS and the peak at 1037 cm^{-1} relative to the C-O bond of cellulose present in the Miscanthus was evaluated (see table II-2) and correlated with the weight gain after the PMMS grafting. The content of PMMS reached to 20 wt % when the PMMS concentration is 200 g/mol compared to only 5 wt % when the concentration of PMMS is about 40 g/mol. The PMMS that was just adsorbed on the MIS surface, was eliminated after extraction with dichloromethane. Consequently, the ratio R_1 decreased from 0.48 to 0.20. By a gravimetric analysis it was more difficult to evaluate the presence of PMMS, inferior to 1 %. Although the content of PMMS is not measurable by gravimetric analysis after extraction, it is possible to show the presence of PMMS by FTIR-ATR that is a more sensitive method.

XPS analyses were performed in order to gain more insight into the chemical functionalization on the MIS surface (see figure II-4). Before XPS analysis, three extractions with dichloromethane as solvent were carried out to eliminate the adsorbed PMMS that is not covalently grafted. The XPS

spectrum of the Miscanthus shows the presence of carbon at 284.6eV, oxygen at 533 eV and nitrogen at 396.91 eV [36, 37]. The peaks occuring at 163 and 103 eV, that were not present in native MIS, are characteristic of the presence of S(2p) and Si(2p) atoms on the grafted MIS surfaces. The thermogravimetric analysis (TGA) results are presented in figure II-5. They are in agreement with literature results for Miscanthus [38] with a mass loss between 250 and 350 °C. The temperatures of the maximum mass loss rate for hemicellulose (25 wt %) cellulose (34 wt %), and lignin (36 wt %) are respectively 275, 342 and 380 °C. We can observe that PMMS grafting onto MIS does not affect the thermal stability of MIS fibers.
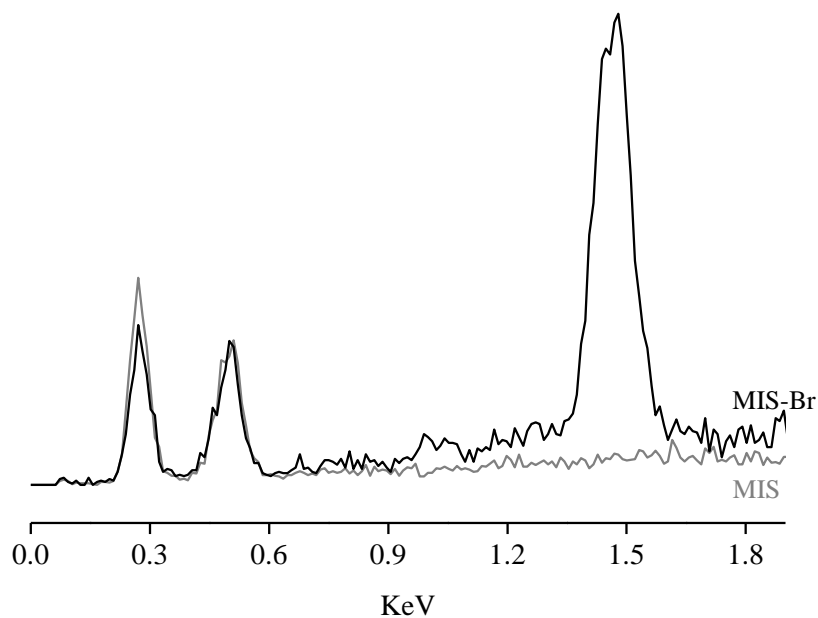
Figure II-2. EDX spectra of MIS and MIS-Br.
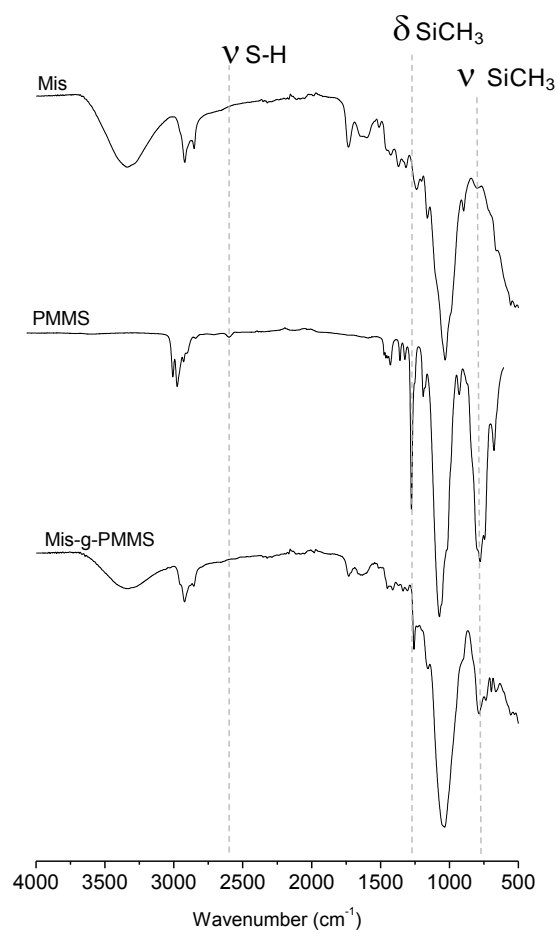
Figure II-3. FTIR-ATR spectra of MIS, PMMS and MIS-g-PMMS.

Compound	[PMMS] [$g*L^{-1}$]	t [h]	R_1[a]	MIS [b] [wt %]
MIS-g-PMMS [c]	40	4	0.32 ± 0.01	5
MIS-g-PMMS [c]	200	4	0.48 ± 0.01	20
MIS-g-PMMS [d]	200	4	0.20 ± 0.01	≤ 1

[a] Determined by FTIR-ATR : $R_1 = I_{1258cm^{-1}}/I_{1037cm^{-1}}$

[b] Determined by gravimetric analysis

[c] Before extraction with CH_2Cl_2

[d] After extraction with CH_2Cl_2

Table II-2. PMMS grafting on MIS determined by gravimetric and FTIR-ATR analyses.
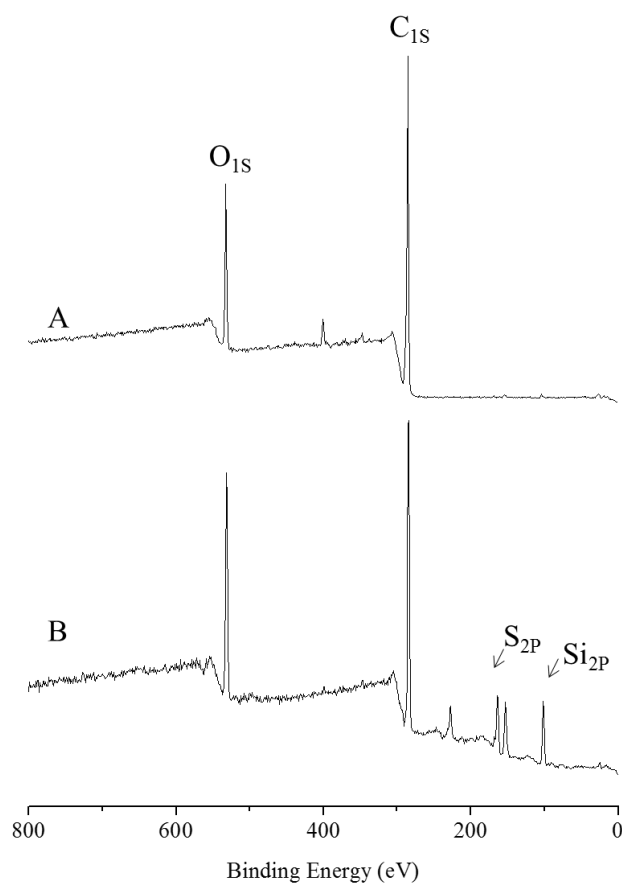
Figure II-4. XPS survey spectra of A) MIS and B) MIS-g-PMMS.
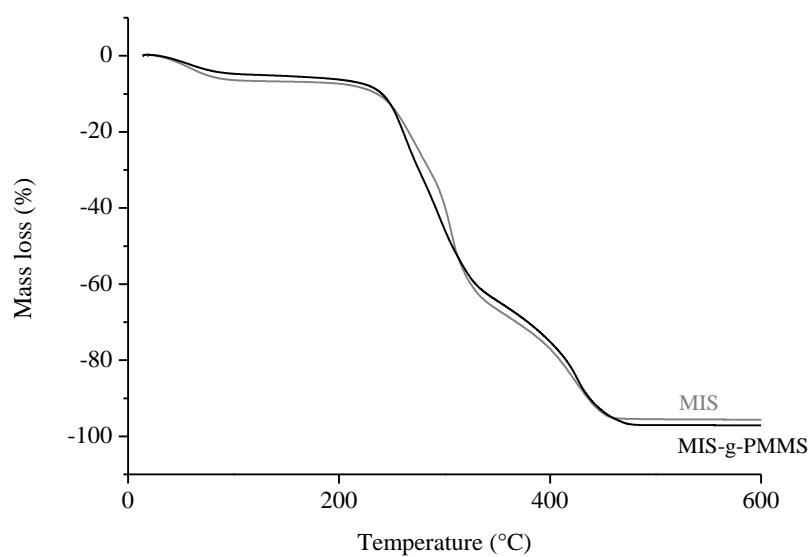
Figure II-5. TGA analysis of MIS and MIS-g-PMMS.

II-3.2. PREPARATION OF BIOCOMPOSITES, PCL$_x$MIS$_Y$

Two methods were developed to prepared biocomposites. The first one, (scheme II-1, way **A**) consists to use MIS coated by PMMS. Then, PCL and MIS were mixed together in a lab-scale twin-screw extruder with or without BPO. The percentage of radical initiator (5 wt %) is a typical concentration used for grafting reactions in the case of biocomposites manufacturing [39]. This latter, considered as a thermal initiator, is responsible for the formation of reactive radicals through its decomposition at high temperature. In the second method, (scheme II-1, way **B**) PCL was mixed with the MIS-g-PMMS. Subsequently, three extractions in dichloromethane were carried out on the biocomposites obtained in order to remove the PCL that was not grafted on MIS. The extracted MIS were then studied by FTIR. This analysis was performed in order to verify if PCL can be efficiently grafted using coated or grafted MIS.

The ratio R_2 between the peak at 1740 cm^{-1} relative to symmetric stretching of carbonyl group of PCL and MIS was evaluated (see table II-3). PCL was covalently grafted onto MIS in all cases thanks to the presence of BPO during the extrusion process. When the peroxide is heated during extrusion it decomposes in free radicals that present the ability to abstract a hydrogen from the polymer and MIS. The radicals initiate the reaction between the two phases present in the composites as it was previously mentioned in the case of PHB/cellulose biocomposites [40]. We notice here that when PCL is mixed with raw fibers in the absence of BPO initiator, the resulting spectrum of the extracted fibers shows a zero value for the ratio R_2, while in the presence of BPO this ratio increases demonstrating the presence of polymer on the surface fibers due to the grafting reaction. Moreover the presence of PMMS influences the final value for this ratio. The best result in term of R_2 is obtained when MIS was only coated by PMMS. This can be explained by the presence of more SH groups than in the case of a MIS previously grafted with PMMS.

Sample	Type of MIS	Method	BPO [wt %]	R_2
PCL$_{80}$MIS$_{20}$	raw	Blend	-	0
PCL$_{78}$MIS$_{19.8}$PMMS$_{2.2}$	coated	A	5	3.6
PCL$_{79.5}$ MIS$_{20}$PMMS$_{0.5}$	grafted	B	5	2.2

Table II-3. Comparison between R_2 values determined by FTIR-ATR analysis.

II-3.3. CHARACTERIZATION OF BIOCOMPOSITES

Mechanical results of loading-unloading tests (See table II-A3 in appendix II-A) showed that at 20 wt % of raw fibers there is a sensible increase in Young Modulus, demonstrating that fibers act as reinforcement for the PCL and that 20 wt % seems to be the good composition to achieve high mechanical properties of the final composites. However, these biocomposites showed a decrease in final strength when fibers were not treated by a chemical agent (figure II-A1 in appendix II-A).

The focus of this work was to understand the mechanical behavior of biocomposites when PMMS and BPO were used together to improve the interface bond between the fibers and the matrix. To this aim, five different biocomposites (labeled **1** to **5** in table II-4) were elaborated with 20 wt % of MIS using the two ways previously described. PCL exhibited an initial linear behavior followed by a nonlinear part indicating the occurrence of plastic deformation. The insertion of 20 wt % MIS in the pure matrix produces a marked change on the curve, reducing the nonlinear part (Figure II-6). These effects are largely described in previous works [6, 20, 41-43]. Comparing PCL and $PCL_{80}MIS_{20}$ we observed an increase of the modulus from 322 MPa to 819 MPa but at the same time a decrease in tensile strength from 26 to 13 MPa. MIS acts as reinforcement for the matrix, making it more rigid. This effect is revealed by the difference between the initial slopes of the PCL curve and that of composites materials, the latter being more important. At the same time, the final strength decrease from 26 to 13 MPa because of the low interfacial adhesion between fiber and matrix. This last is a very common phenomenon in composites materials reinforced with natural fibers in which the insertion of a lot of interfaces in an homogeneous matrix make the transmission of the stress during the traction test less efficient [6, 41, 42]. This problem can be solved using a coupling agent in order to have stronger and stiffer materials [43].

In the case of samples **2** and **4,** the presence of BPO played an important role on the final strength of these materials, respectively 26 and 20 MPa. This increase of tensile strength revealed the good adhesion between the fibers and the matrix due to chemical radical reactions between the PMMS and the PCL. This reaction takes place in the extruder by mixing MIS coated or grafted with PMMS and PCL. Composite **2** shows the highest tensile strength (σ_r, no loss with respect to PCL) and fracture strain (ε_r) but also the smallest Young modulus (E) among all the composites. Sample **5** shows the highest Young modulus but also the lowest tensile strength and fracture strain. Sample **4** shows quite high values for all these mechanical properties.

In order to quantitatively compare the composites, a *global mechanical performance index* was defined as: $\eta_{comp} = \omega_E \times E_{comp}/E_{PCL} + \omega_\varepsilon \times \varepsilon_{r,comp}/\varepsilon_{r,PCL} + \omega_\sigma \times \sigma_{r,comp}/\sigma_{r,PCL}$. The global mechanical performance index is a novel concept to drive material and process selection. It allows combining and comparing mechanical parameters which may not have the same physical units or meaning in material and process selection. This index measures the total gain in mechanical performance of the composite with respect to the PCL. Coefficients ω are weights which should be set according to the significance of each mechanical parameter with respect to a specific application. In this paper, no specific application is targeted and all the weights were set to the same value (one third). Overall, the best mechanical performances are obtained when the PMMS is photo-grafted on MIS before the extrusion process (sample **4**) attesting the fact that only 0.5 wt % PMMS are sufficient to assure a good adhesion between matrix and fibers because this polymer contains a large proportion of SH groups able to interact with natural fibers. Moreover, the highest values of η are obtained when BPO is used (samples **4** and **2**) revealing the relevance of this thermal initiator.

We noticed that the most important effect of chemical modification is visible on the tensile strength. In the absence of a compatibilizing agent (sample **1**), the poor adhesion between fibers and matrix results in numerous voids at the interfaces. In these regions there is a concentration of stresses with a subsequently formation of microcracks during the traction test, which propagate in the sample till the final break. On the contrary, when PMMS grafting were used, the mechanical behavior of composites totally changes. Microcracks are not so quickly formed during the traction tests because of the improvement of the fiber/matrix adhesion with an increase of the final strength and a failure typical of a brittle material (see figure II-6).

To illustrate the role of the mechanical behavior of the fibers-matrix interface in terms of stress transmission, a bidimensional finite element model is here proposed. The aim of this numerical illustration is to present the different stress repartition inside the composite volume, and thus the stress concentration phenomena in the matrix. That is why we present two limit situations: first, a perfect contact between the two phases is considered to obtain a perfect stress transmission across the interface (case of figure II-7c); second, we consider a non-cohesive behavior of the interface (case of figure II-7b).

The real two interface transmission properties with the presence or not of compatibilizing agent stay between these two limit situations, the grafted case being closer to the perfect contact situation. This is only a toy model that is developed to deeply understand the underlying phenomena and the geometry and the quantitative results of this model are not relevant to the reality of our composites.

In Figure II-7, this toy composite is made of an elliptic inclusion embedded in a matrix. The mechanical properties of the inclusion, respectively the matrix, are chosen to mimic the properties of Miscanthus, respectively PCL. According to the symmetry of the geometry (see figure II-7a), only a quarter of the sample is modeled, setting convenient symmetric boundary conditions (right and bottom boundaries in figures II-7b and II-7c). A displacement is imposed on the left boundary whereas the top boundary is free. We use the Structural Mechanics Module of the using the COMSOL Multiphysics software and considered almost 70000 degrees of freedom to compute the following results. In figure II-7c, the matrix-inclusion interface maintains the contact between the two phases, contrary to the case in figure II-7b where the two material domain can be separated by the mechanical loading conditions. A comparison between these two figures clearly shows that the grafting helps to propagate the stress inside the inclusion, decreasing the peak stress value in the PCL and thus increasing the effective tensile strength of the composite. SEM micrographs of fracture surfaces are presented in figure II-8. The unmodified blend **1** and composite **2** show poor polymer/fiber interfacial adhesion, whereas the fracture surfaces of compatibilized composites **4** shows a good interfacial adhesion, resulting in a coating of the fiber surface with PCL. The fibers are embedded into the PCL matrix confirming the occurrence of strong interactions between MIS and PCL. This further suggested that this interfacial adhesion between MIS and PCL was due to grafting. In particular, the composite failure occurs with a mechanism that clearly involves fiber fracture more than fiber pull out from the material.

Wide angle X-Ray diffraction was used to determine changes in the crystalline structure of PCL matrix. Cellulose is a crystalline material with characteristic peaks at 22.6° and 15.8° [44]. PCL contains reflections at 21.4, 22.0 and 23.7° attesting of the orthorhombic crystal structure [45]. The crystallographic structure of the polymer can be influenced by the presence of Miscanthus or by the processing temperature. The crystallinity of matrix decreased from 62 % (PCL) to 46 % (sample **1**) when 20 % wt of MIS was added. These results suggest that the increase of mechanical properties is not due to a change of crystallinity of PCL but to the crosslinking reactions induced by the presence of the initiator BPO. This effect is more marked when PMMS is present.

Reference	Sample	Method	BPO [wt %]	E [MPa]	ε_r [%]	σ_r [MPa]	η
	PCL		-	322 ± 7	906 ± 226	26.0 ± 6.0	1
1	$PCL_{80}MIS_{20}$	Blend	-	819 ± 34	5.7 ± 0.6	13.7 ± 0.6	1.025 ± 0.034
2	$PCL_{78}MIS_{19.8}PMMS_{2.2}$	A	5	708 ± 4	16.3 ± 1.2	26.0 ± 0.8	1.072 ± 0.015
3	$PCL_{78}MIS_{19.8}PMMS_{2.2}$	A	0	811 ± 49	5.3 ± 0.6	13.6 ± 0.8	1.017 ± 0.050
4	$PCL_{79.5}MIS_{20}PMMS_{0.5}$	B	5	844 ± 33	11.8 ± 0.4	19.5 ± 2.1	1.128 ± 0.007
5	$PCL_{79.5}MIS_{20}PMMS_{0.5}$	B	0	860 ± 28	4.7 ± 0.6	12.0 ± 1.0	1.046 ± 0.041

Table II-4. Tensile properties of the realized composites samples. E: Young modulus; ε_r: failure strain; σ_r: tensile strength; η: global mechanical performance index.
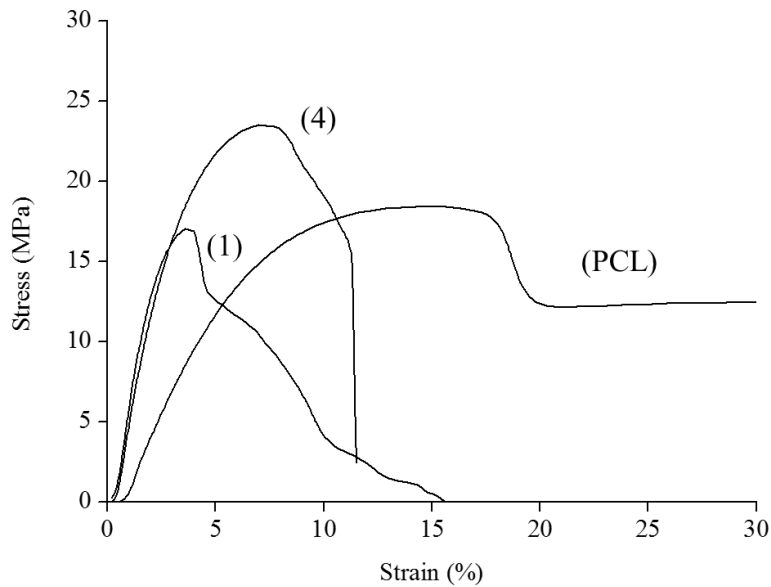
Figure II-6. Strain-stress curves of $PCL_{80}MIS_{20}$ (sample **1**) and $PCL_{79.5}MIS_{20}PMMS_{0.5}$ (sample **4**).

a/ Geometry

b/ Results: PMMS non-grafted interface

c/ Results: PMMS grafted interface
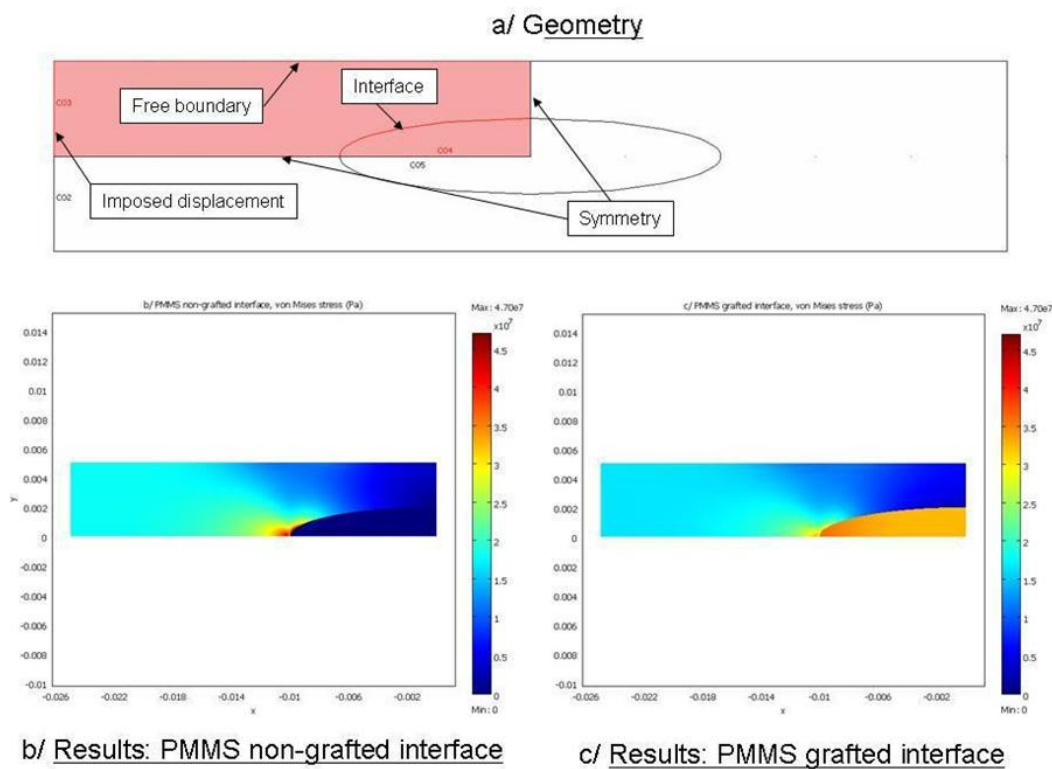
Figure II-7. Numerical toy model to illustrate the role of the interface grafting. a/ Geometry; b/ Results: PMMS non-grafted interface; c/ Results: PMMS grafted interface.
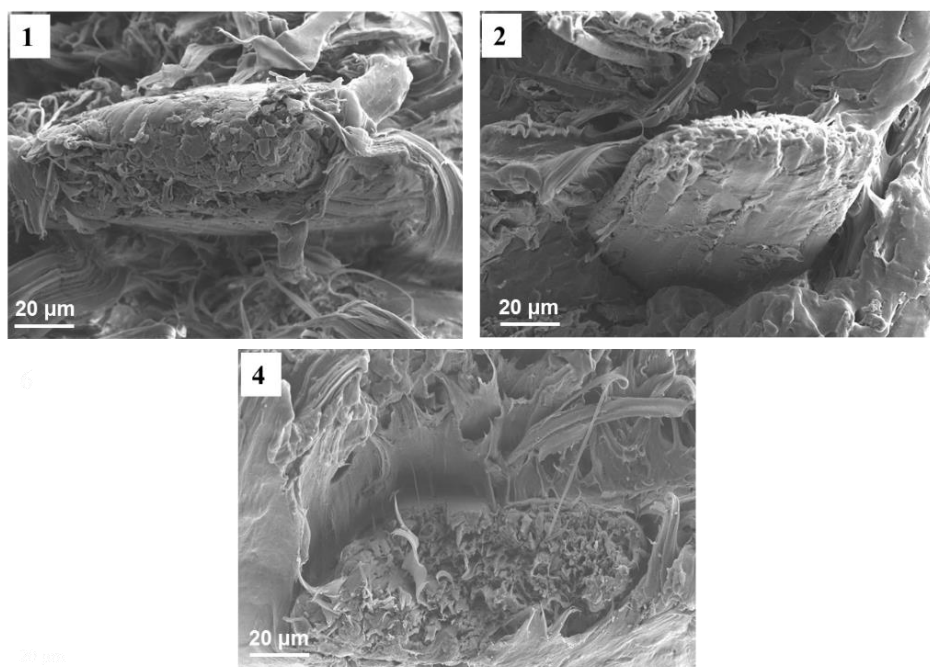
Figure II-8. SEM images of $PCL_{80}MIS_{20}$ (sample **1**), $PCL_{78}MIS_{19.8}PMMS_{2.2}$ (sample **2**) and $PCL_{79.5}MIS_{20}PMMS_{0.5}$ (sample **4**).

II-4. CONCLUSIONS AND PERSPECTIVES

Composites from PCL and Miscanthus *giganteus* fibers were successfully prepared. The incorporation of 20 wt % of fibers is sufficient to increase the Modulus (E) of these composites. Although Miscanthus acts as reinforcement for the pure PCL, the poor adhesion between fibers and matrix causes a decrease of the tensile strength and the presence of microcracks. Higher values of tensile strength were achieved by melting PCL with a MIS treated with PMMS as compatibilizing agent. An excellent balance of mechanical properties was achieved using fibers that were previously treated with a photo-induced thiol-ene addition. BPO was employed as a reactant to enhance the reaction between the different constituents, improving the adhesion between fibers and matrix. This evidence was confirmed by SEM images where fibers previously photo-grafted with PMMS were totally imbedded with the PCL, do not pull out from the material but rather break during tensile tests. Moreover, the composites did not show variations in the degree of crystallinity or thermal degradation as a result of the manufacturing process. Consequently, the increase of mechanical properties is likely due to a crosslinking effect which is more important when PMMS is present in the melt. This method of functionalization of natural fibers appears to be a very promising and versatile way to improve the mechanical properties of any type of polyester. These latest results push for a more detailed investigation of the BPO effect on the crosslinking of the matrix, discussed in appendix II-5B of this work. Moreover, the non-renewable origin of PCL and its poor thermal resistance are two main factors which encouraged us to find other possible matrixes which can possess the requirements of both biodegradability and bio-based origin. The investigation of the mechanisms involving the interface matrix/fibers and the consequent effect on the mechanical properties of the biocomposites constitute undoubtedly an interesting perspective to complete this work.

II-5. APPENDIX

II-5A. EFFECT OF FIBERS CONTENT ON PCL

In order to investigate the effect of fibers content on the mechanical behavior of poly(ϵ-caprolactone), different biocomposites were realized by extrusion and injection molding varying the weight fraction of Miscanthus fibers from 0 to 20 wt %. The processing parameters were chosen in order to achieve a good dispersion of the reinforcement in the matrix. The optimized parameters were described in the table II-A1.

Sample	T_E [°C]	T_I [°C]	T_m [°C]	n [t/min]
PCL	140	150	20	60
$PCL_{95}MIS_5$	140	150	20	60
$PCL_{90}MIS_{10}$	140	150	20	60
$PCL_{80}MIS_{20}$	140	150	20	60

Table II-A1 Processing parameters for PCL/MIS composites with 0, 5, 10 and 20 wt % of MIS fibers. T_E: extrusion temperature; T_I: injection temperature; T_m: mold temperature; n: rpm.

During the extrusion process, the values of pressure and torque were recorder after incorporation of fibers to the matrix. These values are listed in the table II-A2. At high fibers content both pressure and torque increase.

Sample	P [bar]	ΔP [bar]	M [N*cm]
PCL	4	2	16
$PCL_{95}MIS_5$	8	3	18
$PCL_{90}MIS_{10}$	8	4	20
$PCL_{80}MIS_{20}$	16	7	28

Table II-A2. Pressure and torque values for PCL/MIS composites during extrusion process.

Once specimens realized, they were tested using an Instron 5965 Universal Testing Machine equipped of a cell load of 2kN. Five specimens of each type of composite with standard dimensions according to ASTM638 were tested at a crosshead displacement rate of 50 mm/min at room temperature (23°C). The results of tractions tests are showed in figure II-A1. The Young modulus of the same specimens was also evaluated using a series of 8 loading-unloading cycles, from a minimum load of 3 N to a maximum load of 11 N at a cross-speed of 0.05 N/s. The results obtained are listed in the table II-A3.
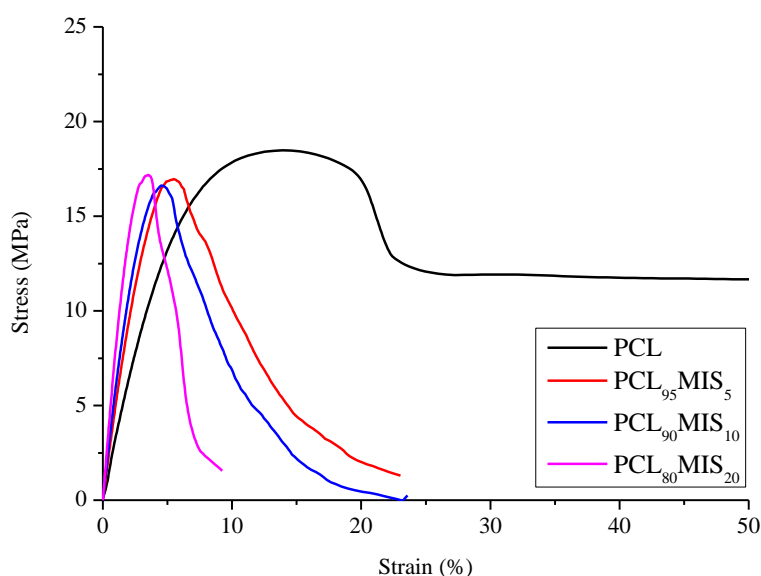
Figure II-A1. Strain-stress curves for PCL/MIS composites with variable weight fraction of MIS fibers from 0 to 20 wt %.

Sample	Slope of unloading phase [N/mm]	Young Modulus [MPa]
PCL	62 ± 3	399 ± 21
PCL$_{95}$MIS$_5$	65 ± 5	415 ± 30
PCL$_{90}$MIS$_{10}$	81 ± 6	519 ± 40
PCL$_{80}$MIS$_{20}$	114 ± 6	729 ± 38

Table II-A3. Results of loading-unloading cycles for PCL/MIS composites.

The results showed that biocomposites with 20 wt % of raw fibers possess a good Young modulus if compared to the neat matrix and to biocomposites with low content of fibers. This result allowed us to choose 20 wt % as the good content of reinforcement for the realization of all biocomposites presented in this work.

II-5B. EFFECT OF BPO ON PCL/MIS BIOCOMPOSITES

In the previous paragraphs the peroxide was added to the material molten in situ and in the presence of fibers that were already modified with PMMS. The objective of this section is to investigate the effect of BPO on the mechanical properties of biocomposites realized with 5 and 20 wt % of raw fibers. Once realized, specimens were tested with the same procedure showed in the appendix A (see table II-B1). Figures II-B1 and II-B2 showed the mechanical behavior for composites with 5 and 20 wt % of fibers respectively.

The BPO seems to have no influence on the Young modulus of the biocomposites, being this last essentially dependent on the fibers content. However, the materials became brittle and an increase in final strength is visible for the composites realized in the presence of the peroxide. This increase is more important for composites with high content of MIS fibers. The results obtained could be explained by an improvement of the adhesion matrix/fibers and by a cross-linking phenomenon of the matrix. The rapidity of the process and the improvement of the mechanical properties obtained are two factors that have led us to retain the reactive extrusion as a good process for the next chapters.
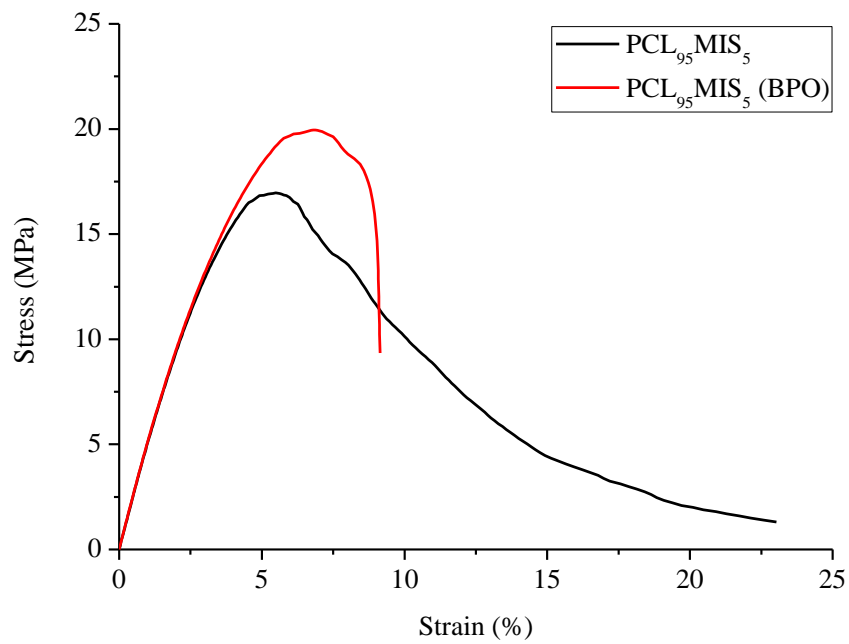
Figure II-B1. Strain-stress curves for PCL/MIS composites with 5 wt % of fibers with and without BPO.
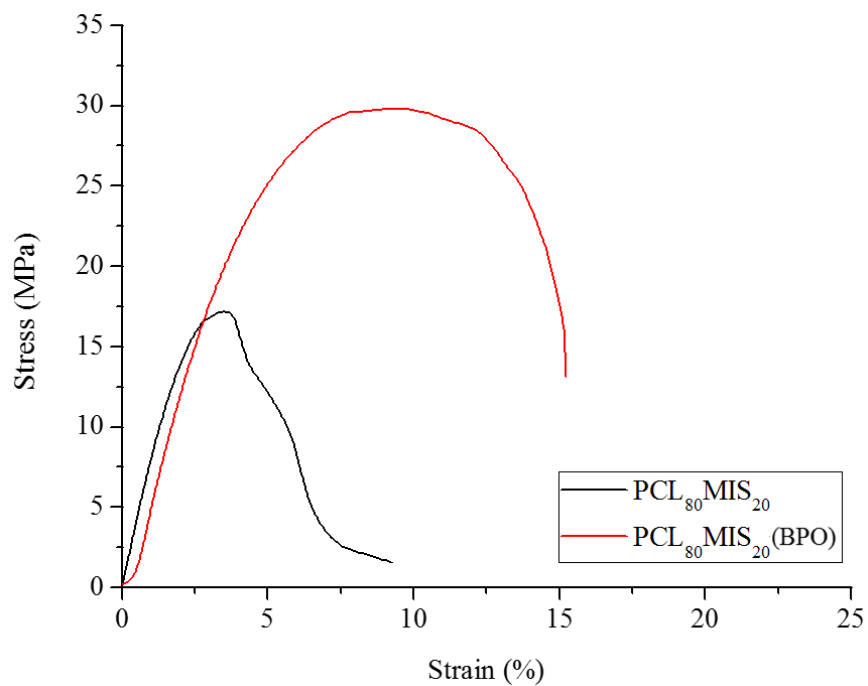
Figure II-B2. Strain-stress curves for PCL/MIS composites with 20 wt % of fibers with and without BPO.

Sample	BPO [%]	E [MPa]	σ_{max} [MPa]	σ_r [MPa]	ε_r [%]
$PCL_{95}MIS_5$	-	497 ± 4.7	17.7 ± 1.0	14.0 ± 0.8	23 ± 3.0
$PCL_{95}MIS_5$	5	517 ± 21	21.2 ± 1.6	20.7 ± 1.3	9.3 ± 1.1
$PCL_{80}MIS_{20}$	-	819 ± 34	17.5 ± 0.6	13.7 ± 0.6	5.7 ± 0.6
$PCL_{80}MIS_{20}$	5	822 ± 107	30.0 ± 1.2	22.0 ± 2.4	15 ± 2.4

Table II-B1. Mechanical results for PCL/MIS composites with 5 and 20 wt % of fibers realized in the presence or not of BPO.

II-6. REFERENCES

1. Mohanty, A.K. et al., Biofibres, biodegradable polymers and biocomposites: An overview. *Macromolecular Materials and Engineering* 276-277(1), p. 1-24 (**2000**).
2. Belgacem, M. et al., Monomers, Polymers and Composites from Renewable Resources. Elsevier (**2011**).
3. Alvarez, V.A. et al., Degradation of sisal fibre/Mater Bi-Y biocomposites buried in soil. *Polymer Degradation and Stability* 91(12), p. 3156-3162 (**2006**).
4. Zini, E. et al., Biodegradable Polyesters Reinforced with Surface-Modified Vegetable Fibers. *Macromolecular Bioscience* 4(3), p. 286-295 (**2004**).
5. Shibata, M. et al., Biocomposites Made from Short Abaca Fiber and Biodegradable Polyesters. *Macromolecular Materials and Engineering* 288(1), p. 35-43 (**2003**).
6. Wollerdorfer, M. et al., Influence of natural fibres on the mechanical properties of biodegradable polymers. *Industrial Crops and Products* 8(2), p. 105-112 (**1998**).
7. Mohanty, A.K. et al., Sustainable Bio-Composites from Renewable Resources: Opportunities and Challenges in the Green Materials World. *Journal of Polymers and the Environment* 10(1), p. 19-26 (**2002**).
8. Avella, M. et al., Poly(lactic acid)-based biocomposites reinforced with kenaf fibers. *Journal of Applied Polymer Science* 108(6), p. 3542-3551 (**2008**).
9. Bogoeva-Gaceva, G. et al., Natural fiber eco-composites. *Polymer Composites* 28(1), p. 98-107 (**2007**).
10. Dimzoski, B. et al., Preparation and characterization of poly(lactic acid)/rice hulls based biodegradable composites. *Journal of Polymer Engineering* 28(6-7), p. 369-383 (**2008**).
11. Faruk, O. et al., Biocomposites reinforced with natural fibers: 2000–2010. *Progress in Polymer Science* 37(11), p. 1552-1596 (**2012**).
12. Joseph, K. et al., Effect of chemical treatment on the tensile properties of short sisal fibre-reinforced polyethylene composites. *Polymer* 37(23), p. 5139-5149 (**1996**).
13. Fischer, G. et al., Biomass potentials of miscanthus, willow and poplar: results and policy implications for Eastern Europe, Northern and Central Asia. *Biomass and Bioenergy* 28(2), p. 119-132 (**2005**).
14. Collura, S. et al., Thermal behaviour of Miscanthus grasses, an alternative biological fuel. *Environmental Chemistry Letters* 5(1), p. 49-49 (**2007**).
15. Raj, R.G. et al., Use of wood fibers in thermoplastic composites: VI. Isocyanate as a bonding agent for polyethylene–wood fiber composites. *Polymer Composites* 9(6), p. 404-411 (**1988**).
16. Devi, L.U. et al., Mechanical properties of pineapple leaf fiber-reinforced polyester composites. *Journal of Applied Polymer Science* 64(9), p. 1739-1748 (**1997**).
17. Wong, S. et al., Interfacial improvements in poly(3-hydroxybutyrate)-flax fibre composites with hydrogen bonding additives. *Composites Science and Technology* 64(9), p. 1321-1330 (**2004**).
18. Shanks, R.A. et al., Thermoplastic biopolyester natural fiber composites. *Journal of Applied Polymer Science* 91(4), p. 2114-2121 (**2004**).
19. Lee, S.G. et al., Characterization of surface modified flax fibers and their biocomposites with PHB. *Macromolecular Symposia* 197(1), p. 089-100 (**2003**).
20. Haque, M.M.-U. et al., Functionalization and Compatibilization of Poly(ε-caprolactone) Composites with Cellulose Microfibres: Morphology, Thermal and Mechanical Properties. *Macromolecular Materials and Engineering* 297(10), p. 985-993 (**2012**).
21. Shibata, M. et al., Poly(ε-caprolactone) composites reinforced with short abaca fibres. *Polymers and Polymer Composites* 11(5), p. 359–367 (**2003**).
22. Kusumi, R. et al., Cellulose alkyl ester/poly(ε-caprolactone) blends: characterization of miscibility and crystallization behaviour. *Cellulose* 15(1), p. 1-16 (**2008**).
23. Wong, S. et al., Properties of Poly(3-hydroxybutyric acid) Composites with Flax Fibres Modified by Plasticiser Absorption. *Macromolecular Materials and Engineering* 287(10), p. 647-655 (**2002**).
24. Mohanty, A.K. et al., *Anhydride functionalized polyhydroxyalkanoates, preparation and use thereof.* 2005.
25. Chen, C. et al., Synthesis and characterization of maleated poly(3-hydroxybutyrate). *Journal of Applied Polymer Science* 88(3), p. 659-668 (**2003**).

26. Carlmark, A. et al., ATRP Grafting from Cellulose Fibers to Create Block-Copolymer Grafts. *Biomacromolecules* 4(6), p. 1740-1745 (**2003**).

27. Lönnberg, H. et al., Grafting of Cellulose Fibers with Poly(ε-caprolactone) and Poly(l-lactic acid) via Ring-Opening Polymerization. *Biomacromolecules* 7(7), p. 2178-2185 (**2006**).

28. Samain, X. et al., Grafting biodegradable polyesters onto cellulose. *Journal of Applied Polymer Science* 121(2), p. 1183-1192 (**2011**).

29. Adler, E., Lignin chemistry—past, present and future. *Wood Science and Technology* 11(3), p. 169-218 (**1977**).

30. Nimz, H., Beech Lignin—Proposal of a Constitutional Scheme. *Angewandte Chemie International Edition in English* 13(5), p. 313-321 (**1974**).

31. Piló-Veloso, D. et al., Isolamento e Análise Estrutural de Ligninas. *Quimica Nova* 16 (5), p. 435–448 (**1993**).

32. Aoyama, M. et al., Hydrolysis of lignin with dioxane-water (XVII). Isolation of a new lignol from hardwood lignin. *Mokuzai Gakkaishi* 25(10), p. 644-646 (**1979**).

33. Nascimento, M.S. et al., Phenolic Extractives and Natural Resistance of Wood, in *Biodegradation - Life of Science*, R. Chamy and F. Rosenkranz, Editors. InTech. (**2013**), p. 378.

34. Heo, J. et al., Improved Performance of Protected Catecholic Polysiloxanes for Bioinspired Wet Adhesion to Surface Oxides. *Journal of the American Chemical Society* 134(49), p. 20139-20145 (**2012**).

35. Zhou, C. et al., Poly[(mercaptopropyl)methylsiloxane] (PMMS)-based antibacterial polymer coatings prepared by a two-step sequential thiol–ene click chemistry. *Chinese Chemical Letters* 27(5), p. 685-688 (**2016**).

36. Popescu, C.-M. et al., XPS characterization of naturally aged wood. *Applied Surface Science* 256(5), p. 1355-1360 (**2009**).

37. Inari, G.N. et al., XPS characterization of wood chemical composition after heat-treatment. *Surface and Interface Analysis* 38(10), p. 1336-1342 (**2006**).

38. Dufour, A. et al., The Origin of Molecular Mobility During Biomass Pyrolysis as Revealed by In situ 1H NMR Spectroscopy. *ChemSusChem* 5(7), p. 1258-1265 (**2012**).

39. Wei, L. et al., Interfacial improvements in biocomposites based on poly(3-hydroxybutyrate) and poly(3-hydroxybutyrate-co-3-hydroxyvalerate) bioplastics reinforced and grafted with [small alpha]-cellulose fibers. *Green Chemistry* 17(10), p. 4800-4814 (**2015**).

40. Wei, L. et al., Grafting of Bacterial Polyhydroxybutyrate (PHB) onto Cellulose via In Situ Reactive Extrusion with Dicumyl Peroxide. *Biomacromolecules* 16(3), p. 1040-1049 (**2015**).

41. Cyras, V.P. et al., Relationship between processing and properties of biodegradable composites based on PCL/starch matrix and sisal fibers. *Polymer Composites* 22(1), p. 104-110 (**2001**).

42. Keller, A., Compounding and mechanical properties of biodegradable hemp fibre composites. *Composites Science and Technology* 63(9), p. 1307-1316 (**2003**).

43. Ganster, J. et al., Novel cellulose fibre reinforced thermoplastic materials. *Cellulose* 13(3), p. 271-280 (**2006**).

44. Pracella, M. et al., Functionalization, Compatibilization and Properties of Polyolefin Composites with Natural Fibers. *Polymers* 2(4), p. 554– 574 (**2010**).

45. Han, J.T. et al., Biomimetic Fabrication of Vaterite Film from Amorphous Calcium Carbonate on Polymer Melt: Effect of Polymer Chain Mobility and Functionality. *Chemistry of Materials* 17(1), p. 136-141 (**2005**).

Chapter III

"Only when the last tree has been cut down,
the last fish been caught
and the last stream poisoned,
will we realize that we cannot eat money."

(Cree Indians Prophecy)

STUDY OF MECHANICAL PROPERTIES OF PHBHV/MISCANTHUS GREEN COMPOSITES COMBINING EXPERIMENTAL AND MICROMECHANICAL APPROACHES

The need to reduce the proliferation of synthetic and not-biodegradable plastics has been already underlined in the previous chapters. The low melting temperature of PCL and its not bio-based character are some aspects that have led us to the investigation of new bio-based and biodegradable plastics with interesting mechanical properties. To this aim, the bacterial poly(3-hydroxybutyrate-co-3-hydroxyvalerate) (PHBHV) has been chosen as alternative to PCL to realize totally green biocomposites by adding Miscanthus giganteus (MIS) fibers as reinforcement, improving in this way its mechanical properties. This work aims to be a preliminary study on the characteristics of these biocomposites before any chemical treatment of vegetal fibers. All the manufactured materials were studied from their synthesis to the characterization of their mechanical properties. These last are related to the underlying microstructure using both experimental and modeling approaches. In this study, PHBHV with 12 % of HV units ($PHB_{88}MIS_{12}$) was chosen as matrix. Different contents of Miscanthus giganteus fibers, 5, 10, 20, 30 weight percent were thus combined with the matrix. The samples were manufactured by extrusion and injection molding processing at lab scale already treated in the previous chapter. The obtained samples were then characterized by cyclic-tensile tests and microscopy. In parallel, the measured properties of the biocomposite were also estimated using a Mori-Tanaka approach to derive the effective behavior of the composite. As expected, the addition of reinforcement to the polymer matrix results in composites with higher tensile moduli on the one hand, and lower failure strains and tensile strengths on the other hand.

III-1. INTRODUCTION

In recent years the market for Wood Plastic Composites (WPCs) has grown exponentially and is expected to exceed $ 4.5 billion in 2019 [1]. The different applications for these materials, such as in building and construction field or automotive, make this market highly fragmented but at the same time very attractive for many research groups and industries. Today, most of these materials are constituted by matrixes derived from oil such as polyethylene (PE) or polypropylene (PP). Even though natural cellulosic fibers have been successfully used with petroleum-derived polymers, the environmental benefits of natural fiber composites can be enhanced considerably if biodegradable polymers are used [2]. These biocomposites can be easily disposed of or composted at the end of their life without harming the environment, which is not possible with synthetic fiber based polymer composites.

Poly(3-hydroxyalkanoates) (PHAs) are a class of natural biodegradable polyesters accumulated by many bacteria as carbon and energy supply when an essential nutrient is limited [3, 4]. Using various substrates, a wide variety of PHAs can be synthesized, differing notably in the length of their side chains [3, 5]. Two types of PHAs can be distinguished; (i) short chain length PHAs, or scl-PHAs, possessing alkyl side chains having up to two carbon atoms, as for example the widely used poly(3-hydroxybutyrate-*co*-3-hydroxyvalerate) PHBHV that is considered hereafter; (ii) medium chain length PHAs, or mcl-PHAs, with at least three carbon atoms in their side chains. (PHAs) have been suggested as green substitutes for conventional plastics, due to their synthesis from renewable resources and their biodegradation by enzymatic action [6]. Owing to their biocompatibility and their biodegradability, PHAs proved to be good candidates for biomedical applications including the design of devices, biodegradable drug carriers and tissue engineering (TE) scaffolds [7-10]. They also have been combined with natural cellulosic fibers such as hemp jute flax carnauba fibers, miscanthus, bamboo [11-13], pineapple fibers [14], recycled wood fiber [15] and cellulose [16-18] to prepare biocomposites.

Among all the existing PHAs, poly(3-hydroxybutyrate) (PHB) is certainly one of the most important. It possesses a melting point close to that of polypropylene, better oxygen barrier property and similar mechanical properties [6]. However, its brittleness and narrow processing temperature window limit its application. To overcome the inferior properties of PHB, a variety of copolymers have been synthesized by bioconversion such as the poly(3-hydroxybutyrate-*co*-3-hydroxyvalerate) (PHBHV). In this study, a PHBHV with 12 % of valerate units was chosen to realize composite

materials. Among the different vegetable fibers that can be used, Miscanthus (Miscanthus *giganteus*) was retained. This last is a perennial crop, highly productive, with a very efficient nitrogen-recycling system and a very interesting energy balance due to the absence of nitrogen [19] and recently used in composites [20-22]. A well-known phenomenon in these materials is the incompatibility between fibers and matrix caused by the hydrophobicity of the polymer and the hydrophilic nature of the fibers. This effect has serious consequences on the mechanical seal of the final material and this is the reason why the presence of compatibilizer agents or additives improving the cohesion at the matrix / fiber interface is often necessary [23]. Thus, we recently showed the possibility to improve the adhesion between poly(ε-caprolactone) and vegetal fibers using photo-activated grafting of a bounding agent [24]. Such a functionalization of the fibers to improve their adhesion is out of the scope of this paper since it is first important to present here a complete study of our PHBHV/Miscanthus composites from their synthesis to their testing and *in silico* characterization.

Considering different contents of Miscanthus fibers, the purpose of the present paper is to propose a rigorous method to produce these composites and then determine their mechanical properties. This characterization is performed using a twofold approach since, in addition to classical mechanical testing, a micromechanical approach taking into account the geometry, volume fraction and organization of the fibers in the matrix is carried out to estimate the effective mechanical properties of the composite. Thus, this modelling approach could be useful to derive a model-driven optimization of the composite synthesis in a further step.

III-2. MATERIALS AND METHODS

III-2.1. MATERIALS

Poly(3-hydroxybutyrate-*co*-3-hydroxyvalerate) ($PHB_{88}HV_{12}$), containing 12 % of valerate was purchased from Goodfellow in a pelletized form. Miscanthus *giganteus* (MIS) fibers were provided by Miscanplus, France. MIS fibers came from a 2014 spring crop roughly chopped and subsequently milled until fiber length ranged between 1 and 5 mm.

III-2.2. COMPOSITE PROCESSING

Thermogravimetric analysis revealed that the MIS has ambient moisture of 5 %. For this reason, prior to processing, both PHBHV and Miscanthus were dried in a conventional oven at 80°C for 5 h in order to remove any moisture and then they were stored in a desiccator containing K_2HPO_4 prior to processing. To investigate the effect of the fiber content on composite mechanical properties, the following nominal values were investigated: 0, 5, 10, 20 and 30 wt %. The nominal mass content corresponds to the mass content of MIS at the beginning of the composite processing. As shown later (see section III-3.4), the fiber mass content of the final product may be slightly lower. Notwithstanding this observation, the classical use of nominal contents is adopted hereafter to present the results.

According to the nominal mass content of each phase, PHBHV and MIS were mixed together in a lab-scale twin-screw extruder (Minilab Thermo Scientific Haake). The experiments were performed at 160°C (T_E) with a screw speed of 60 rpm (n). The retention time for the pure matrix was of 1 minute; this time was increased to 2 minutes in order to fully disperse the fibers into the matrix. After recirculation, the extruded molten material was transferred by means of a preheated piston-cylinder assembly and was shot in the micro-injection unit (MiniJet Thermo Scientific Haake) at the injection pressure for 30 seconds. A maintenance pressure, lower than that used during the phase of injection, was applied for other 30 seconds. The collector and the mold temperatures were set at 165°C (T_I) and 45° (T_m) respectively. Parameters during the phase of injection of the material were adjusted according to the increase of the polymer melt viscosity with the fiber content. Some of the final optimized parameters used for the entire process are resumed in table III-1.

T_E [°C]	n [tr/min]	T_I [°C]	T_m [°C]
160	60	165	45

Table III-1. Some of the extrusion and injection molding parameters. T_E: extrusion temperature; n: rotational speed; T_I: injection temperature; T_m: mold temperature.

III-2.3. MATERIALS CHARACTERIZATION

III-2.3.1. Scanning electron microscope (SEM)

SEM observations were performed using a Merlin Carl Zeiss scanning electron microscope. Prior to observation, the cross sections of specimens at different fiber content were sputter-coated with a thin layer of palladium in a Cressington 208 HR sputter-coater. Images were recorded with an acceleration voltage of 10keV and at different magnifications.

III-2.3.2. Mechanical properties

The mechanical properties of the composites were evaluated using an Instron 5965 Universal Testing Machine equipped with a cell load of 100 N. All specimens presented standard dimensions according to ASTM638. Two types of tests were made. On the one hand, a simple traction test was set up at a rate of 5 mm/min in order to evaluate the mechanical behavior of the composites, typically its failure strain and tensile strength. Five samples were tested for each fiber content value. These tests were performed 2 days after the day of realization of the biocomposites. On the other hand, a cyclic traction test was set up to evaluate the Young modulus. Ten specimens for each fiber content value were tested in this setup. Prior to testing, specimens were stored 8 days at 23 °C. The cyclic traction test was set up with increasing values of the maximum load applied by the testing machine from one cycle to another. The initial maximum state stress was set to 3 N and the final one to 10 N with an increment of 1 N from one cycle to another (that is 8 cycles overall). The lower and upper limits are related to the sensitivity of the experimental device threshold and to the yield stress of the PHBHV, respectively.

We moreover checked *a posteriori* that the cyclic loading curves remain in the elastic domain. All cycles were made at a constant speed of 0.05 N/s. In the absence of extensometer or other devices

allowing direct measures of stress and strain on the specimens, the elastic modulus was calculated using the procedure showed in the appendix III-6A.

III-2.3.3. Fiber-size distribution

After processing, specimens with different fiber contents were solubilized three times in dichloromethane during 30 minutes. After filtration, the collected Miscanthus fibers were observed using a 3B Scientific Physics microscope at a magnification of 4x. A series of 30 observations was made per specimen.

III-2.3.4. Density measurements

Average density of pure matrix and composites were evaluated using a helium AccuPyc 1330 Micromeritics pycnometer on around 40 mg of mass taken from the central section of the specimens used for tensile tests. The density calculated with this method was compared with that calculated using the ratio between the mass and the volume of the specimens.

III-2.3.5. Thermal analyses

Differential scanning calorimetry experiments were performed on a PerkinElmer Diamond DSC Apparatus. Sample of around 10 mg sealed in aluminum pans were initially heated from -60°C to 200°C at 20°C/min, cooled down rapidly and then reheated in the same conditions used in the first heating run. Melting point (T_M) and melting enthalpy (ΔH_M) were determined during the first heating. The degree of crystallization (X_c) was then calculated using the following equation:

$$X_c(\%) = \frac{\Delta H_M}{\Delta H_0 * W} * 100 \tag{III-1}$$

where ΔH_0 corresponds to the melting enthalpy of a 100% crystalline PHBHV (146 J/g) and W is the polymer fraction present in the composite [25].

III-2.4. MODELING

Among the several methods predicting the elastic properties of fiber-reinforced composites, the rule of mixtures (ROM) is probably the quickest and easiest one. Using the elastic moduli E_F and E_M of the fiber and matrix phases, and the volume fraction of the fibers ϕ_F, the effective Young modulus of the composite reads:

$$E_C = \phi_F E_F + (1 - \phi_F) E_M \qquad\qquad (\text{III-2})$$

Much more sophisticated models were also developed to evaluate the effective elastic behavior of the composite using homogenization approaches. Homogenization theories can estimate the effective elastic tensor C_{hom} of a multiphase material based on information about its microstructural organization. Among others, continuum micromechanics [26, 27] proved quite useful when dealing with composite materials of matrix-inclusion type [28, 29]. Continuum micromechanics uses the solution of the matrix-inclusion problem provided by Eshelby in the fifties [30] to estimate the effective elastic tensor C_{hom} of a multiphase material as [31]:

$$C_{\text{hom}} = \sum_r \phi_r C_r : A_r , \qquad\qquad (\text{III-3})$$

where ϕ_r, C_r and A_r are the volume fraction, (4th-order) elastic tensor and (4th-order) localization tensor of phase r, and the sum runs over all the constituent phases. The localization tensor A_r accounts for the nature and geometrical organization of the phase r within the *effective matrix* and its expression depends, in general, on the volume fraction and elastic tensor of all the phases. Different estimates of C_{hom} can be obtained by suitable choices of the effective matrix. As long as one actual phase can be identified as a "matrix" phase, the relevant estimate of C_{hom} is provided by the Mori-Tanaka model. The idea behind this approach is sketched in figure III-1.

Our case is well described by the Mori-Tanaka model, since MIS fibers (inclusion phase) are disconnected with one another and fully embedded in the PHBHV (matrix phase). Thus, the information required by the model concerns the elastic tensors of the MIS and PHBHV and the volume fraction and geometrical organization of the MIS fibers. We assumed both MIS ad PHBHV to be elastic isotropic materials (see table III-2). The volume fraction of the MIS fibers ϕ_F was computed based on the measured mass fraction using the procedure outlined in the appendix III-6B. Eventually, we assumed the MIS fibers to be either cylinder shaped and aligned with the sample main axis (that is, the injection direction) or spherical particles. Note that these two hypotheses lead to homogenized materials which are transversely isotropic and isotropic, respectively.

Constituents	Young's Modulus [GPa]	Poisson's coefficient [-]
Miscanthus *giganteus*	4.5 [a]	0.3 [c]
PHBHV	1.0 [b]	0.3 [c]

Table III-2. Technical data of Young Modulus and Poisson coefficient for Miscanthus *giganteus* and PHBHV. (a) Adapted from [32] (b) Experimental value. (c) Assumed.
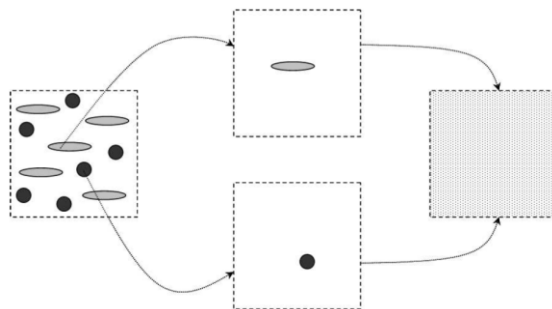
Figure III-1. Schematic of the Mori-Tanaka model. On the left: actual, heterogeneous material; on the right: effective, homogeneous material. The intermediate step represents the homogenization procedure where individual inclusions are considered as embedded in the matrix phase and contribute to the overall elasticity of the homogenized material.

III-3. RESULTS

III-3.1. MECHANICAL PROPERTIES OF BIOCOMPOSITES

The tensile modulus, the tensile stress and the ultimate strain of the PHBHV/MIS composites were evaluated using classical tensile tests (see table III-3). For rather low nominal contents of fibers, typically 5, 10 and 20 wt %, the properties change rather slowly. It is necessary to reach 30 wt % of fibers mass content to observe a significant effect of the reinforcement in the matrix. This gradual increase of the tensile modulus is clearly visible comparing the initial slopes of the curves obtained from tensile tests (figure III-2).

In parallel, a series of cyclic loading-unloading tensile tests was performed. First, a pure matrix sample was tested to quantify its damage limit. Through these tests it was possible to identify the applied force beyond which damage appears in the matrix, which turned out to be about 10 N. This value was used to set up the upper limit of the 8-cycle loading-unloading tensile test performed on all

the composite samples (see sec. III-2.3.2), in order to prevent rupture of the samples. For each test, the slope of each unloading phase was computed and used to obtain the tensile modulus of the composite. This last was definitively corrected using the procedure showed in appendix III-6A and the final values are showed in table III-4.

Slope, and thus tensile modulus, increased with increasing fiber content, but also the standard deviations of these values increased. Furthermore, the values obtained with a simple tensile test are lower from those obtained with the cyclic procedure (figure III-3). Another important point of these tests is the difference between the slopes of the curve during the loading and unloading phases, the latter being more important (figure III-4).

Samples	Tensile Modulus [MPa]	Tensile strength [MPa]	Ultimate strain [%]
PHBHV	889 ± 41	22.0 ± 0.48	9.9 ± 1.1
PHBHV$_{95}$MIS$_5$	1074 ± 44	17.0 ± 1.54	4.2 ± 0.7
PHBHV$_{90}$MIS$_{10}$	1238 ± 74	16.8 ± 1.67	4.4 ± 0.9
PHBHV$_{80}$MIS$_{20}$	1267 ± 90	15.8 ± 0.77	3.9 ± 0.2
PHBHV$_{70}$MIS$_{30}$	1891 ± 172	16.9 ± 1.03	3.3 ± 0.7

Table III-3. Results of tensile tests on PHBHV/MIS composites at different fiber content (0, 5, 10, 20, 30 wt %).

Samples	Slope of unloading phase [N/mm]	Tensile Modulus [MPa]
PHBHV	115 ± 5.0	1012 ± 48
PHBHV$_{95}$MIS$_5$	134 ± 5.3	1185 ± 44
PHBHV$_{90}$MIS$_{10}$	159 ± 7.0	1408 ± 63
PHBHV$_{80}$MIS$_{20}$	196 ± 15.2	1736 ± 137
PHBHV$_{70}$MIS$_{30}$	228 ± 22.3	2032 ± 191

Table III-4. Results of cyclic loading-unloading test on PHBHV/MIS composites at different fiber content (0, 5, 10, 20, 30 wt %).
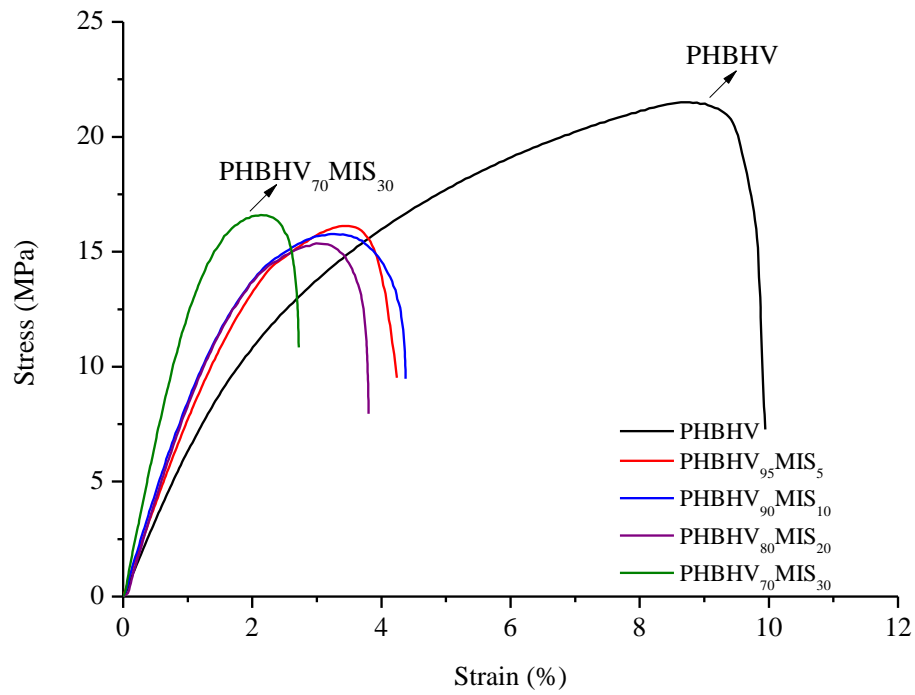
Figure III-2. Strain-stress curves for PHBHV/MIS composites (the weight percent contents are indicated).
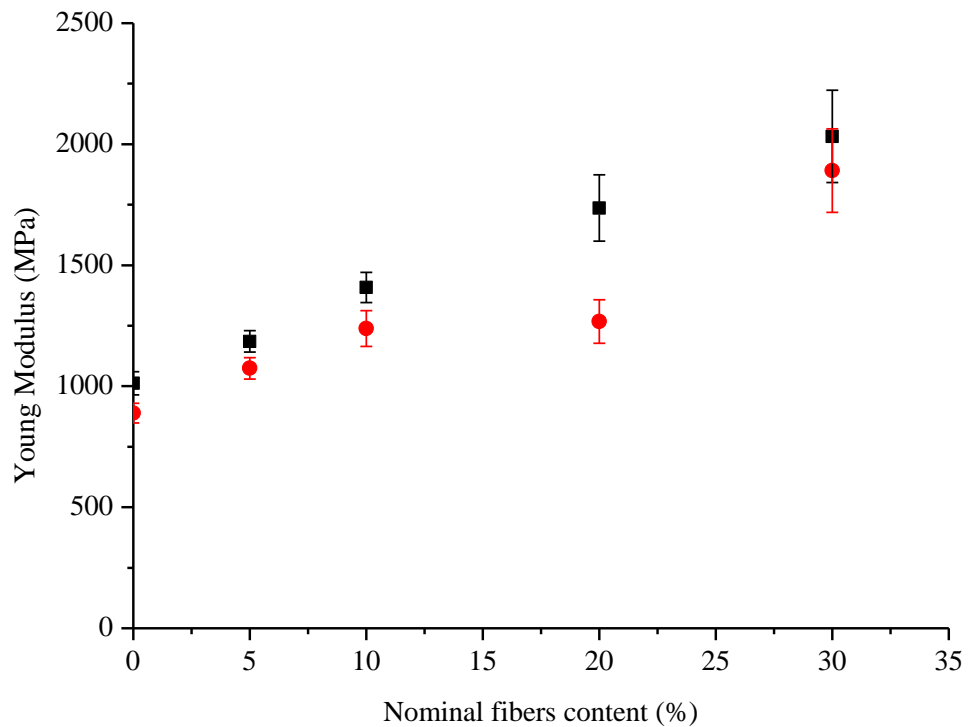
Figure III-3. Young Modulus vs Nominal fibers content calculated with the two methods of loading-unloading tests (■) and traction tests (●).
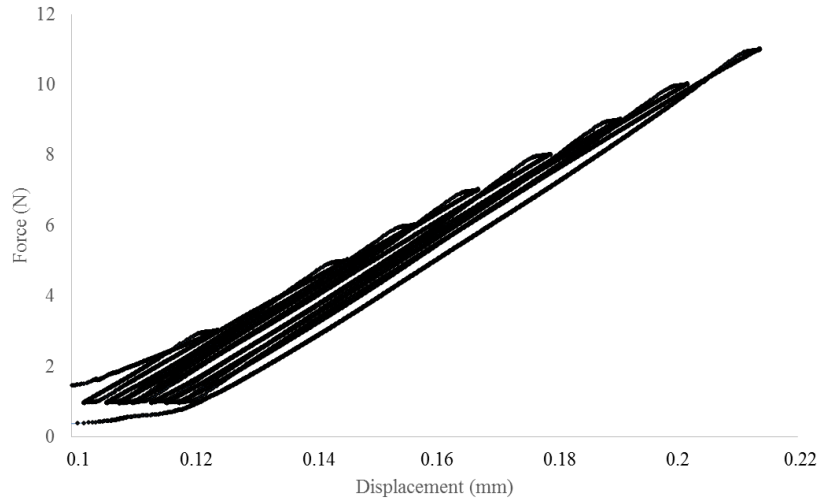
Figure III-4. Loading-unloading cycle for a PHBHV$_{95}$MIS$_5$ specimen.

III-3.2. SCANNING ELECTRON MICROSCOPY (SEM)

The cross sections of composites at different content of fibers were characterized by SEM and the results are shown in figure III-5. At lower fiber contents, typically at 5 and 10 wt %, the fibers are isolated in the matrix and perfectly identifiable. At higher fiber contents, fibers tend to form aggregates in all the section. In all samples, fibers pull out from the matrix.
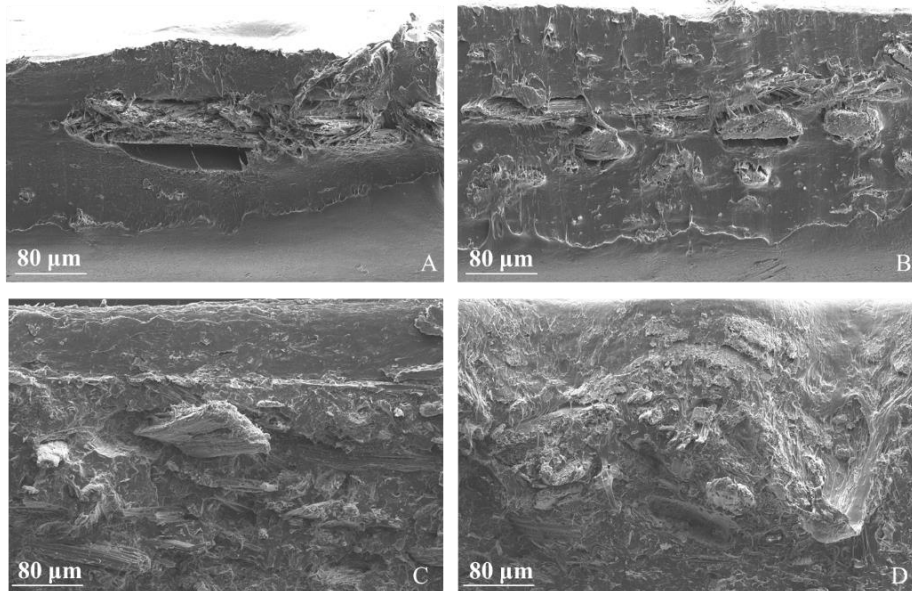
Figure III-5. SEM images of the cross section of PHBHV/MIS composites:
(A) PHBHV$_{95}$MIS$_5$; (B) PHBHV$_{90}$MIS$_{10}$; (C) PHBHV$_{80}$MIS$_{20}$; (D) PHBHV$_{70}$MIS$_{30}$.

III-3.3. Fiber-size distribution

Average values of width (*d*) and length (*l*) of the fibers and the *l/d* ratio are reported in Table III-5. The fibers aspect ratio decreases when fiber content increases. This indicates that the composite synthesis based on an injection molding processing does damage the fibers for higher content. Indeed, due to the narrow pathway in the injector, it is reasonable to assume that high fiber contents correspond to stronger deterioration of the fibers.

Samples	Width, *d* [mm]	Length, *d* [mm]	*l/d*
PHBHV$_{95}$MIS$_5$	0.27 ± 0.04	1.72 ± 0.33	6.4
PHBHV$_{90}$MIS$_{10}$	0.20 ± 0.06	1.11 ± 0.44	5.6
PHBHV$_{80}$MIS$_{20}$	0.16 ± 0.01	0.82 ± 0.10	5.1
PHBHV$_{70}$MIS$_{30}$	0.18 ± 0.08	0.80 ± 0.09	4.6

Table III-5. Evaluation of fiber-size distribution.

III-3.4. Density of Miscanthus and composites

In table III-6, the fiber and composites densities are presented. First, using the procedure presented in appendix III-6B to calculate the volumetric fraction of the MIS fibers, the fiber mass M_F is obtained and then their density ρ_F is determined thanks to Eq. III-B.1. The fiber mass measurements clearly show that discrepancies between the nominal and actual MIS mass contents do exist, the actual value being slightly lower. This trend may be due to a clogging effect at the injection point. Actually, during the injection process, the mixture is cooled quickly from $T_I = 165°C$ in the collector to $T_m = 45°C$ in the mold, leading to a progressive clogging at the injection point which increasingly prevents fibers from entering the mold. According to this hypothesis, the bulk of the mold should be richer in fibers than the space near the mold walls, this latter being essentially filled by pure matrix. This phenomenon is clearly visible in the SEM images of figures III-5A and III-5B where there are no fibers in the boundary of the sample. The density of MIS roughly ranged from 0.7 to 1 g/cm^3 after the injection molding procedure. Note that the MIS fibers extracted from specimens at 5 and 10 wt %, respectively from specimens at 20 and 30 wt %, have similar densities. Secondly, the density of the biocomposites was evaluated through the pycnometer and compared with that obtained from a weighing procedure. Results obtained with the two methods are coherent for 5, 10 and 20 wt %, whereas they differ for the pure PHBHV and the 30 wt % case. We attribute this to a

potential misuse of the pycnometer. Actually, this last is not able to measure the exact density of composites realized by injection molding, being these last free from evident pores. In this case, values obtained by the weighing procedure seem to be more accurate.

Samples	ν_{MIS_n}	ν_{MIS_m}	$<\rho_{MIS}>$ [g/cm^3]	$<\rho_{C\_calc}>$ [g/cm^3]	$<\rho_{C\_exp}>$ [g/cm^3]
PHBHV	0	0	-	1.25[a]	1.083[b]
PHBHV$_{95}$MIS$_5$	5	4.4 ± 0.1	0.75 ± 0.03	1.214 ± 0.003[a]	1.233[b]
PHBHV$_{90}$MIS$_{10}$	10	7.9 ± 1.6	0.76 ± 0.05	1.187 ± 0.002[a]	1.176[b]
PHBHV$_{80}$MIS$_{20}$	20	17.5 ± 2.1	0.96 ± 0.01	1.186 ± 0.005[a]	1.184[b]
PHBHV$_{70}$MIS$_{30}$	30	27.1 ± 0.2	0.93 ± 0.03	1.143 ± 0.012[a]	1.240[b]

Table III-6. Density values for MIS fibers and composites materials calculated with weight values (a) and with a Helium pycnometer (b). ν_{MIS_n}: nominal mass fraction of Miscanthus; ν_{MIS_m}: measured mass fraction; $<\rho_{MIS}>$: average density of Miscanthus; $<\rho_{C\_calc}>$: calculated average density of composites; $<\rho_{C\_exp}>$: experimental average density of composites.

III-3.5. RESULTS OF NUMERICAL SIMULATION

A Mori-Tanaka model was used to estimate the overall homogenized elastic modulus of PHBHV/MIS composites in the direction of application of the stress (E3). In a first case it is assumed that the fibers had a cylindrical shape and were aligned along the axis of stress, leading to a transversely isotropic effective behavior. In a second case, it is assumed that fibers had a spherical shape realizing an isotropic system. Both models require knowledge of the volumetric fractions of fibers in the biocomposites and the mechanical properties of the constituents. In both models, both matrix and fibers are assumed to be isotropic. Then, their elastic behavior is fully described by their Young modulus and Poisson ratio.

The experimental values calculated with the loading-unloading cycles lie between the two simulations, which constitute the upper and lower limits for the elastic modulus E3.

The model with cylindrical fibers aligned in the direction of the stress seems to get closer to the experimental values than the model with spherical fibers. Moreover, result obtained from the cylindrical fiber model are perfectly overlapped with those obtained using the rule of mixtures (ROM). All these results are shown in figure III-6.
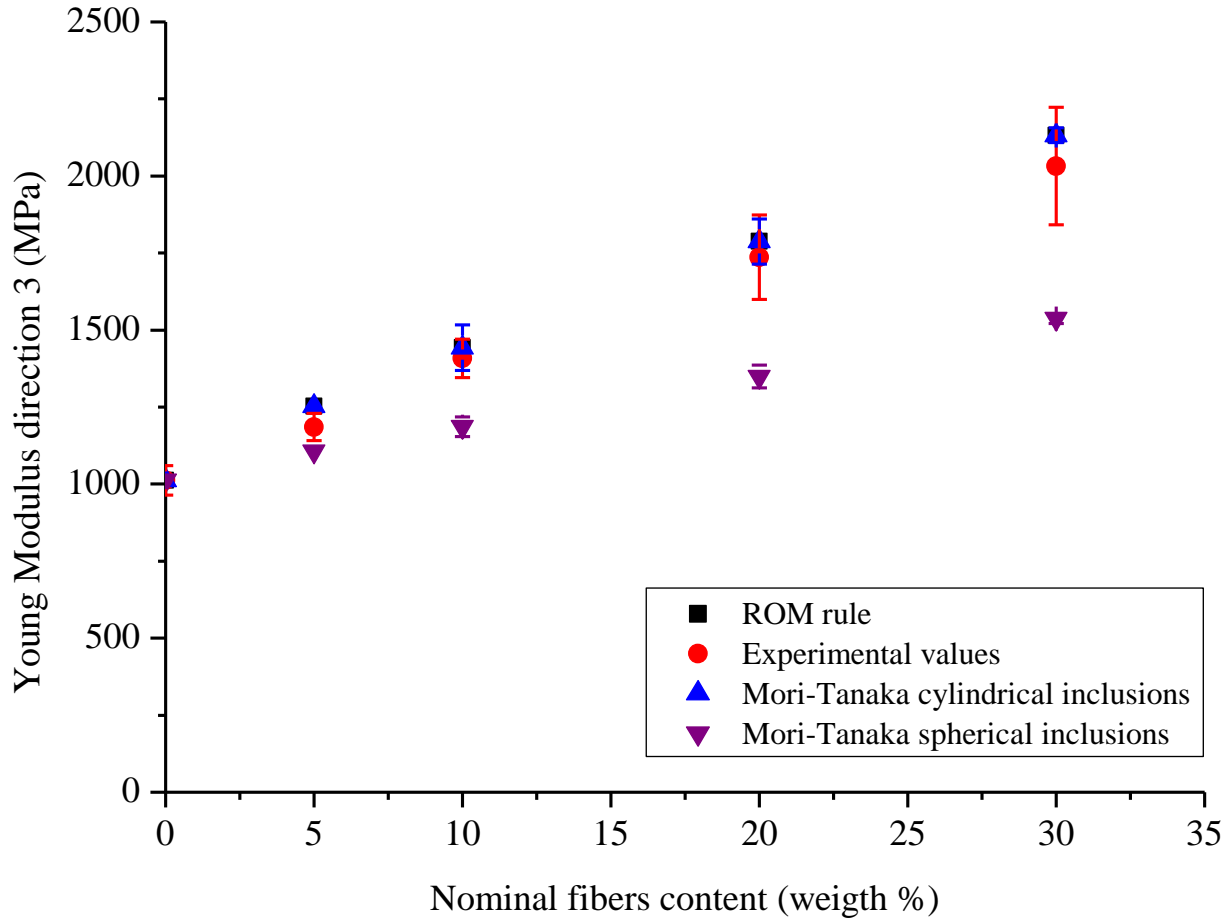
Figure III-6. Results of numerical simulation: the values obtained with ROM rule are superposed with those obtained with the Mori-Tanaka with cylindrical inclusions.

III-4. DISCUSSION

III-4.1. THE MECHANICAL BEHAVIOR OF PHBHV/MIS COMPOSITES

A familiar behavior in composite materials is an increase of Young's modulus and a decrease in failure strain and stress with increase of fiber mass content. This general trend was showed in many previous works [32-36] and it seems to be independent from the nature of the polymer matrix. Biocomposites realized with other bio-based matrix like PLA have shown an increase by 20% when reinforced with 20 wt % of Miscanthus fibers and a slighty decrease in Young Modulus for percentage over 20 wt %, this last probably due to the formation of aggregates [21, 37]. Comparing the tensile modulus and strength of the polypropylene (PP) based wood fiber composites with PHBHV–wood fiber composites, composites realized with polypropylene have higher order of tensile properties [38]. As reported in literature the modulus and the strength of a PP composite reinforced with 30 wt % of wood fibers are 3.33 GPa and 27.1 MPa respectively [39]. In the present work, all the phenomena previously described were highlighted by simple tensile tests (see table III-3) and by loading-unloading tests (see table III-4). For our samples the tensile modulus was increased by 100 % and tensile strength decreased by 23% when reinforced with 30 wt % of Miscanthus fibers as compared to neat PHBHV.

Although the tensile modulus was calculated with the two methods, the values obtained with tensile tests are lower from those obtained with the cyclic procedure (figure III-3). Another important point of these tests is the difference between the slopes of the curve during the loading and unloading phases, the latter being more important (figure III-4). These phenomena may be explained by the fact that the matrix is subjected to crystallization during time. PHBHV is a semicrystalline polymer and changes in the microstructure of the polymer are possible at temperatures higher than the glass transition one. In our case, the tests were carried out at a temperature (23°C) that is slightly higher than the glass transition temperature of the neat matrix (5°C) evaluated in a precedent work [40]. A possible mechanism occurring during the traction tests consists of different deformation steps. In particular, in the first stage of deformation, changes occur exclusively in amorphous zones that stretch. Successively, the crystalline areas start to slide parallel to the traction axis pulled from the stretched amorphous zones and, at the end, the highly stretched polymer chains align with the axis. Since the polymer chains may vary during the loading, slopes in the loading and unloading phases

can be different from each other. The crystallization phenomenon occurring during time was checked "*a posteriori*" using both mechanical and thermal tests as showed in appendix III-6C.

III-4.2. INTERNAL MORPHOLOGY AND DENSITY OF THE BIO COMPOSITES

The morphology of the biocomposites can be perfectly identified by SEM images. Moreover, optical microscopy can provide important information on the effect of the processing on the fibers. Generally, when a compatibilizing agent is not used, fibers pull-out from matrix because of the poor adhesion between the two constituents. In the case of the biocomposites manufactured by extrusion and injection molding, a multi-layer effect along the cross section was also observed. This phenomenon was likely caused by the flow of melted material in the mold during the phase of injection molding and has a clear effect on the dispersion of the fibers in the matrix. These latter are mainly located in the upper part of the cross section while pure matrix is visible in the lower part (see figures III-5A and III-5B). This effect can be explained as the result of low interfacial adhesion between the fibers and the matrix.

The fabrication procedure, from milling to injection molding, strongly impacts the length of the fibers, preserving their width (see table III-5). At low contents of reinforcement in the matrix, the fibers appear intact and long, while at high levels they are reduced to a finer powder. Keeping constant the rotational speed and time of mixing during the extrusion process, the mechanical torque of the extruder machine was observed to increase with the fiber content. As expected, after processing, there is a reduction of the aspect ratio due to the breakup of the fibers during processing. Moreover, the density of the fibers and consequently that of the composites is influenced by the degree of compression imposed during the step of injection.

III-4.3. NUMERICAL SIMULATION

For the numerical simulation, a Mori-Tanaka model was adopted considering either cylindrical or spherical inclusions (see sec III-2.4). The hypothesis of cylindrical fibers seems to be confirmed from SEM observations, while the hypothesis of a transversal isotropic organization seems to be plausible and suggested by the method adopted to realize the biocomposites. In particular, the injection molding procedure requires the injection of the extruded material into a mold along the vertical direction. Fibers and polymer chains are forced to enter into the mold and to basically align with the flow direction. Accordingly, both the Young modulus calculated using the ROM (see Eq.

III-2) and the E3 modulus provided by the Mori-Tanaka model with cylindrical inclusions correspond to the fiber direction. Although the transversely isotropic model with cylindrical inclusions is closer to the experimental results than the one with spherical inclusions (see figure III-6), it remains a relatively rough model, showing that the reality is different and more complex than assumed. The fibers are likely oriented in several directions resulting in an anisotropic material. Moreover, the method used for manufacturing the materials causes a reduction of fiber size, with effects on their shape, the latter not being perfectly cylindrical. An avenue of research to investigate these effects consists in performing a direct Finite Element (FE) analysis from constructed geometries mimicking the composite or from grid built from 3D micro-CT images of the composite. Such a FEM based analysis is proposed in the next chapter.

III-5. CONCLUSIONS AND PERSPECTIVES

Biocomposites from PHBHV and Miscanthus *giganteus* fibers were fabricated using extrusion followed by injection molding. Tensile properties were evaluated using loading-unloading and simple traction tests. Young modulus increased slowly for low fiber contents, typically 5, 10, 20 wt %. It is necessary to attain 30 wt % of fibers to observe a significant difference in the Young modulus. Although composites appear to be more rigid when compared to the pure matrix due to the presence of the reinforcement, they exhibit a decrease of the tensile strength. This effect can be justified by the lack of adhesion between the fibers and the matrix, which causes a loss of mechanical seal under tensile stress. An evidence of this lack of adhesion is that the fibers pull out from the composites instead of being totally immersed in the matrix as shown by SEM images. Moreover, a difference in the Young modulus values calculated with the two methods (tensile tests and loading-unloading tests) was observed, indicating that PHBHV crystallize during time. This phenomenon was demonstrated by mechanical and thermal tests conducted "*a posteriori*" on the biocomposite with 5 wt % of raw fibers at different times.

The mechanical behavior of these materials was modeled by a two-phase Mori-Tanaka model where fibers were assumed either of cylindrical shape and oriented along the stress axis or spherical. The first model provides a better approximation of the experimental values of the Young Modulus, although in the reality fibers are not perfectly cylindrical and oriented in one direction. Indeed, fiber size [41, 42], shape [41] and orientation [42] may strongly affect the effective elastic properties of the composite and can explain the gap between the model and the experimental behavior. A better understanding of fibers orientation and shape via micro-CT images may be useful to implement a more accurate model. Moreover, the realization of PHBHV-based composites with different fibers size could be an interesting perspective in order to further improve the mechanical properties of these biocomposites. Lastly, as seen in the previous chapter, the adhesion between fibers and matrix can be improved by the chemical modification of vegetal fibers [24] or by a simple reactive extrusion. To this purpose, a green chemical modification of vegetal fibers could be adopted in order to obtain eco-friendly composites with improved properties. However, before studying in detail the influence of any chemical treatment on fiber/matrix adhesion, it seems more appropriate to investigate the effect of the size and arrangement of the fibers in the matrix and their influence on the mechanical behavior of the biocomposites, which will be the focus of the next chapter.

III-6. APPENDIX

III-6A. IDENTIFICATION OF THE YOUNG MODULUS OF THE MATRIX

The Young modulus of the matrix was identified by inverse analysis using as input data. Our raw input data are the slopes of the force/displacement curves of pure PHBHV samples in the unloading phase of the loading-unloading tests (see table III-4). No extensometer or other devices allowing direct measures of stress and strain were available. The average value of these slopes, *i.e.* 115 N/mm, was assumed to be the stiffness of the PHBHV sample, K_s.

A 2D Comsol model was then developed to model the part of the actual sample between the clamps of the testing machine, see figure III-A1. The effective thickness of the model was set to that of the actual sample, *i.e.* H = 0.93 mm, the material was defined as linearly elastic and homogeneous, and simple traction conditions were applied on the left and right boundaries. A parametric analysis was then performed by letting the Young modulus of the material, E_M, vary (while keeping fixed the Poisson ratio to 0.3) and the stiffness of the sample was computed as the ratio between the total force applied on the boundaries and the calculated elongation of the sample. The value of E_M best matching the experimental value was found to be about 1 GPa.
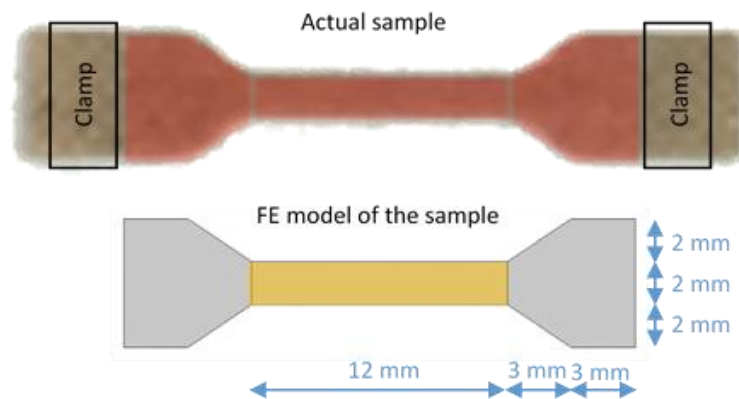
Figure III-A1. Actual sample (on the top) and 2D FE model of the sample (on the bottom); the "active" part is coloured in yellow.

Since the numerical models developed afterward focus only on the "active" part of the sample, i.e. the central rectangular region sized L × B = 12 mm × 2 mm, a shape factor χ was calculated to transform the experimental values measured on the whole sample into values corresponding to its

active part only. This shape factor is the ratio between the stiffness of the active sample, i.e. $K_a = E_M \times (B \times H)/L$, and the stiffness of the sample K_s (numerically computed). It turned out that $\chi = K_a/K_s = 1.37$. Assuming that this shape factor does not change when considering a composite sample, it allows computing the tensile modulus of composite material, E_c, based on the experimental value of the stiffness of the composite sample, K_c, namely: $E_c = \chi \times K_c \times L/(B \times H)$.

III-6B. ESTIMATION OF VOLUMETRIC FRACTION OF FIBERS IN THE SPECIMENS

The Mori-Tanaka method requires the knowledge of the volumetric fraction of the fibers in each composite specimen. This parameter $\phi_F = {V_F}/{V_C}$ is defined as the ratio between the volume of the fibers V_F and the total volume of the composite $V_C = V_F + V_M$, the volume of the matrix phase being V_M. Note that we can measure the composite volume V_C from the sample geometry. In order to obtain ϕ_F, we adopted an invasive procedure in order to separate the matrix from the fibers. First of all, every specimen manufactured by extrusion and injection molding was weighed and then solubilized under pressure and high temperature in 100 mL of dichloromethane with a rotation speed of 200 rpm for 30 minutes. After stirring, the solution was filtered and the solvent was evaporated in a static manner. Fibers were washed for 2 times with the same procedure in order to eliminate the matrix attached. The matrix and the fibers were finally collected and their mass values M_M and M_F were obtained. Then, knowing the matrix density ρ_M from the commercial provider, the fiber density ρ_F, which may vary with processing due to the various degree of compression during the injection molding procedure, is finally expressed as:

$$\rho_F = \frac{M_F}{V_C - {M_M}/{\rho_M}} \qquad \text{(III-B.1)}$$

Finally, the fiber volume $V_F = {M_F}/{\rho_F}$ can be deduced and thus the fiber volume content ϕ_F.

III-6C. EFFECT OF TIME ON MECHANICAL AND THERMAL PROPERTIES OF PHBHV-BASED COMPOSITES

In order to evaluate the change in mechanical properties due to the time, traction tests were carried out on specimens of PHBHV$_{95}$MIS$_5$ after 8 days and then after 8 months. Results of these tests are showed in figure III-C1. An increase in modulus and a decrease in the elongation at break

are visible after 8 months, confirming that the crystallization phenomenon during time observed from other researchers is valid also for our composites. In a second time, we used differential scanning calorimetry (DSC) as an additional analysis to evaluate the crystalline behavior of the biocomposites and the results obtained are showed in figure III-C2. A shift in the melt temperature from 157 to 162°C and an increase in the crystallinity degree from 28 % to 34 % are visible after 8 months. This result is a further confirmation of the crystallization phenomenon.
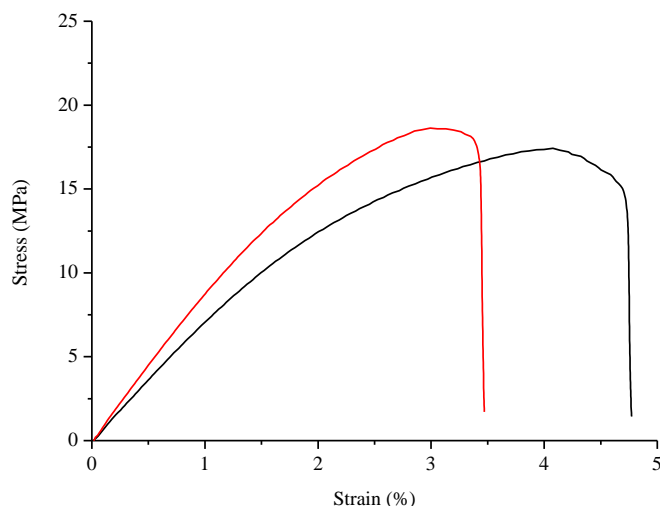
Figure III-C1. Strain-stress average curves for PHBHV$_{95}$MIS$_5$ composites tested after 8 days (black curve) and after 8 months (red curve).
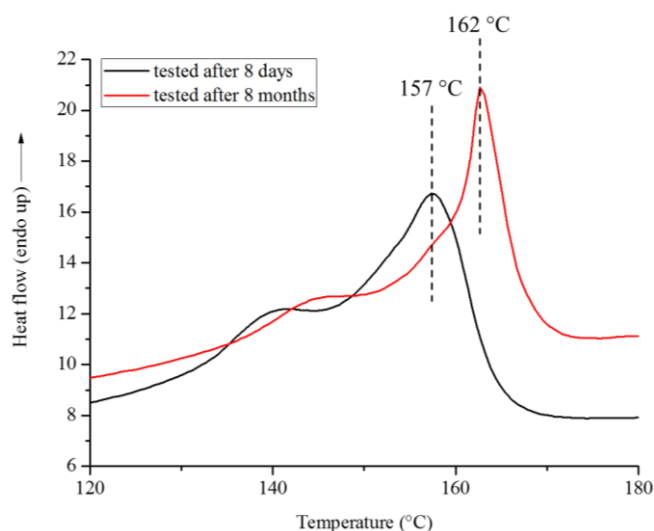
Figure III-C2. DSC first heating thermograms of PHBHV95MIS5 biocomposites tested after 8 days (black curve) and after 8 months (red curve).

III-7. REFERENCES

1.   Available from: http://www.marketsandmarkets.com/Market-Reports/wood-plastic-composite-market-170450806.html,. June 10, 2016.

2.   Gurunathan, T. et al., A review of the recent developments in biocomposites based on natural fibres and their application perspectives. *Composites Part A: Applied Science and Manufacturing* 77, p. 1-25 (**2015**).

3.   Müller, H.-M. et al., Poly(hydroxyalkanoates): A Fifth Class of Physiologically Important Organic Biopolymers? *Angewandte Chemie International Edition in English* 32(4), p. 477-502 (**1993**).

4.   Lao, H.-K. et al., Modification of Poly(3-hydroxybutyrate-co-3-hydroxyvalerate) Film by Chemical Graft Copolymerization. *Biomacromolecules* 8(2), p. 416-423 (**2007**).

5.   Brandl, H. et al., Plastics from bacteria and for bacteria: Poly(β-hydroxyalkanoates) as natural, biocompatible, and biodegradable polyesters. *Advances in Biochemical Engineering / Biotechnology* 41, p. 77–93 (**1990**).

6.   Chen, G.-Q. et al., Plastics Derived from Biological Sources: Present and Future: A Technical and Environmental Review. *Chemical Reviews* 112(4), p. 2082-2099 (**2012**).

7.   Vergnol, G. et al., Multilayer approach for tuning the drug delivery from poly(3-hydroxyalkanaoate)s coatings. *Reactive and Functional Polymers* 72(4), p. 260-267 (**2012**).

8.   Modjinou, T. et al., Poly(3-hydroxyalkanoate) sulfonate: From nanoparticles toward water soluble polyesters. *European Polymer Journal* 68, p. 471-479 (**2015**).

9.   Vergnol, G. et al., Electrografting of a biodegradable layer as a primer adhesion coating onto a metallic stent: in vitro and in vivo evaluations. *Journal of Materials Science: Materials in Medicine* 24(12), p. 2729-2739 (**2013**).

10.   Babinot, J. et al., Poly(3-hydroxyalkanoate)-derived amphiphilic graft copolymers for the design of polymersomes. *Chemical Communications* 48(43), p. 5364-5366 (**2012**).

11.   Dufresne, A. et al., Lignocellulosic flour-reinforced poly(hydroxybutyrate-co-valerate) composites. *Journal of Applied Polymer Science* 87(8), p. 1302-1315 (**2003**).

12.   Christian, S.J. et al., Mechanical response of PHB- and cellulose acetate natural fiber-reinforced composites for construction applications. *Composites Part B: Engineering* 42(7), p. 1920-1928 (**2011**).

13.   Melo, J.D.D. et al., A biodegradable composite material based on polyhydroxybutyrate (PHB) and carnauba fibers. *Composites Part B: Engineering* 43(7), p. 2827-2835 (**2012**).

14.   Luo, S. et al., Mechanical and thermal properties of environment-friendly "green" composites made from pineapple leaf fibers and poly(hydroxybutyrate-co-valerate) resin. *Polymer Composites* 20(3), p. 367-378 (**1999**).

15.   Javadi, A. et al., Processing and characterization of solid and microcellular PHBV/PBAT blend and its RWF/nanoclay composites. *Composites Part A: Applied Science and Manufacturing* 41(8), p. 982-990 (**2010**).

16.   Ten, E. et al., Effects of Cellulose Nanowhiskers on Mechanical, Dielectric, and Rheological Properties of Poly(3-hydroxybutyrate-co-3-hydroxyvalerate)/Cellulose Nanowhisker Composites. *Industrial & Engineering Chemistry Research* 51(7), p. 2941-2951 (**2012**).

17.   Ten, E. et al., Preparation and properties of aligned poly(3-hydroxybutyrate-co-3-hydroxyvalerate)/cellulose nanowhiskers composites. *Carbohydrate Polymers* 92(1), p. 206-213 (**2013**).

18.   Samain, X. et al., Grafting biodegradable polyesters onto cellulose. *Journal of Applied Polymer Science* 121(2), p. 1183-1192 (**2011**).

19.   Fischer, G. et al., Biomass potentials of miscanthus, willow and poplar: results and policy implications for Eastern Europe, Northern and Central Asia. *Biomass and Bioenergy* 28(2), p. 119-132 (**2005**).

20.   Johnson, R.M. et al., Impact performance of Miscanthus/Novamont Mater-Bi® biocomposites. *Polymer Testing* 22(2), p. 209-215 (**2003**).

21.   Bourmaud, A. et al., Investigations on mechanical properties of poly(propylene) and poly(lactic acid) reinforced by miscanthus fibers. *Composites Part A* 39(9), p. 1444–1454 (**2008**).

22. Gamon, G. et al., Twin-screw extrusion impact on natural fibre morphology and material properties in poly(lactic acid) based biocomposites. *Industrial Crops and Products* 46, p. 173-185 (**2013**).
23. Selke, S.E. et al., Wood fiber/polyolefin composites. *Composites Part A: Applied Science and Manufacturing* 35(3), p. 321-326 (**2004**).
24. Rodi, E.G. et al., Functionalization of Miscanthus by Photoactivated Thiol–Ene Addition to Improve Interfacial Adhesion with Polycaprolactone. *ACS Sustainable Chemistry & Engineering* 4(10), p. 5475-5482 (**2016**).
25. Berthet, M.A. et al., Impact of fibre moisture content on the structure/mechanical properties relationships of PHBV/wheat straw fibres biocomposites. *Composites Science and Technology* 117(Supplement C), p. 386-391 (**2015**).
26. Nemat Nasser, S. et al., Micromechanis: overall properties of heterogeneous materials, 2nd ed., Applied Mathematics and Mechanics. *North-Holland* (**1999**).
27. Qu, J. et al., Fundamentals of micromechanics of solids. Wiley & Sons, Hoboken, New Jersey (**2006**).
28. Tan, H. et al., The Mori–Tanaka method for composite materials with nonlinear interface debonding. *International Journal of Plasticity* 21(10), p. 1890-1918 (**2005**).
29. Benveniste, Y., A new approach to the application of Mori-Tanaka's theory in composite materials. *Mechanics of Materials* 6(2), p. 147-157 (**1987**).
30. Eshelby, J.D., The Determination of the Elastic Field of an Ellipsoidal Inclusion, and Related Problems. *Proceedings of the Royal Society of London. Series A. Mathematical and Physical Sciences* 241(1226), p. 376 (**1957**).
31. Sansalone, V. et al., A stochastic homogenization approach to estimate bone elastic properties. *Comptes Rendus Mécanique* 342(5), p. 326-333 (**2014**).
32. Kaack, K. et al., Variation in morphology, anatomy and chemistry of stems of Miscanthus genotypes differing in mechanical properties. *Industrial Crops and Products* 17(2), p. 131-142 (**2003**).
33. Johnson, M. et al., Improvement of the impact performance of a starch based biopolymer via the incorporation of Miscanthus giganteus fibres. *Industrial Crops and Products* 22(3), p. 175-186 (**2005**).
34. Singh, S. et al., Wood fiber reinforced bacterial bioplastic composites: Fabrication and performance evaluation. *Composites Science and Technology* 67(9), p. 1753-1763 (**2007**).
35. Ahankari, S.S. et al., Mechanical behaviour of agro-residue reinforced poly(3-hydroxybutyrate-co-3-hydroxyvalerate), (PHBV) green composites: A comparison with traditional polypropylene composites. *Composites Science and Technology* 71(5), p. 653-657 (**2011**).
36. Gunning, M.A. et al., Mechanical and biodegradation performance of short natural fibre polyhydroxybutyrate composites. *Polymer Testing* 32(8), p. 1603-1611 (**2013**).
37. Ragoubi, M. et al., Effect of corona discharge treatment on mechanical and thermal properties of composites based on miscanthus fibres and polylactic acid or polypropylene matrix. *Composites Part A: Applied Science and Manufacturing* 43(4), p. 675-685 (**2012**).
38. Bledzki, A.K. et al., Mechanical performance of biocomposites based on PLA and PHBV reinforced with natural fibres – A comparative study to PP. *Composites Science and Technology* 70(12), p. 1687-1696 (**2010**).
39. Stark, N.M. et al. Effect of species and particle size on properties of wood–flour-filled polypropylene composites, functional fillers for thermoplastics, thermosets and elastomers. in *Intertech Conferences*. 1997. San Diego, California.
40. Lorenzini, C. et al., High glass transition temperature bio-based copolyesters from poly(3-hydroxybutyrate-co-3-hydroxyvalerate) and isosorbide. *Reactive and Functional Polymers* 73(12), p. 1656-1661 (**2013**).
41. Sansalone, V. et al., Nanostructure and effective elastic properties of bone fibril. *Bioinspired, Biomimetic and Nanobiomaterials* 1(3), p. 154-165 (**2012**).
42. Sansalone, V. et al., Multiscale modeling of materials by a multifield approach: Microscopic stress and strain distribution in fiber–matrix composites. *Acta Materialia* 54(13), p. 3485-3492 (**2016**).

Chapter IV

"Knowledge would be fatal.
It is the uncertainty that charms one.
A mist makes things wonderful."

(Oscar Wilde)

Effect of fiber content, length and arrangement on the mechanical modulus of PHBHV/Miscanthus fiber composites: contribution of a finite element model

The analytical models of Mori-Tanaka applied to the biocomposites manufactured in the previous chapter have shown the limits of this homogenization technique which is not able to well approximate the real elastic behavior of the biocomposites at high fibers content. Moreover, the lack of knowledge concerning the distribution of fibers into the matrix and their effective size after processing are two of the main factors which could affect the success of the models implemented. For this reason, this chapter focuses on the effect of the fiber length and arrangement on the mechanical properties of composites made of poly(3-hydroxybutyrate-co-3-hydroxyvalerate) matrix (PHBHV) and Miscanthus giganteus fibers. Two fiber weight fractions (5% and 20%) and two different lengths (1 mm and 45 μm) were investigated. Composites of standard dimensions were realized by extrusion and injection molding processing. The samples were characterized by cyclic tensile tests and traction tests. Microscopy and micro-tomography were used as fundamental techniques to have information about fibers structure, size and arrangement in the biocomposites. Mori-Tanaka models were implemented in a different manner, considering now that cylinders and spheres can be used to represent long and short fibers respectively. 2D and 3D Finite element models with different fibers patterns were used to determine not only the elastic modulus of biocomposites but also to describe the different distribution of the stress in the matrix, taking into account by this way the non-linear behavior of the material. This work elucidates on the effect of the fibers size and it provides important information about the better orientation of fibers to achieve in the matrix in order to have composite with improved mechanical properties. This last information is strictly related to the processing method used, which is responsible of the homogeneous distribution of fibers in the matrix and also of their partial alignment in a specific direction.

IV-1. INTRODUCTION

In these last years, polymer scientists focused their researches on the development of new biodegradable polymer composite materials obtained from renewable resources [1, 2]. Wood plastic composites (WPCs) are composed by plastics, such as polyesters and natural fillers. These latter generally refer to cellulosic materials derived from wood and they are available in different forms (particles or single fibers for example), causing different properties of the final material. Despite the extraordinary progress that was made in the field of realization of biocomposites using techniques such as injection molding and extrusion [3], a reduction of the tensile strength of the final composite is often observed because of the lower interfacial adhesion between the hydrophilic fibers and the hydrophobic matrix. However, the several advantages of natural fillers such as their low cost, renewable nature, low density, high specific strength and stiffness [4, 5] and the increasing demand for these composites have drawn the attention of many researchers to investigate the fiber properties in order to design specific mechanical properties [6, 7]. Many research groups showed that the fiber content and length affect the overall properties of bio-composites [7-14]. In particular these two parameters impact the mechanical behavior of the composites. Actually, the tensile strength and the elastic modulus of the composites mainly depend on the nature of the fiber-matrix interface and on the fiber content, respectively [15]. Moreover, many studies revealed that processing methods adopted to manufacture composite strongly affect fibers sizes, varying in this way the mechanical properties of the final biocomposites [16].

In this study the effect of different fiber contents (5 and 20 weight %) and sizes (1 mm and 45 μm) on the mechanical properties of PHBHV and Miscanthus *giganteus* composites were investigated. Microscopy analysis was used to have information about fibers sizes after processing and their distribution in the biocomposites. These analyses were used as guide for the implementation of both analytical and numerical models, aiming to provide information about the elastic behavior of the materials. Results obtained by models were systematically compared to the experimental values obtained by cyclic tensile tests. Mori-Tanaka models with cylindrical and spherical inclusions were used to model the behavior of composites with long and short fibers respectively. Different 2D and 3D Finite element (FE) models, taking into account not only the fibers content and size, but also their arrangement in the matrix, were also create. To this aim four models with different degree of matrix coverage were implemented.

In this work, FE models were used not only to provide information about the elastic behavior of the composite, but also about the stress distribution in the final materials. Actually, these models are able to predict the high-stress region, gaining insights on the non-linear behavior of composites. Moreover, the results provided by the models can be useful in refining the processing methods, indicating not only the quantity of fibers but also the orientation that they must possess in order to create composite with improved mechanical properties.

IV-2. EXPERIMENTAL INVESTIGATION

In this section the materials and methods used to realize biocomposites and to characterize them were described. Extrusion and injection molding at the lab scale were chosen as processing techniques to manufacture specimens of neat matrix and biocomposites, varying the content of fibers (5 and 20 wt %) and their lengths (1 mm and 45 μm), these last obtained with sieves of specific opening mesh. The part dedicated to the characterization focused essentially on the morphology of fibers and to their effect on the mechanical properties of biocomposites. To this aim, microscopy, cyclic and tensile tests were used.

IV-2.1. MATERIALS AND PROCESSING

IV-2.1.1. Materials

Poly(3-hydroxybutyrate-*co*-3-hydroxyvalerate) ($PHB_{88}HV_{12}$) containing 12% of valerate was purchased from the company Goodfellow in a pelletized form. Miscanthus *giganteus* (MIS) was provided by Miscanplus (France) in the form of roughly cut stems. These latter were chopped and then sieved with 1 mm and 45 μm opening mesh sieves. Fibers so obtained will be referred to as long and short fibers, respectively. Note that the sieve mesh size does not correspond to the fiber size in the composite due to the effect of processing inducing a decrease in fibers dimensions.

IV-2.1.2. Composite processing

To investigate the effect of fiber amount and size on the mechanical properties of the composites, the PHBHV and the fibers were mixed together in a lab-scale twin-screw extruder (Minilab Thermo Scientific Haake). Composites with two different contents of fibers (5 and 20 wt %) were realized. The retention time for the pure matrix was of 1 minute; this time was increased to 2 minutes in order to fully disperse the fibers into the matrix. After recirculation, the extruded molten material was shot in the micro-injection unit (MiniJet Thermo Scientific Haake). The injection pressure was adjusted according to the increase of the polymer melt viscosity with the fiber content in order to obtain entire specimens of 60 mm x 20 mm x 1 mm. Final optimized parameters used for extrusion and injection-molding processing are resumed in table IV-A1 (see appendix IV-6A).

IV-2.2. MATERIALS CHARACTERIZATION

IV-2.2.1. Scanning electron microscopy

Scanning electron microscopy (SEM) observations were performed on the MIS fibers and on the sections of specimens used in traction tests (see section IV-2.2.3) using a JEOL JSM6301F scanning electron microscope. Prior to observation, the fibers and the cross sections of analyzed specimens were sputter-coated with a thin layer of gold. Images were recorded with an acceleration voltage of 20keV at a working distance of 15 mm. These images give information about the shape of the fibers and their orientation, distribution and adhesion to the matrix.

IV-2.2.2. Morphology of the fibers

In this section it seems necessary to investigate more in detail the fiber size after processing. As previously explained, processing techniques such as extrusion and injection molding in which high shear stresses are applied, have a great impact on the aspect ratio of fibers, affecting in particular their length as reported in other works [16].

The average dimensions of these fibers were analyzed through optical microscopy. To this aim, fibers were extracted from biocomposites by dissolving PHBHV in 100 mL of dichloromethane for 30 minutes and then washed for 3 times at 54°C in the same solvent to remove any trace of matrix. This procedure was successful only for long-fiber composites but failed for short-fiber composites. Actually, separation of short fibers from the matrix results in a great loss of fibers and in the impossibility to completely remove the matrix. Length (l) and width (d) were manually measured using an Olympus BX 50F optical microscope at 50x and about 30 fibers per sample were measured. Fibers were labeled to avoid duplicates and the aspect ratio (l/d) was then calculated.

IV-2.2.3. Mechanical properties of the composite

The mechanical properties of the composites were evaluated through an Instron 5965 Universal Testing Machine equipped with a cell load of 100 N. All the specimens presented standard dimensions according to ASTM638. After realization, specimens were stored for 8 days at 23°C before testing. First, cyclic tensile tests were conducted on ten specimens of each type of composite (5 wt % and 20 wt % MIS content, long and short fibers). The initial maximum load for cyclic tests was set to 3 N and the final one to 10 N with an increment of 1 N from one cycle to another (that is, 8 cycles overall). All cycles were performed at a constant speed of 0.05 N/s. Then, for each type of composite, five

specimens out of ten were tested in monotonic traction tests at a speed of 5 mm/min in order to evaluate the tensile strength and the failure stress and strain of the composites.

IV-2.3. EXPERIMENTAL RESULTS

IV-2.3.1. Scanning electron microscopy (SEM) and fibers characterization

Fibers used in this work were characterized by SEM in order to provide information about their real shape and structure before processing. Figure IV-1 shows that fibers milled with 1 mm mesh sieve maintain their classical structure with an elongated shape, while fibers milled with a 45 μm mesh sieve appear as a heterogeneous set of fibers whose structure has been destroyed by the sealing operation.
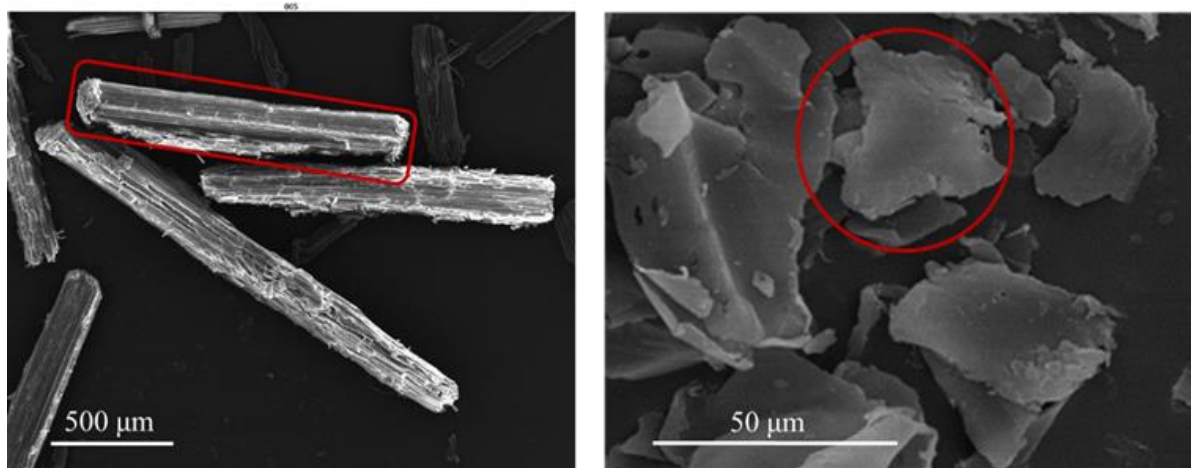
Figure IV-1. SEM images of long fibers (on the left) and short fibers (on the right) before processing.

Using the procedure outlined in section IV-2.2.2, the average fiber length and width of long-fiber composites were evaluated. All these values are reported in table IV-1. It turns out that fibers in 5 wt % MIS samples are bigger and more elongated than in 20 wt % MIS samples.

Samples	Fiber width, d [mm]	Fiber length, l [mm]	Aspect ratio, l/d
PHBHV₉₅MIS₅	0.27 ± 0.04	1.72 ± 0.33	6.4
PHBHV₈₀MIS₂₀	0.16 ± 0.01	0.82 ± 0.10	5.1

Table IV-1. Fiber size distributions in long-fiber composites with 5 and 20 wt % of MIS.

The SEM images provide important information on the shape of the fibers that will have to be taken into account in the numerical model. More precisely, it seems appropriate to assimilate the long fibers to either elongated bars or cylinders and the short ones to either cubes or spheres.

The cross sections of long- and short-fiber composites with different fiber contents (5% and 20%) were also characterized by SEM as shown in figure IV-2. For the composite realized with 5% of long fibers (figure IV-2, A1), it is possible to notice that the fibers are isolated in the matrix and perfectly identifiable. At higher fiber contents (20%), fibers tend to form aggregates (figure IV-2, B1). In all samples realized with long fibers, fibers pull out from the matrix. For what concerns the sections of the composites realized with short fibers (figure IV-2, A2 and B2), these latter are fully dispersed in the matrix and their identification is rather difficult.
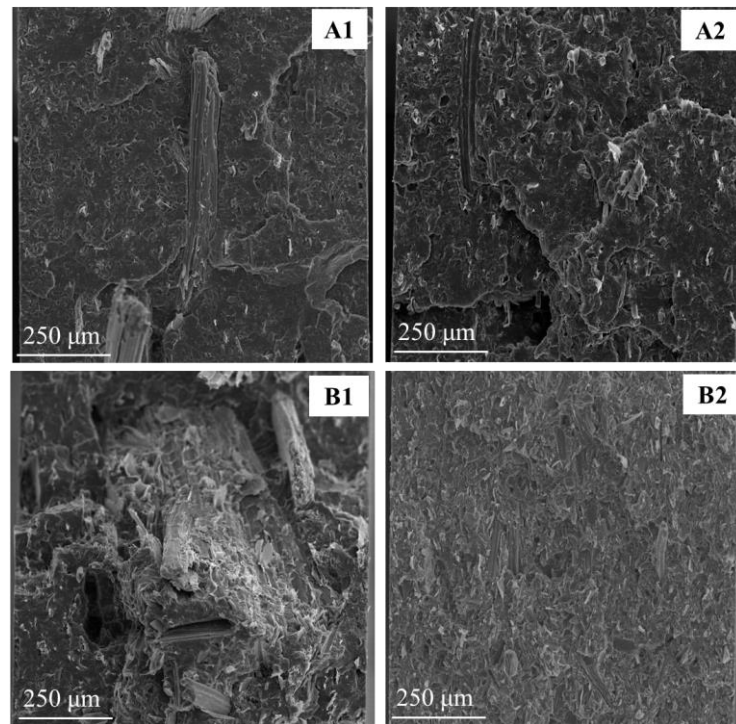
Figure IV-2. SEM images of PHBHV₉₅MIS₅ composites with long (A1) and short (A2) fibers and of PHBHV₈₀MIS₂₀ composites with long (B1) and short (B2) fibers.

IV-2.3.2. Mechanical properties of the biocomposites

The mechanical properties of the PHBHV/MIS composites were evaluated using classical tensile tests. The effect of fiber length is more pronounced in 5 wt % MIS composites (see figure IV-3) than in 20 wt % MIS composites (see figure IV-4). The presence of the fibers in the matrix causes an increase in the tensile modulus and a decrease in the tensile strength and failure strain of the composite as showed in tables IV-2 and table IV-3. For the tensile modulus, we refer to the cyclic tests which provide more reliable results than monotonic traction tests. The tensile modulus of the composites was computed based on the slope of the unloading phases in the loading-unloading tests (see table IV-2) using the procedure described in appendix III-6A in Chapter III.
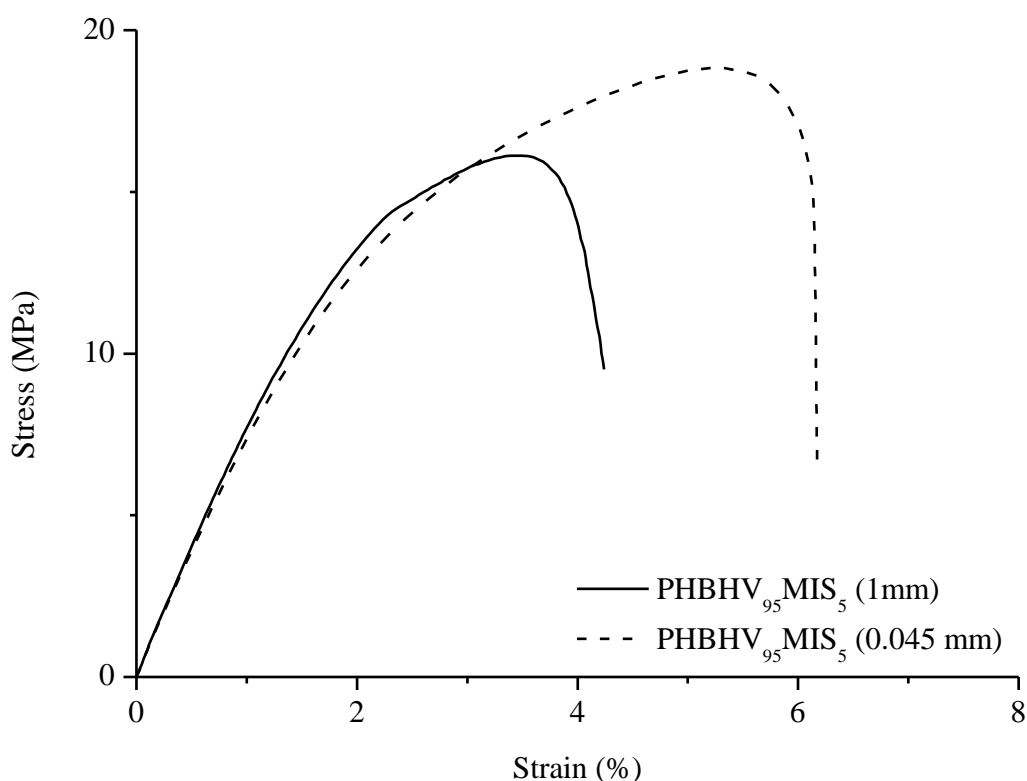
Figure IV-3. Comparison between strain-stress curves for PHBHV$_{95}$MIS$_5$ composites realized with long (solid line) and short (dashed line) fibers.
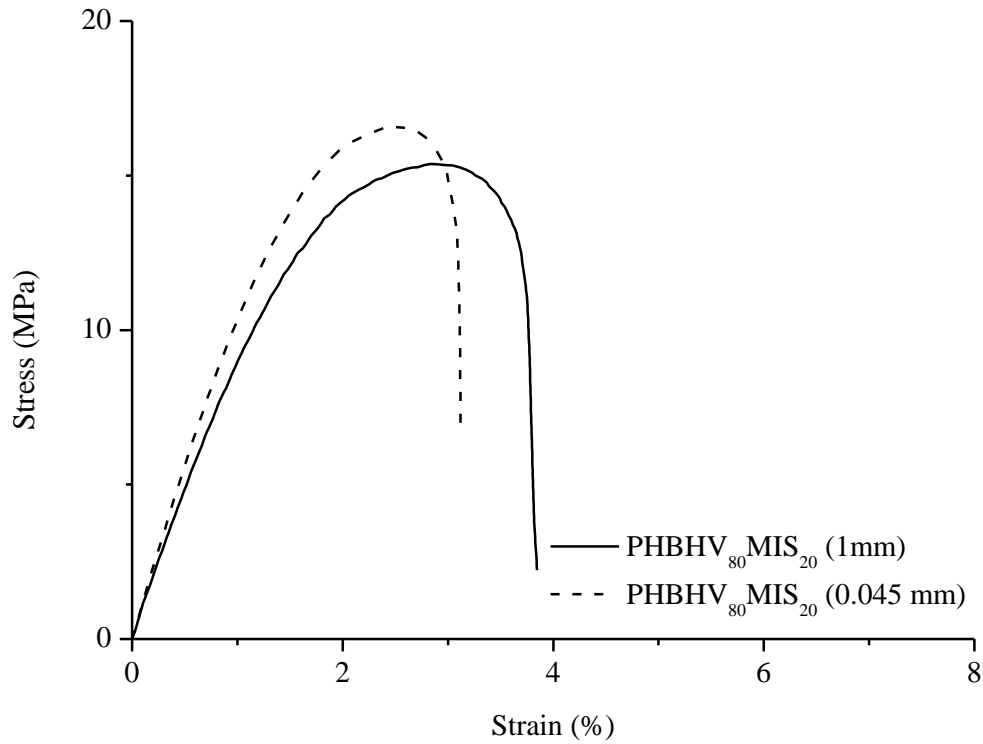
Figure IV-4. Comparison between strain-stress curves for PHBHV$_{80}$MIS$_{20}$ composites realized with long (solid line) and short (dashed line) fibers.

MIS Length	Sample	Slope of unloading phase [N/mm]	Tensile modulus (*) [MPa]
-	PHBHV	115 ± 5	1012 ± 48
45 μm	PHBHV$_{95}$MIS$_{5}$	116 ± 2	1040 ± 40
	PHBHV$_{80}$MIS$_{20}$	172 ± 11	1515 ± 93
1 mm	PHBHV$_{95}$MIS$_{5}$	134 ± 5	1185 ± 44
	PHBHV$_{80}$MIS$_{20}$	196 ± 15	1736 ± 137

Table IV-2. Results of cyclic loading-unloading tests on PHBHV/MIS composites with different fiber contents (0, 5, 20 wt %). (*) Identified, see Appendix III-6A in Chapter III.

MIS Length	Sample	Tensile modulus (*) [MPa]	Failure stress [MPa]	Failure strain [%]	Tensile strength [MPa]
-	PHBHV	889 ± 41	20 ± 0.9	11 ± 1.6	23.0 ± 0.5
45 µm	PHBHV$_{95}$MIS$_5$	1021 ± 20	16 ± 0.6	6.1 ± 0.8	18.8 ± 1.0
	PHBHV$_{80}$MIS$_{20}$	1525 ± 84	15 ± 0.7	2.9 ± 0.3	16.9 ± 0.7
1 mm	PHBHV$_{95}$MIS$_5$	1074 ± 44	14 ± 1.0	4.2 ± 0.9	16.1 ± 1.7
	PHBHV$_{80}$MIS$_{20}$	1267 ± 90	14 ± 0.4	3.5 ± 0.3	15.4 ± 1.1

Table IV-3. Results of tensile tests on PHBHV/MIS composites with different fiber contents (0, 5, 20 wt %) realized with two lengths of fibers (1 mm and 45 µm). (*) Identified, see appendix III-6A in Chapter III.

The tensile modulus increases with the fiber content irrespective of the fiber size, being almost 50 % higher in PHBHV$_{80}$MIS$_{20}$ than in PHBHV$_{95}$MIS$_5$. Moreover, the tensile modulus is higher in long-fiber composites than in short-fiber composites irrespective of the fiber content. Short-fiber composites show higher tensile strength and failure strain than long-fiber composites. This effect is quite apparent in 5 wt % MIS composites whereas it is not significant in 20 wt % MIS composites.

IV-3. NUMERICAL INVESTIGATION

Different numerical models were used to investigate the dependency of the tensile modulus of the composite in terms of its microstructure. Two modeling approaches are considered in the following sections, namely, a Finite Element (FE) approach, where the microstructure is explicitly modeled, and a homogenization approach, where a simplified representation of the microstructure is assumed. In both approaches, the focus is set on the micro-architectural features of the composite (fiber amount, size, and arrangement) while keeping fixed the elastic properties of its constituent phases. Both the matrix and fibers were considered as linearly elastic, isotropic materials and their relevant elastic moduli are shown in table IV-4. Moreover, all models consider a perfect adhesion between the fibers and the matrix.

Material	Young Modulus [GPa]	Poisson coefficient [-]	Mass density [g/cm³]
Miscanthus *giganteus*	4.5 [b]	0.3 [c]	0.70 [e]
PHBHV	1.0 [a]	0.3 [c]	1.25 [d]

Table IV-4. Elastic moduli and mass density of the constituent phases of the composite used in the numerical models. (a) Experimental value; (b) adapted from [17]; (c) Assumed; (d) Technical data; (e) Calculated according to the procedure in appendix III-6B in Chapter III.

IV-3.1. FINITE ELEMENT MODELS

Both 2D and 3D finite element (FE) models have been developed to study the effect of the micro-architectural features of the composite on its axial modulus, see table IV-5. FE models were implemented in the commercial software COMSOL Multyphysics 5.2a using the Structural Mechanics module. FE models refer to the whole active part of the sample, that is a parallelepiped domain 12 mm long (*L*), 2 mm wide (*B*) and 0.93 mm thick (*H*), see figure IV-5.

Model nb.	Model features	Effect of fiber size & amount	Effect of fiber pattern	Effect of model dimension	Fiber volume fraction	Nb. of elements	Nb. of DOFS
1	2D, Short, 5%, *Unif*	*			0.0710	39770	398906
2	2D, Short, 20%, *Unif*	*			0.2300	46368	464862
3	2D, Long, 5%, *Unif*	*		*	0.0774	554	5662
4	2D, Long, 20%, *Unif*	*	*	*	0.2296	2046	20742
5	2D, Long, 20%, *Clust*		*		0.2187	24483	245038
6	2D, Long, 20%, *RndNoise*		*		0.2203	8140	81806
7	2D, Long, 20%, *RndPattern*		*		0.2303	19067	191202
8	3D, Long, 5%, *Unif*	*		*	0.0786	13939	63201
9	3D, Long, 20%, *Unif*	*		*	0.2257	125005	521130

Table IV-5. FE model information. Column "Model features" provides information on the model dimension (either 2D or 3D), type of fibers (either long or short), nominal fiber weight fraction (%), and fiber pattern (either uniformly distributed (*Unif*), clustered (*Clust*), or randomly

distributed fibers (*RandNoise* and *RandPattern Unif*, see paragraph IV-3.1.1 for details). Columns 3 to 5 indicate the study that the models were used for. Note that the numbers of elements and degrees of freedom (DOFS) are also presented.
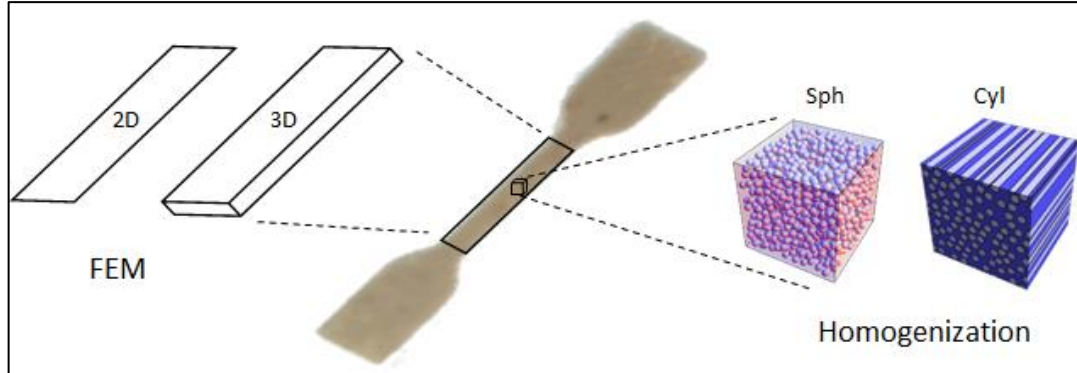
Figure IV-5. Numerical models developed in this study. On the left: FE models (2D and 3D); on the right: homogenization models (spherical and cylindrical inclusions).

For the long fibers the dimensions measured after sample processing were given and reported in table IV-1. Lacking precise information on the size of short fibers after processing, they were assumed to be equal to the nominal size of the corresponding sieve, *i.e.* 45 μm.

In each model, the number of fibers was set so as to best approximate the target nominal fiber volume fraction (about 7% and 22-24% for $PHBHV_{95}MIS_5$ and $PHBHV_{80}MIS_{20}$, respectively) while preserving a specific spatial pattern. Thus, the effective fiber volume fraction may slightly differ from the target value. Quadratic Lagrange elements either triangles in 2D or tetrahedra in 3D were used. Basic information about the FE models is reported in table IV-5. A uniformly distributed load (increasing from 0 to 20 MPa) was applied on the left and right boundaries of the simulated domain and the displacements of specific points were restricted so as to avoid rigid movements. The FE solution provided the distribution of stress and strain in the composite. The tensile modulus was eventually computed as the ratio between the average axial stress and strain in the composite.

IV-3.1.1. 2D FE models

The 2D FE models were used to investigate the effects of fiber amount, size, and distribution on the mechanical properties of the composite. The models were set up in plane stress conditions. Long fibers were modeled as rectangular domains and fiber length and width were set up according to table IV-1. Short fibers were modeled as square domains with edge length equal to the mesh sieve opening (45 μm).

The effects of fiber amount and size was investigated with respect to the models shown in figure IV-6. Fibers were uniformly distributed in the sample in a staggered pattern and spacing was adapted to best fill the whole sample according to the target fiber volume fraction.
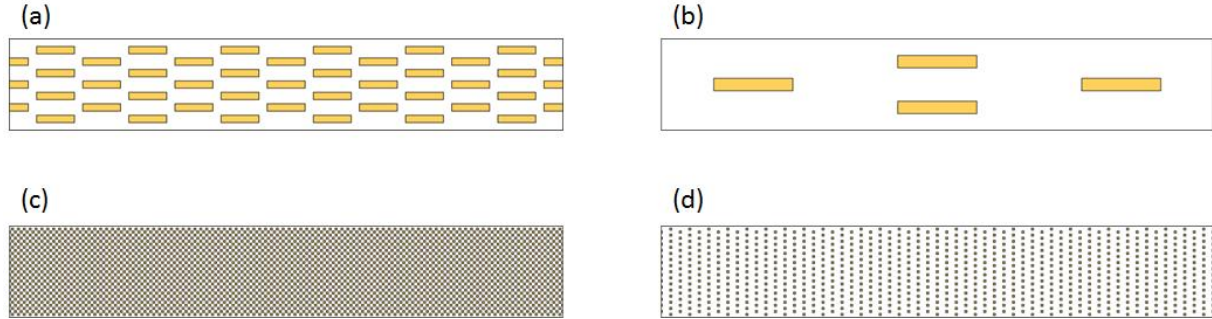
Figure IV-6. 2D FE models of long-fiber (top row) and small-fiber (bottom row) composites with 20 wt % (left column) and 5 wt % (right column) MIS fiber content.

The effects of fiber distribution was investigated by referring to long-fiber models with 20 wt % MIS fibers. Several fiber patterns were considered, namely: uniformly distributed (*Unif*), clustered (*Clust*), and randomly distributed fibers (*RandNoise* and *RandPattern*) (see figure IV-7). In the *Unif* fibers models, fibers were uniformly distributed in the sample in a staggered pattern and spacing was adapted to best fill the whole sample according to the target fiber volume fraction. In the *Clust* fibers model, fibers were placed close the center of the sample in a staggered pattern with horizontal and vertical spacing equal to 10 % of their length and width, respectively. Two types of randomly distributed fibers were considered. In the *RandNoise* models, fibers of the *Unif* models were randomly displaced by adding a random noise to their position and orientation. More precisely, random translations (tx and ty) and rotations (α) of the fibers were modeled through a centered normal distribution with standard deviations ($\sigma_{tx}=0.2\times l$, $\sigma_{ty}=0.2\times b$, $\sigma_{\alpha}=20$) and were sampled using a custom Matlab computer code. In the *RandPattern* model, fibers were randomly placed in the domain. Random position (x,y) and orientation (α) of the fibers were modeled through a uniform and a centered normal distribution ($\sigma_{\alpha}=20°$), respectively, and were sampled using a custom Matlab computer code.
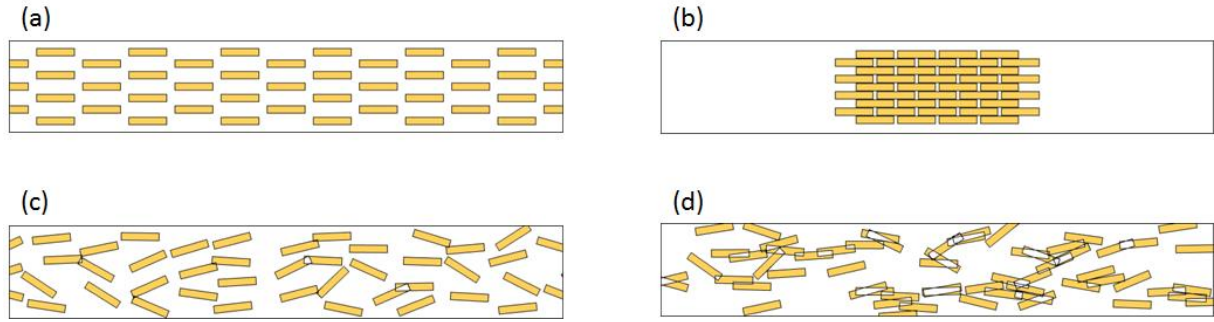
Figure IV-7. 2D FE models with different patterns of long fibers: clustered (a), staggered (b), random with small (c) and large (d) levels of randomness.

IV-3.1.2. 3D FE models

A few 3D models were also developed to investigate the effects of model dimension (2D *vs.* 3D) for 5 wt % and 20 wt % MIS composites. For sake of computational time, only long-fiber models were considered, see figure IV-8. Fibers were uniformly distributed in the sample in a 3D staggered pattern and spacing was adapted to best fill the whole sample according to the target fiber volume fraction.
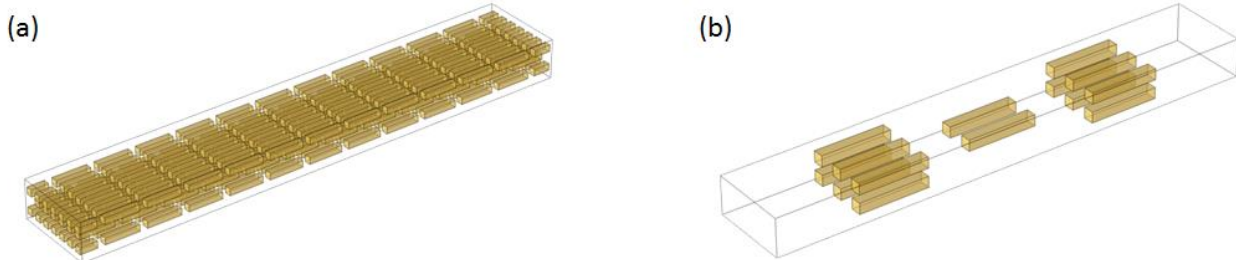
Figure IV-8. 3D FE models of long-fiber composites with 20 wt % (on the left) and 5 wt % (on the right) MIS fiber content.

IV-3.2. HOMOGENIZATION MODELS

Our homogenization approach is based on the Continuum Micromechanics (CµM) theory [18, 19]. CµM allows computing the elastic properties of a multiphase material by extending the solution of the matrix/inclusion problem obtained by Eshelby in the fifties [20]. In this framework, a simplified geometric representation of the microstructure is adopted (in particular, each phase is assumed to be made of particles of ellipsoidal shape) and the whole elastic tensor of the homogenized medium is obtained through analytical or semi-analytical formulae.

Different approximations exist in the scope of the CµM theory. For our composite, a two-phase medium of matrix/inclusion type with a small content of inclusions, the Mori-Tanaka (MT) approximation was applied [21]. Since we do not have precise information about the shape of the fibers, we considered two limit cases, namely spherical and cylindrical inclusions, corresponding to roughly spheroidal and very elongated fibers, respectively, see figure IV-5. The corresponding models will be referred to as *MT/Sph* and *MT/Cyl*, respectively and are meant to represent short- and long-fiber composites, respectively. It should be noted that the actual size of the inclusions does not enter the MT model. The *MT/Sph* and *MT/Cyl* models lead to homogenized materials showing isotropic and transversely isotropic elastic symmetry, respectively.

IV-3.3. NUMERICAL RESULTS

IV-3.3.1. Tensile modulus

The tensile moduli computed through the different numerical models (with uniformly distributed fibers) and MT models are resumed in table IV-6 and table IV-7.

MIS information		Tensile modulus [GPa]				Error in tensile modulus [%]		
[wt %]	Size	Exp	MT	2D FEM	3D FEM	MT	FEM 2D	FEM 3D
5	Short	1.04	1.11	1.09	-	6.3%	4.4%	-
	Long	1.19	1.25	1.15	1.17	5.7%	-2.9%	-1.2%
20	Short	1.52	1.36	1.30	-	-10.4%	-14.5%	-
	Long	1.74	1.80	1.51	1.62	3.9%	-12.7%	-6.4%

Table IV-6. Experimental values and numerical predictions of the tensile modulus of the composites. Exp: experimental value; MT: Mori-Tanaka model; 2D FEM and 3D FEM: FEM models with uniformly distributed fibers.

Fiber pattern	Tensile modulus [GPa]
Unif	1.51
Clust	1.29
RandNoise	1.42
RandPattern	1.45

Table IV-7. Tensile moduli of long-fiber, 20 wt % MIS composite predicted by 2D FE models with different fiber patterns. *Unif*: uniformly distributed fibers; *Clust*: clustered fibers; *RandNoise* and *RandPattern*: randomly dispersed fibers (see paragraph IV-3.1.1 for details).

Table IV-6 is aimed at highlighting the effects of fiber size and amount. Results of the MT, 2D FE (*Unif* fiber pattern), and 3D FE (*Unif* fiber pattern) models are reported and compared with the experimental results. The same results are shown in figure IV-9.
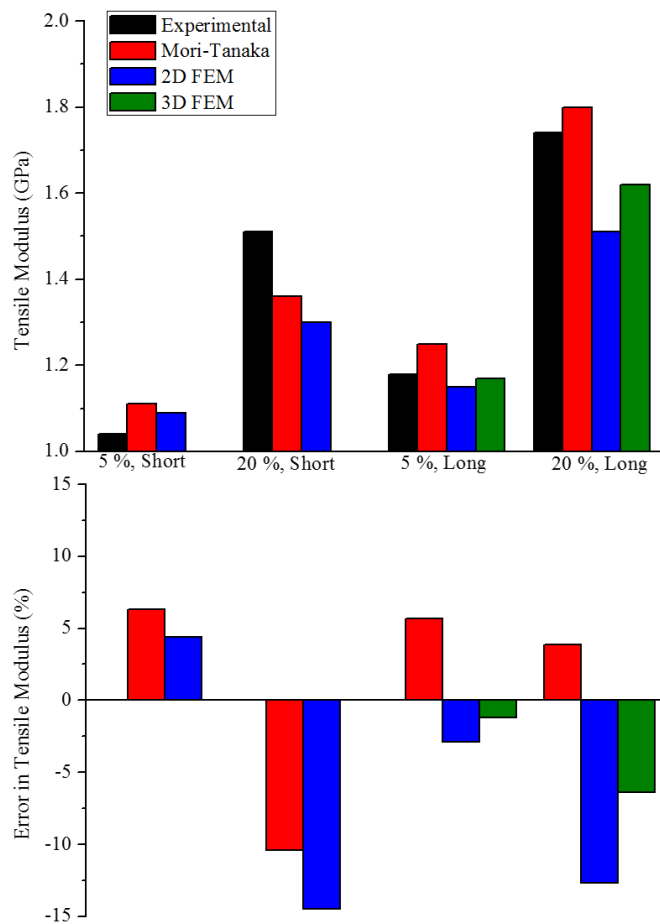
Figure IV-9. Top: Experimental and numerical values of the tensile moduli. Bottom: Relative errors of the numerical predictions with respect to the experimental measures. FE results refer to the *Unif* fiber pattern.

Results reported in table IV-7 are aimed at providing insights on the effect of the fiber pattern on the tensile modulus of the composite. The elastic moduli of long-fiber, 20 wt % MIS composites computed through 2D FE models with four different fiber patterns (*Unif*, *Clust*, *RandNoise*, and *RandPattern*) are reported.

IV-3.3.2. Stress distribution

FE models can provide useful information about the stress distribution in the composite which, in turn, can help to gain insights on the nonlinear behavior of the composites. Information about high-stress regions is reported in table IV-8. Let $\sigma_{m,y}=10$ MPa be an alias of the yield stress of the matrix and $\sigma_{c,u}=15$ MPa an alias of the tensile strength of the composite (see figures IV-3 and IV-4). Moreover, let φ_{m1} and φ_{m2} represent the volume fractions of matrix (with respect to the total volume of matrix) where the first principal stress σ_{p1} exceeds the yield stress $\sigma_{m,y}$ as the boundary traction σ is equal to $\sigma_{m,y}$ or $\sigma_{c,u}$, respectively. Values of φ_{m1} and φ_{m2} relative to several FE models are reported in table IV-8.

Model nb.	Model features	φ_{m1} [%]	φ_{m2} [%]
1	2D, Short, 5%, *Unif*	41.3	97.7
2	2D, Short, 20%, *Unif*	46.5	91.6
3	2D, Long, 5%, *Unif*	28.5	88.9
4	2D, Long, 20%, *Unif*	15.1	55.3
5	2D, Long, 20%, *Clust*	39.1	86.1
6	2D, Long, 20%, *RndNoise*	13.4	73.4
7	2D, Long, 20%, *RndPattern*	11.4	74.6
8	3D, Long, 5%, *Unif*	31.6	80.9
9	3D, Long, 20%, *Unif*	8.6	30.1

Table IV-8. Volume fractions φ_{m1} and φ_{m2} of highly stressed matrix when the boundary traction is equal to $\sigma_{m,y}$ and $\sigma_{c,u}$, respectively (see paragraph IV-3.3.2 for details). Column "Model features" provides information on the model dimension (either 2D or 3D), type of fibers (either long or short), nominal fiber weight fraction (%), and fiber pattern (either *Unif*, *Clust*, *RndNoise*, or *RndPattern*).

FE models predict that high-stress regions are larger in short-fiber composites ($\varphi_{m1} > 40\%$ and $\varphi_{m2} > 90\%$) (models **1** and **2**) than in long-fiber ones (models from **3** to **7**). In short-fiber models, the

values of φ_{m1} and φ_{m2} are similar irrespective of the MIS content. However, in long fiber-models, the values of φ_{m1} and φ_{m2} are higher in 5 wt % (model **3**) than in 20 wt% MIS models (models **4**, **6** and **7**). The only exception is constituted by the *Clust* pattern (model **5**).

The effect of the model dimension (2D *vs.* 3D) was investigated with respect to long-fiber models with *Unif* fiber pattern. 2D and 3D FE models provided similar results for a MIS content of 5 wt % (see models **3** and **8**) but not for 20 wt %, when the 2D model (model **4**) predicted high-stress regions almost two times larger than the 3D model (model **9**).

A deeper insight can be gained by looking at the distribution of high-stress regions shown in figure IV-10. Regions of the matrix where σ_{p1} exceeds $\sigma_{m,y}$ and $\sigma_{m,u}$ (the tensile strength of the PHBHV, equal to 23 MPa (see table IV-3) are depicted in gray and in red, respectively. It can be noticed that the matrix in short-fiber models is much more stressed than in long-fiber models. Moreover, σ_{p1} never exceeds $\sigma_{m,u}$ in the 2D *Unif* model whereas it does in the 2D *RandPattern* model (small red regions indicated by red arrows) which is characterized by higher stress concentration. Stress concentration appears even more in the 3D model despite the regular distribution of fibers.
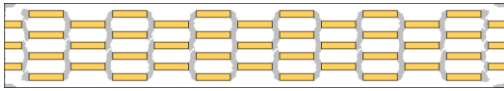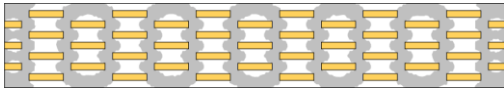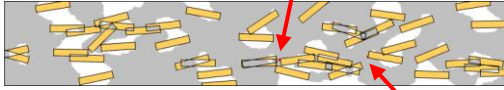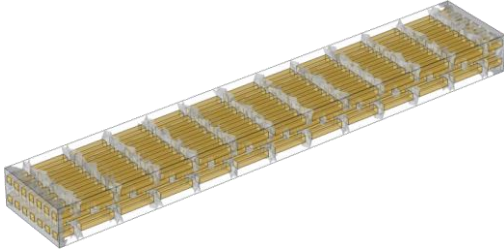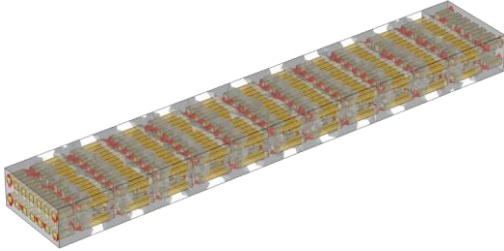
	Boundary traction = 10 MPa	*Boundary traction = 15 MPa*
2D, Short, *Unif*		
2D, Long, *Unif*		
2D, Long, *RandPattern*		
3D, Long, *Unif*		

Figure IV-10. Highly stressed regions in the matrix. Results refer to 2D and 3D FE models of 20 wt % MIS composites (namely models **2**, **4**, **7**, and **9**). Gray regions: $\sigma_{p1} > \sigma_{m,y}$; Red regions $\sigma_{p1} > \sigma_{m,u}$ (See paragraph IV-3.3.2 for details).

IV-4. DISCUSSIONS

IV-4.1. EFFECT OF FIBER LENGTH AND CONTENT ON THE MECHANICAL BEHAVIOR OF THE BIOCOMPOSITES

A familiar behavior in PHBHV based composites is an increase in tensile modulus and a decrease in failure strain and stress with increase of fiber mass content [22, 23]. These phenomena were highlighted by cyclic and monotonic tensile tests (see tables IV-2 and IV-3, respectively) and numerical simulations were used to gain further insight.

IV-4.1.1. Tensile modulus

Although the tensile modulus was calculated with both monotonic and cyclic tensile tests, we consider only these latter in our discussion. As expected, the tensile moduli increase with the fiber content, 20 wt % MIS composites showing a tensile modulus almost 50 % higher than short-fiber composites. The numerical predictions of elastic moduli globally agree with the experimental measures but in some cases substantial errors are observed (table IV-6 and figure IV-9). Despite their simplicity, MT models perform quite well for the long-fiber composites and in particular for 20 wt % MIS fibers composites. Therefore, the computational cost of such a model is absolutely negligible with respect to that of a FE simulation. FE models (*Unif* fiber pattern) perform even better for the 5 wt % MIS composites (errors < 5%) but their accuracy decrease noticeably for 20 wt % MIS composites, for which errors as high as 15% can be observed. As expected, being more realistic, 3D FE models perform better than 2D ones.

Irrespective of the fiber content, long-fiber composites are stiffer than short-fiber ones. This may be due to a shielding effect of long fibers which disappears as soon as the fibers become too short. This shielding effect can be easily observed in the stress distributions predicted by the FE models of short- and long-fiber composites shown in figure IV-10. Indeed, the region of matrix characterized by high stress in long-fiber composites is much smaller than in short-fiber composites. The difference between short- and long-fiber composites is more pronounced for 20 wt % MIS content. Actually, the very low amount of fibers in 5 wt % MIS composites is likely unable to shield the matrix. These conclusions are also supported by the values of φ_{m1} reported in table IV-8. Short-fiber models (FE models **1** and **2**) show the highest values of φ_{m1} (more than 40%), supporting the idea that the matrix is largely involved in carrying the stress. In long-fiber models, matrix is more

stressed in 5 wt % MIS models ($\varphi_{m1} \approx 30\%$) than in 20 wt % MIS models (see FE models **3** & **8** vs. **4** & **9**).

Comparing the experimental measures with the numerical results, it turns out that the elastic moduli of the long-fiber composites are overestimated by the MT models and underestimated by the FE models, irrespective of the fiber content. By contrast, all the numerical models behave similarly with respect to short-fiber composites: experimental measures are overestimated at 5 wt % and underestimated at 20 wt % fibers content.

The above discussion concerned models featuring regular fiber patterns. However, actual fiber patterns are not regular. Figure IV-11 shows the microstructures of long-fiber, 5 wt % MIS (on the left) and 20 wt % MIS (on the right) composites as imaged through micro-computed tomography (µCT). On the right, a few individual fibers are colored differently to highlight their pattern. It is apparent that in both composites fibers are randomly oriented and, although most of them are roughly aligned with the sample axis, a significant fraction is not. Fiber distribution may affect the elastic modulus of the composites and was investigated by means of 2D FEM models of long-fiber, 20 wt % MIS composites. On the one hand, results reported in table IV-7 show that *Unif*, *RandNoise* and *RandPattern* patterns provide similar estimates of the tensile modulus, the former leading to the higher value. In view of the µCT images in figure IV-11, it appears that the concept of representative volume element (RVE) that was defined in the introductive chapter may be delicate to be properly defined here. Indeed, the scale separation between inclusions and the sample seems quite limited and the statistical distribution and orientation of the fibers may vary for different samples. Notwithstanding this limitation to provide a convenient theoretical representation of the various synthetized composites, the *RandPattern* pattern seems to be the most realistic one. However, the best estimate of the experimental elastic modulus is provided by the *Unif* pattern. On the other hand, the *Clust* pattern provides a much smaller estimate of the tensile modulus and results in a quite compliant composite. These results point out the importance of controlling the fiber pattern during the processing of the composite. Indeed, a fiber pattern as regular as possible is likely to increase the elastic modulus of the composite whereas the presence of clusters of fibers should be prevented since it is expected to have a negative effect.
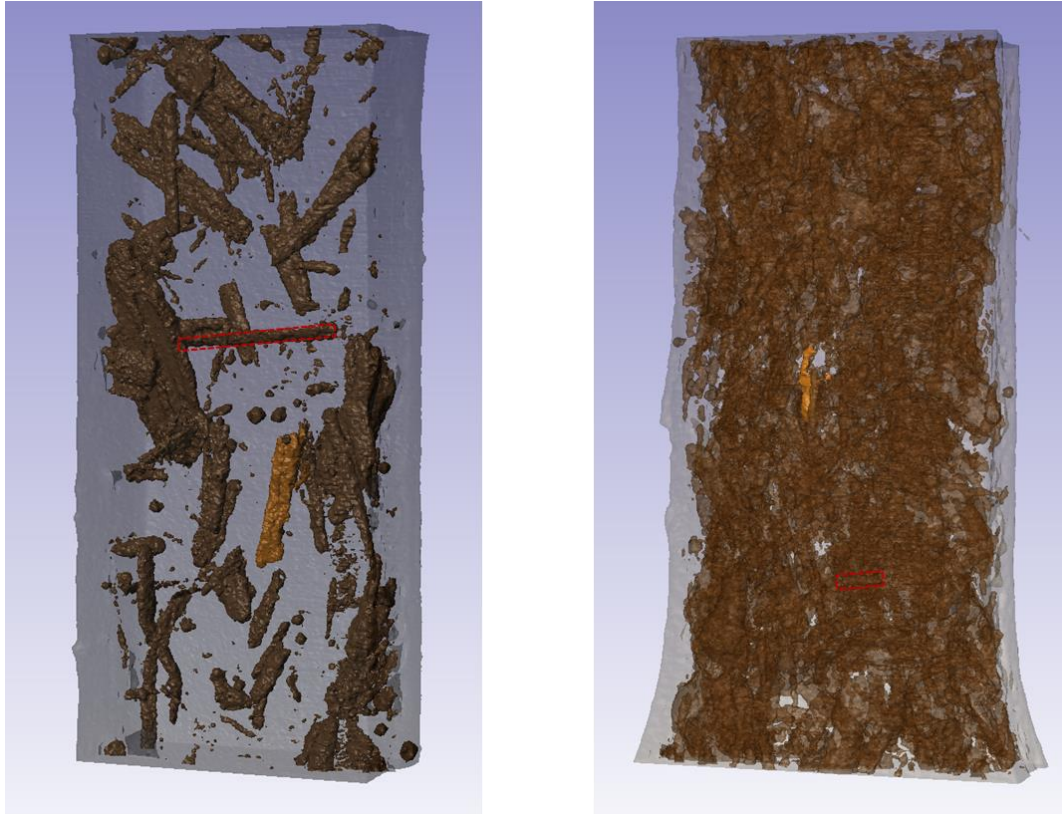
Figure IV-11. Images of long-fiber, 5 wt % MIS (on the left) and 20 wt % MIS (on the right) composites obtained through micro-computed tomography. A few individual fibers are colored differently to highlight their pattern.

IV-4.1.2. Tensile strength

The increase in final strength observed in short-fiber with respect to long-fiber composites (See figures IV-3 and IV-4) may be due to the fact that, at the same fiber content, shorter fibers are better distributed within the volume of the sample, making the composite material more homogeneous. In this case, the transmission of the applied stress is much more efficient and the propagation of microcracks is more difficult than in long-fiber composites. In the case of composites realized with long fibers, the stress concentration around the fibers is higher and the propagation and merging of microcracks is easier due to the deflection and guidance phenomena occurring along the fibers.

Numerical results point in the same direction. Indeed, looking at the stress distribution in the matrix shown in figure IV-10, it is apparent that the matrix in short-fiber composites is more homogeneously stressed than in long-fiber ones where stress concentration around the fibers arise (gray regions). This means that most of the matrix is involved in carrying stress in short-fiber composites whereas, in long-fiber composites, only a small part of the matrix is concerned with

transferring stress between the fibers therefore locally reaching higher values of stress. Stress concentration is even more pronounced considering realistic fiber patterns or 3D models. In these latter cases, very high stress levels appear in the matrix (red regions). These conclusions are supported by the values of φ_{m1} and φ_{m2} reported in table IV-8. Indeed, the larger values of φ_{m1} and φ_{m2} are observed in short-fiber composites (models **1** and **2**).

Experimental results show that the impact of fiber length on the tensile strength of the composite is stronger for low contents of fibers, typically 5 wt % (see figure IV-3). At 20 wt % of fiber content, the effect of fiber length on the mechanical properties of the final composites is reduced (see figure IV-4). This effect can be explained by the fact that at high fiber contents, the composite cannot be considered as a real diluted and homogeneous system. For both long and short fibers, the interaction between fibers is predominant than the interaction between matrix and fibers. These latter tend to improve the formation of aggregates and are distributed in all the section independently of their length, thus the stress is transmitted in the same way through the sections of the composites and this may explain the fact that the final tensile strength does not increase.

Numerical results do not agree with the experimental results. Indeed, according to the values of φ_{m1} and φ_{m2} reported in table IV-8, one would expect the main differences between short- and long-fiber composites to appear at 20 wt % of fiber content. For instance, referring to the 2D FE models with *Unif* fiber pattern (models **1** to **4**), the ratio between the values of φ_{m1} in short- and long-fiber models is about 3 at 20 wt % and about 1.5 at 5 wt % fiber content. A possible explanation is related to the fact that the results of the FE models have been obtained through a linear analysis which cannot account for microcracks transmission and deflection. Since these phenomena are likely the main determinants of the tensile strength of the composites, an important feature is missed in these models.

IV-5. CONCLUSIONS

Biocomposites realized with PHBHV as matrix and Miscanthus *giganteus* as reinforcement were realized by extrusion and injection molding processing. The effect of fiber content, length and arrangement were studied by the realization of composites at 5 wt % and 20 wt % of MIS fibers and with two different lengths (1 mm and 45 µm). First results showed that processing has a great impact on fibers size and orientation in the matrix. This limits the possibility to properly derive a convenient RVE. The large surface area exposed from 45 µm particles facilitate stress transfer to the matrix phase, increasing the final strength of the composites realized with 5 wt % of fibers. For composites with higher content of fibers, typically 20 wt %, the particle-particle interaction is predominant on the matrix-particle one and there is no evident effect of fiber length on the tensile strength. These results were also supported by numerical simulations. The transmission of the applied stress is much more efficient in the case of composites realized with short fibers, making more difficult the propagation of microcracks than in long-fiber composites where fibers guide the cracks propagation. Irrespective of the fiber content, long-fiber composites are stiffer than short-fiber ones. This effect might be due to a shielding effect of long fibers which is not visible for short-fiber composites. This effect is more pronounced for 20 wt % MIS content.

The developed models aim at understanding the elastic behavior of the biocomposites by mimicking a tensile test and thus determining their elastic moduli. This parameter depends both on fibers content and fibers distribution. Biocomposites with 20 wt % MIS fibers exhibit a modulus higher than those with 5 wt % MIS fibers. Irrespective of the fiber content, the Mori-Tanaka models overestimate the experimental values of long-fiber composites. Despite their simplicity, this technique allow to a good approximation of the elastic behavior of composites realized with 20 wt % of long fibers. Among all FE models implemented, undoubtedly 3D FE models are more realistic than their corresponding 2D. However, it seems that no model represents perfectly the experimental elastic modulus of biocomposites, overestimating or underestimating the real value of elastic modulus. Despite this result, an important conclusion can be deducted from models with different fibers distribution. In this case, composites with uniform pattern of fibers provide the best estimate of the experimental elastic modulus, while composites with clusters of fibers provide the worsts. This result suggests that the processing methods have to be better controlled, both during the homogenization step occurring in the extruder and during the injection of fibers, this last causing a partial alignment of fibers. Due to the numerical cost of 3D FEM analysis that is very much higher than applying the Mori-Tanaka approach and the remaining uncertainties induced by the processing,

it seems that the simpler second method should be preferred to *in silico* tailor the mechanical properties of the composites.

IV-6. APPENDIX

IV-6A. PROCESSING PARAMETERS DURING EXTRUSION AND INJECTION MOLDING

Biocomposites realized with different content of fibers (5 and 20 wt %) and two different fibers lengths (1 mm and 45 µm) were realized by extrusion and injection molding. Some of the parameters adopted during the processing steps are reported in table IV-A1. The processing temperatures T_E, T_I and T_m corresponding to the extrusion, injection and mold temperatures respectively were maintained the same in order to compare all the specimens. The screw speed was set to a fixed value of 60 t/min.

T_E [°C]	n [t/min]	T_I [°C]	T_m [°C]
160	60	165	45

Table IV-A1. Final parameters used in extrusion and injection molding procedure.

IV-7. REFERENCES

1. Sahari, J. et al., Natural fibre reinforced biodegradable polymer composites. *Rev. Adv. Mater. Sci* 30(2), p. 166-174 (**2011**).
2. Mohanty, A.K. et al., Natural fibers, biopolymers, and biocomposites. CRC press (**2005**).
3. Zhang, K. et al., Co-Injection Molded New Green Composites from Biodegradable Polyesters and Miscanthus Fibers. *Macromolecular Materials and Engineering* 299(4), p. 436-446 (**2014**).
4. Mohanty, A. et al., Sustainable bio-composites from renewable resources: opportunities and challenges in the green materials world. *Journal of Polymers and the Environment* 10(1), p. 19-26 (**2002**).
5. Azizi Samir, M.A.S. et al., Review of recent research into cellulosic whiskers, their properties and their application in nanocomposite field. *Biomacromolecules* 6(2), p. 612-626 (**2005**).
6. Gallagher, L.W. et al., The effect of micron sized wood fibers in wood plastic composites. *Maderas. Ciencia y tecnología* 15(3), p. 357-374 (**2013**).
7. Stark, N.M. et al., Effects of wood fiber characteristics on mechanical properties of wood/polypropylene composites. *Wood and fiber science* 35(2), p. 167-174 (**2007**).
8. Klyosov, A.A., Wood-plastic composites. John Wiley & Sons (**2007**).
9. Migneault, S. et al., Effect of fiber length on processing and properties of extruded wood-fiber/HDPE composites. *Journal of Applied Polymer Science* 110(2), p. 1085-1092 (**2008**).
10. Bouafif, H. et al., Effects of fiber characteristics on the physical and mechanical properties of wood plastic composites. *Composites Part A: Applied Science and Manufacturing* 40(12), p. 1975-1981 (**2009**).
11. Basiji, F. et al., The effects of fiber length and fiber loading on the mechanical properties of wood-plastic (polypropylene) composites. *Turkish Journal of Agriculture and Forestry* 34(3), p. 191-196 (**2010**).
12. Zaini, M.J. et al., The effect of filler content and size on the mechanical properties of polypropylene/oil palm wood flour composites. *Polymer International* 40(1), p. 51-55 (**1996**).
13. Venkateshwaran, N. et al., Effect of fiber length and fiber content on mechanical properties of banana fiber/epoxy composite. *Journal of Reinforced Plastics and Composites* 30(19), p. 1621-1627 (**2011**).
14. Fu, S.-Y. et al., Effects of fiber length and fiber orientation distributions on the tensile strength of short-fiber-reinforced polymers. *Composites Science and Technology* 56(10), p. 1179-1190 (**1996**).
15. Thomason, J.L. et al., Influence of fibre length and concentration on the properties of glass fibre-reinforced polypropylene: 1. Tensile and flexural modulus. *Composites Part A: Applied Science and Manufacturing* 27(6), p. 477-484 (**1996**).
16. Gamon, G. et al., Twin-screw extrusion impact on natural fibre morphology and material properties in poly (lactic acid) based biocomposites. *Industrial crops and products* 46, p. 173-185 (**2013**).
17. Kaack, K. et al., Variation in morphology, anatomy and chemistry of stems of Miscanthus genotypes differing in mechanical properties. *Industrial crops and products* 17(2), p. 131-142 (**2003**).
18. Continuum Micromechanics. 1 ed. CISM International Centre for Mechanical Sciences. Springer-Verlag Wien (**1997**).
19. Zaoui, A., Continuum micromechanics: survey. *Journal of Engineering Mechanics* 128(8), p. 808-816 (**2002**).
20. Eshelby, J.D., The Determination of the Elastic Field of an Ellipsoidal Inclusion, and Related Problems. *Proceedings of the Royal Society of London. Series A. Mathematical and Physical Sciences* 241(1226), p. 376-396 (**1957**).
21. Nemat-Nasser, S. et al., Micromechanics: overall properties of heterogeneous materials. Elsevier.Vol. 37. (**2013**).
22. Singh, S. et al., Renewable resource based biocomposites from natural fiber and polyhydroxybutyrate-co-valerate (PHBV) bioplastic. *Composites Part A: Applied Science and Manufacturing* 39(5), p. 875-886 (**2008**).
23. Avella, M. et al., Poly(3-hydroxybutyrate-co-3-hydroxyvalerate)-based biocomposites reinforced with kenaf fibers. *Journal of Applied Polymer Science* 104(5), p. 3192-3200 (**2007**).

Chapter V

*"Experience is the name
everyone gives
to his mistakes."*

(Oscar Wilde)

BIOCOMPOSITES BASED ON POLY(3-HYDROXYBUTYRATE-*CO*-3-HYDROXYVALERATE) (PHBHV) AND MISCANTHUS *GIGANTEUS* FIBERS : MULTIPHASE MODELING OF THE EFFECTIVE MECHANICAL BEHAVIOR OF BIOCOMPOSITE WITH IMPROVED FIBER/MATRIX INTERFACE

This chapter is dedicated to the realization of green biocomposites based on Poly(3-hydroxybutyrate-co-3-hydroxyvalerate) (PHBHV) and Miscanthus giganteus fibers (MIS) prepared in the presence of dicumyl peroxide (DCP) via reactive extrusion. The objective of this study was to optimize the interfacial adhesion between the reinforcement and the matrix, improving the mechanical properties of the final material. To this aim, two fibers mass fractions (5 and 20 wt %) and two different fibers sizes obtained by two opening mesh sieves (1 mm and 45 μm) were investigated. The impregnation of fibers with DCP before processing was carried out in order to promote the PHBHV grafting onto MIS fibers during the process, favoring in this way the interfacial adhesion between fibers and matrix instead of the cross-linking of the matrix. All composites were realized by extrusion and injection molding processing and then characterized by tensile tests, FTIR-ATR, SEM, DSC and XRD. According to the improved adhesion of fibers to matrix due to DCP, we carried out an implementation of both analytical and numerical models involving a perfect interface that can predict the effective mechanical properties of the biocomposites. Three phases were taken into account here: cylindrical inclusions mimicking aligned fibers and cross-linked or not matrix fractions. Due to the complexity of the system (matrix-crosslinked matrix-fibers) and to the lack of knowledge about all the phenomena occurring during the reactive extrusion, a mathematical approach was considered in order to obtain information about the modulus of the cross-linked matrix and its fraction in the composites. This study aims to estimate these last values and to clarify the effect caused by the presence of vegetal fibers in a composite in which different reaction are promoted by DCP.

V-1. INTRODUCTION

In recent years, the attention of both academia and industry was focused on eco-friendly materials from renewable resources due to the growing concern over environmental issues. The pollution caused by non-biodegradable synthetic plastics led to the investigation of totally bio-based polymers that could replace the first ones [1-7] . A class of polyesters of great interest is microbial polymers known as poly(3-hydroxyalkanoate)s (PHAs). This family of polymers is known for the good biodegradability and biocompatibility, being derived from bacterial synthesis [8-10]. These polymers have been used for a wide range of applications, starting from biomedical such as for tissue engineering and bone replacement to packaging, agriculture and personal disposal articles [8, 11-13].

Among PHAs, two of major polymers that have been largely investigated are the poly(3-hydroxybutyrate) (PHB) and poly(3-hydroxybutyrate-*co*-3-hydroxyvalerate) (PHBHV). The difficulty in processing and the very brittle character of PHB are two reasons explaining our interest on the second polymer. Notwithstanding its better flexibility due to the HV units, its high cost limits the usage of PHBHV in industrial applications. In this context, green composites associating such bio-based polymers and vegetal fibers constitute an attractive alternative due to their lower cost, biodegradability, renewability, and pretty good mechanical properties [14-27].

Among all vegetal fibers, Miscanthus *giganteus* has a great number of advantages, like the possibility to be cultivated on poor quality soil and in the presence of very little amount of herbicide and water [28-30], the high productivity in particular in temperate climates [31, 32] with good yield also in relatively cold zones [33]. These features and the variegated mechanical properties [34, 35] make Miscanthus as a good candidate for the production of fuels and chemicals [36] and also as reinforcement [37]. Although all these advantages, the hydrophilic character of vegetal fibers and the hydrophobic one of bio-based polyesters, affect the transmission of the stress, resulting in poor mechanical properties [38].

Interfacial adhesion could be improved by different techniques already tested [39-47]. Recently the free radical grafting initiated by peroxides has been largely used in different polymeric blends to induce coupling between molecular chains [44, 48] but also to graft cellulosic fibers or wood derivatives to different matrixes [49-53]. Although the biocomposites realized in precedent works were fully characterized by mechanical and thermal tests, indicating a decrease in crystallinity after addition of the reinforcement and DCP, no studies were carried out to predict the effective mechanical behavior of these types of composites with compatibilized interface matrix/fibers.

Numerical models based on a kinetic approach were implemented in past years to predict the molecular weight distribution as function of time for polyolefin crosslinked in the presence of peroxides [54-57]. Other models based on statistical approaches [58-60] and Monte Carlo simulations tried to predict a series of reactions that may occur during the crosslinking in order to fully characterize this complex process [61]. Among all these methods, kinetics models were preferred to statistical ones due to the impossibility of these last to predict the reactions as function of time, but only as function of conversion. However, in such cases the mathematical analyses implemented were too much simplistic for real polymers or too much specific to particular compositions or reactions [61]. In this study we proposed an approach based on the reactive grafting initiated by DCP in order to improve the adhesion of Miscanthus fibers to a PHBHV matrix with a consequent improvement of the mechanical properties of the final composite. The reaction was conducted in situ using extrusion followed by injection molding processing and the final materials were fully characterized to detect any possible change in the crystalline structure. Starting from the experimental procedure, a modeling strategies based on the inclusion theory of Eshelby was proposed to calculate the effective elastic behavior of a composite realized by this technique. The confrontation between experimental and numerical results doesn't provide a perfect agreement, showing that the complexity of the system and the lack of knowledge about cross-linking and grafting phenomena occurring during the reactive process need to be clarify more in details. In particular the elastic properties of the cross-linked matrix and its exact fraction in the composites constitute two great limits for the implementation of realistic models. To this aim a mathematical approach was considered in order to evaluate the change of the elastic modulus of the cross-linked matrix as function of its fraction in the composites. This procedure clarify the role of DCP and that of fibers in the reactive blend, quantifying a range of cross-linked fraction matrix generated by a given content of DCP and for a given content of fibers.

V-2. EXPERIMENTAL

V-2.1 MATERIALS

Poly(3-hydroxybutyrate-*co*-3-hydroxyvalerate) (PHBHV) containing 12 % of valerate was purchased from Goodfellow. Miscanthus *giganteus* (MIS) was provided by Miscanplus, France. It came from a 2014 spring crop roughly chopped and subsequently milled with two different sieves with an opening mesh of 1 mm and 45 µm. For simplicity, in this work fibers so obtained will be referred to as long and short fibers, respectively. Dicumyl peroxide (DCP) at 98% was purchased from Sigma-Aldrich.

V-2.2 CHEMICAL TREATMENT OF MISCANTHUS GIGANTEUS FIBERS

The surface of Miscanthus *giganteus* fibers was modified using the dicumyl peroxide (DCP). All kinds of fibers were dried at 80°C in a conventional oven for 4 hours and then impregnated in a solution (8 mg/ml) of DCP in acetone. The quantity of DCP was varied from 0.25 to 2.2 and 5 wt % of the total mass used during the compounding step. Solutions were stirred for 30 minutes at 200 rpm and fibers were then dried statically before the realization of composites until total evaporation of the solvent, this last evaluated by gravimetric analysis.

V-2.3 COMPOSITE MANUFACTURING

Before processing, PHBHV pellets and raw fibers were dried under vacuum at 80°C for 4 hours in order to avoid the presence of moisture during the mixing step. Composites with two different content of fibers (20 wt % and 5 wt %) were realized by mixing together the matrix and the fibers, modified or not, in a lab-scale twin-screw extruder (Minilab Thermo Scientific Haake). The experiments were performed at 160°C (T_E) with a screw speed of 60 rpm (n). The retention time for the pure matrix was of 1 minute; this time was increased to 2 minutes in order to fully disperse the fibers into the matrix. After recirculation, the molten material was shot in a micro-injection unit (MiniJet Thermo Scientific Haake) at a variable pressure depending on the fibers weight fraction applied for 30 seconds. A maintenance pressure, lower than that used during the phase of injection, was applied for other 30 seconds. The collector and the mold temperatures were set at 165°C (T_I) and 45° (T_m) respectively. The injection pressure was adjusted according to the increase of the polymer melt viscosity with the fiber content in order to have entire specimens of 60 mm x 20 mm x 1 mm.

V-2.4 MATERIALS CHARACTERIZATION

V-2.4.1 Gel fraction

After processing, the gel content for the composite $PHBHV_{80}MIS_{20}$ (DCP) was evaluated by solvent extraction. Samples (2 g) were extracted with 150 mL of $CHCl_3$ using a Soxhlet for 24 hours. The non-reacted PHBHV was extracted by the solvent, while gel and fibers were recovered after extraction and dried until recovering constant weight. The knowledge of the total mass (gel + fibers) and the knowledge of the fibers mass fraction present in the composite, allow to calculate the exact weight of the gel and as consequence its percentage by gravimetric analysis using the following expression:

$$Gel\ (\%)= \frac{W_{gel}}{W_0}\ 100 \qquad\qquad (V-1)$$

where W_{gel} and W_0 are respectively the dry weights of isolated gel and of initial material.

V-2.4.2 Mechanical testing

Tensile modulus, tensile strength and failure strain for all realized composites were evaluated using an Instron 5965 Universal Testing Machine equipped with a cell load of 100 N. All specimens presented standard dimensions according to ASTM638 and they were stored at 23°C before testing 8 days after the realization day. The mechanical characteristics of composites were evaluated by tensile tests. For each type of composite 10 specimens were tested at a speed of 5 mm/min. At the end of the mechanical procedures curves were averaged in order to obtain one averaged curve representative of each type of composite. Tensile modulus values were calculated using the procedure already described in the chapter III (see appendix 6A).

V-2.4.3 Scanning electron microscopy (SEM)

SEM observations were performed on the fracture sections of composites using a JEOL JSM6301F scanning electron microscope. Prior to observation, the cross sections of analyzed specimens were sputter-coated with a thin layer of gold. Images were recorded with an acceleration voltage of 20keV at a working distance of 15 mm.

V-2.4.4 Fourier Transform Infrared Spectroscopy (FTIR)

Specimens of PHBHV/MIS and PHBHV/MIS/DCP composites realized with fibers of 1 mm length were solubilized in dichloromethane in order to separate fibers from matrix. Then, the collected fibers were extracted for 3 times in 100 mL of dichloromethane at 54°C, stirring for 30 minutes at 200 rpm. Fibers were then dried before analysis. Infrared spectra of the extracted fibers were recorded using a TENSOR27 Brucker apparatus equipped with an attenuated internal reflection accessory using a diamond crystal (Digi Tech DLATGS Detector, 32 scans, 4 cm^{-1}) in the range 500-4000 cm^{-1}. These spectra were then compared with that of raw Miscanthus fibers. In order to quantify the grafting of PHBHV on the MIS fibers due to the DCP, the ratio R_1 was calculated as follows:

$$R_1 = \frac{I_{1726\ cm^{-1}}}{I_{1604\ cm^{-1}}} \qquad\qquad (V\text{-}2)$$

where I_{1726} corresponds to the intensity of carbonyl group of PHBHV and I_{1604} corresponds to the intensity of the esters present in the lignin structure. A measure of crystallinity was also evaluated using another index: the crystallinity index (*CI*) [50] which is the ratio of intensity of the band sensitive to crystallization to the band insensitive to the crystallization, in our case defined as follows:

$$CI = \frac{I_{1225\ cm^{-1}}}{I_{1452\ cm^{-1}}} \qquad\qquad (V\text{-}3)$$

where I_{1225} is assigned to the C-O-C stretching mode of the crystalline parts and I_{1452} corresponds the asymmetric deformation of the methylene groups.

V-2.4.5 Differential Scanning Calorimetry (DSC)

Differential scanning calorimetry experiments were performed on a PerkinElmer Diamond DSC Apparatus. Sample of around 10 mg sealed in aluminum pans were initially heated from -60°C to 200°C at 20°C/min, cooled down rapidly and then reheated in the same conditions used in the first heating run. Melting point (T_M) and melting enthalpy (ΔH_M) were determined during the first heating. The degree of crystallization (X_c) was then calculated using the following equation:

$$X_c(\%) = \frac{\Delta H_M}{\Delta H_0 * W} * 100 \qquad\qquad (V\text{-}4)$$

where ΔH_0 corresponds to the melting enthalpy of a 100% crystalline PHBHV (146 J/g) [62] and *W* is the PHBHV weight fraction present in each the blend realized.

V-2.4.6 X-ray Diffraction (XRD)

Structural characterizations of Miscanthus fibers and PHBHV/MIS composites with and without DCP were determined by X-Ray diffraction (XRD) using a D8 advance Bruker diffractometer operating at 40kV and 40 mA with a CuKα radiation. The whole area investigated was in the range $2\theta \approx 5\text{-}40°$ at a scanning rate of 0.2°/min.

V-3. RESULTS AND DISCUSSION

V-3.1 EVALUATION OF PHBHV GRAFTING ONTO MIS SURFACE DURING PROCESSING EVALUATED BY FTIR-ATR ANALYSIS

During the extrusion process, the peroxide decomposes creating free radicals that can react with the macromolecular chains of the PHBHV forming ternary radicals. These last have two possibilities, they can react with vegetal fibers constituents or they can react each other with a cross-linking effect on the PHBHV. In this work DCP was not directly added into the extruder but fibers were previously impregnated with DCP and then they were processed in the extruder with the matrix. This procedure was preferred in order to promote the grafting effect instead of the cross-linking of the matrix. Using this technique, different biocomposites were prepared varying the content of fibers (5 and 20 wt %), the length of fibers (1 mm and 45 µm) and the content of DCP (0, 0.25 and 2.2 wt %). All composites realized are listed in Table V-1.

Reference	Sample	MIS length	DCP [wt%]
	PHBHV	-	0
1	PHBHV$_{95}$MIS$_5$	1 mm	0
2	PHBHV$_{95}$MIS$_5$	1 mm	0.25
3	PHBHV$_{95}$MIS$_5$	1 mm	2.20
4	PHBHV$_{95}$MIS$_5$	45 µm	0
5	PHBHV$_{95}$MIS$_5$	45 µm	0.25
6	PHBHV$_{95}$MIS$_5$	45 µm	2.20
7	PHBHV$_{80}$MIS$_{20}$	1 mm	0
8	PHBHV$_{80}$MIS$_{20}$	1 mm	2.20
9	PHBHV$_{80}$MIS$_{20}$	45 µm	0
10	PHBHV$_{80}$MIS$_{20}$	45 µm	2.20

Table V-1. Composition of PHBHV/MIS composites at different fibers content (5 and 20 wt %) length (1 mm and 45 µm) and DCP content (0, 0.25 and 2.2 wt %).

In order to show the presence of PHBHV chains grafted onto MIS surface, FTIR-ATR spectroscopy analyses were carried out on the fibers extracted from biocomposites PHBHV$_{95}$MIS$_5$ realized in the presence or in the absence of DCP (samples **1** and **3**). The ratio (R_1) between the peak at 1726 cm^{-1} corresponding to the carbonyl group of the PHBHV and the peak at 1604 cm^{-1} corresponding to the esters of lignin was evaluated. Figure V-1 shows the superposition of FTIR-

ATR spectra, the first of raw fibers, the second of fibers extracted from a composite with 5 wt % of fibers in the absence of DCP (sample **1**) and the last of fibers extracted from a composite with the same fiber charge and adding 2.2% of DCP (sample **3**).
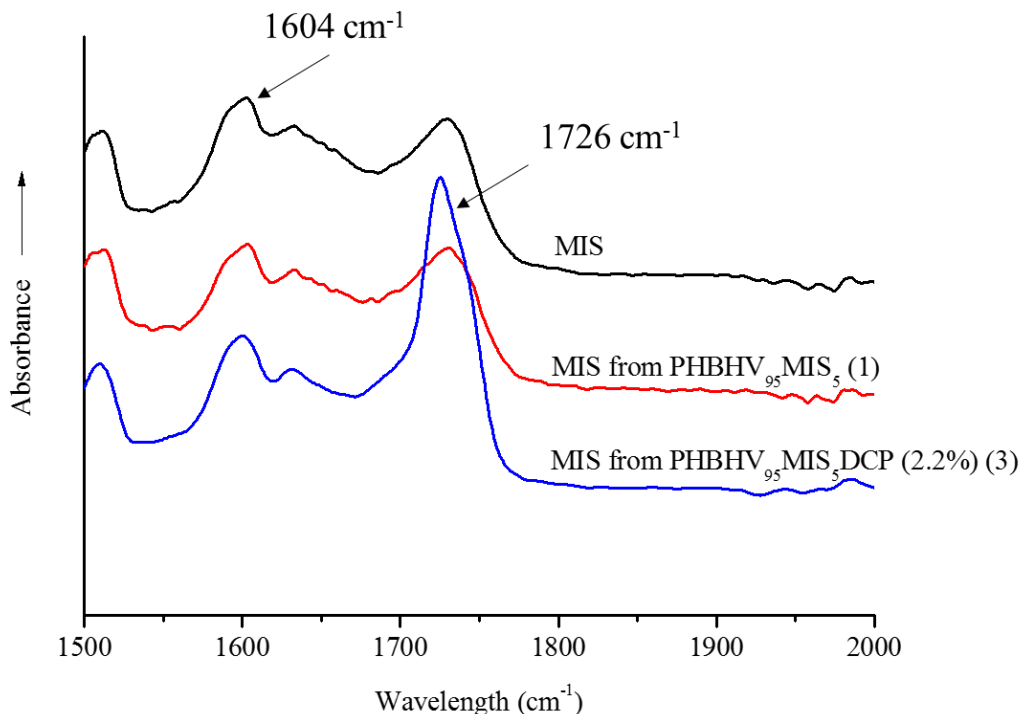
Figure V-1. FTIR-ATR spectra of MIS, MIS extracted from a composite PHBHV$_{95}$MIS$_5$ (sample **1**) and MIS extracted from a composites PHBHV$_{95}$MIS$_5$ DCP (2.2%) (sample **3**).

The figure shows a significant peak at 1726 cm^{-1} typical of the carbonyl group of the matrix for the fibers that were treated in the presence of DCP. This qualitative result suggests that the grafting of PHBHV onto MIS surface occurred. As shown in Table V-2 the ratio R$_1$ increases with increasing the quantity of DCP. This fact means that more PHBHV was grafted onto the surface of the fibers. When DCP is not used, no PHBHV was grafted onto the MIS surface and the ratio R$_1$ is the same of that obtained for the raw Miscanthus.

Reference	Sample	DCP[wt%]	$R_1 = \dfrac{I_{1726\ cm^{-1}}}{I_{1604\ cm^{-1}}}$
	MIS	--	1.3 ± 0.01
1	PHBHV$_{95}$MIS$_5$	0	1.3 ± 0.01
2	PHBHV$_{95}$MIS$_5$	0.25	1.6 ± 0.02
3	PHBHV$_{95}$MIS$_5$	2.20	3.4 ± 0.04

Table V-2. Comparison of R_1 values obtained by FTIR-ATR analysis as function of DCP content for fibers of 1 mm raw and extracted from biocomposites PHBHV$_{95}$MIS$_5$ (samples **1** and **3**).

FTIR is also a useful analysis to evaluate the crystallinity of the PHBHV after processing. The band at 1726 cm^{-1} is representative of the C=O stretch present in the highly crystalline structure of the matrix, while the small shoulder at 1740 cm^{-1} represents the same stretch in the amorphous region. The band around 1378 cm^{-1} corresponds to the symmetrical wagging of the CH$_3$ groups and that at 1452 cm^{-1} to the asymmetric deformation of methylene groups. These bands are considered as insensitive to crystallinity and they can be used to evaluate the crystallinity degree. [16, 50]. In particular, The bands at 1452 cm^{-1} and that at 1225 cm^{-1}, this last corresponding to the C-O-C stretching, were taken into account to calculate the crystallinity index (see figure V-2). This index provides qualitative information about all changes that may occur in the crystalline structure of the matrix.
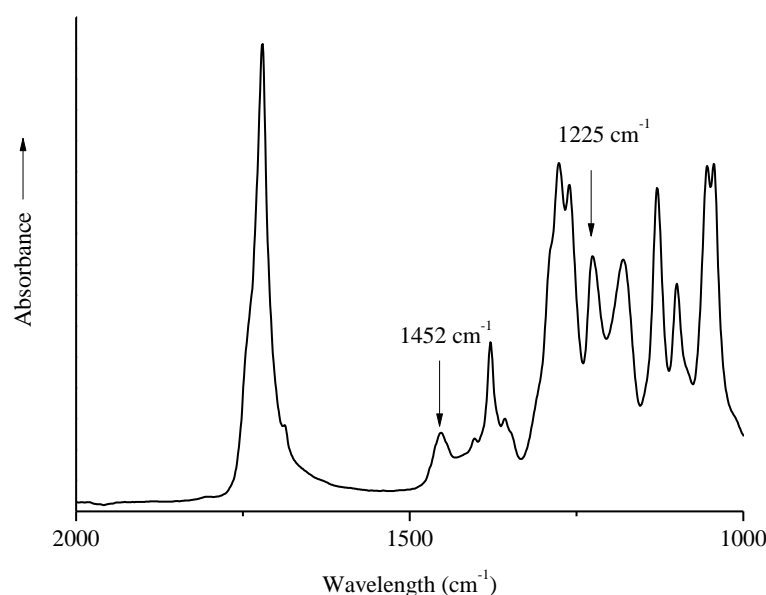
Figure V-2. FTIR-ATR spectrum of a PHBHV specimen in the range 2000-1000 cm^{-1}.

The CI decreased from 1.07 for the neat matrix to 1 for a composite with 20 wt % of raw fibers. Compared to PHBHV/MIS blends, DCP treatment reduced the crystallinity index to 0.94 for a composite with 20 wt % of fibers. However, the decrease in the CI values caused by both fibers length and by the presence of DCP cannot be considered significant.

Reference	Sample	MIS length	DCP [wt%]	CI
	PHBHV		0	1.07 ± 0.1
1	$PHBHV_{95}MIS_5$	1 mm	0	1.06 ± 0.2
3	$PHBHV_{95}MIS_5$	1 mm	2.2	0.98 ± 0.1
4	$PHBHV_{95}MIS_5$	45 µm	0	1.00 ± 0.1
6	$PHBHV_{95}MIS_5$	45 µm	2.2	0.95 ± 0.3
7	$PHBHV_{80}MIS_{20}$	1 mm	0	1.00 ± 0.1
8	$PHBHV_{80}MIS_{20}$	1 mm	2.2	0.94 ± 0.2

Table V-3. Crystallinity parameters of PHBHV and its composites determined by FTIR-ATR analysis.

V-3.2 TENSILE PROPERTIES

Biocomposites at different fibers content, length and DCP percentage were realized by extrusion and injection molding and the results of the mechanical tests are summarized in table V-4. The incorporation of 5 wt % of raw fibers causes an increase in tensile modulus from 889 MPa (value for the neat matrix) to 1074 MPa (sample **1**). This increase is more significant for the composites realized with 20 wt % of fibers, reaching the value of 1525 when fibers of 45 µm were used (sample **9**). For what concern biocomposites with 5 wt % of fibers realized in the presence of DCP, a decrease in tensile modulus is observed for high content of DCP (samples **3** and **6**) compared to their equivalent realized with raw fibers (samples **1** and **4**). DCP is known to cause the cross-linking of the matrix that should exhibit an increase in tensile modulus [51]. Although the increase is not too much high, this

effect is visible only for the composite $PHBHV_{80}MIS_{20}$ (sample **8**). A possible explanation for the decrease in tensile modulus might be the decrease in molar mass due to the presence of high content of DCP. In order to verify this hypothesis PHBHV was treated with DCP and then extruded and injected following the same procedure for the processing of the neat matrix. The tensile modulus and the molar mass were then evaluated by tensile tests and size exclusion chromatography analysis. The PHBHV showed a decrease in tensile modulus from 889 MPa to 782 MPa and a decrease in molar mass from 100,000 to 54,000 $g \cdot mol^{-1}$ indicating that the degradation of the matrix occurred. In the case of the composite $PHBHV_{80}MIS_{20}$ (sample **8**) which exhibit an opposite trend, it may be possible that the high fibers content has a positive effect on the mechanical seal of the biocomposite with DCP, reducing the molecular chains scission and improving the fibers/matrix interactions.

It is well known that the incorporation of vegetal fibers causes an increase in Young Modulus and at the same time a decrease in final strength [24, 63, 64]. This fact is due to a weak interaction between the PHBHV and MIS fibers, impeding stress transfer in the two-phase interface. To improve the adhesion of the fibers to the matrix, Miscanthus fibers were modified with different amounts of DCP as described previously and the optimal DCP content was determined after the results obtained by traction tests. At low content of DCP, typically 0.25 wt %, there is a slightly increase in the final strength (samples **2** and **5**) and this results are independent from the length of the fibers used as showed in figures V-3 and V-4. A content of DCP of 2.2 wt % is sufficient to improve the maximum strength and final strain for all composites and in particular for composites with 20 wt % of fibers, whose tensile strength pass from 15.8 (sample **7**) to 22 MPa (sample **8**) as showed also by figure V-5. When 5 wt % of DCP is used the material molten cannot be extruded because it undergoes a too important crosslinking phenomenon, blocking the material in the recirculation zone of the extruder. A content of 2.2 wt % seems to be a good compromise between the grafting effect and the cross-linking phenomena.

We can affirm that the improvement of the stress transfer between the matrix and the reinforcement can be achieved by using fibers of 45 μm but also by using DCP during the extrusion. Actually the use of DCP allows to better mechanical properties for the biocomposites. However at high content of fibers, typically 20 wt %, the effect of fibers length is not visible on the final strength (sample **9**). Moreover, for the same composition, biocomposites cannot not be realized in the presence of DCP due to a strong interaction between fibers (sample **10**). The reason is that the totally surface area exposed from these particles is very high and in the presence of DCP the material molten undergoes a rapid fiber-fiber interactions accompanied also by a crosslinking phenomenon, this last

preventing the realization of specimens by extrusion and injection molding in the same conditions of the other composites.

The composite $PHBHV_{80}MIS_{20}$ containing 2.2% of DCP and 20 wt% of long fibers (sample **8**) was judged as the optimum composition. In this context, the degradation of the neat matrix showed in the presence of DCP, was strongly limited by the great number of fibers. All the mechanical results are listed in the table V-4. The Soxhlet extraction on this composite has led to the determination of a crosslinked portion of 23 wt % on the total matrix present in the specimens. Assuming a quasi-constant density of the matrix if cross-linked or not (1.3 g/cm^3), this fraction was determinant in the following paragraph to determine the effective mechanical properties of this composite.
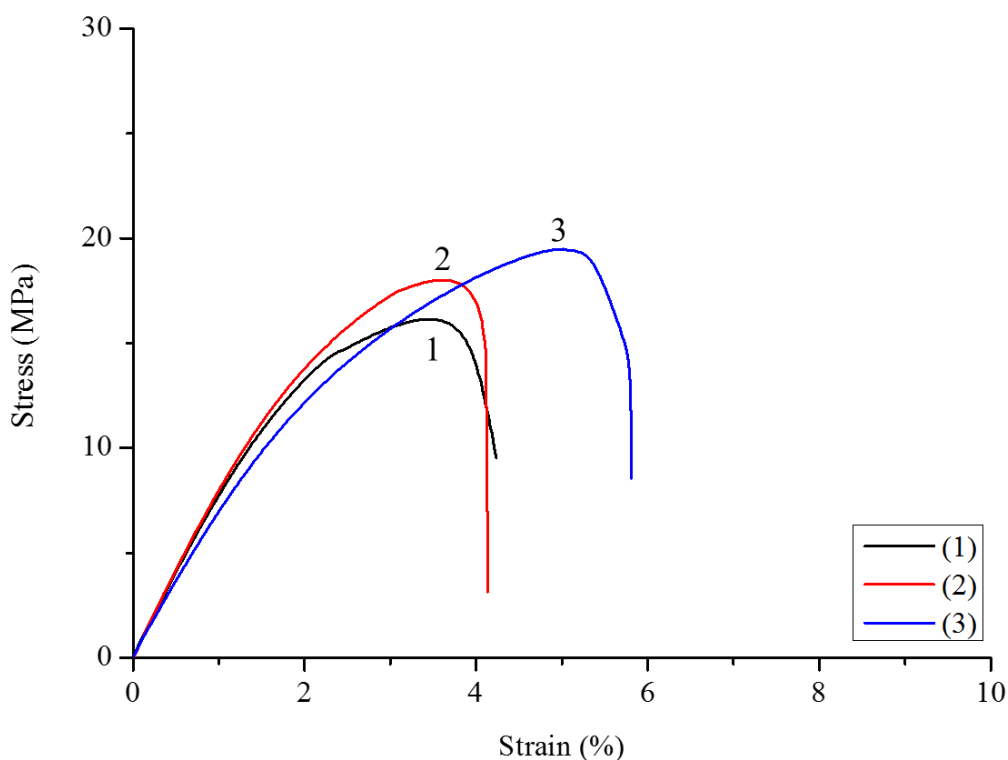
Figure V-3. Strain-Stress curves of composites $PHBHV_{95}MIS_5$ (sample **1**), $PHBHV_{95}MIS_5$ with 0.25 wt % of DCP (sample **2**) and $PHBHV_{95}MIS_5$ with 2.2 wt % of DCP (sample **3**).
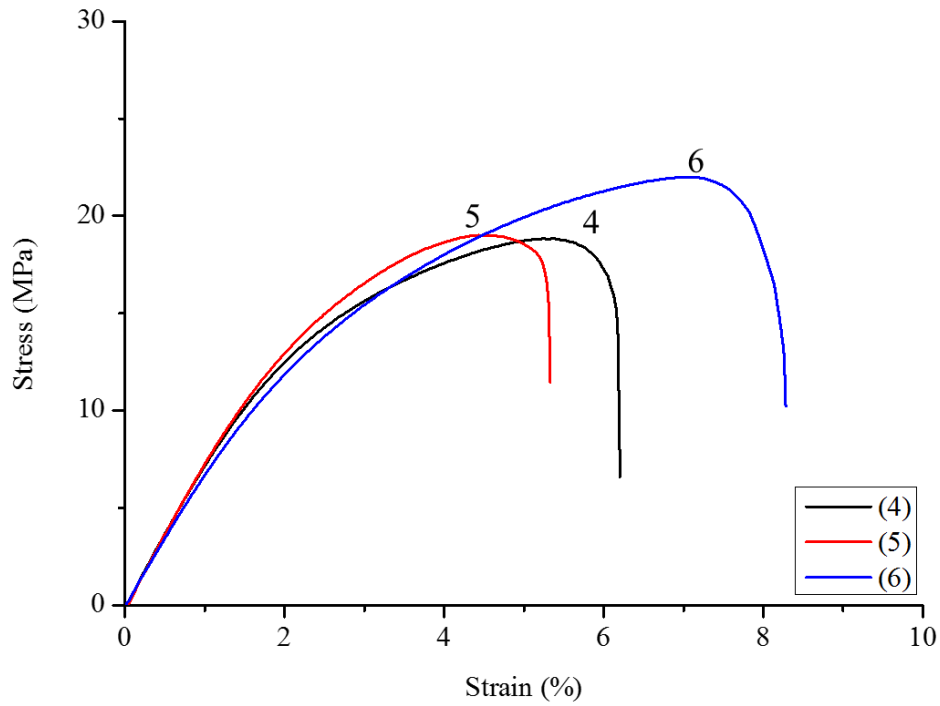
Figure V-4. Strain-Stress curves of composites PHBHV$_{95}$MIS$_5$ (sample **4**), PHBHV$_{95}$MIS$_5$ with 0.25 wt % of DCP (sample **5**) and PHBHV$_{95}$MIS$_5$ with 2.2 wt % of DCP (sample **6**).
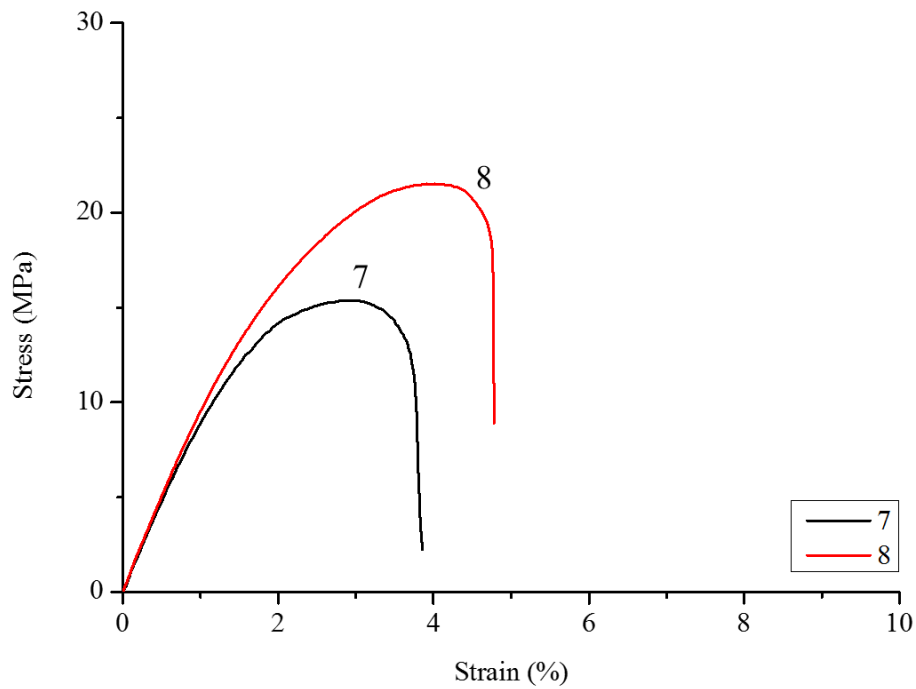
Figure V-5. Strain-Stress curves of composites PHBHV$_{80}$MIS$_{20}$ (sample **7**) and PHBHV$_{80}$MIS$_{20}$ with 2.2 wt % of DCP (sample **8**).

Reference	Sample	MIS length	DCP [wt%]	E [MPa]	σ_{max} [MPa]	ε_r [%]
	$PHBHV_{100}$	-	-	889 ± 41	23.0 ± 0.5	11 ± 1.60
1	$PHBHV_{95}MIS_5$	1 mm	-	1074 ± 44	17.0 ± 1.7	4.5 ± 0.89
2	$PHBHV_{95}MIS_5$	1 mm	0.25	1126 ± 37	18.0 ± 0.7	4.1 ± 0.43
3	$PHBHV_{95}MIS_5$	1 mm	2.2	962 ± 19	20.0 ± 0.9	5.9 ± 0.74
4	$PHBHV_{95}MIS_5$	45 µm	-	1021 ± 20	18.0 ± 0.1	6.3 ± 0.27
5	$PHBHV_{95}MIS_5$	45 µm	0.25	1045 ± 62	20.0 ± 1.0	5.3 ± 0.60
6	$PHBHV_{95}MIS_5$	45 µm	2.2	938 ± 55	22.1 ± 0.4	8.3 ± 1.09
7	$PHBHV_{80}MIS_{20}$	1 mm	-	1267 ± 90	15.8 ± 0.7	3.9 ± 0.22
8	$PHBHV_{80}MIS_{20}$	1 mm	2.2	1358 ± 52	22.0 ± 1.0	4.8 ± 0.46
9	$PHBHV_{80}MIS_{20}$	45 µm	-	1525 ± 84	17.0 ± 0.7	3.1 ± 0.30
10	$PHBHV_{80}MIS_{20}$	45 µm	2.2	-	-	-

Table V-4. Tensile properties of biocomposites determined by tensile tests.

V-3.3 FRACTURE FACIES MORPHOLOGY

After traction tests, the fracture section of each specimen was observed by SEM in order to evaluate the adhesion between the fibers and the matrix. These observations revealed two different effects due to the presence of the DCP as deduced from mechanical tests. The first one is the improvement of the adhesion between matrix and fibers showed in figure V-6A. Indeed, when considering untreated fibers (cf. figure V-6B), a non-cohesive interface can be observed. This indicates that the increase in ultimate strength for treated fibers is due to an improved stress transmission between the composite different phases during the traction test.

The second effect that is less evident and it was evaluated by a zoom on a specific part of the specimen where only matrix is present. In these zones there is an evident structural change of the pure matrix (See figure V-7). This morphological change could be due to a cross-linking effect caused by the presence of DCP. These zones are not homogeneous in all section. Moreover, the type of cross-liking is different if long fibers are used instead of short fibers. In the case of composites realized with short fibers the resulting network seems to be more compact than that obtained in the presence of long fibers (Figure V-7D, V-7E). This fact support the mechanical results in which composites with 5 % of short fibers present better mechanical properties than their equivalent with long fibers and composites with 20% of short fibers cannot be extruded.
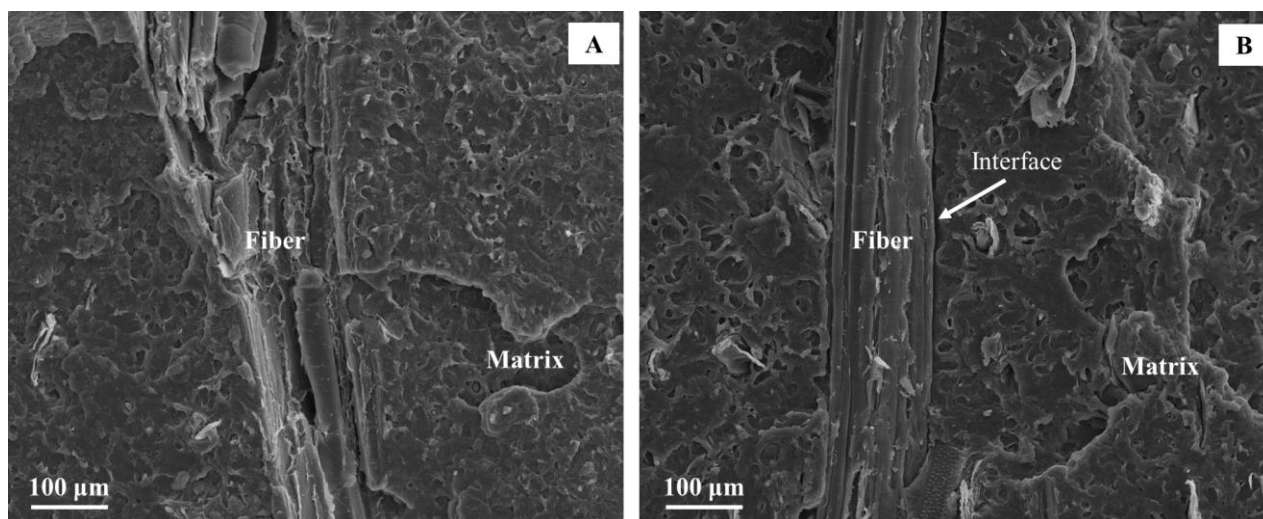
Figure V-6. SEM images of PHBHV$_{95}$MIS$_5$ composites realized with fibers of 1 mm treated with DCP (A) and untreated (B).
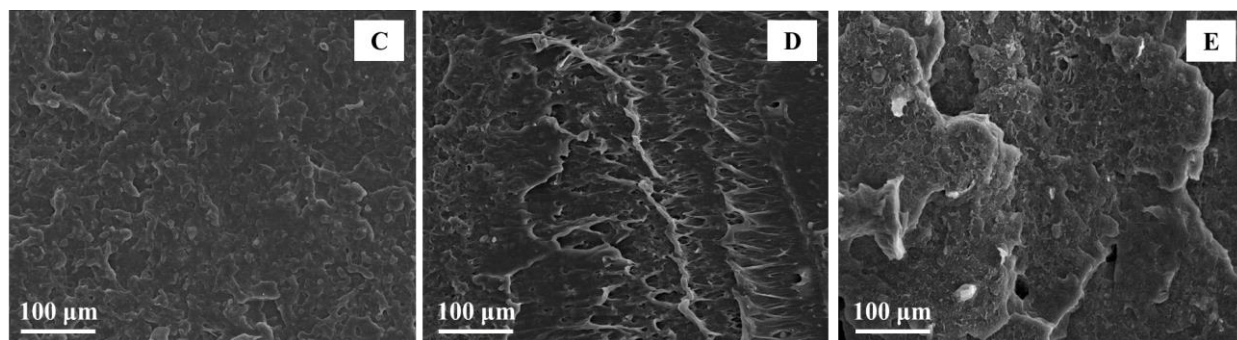
Figure V-7. SEM images of pure PHBHV (C) and of the matrix in the PHBHV$_{95}$MIS$_5$ (DCP) composites realized with fibers of 1 mm (D) (sample **3**) and 45 µm (E) (sample **6**).

V-3.4 CHARACTERIZATION OF BIOCOMPOSITES BY DSC AND XRD ANALYSES

The differential scanning calorimetry (DSC) was used in order to evaluate the thermal behavior of the final composites. All the curves of the composites present two melt peaks due to the repartition of crystallites of different dimensions typical of semi-crystalline polymers (Table V-5). Each peak is characterized by two different melt temperatures (T_{M1} and T_{M2}). Comparing the neat matrix and composites realized with high content of raw fibers, typically 20 wt % (sample **7**), no modification thermal properties was detected. This fact means that Miscanthus fibers do not have an impact on the crystallization behavior of the matrix. The presence of DCP during the processing step causes a modification in melt temperatures, these last passing from 156 to 148°C (T_{M2}) and from 140 to 133°C (T_{M1}) for a composite realized with 20 wt % of fibers in the presence of 2.2 wt % of DCP (sample **8**) as showed in figure V-8. At the same time, no change in crystallinity was detected for the same sample. This result could be explained by the fact that DCP doesn't alter the semicrystalline behavior of the matrix, whose crystallinity degree remains at 31 %, but it could have a significant impact on the crystallites size and shape.

Reference	Sample	DCP [wt%]	MIS length	T_{M1} [°C]	T_{M2} [°C]	ΔH_M [J/g]	X_c [%]
	PHBHV	-	-	140	156	46	31
1	$PHBHV_{95}MIS_5$	-	1 mm	140	154	45	32
3	$PHBHV_{95}MIS_5$	2.2	1 mm	137	154	44	32
4	$PHBHV_{95}MIS_5$	-	45 μm	140	159	48	35
6	$PHBHV_{95}MIS_5$	2.2	45 μm	138	156	43	31
7	$PHBHV_{80}MIS_{20}$	-	1 mm	141	155	37	31
8	$PHBHV_{80}MIS_{20}$	2.2	1 mm	133	148	40	31

Table V-5. DSC data for PHBHV/MIS composites realized with fibers of 1 mm and 45 μm: T_{M1} and T_{M2} (Melt temperatures); ΔH_M (Melt Enthalpy); X_c (Cristallinity degree).
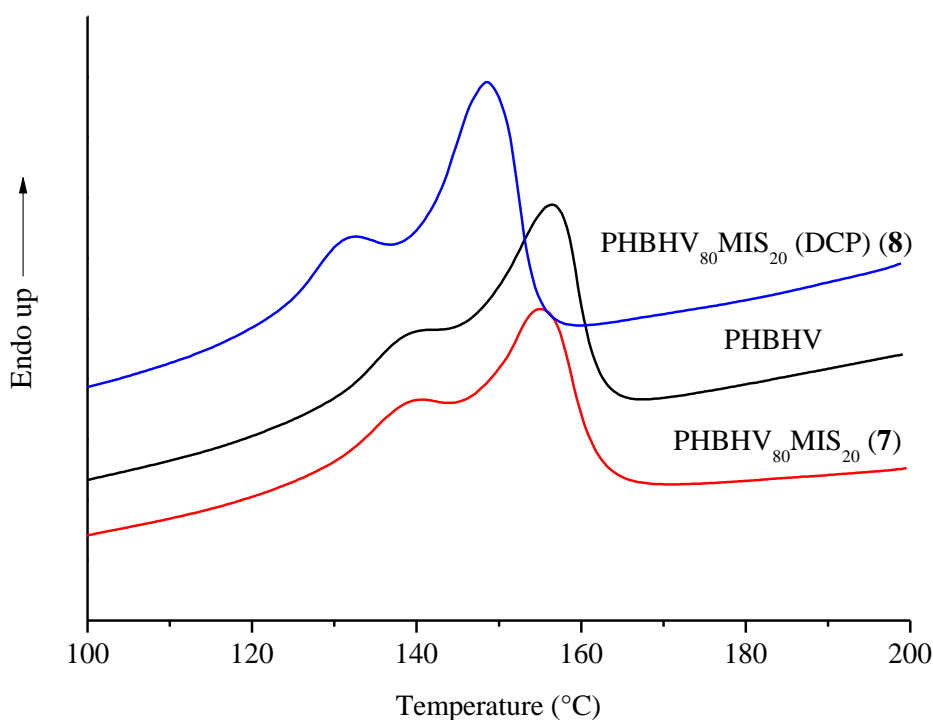
Figure V-8. DSC first heating thermograms of PHBHV, $PHBHV_{80}MIS_{20}$ (sample **7**) and $PHBHV_{80}MIS_{20}$ (DCP) (sample **8**).

This shift at lower fusion temperature suggested a change in the crystallites dimensions. XRD analysis was also conducted on the neat matrix and composites with 20% of long fibers realized with

and without DCP (Figure V-9). PHBHV has a semicrystalline nature with characteristics peaks at 2theta around 13°, 17°, 21°, 22°, 25° and 27°, corresponding to planes (020), (110), (101), (111), (121), (040) respectively in the orthorhombic crystalline lattice. The addition of MIS and DCP does not alter the basic crystal structure of PHBHV, being the reflections located at the same angle. Moreover, the evaluation of Bravais parameters, showed that the lattice volume did not change.
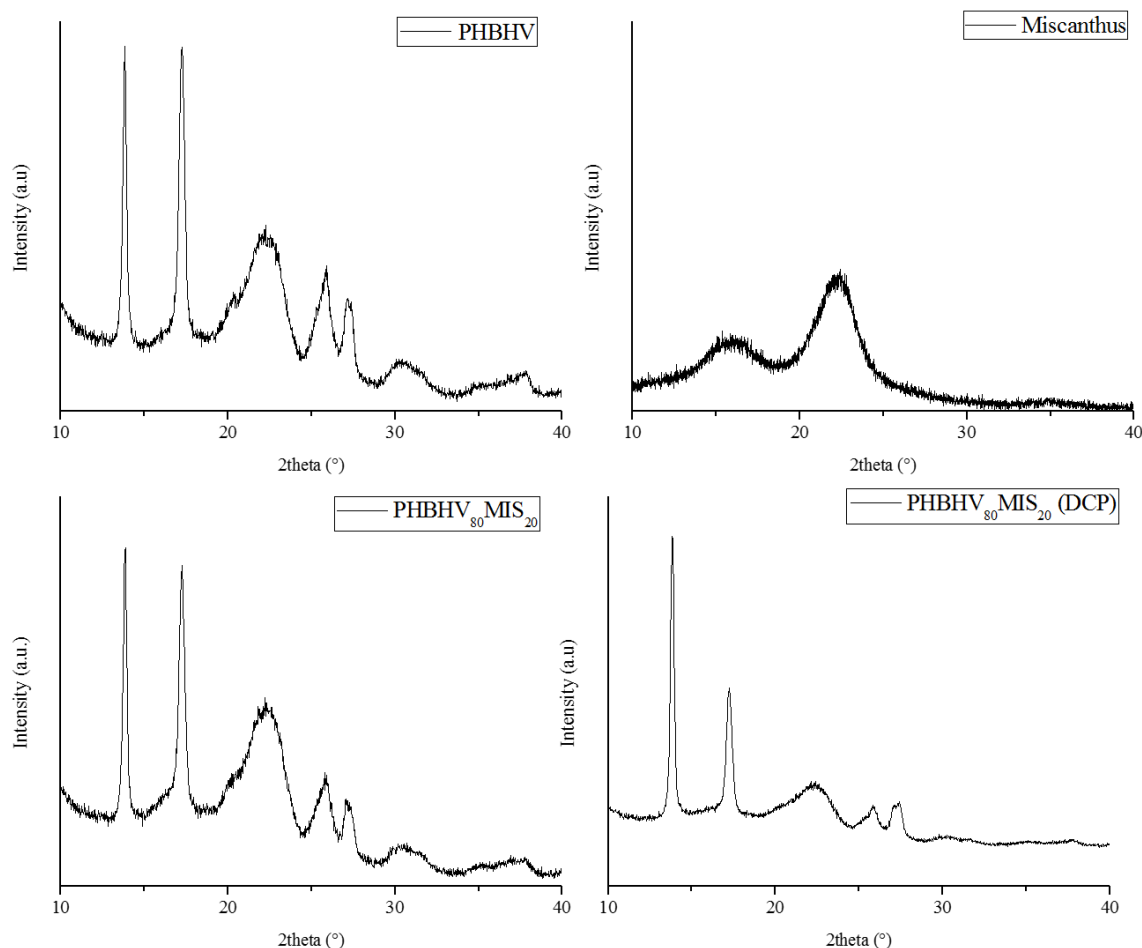
Figure V-9. XRD diffractograms of MIS, PHBHV, PHBHV$_{80}$MIS$_{20}$ (sample **7**) and PHBHV$_{80}$MIS$_{20}$ (DCP) (sample **8**).

V-3.5 ANALYTICAL MODELS

Our goal is now to provide in this section modeling approaches that, if they can mimic the actual behavior of the composites, could be then used to provide an *in silico* design of composites according to various applications. To this aim we used micromechanics analytical approaches [65-68]. In these models, a perfect contact between the inclusions and the matrix was assumed. According to Figure V-6, this assumption seems relevant.

V-3.5.1 Use of a model involving three phases

The rule of mixture (*ROM*), respectively the Mori-Tanaka model (*MT*), are ways to analytically derive the effective Young modulus of a multiphasic medium. Concerning the latter one, it is based on Eshelby's elasticity solution for diluted particle inclusion in infinite matrix [68]. These two methods require to properly describe the different components that form the composite (indexed "*C*"). Here, we chose to consider three phases: the fibers (indexed "*F*"), the gel (cross-linked matrix, indexed "*G*") and the remaining matrix (indexed "*M*"). To apply these methods, it is necessary to know the volume fraction Φ_i and the bulk Young moduli E_i of each phase ($i = F$, G or M). Thus the Young modulus of the composite E_c can be described through two functions of these 6 parameters:

$$E_{ROM} = \sum \Phi_i E_i = f_{ROM}(E_F, E_G, E_M, \Phi_F, \Phi_G, \Phi_M) \tag{V-5}$$

$$E_{MT} = f_{MT}(E_F, E_G, E_M, \Phi_F, \Phi_G, \Phi_M) \tag{V-6}$$

which respectively correspond to the mixing rule or the Mori-Tanaka approach. Knowing five of these six parameters and the effective Young modulus of the composite, it is thus possible to recover the sixth parameter. Note that the conservation of the volume may reduce the number of unknown volume fractions since their sum is one. We decided to focus our attention on PHBHV$_{80}$MIS$_{20}$ (DCP) (sample **8**) and apply to this peculiar specimen the two methods (Mori-Tanaka and rule of mixture) to evaluate its elastic modulus. To this aim, the fraction of gel Φ_G was calculated using the experimental procedure previously described (See section V-2.4.1). The value of Φ_F can be easily deduced from fiber mass content and density. By this way, the knowledge of two volume fractions provides the last one thanks to the volume conservation law ($\Phi_F + \Phi_G + \Phi_M = 1$). The Young modulus of the cross-linked matrix was evaluated experimentally, by testing specimens of neat matrix realized in the presence of DCP (See paragraph V-3.2). The final values used to implement the models are resumed in Table V-6.

Constituents	Young Modulus [GPa]	Volumetric fraction [%]
Miscanthus *giganteus*	4.5 [a]	0.22
PHBHV	0.889 [b]	0.60
Gel	0.782 [b]	0.18 [c]

Table V-6. Technical data for Young Modulus and volumetric fraction for Miscanthus *giganteus*, PHBHV and gel fraction. (a) Adapted from [69]; (b) Experimental value; (c) evaluated according to procedure described in paragraph V-2.4.2.

V-3.5.2. Evaluation of E_G and Φ_G by a mathematical approach

The application of the rule of mixture to composites realized in the absence of DCP showed discrepancies between the real value of Young modulus and that obtained by ROM In particular, for the composite PHBHV$_{80}$MIS$_{20}$ (sample **7**), the error between the experimental value and that obtained with the ROM is quite important around 33%. This great differences could be due to the lack of knowledge of the fibers Young modulus assumed equal to 4.5 GPa, this last value being taken from literature data and possible stress concentrations within the matrix.

The Young modulus of the cross-linked matrix is one of the principal unknown of our system. At first, we apply an experimental procedure to calculate this value. If we consider that the matrix totally cross-links during the manufacturing step, this hypothesis allows to assimilate the Young modulus calculated for specimens of neat PHBHV realized with DCP to that of any cross-linked portion present in our composite. Then, assuming that the nature of the cross-linked portion doesn't change when fibers are present in the blend, it is possible to perform analytical and numerical approaches to estimate the effective modulus of the composite. However, the uncertainties related to the values of E_F, E_G and to the fraction of cross-linked matrix cause the re-opening of the discussion about the value of moduli used in the models and question about the role of vegetal fibers in the blend when DCP is present.

For this reason, at this step, we decided to use MATLAB R2007b software to map the variation of E_G as function of the cross-linked fraction Φ_G, by implementing a function F from the function f$_{ROM}$ defined by Eq. (V-5). If the values of E_G and Φ_G are variable (E_G varied from 0 to 2 GPa and Φ_G from 0 to 1- Φ_F), the other parameters are those obtained through experimental procedures. The function *F* reads as follows:

$$F\left(\varPhi_{G(j)}, E_{G(i)}\right) = \varPhi_F E_F + \varPhi_{G(j)} E_{G(i)} + \left(1 - \varPhi_F - \varPhi_{G(j)}\right) E_M - E_{exp} \qquad (V\text{-}7)$$

The zero-curve obtained from this function provides possible couples ($\varPhi_G, E_G$) checking the experimental effective behavior. Note that this value is characterized by errors due to the standard deviation associated to E_{exp} and to the assumptions made about E_F.

V-3.5.3 Results of analytical and mathematical approach

The results of analytical simulations on the composite PHBHV$_{80}$MIS$_{20}$ (DCP) (sample **8**) are presented in Table V-7. The homogenized models with cylindrical and spherical inclusions constituted the upper and lower boundary for the experimental values, the first one representing a fully oriented configuration whereas the second one remaining isotropic. The discrepancies between the experimental and approximated moduli can be, in part, explained by the bad repartition of the fibers (see previous chapter).

Sample	MT model 3 phases		ROM	Experimental
	E_{MT_cyl} [MPa]	E_{MT_sph} [MPa]	E_{ROM} [MPa]	E_{exp} [MPa]
8	1655	1170	1655	1358 ± 52

Table V-7. Comparison between Mori-Tanaka model, ROM and FE model and the experimental value for the composite PHBHV$_{80}$MIS$_{20}$ (DCP) (sample **8**).

According to the results in Table V-6, models provided unrealistic values compared to the experimental ones. This fact means that the uncertainties presented in the previous paragraph concerning the Young modulus of the cross-linked matrix and the choice made on that of vegetal fibers have a great impact on the determination of the elastic modulus of a composite partially cross-linked.

The mapping operation conducted on specimens of PHBHV$_{95}$MIS$_5$ (sample **2**, **3**, **5** and **6**) presents the various lines of possible. When considering fully cross-linked matrix, that is to say asymptotic values which corresponds to the total cross-link of the matrix, it remains more or less the same notwithstanding the DCP concentration (See Figure V-10). Moreover, the Young Modulus E_G find for these composites ranges between 0.6 and 0.8 GPa. These values agree with the experimental modulus (0.782 GPa) evaluated on specimens of neat matrix totally cross-linked. More precisely, lower values of modulus are obtained for higher DCP content (samples **3** and **6** were realized with

2.2 wt % of DCP), while higher values of modulus for lower DCP content (samples **2** and **5** were realized with 0.25 wt % of DCP).

This result indicates that the cross-linking phenomenon within the matrix is predominant when compared to the grafting of fibers.

At this point, it could be interesting to investigate the effect of the fibers content in order to understand their role when the reaction of PHBHV with DCP takes place. To this aim, composite PHBHV$_{80}$MIS$_{20}$ (sample **8**) was analyzed in the same manner and the result is showed in Figure V-11. For this sample, the value of Φ_G is known and equal to 0.179. It is evident that at this gel fraction, E_G must be negative to obtain the experimental value corresponding to the composite. This fact means that: i/ the analytical rule does not work well for high fiber content; ii/ the fiber content impacts the PHBHV cross-linking process in addition to DCP concentration.

For all described composites it seems that the mechanical behavior oscillates from one (typical of specimens with 5 wt % of fibers) in which the content of fibers is too low to have a remarkable impact on the stiffness of the material, to another (typical of specimens with 20 wt % of fibers) in which the presence of high content of reinforcement influences not only the mechanical behavior but also the reaction of DCP. This threshold effect due to the content of fibers was verified *a posteriori*, realizing PHBHV-based composites with 10 wt % of short MIS fibers and 2.2 wt % of DCP (see appendix V-5A for more details). The properties obtained for the additional specimen demonstrate that the composite is similar to those realized with 5 wt % of fibers in terms of mechanical behavior and in terms of cross-linking phenomena. Moreover, the fact that the realization of this composite by extrusion and injection molding was possible is a further clue that the high fiber content behavior was not reached for this composite (the processing at 20 wt % of short fibers being unrealizable).
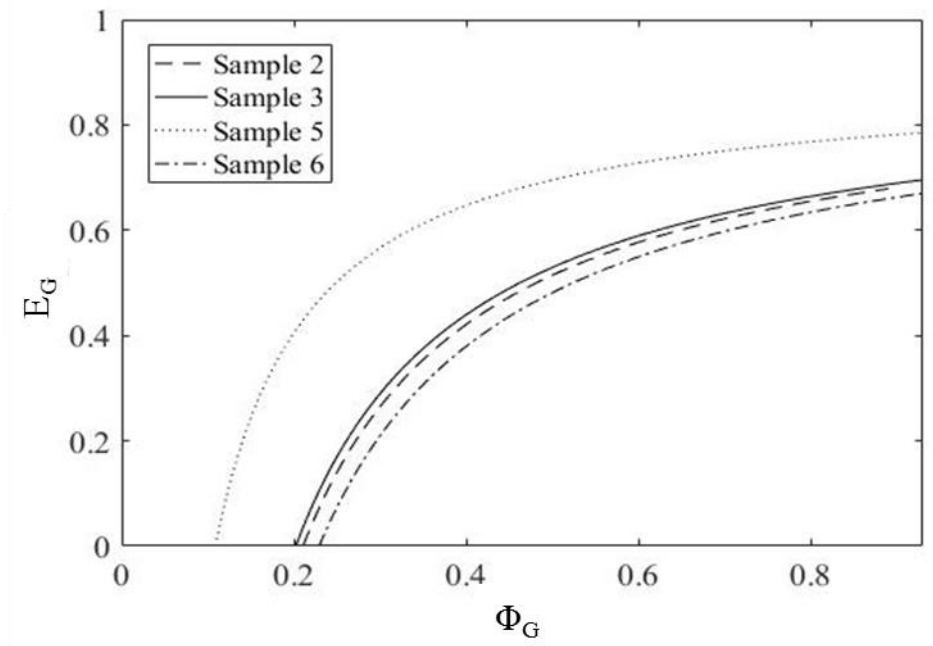
Figure V-10. Evaluation of E_G as function of Φ_G for composites PHBHV$_{95}$MIS$_5$ (samples **2**, **3**, **5** and **6**).
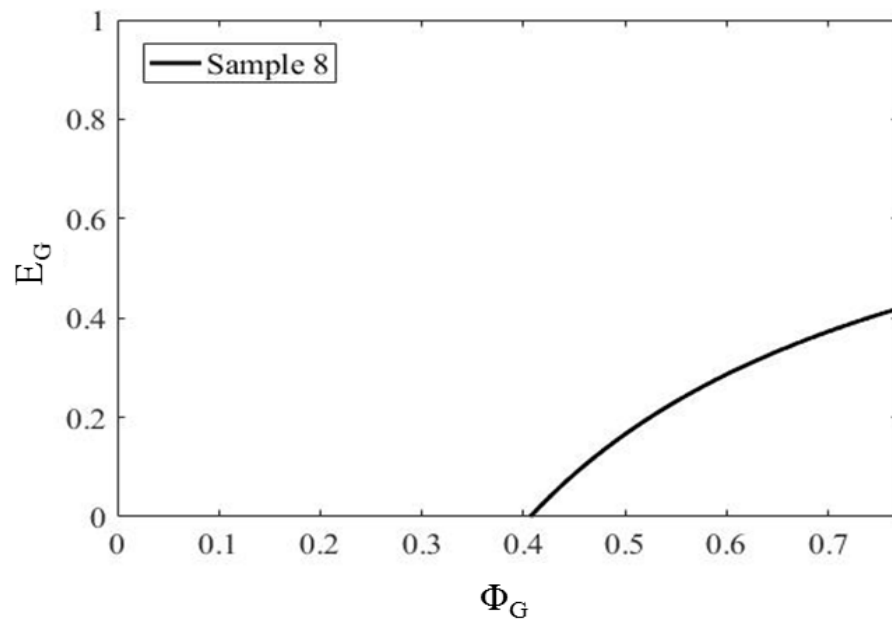
Figure V-11. Evaluation of E_G as function of Φ_G for composites PHBHV$_{80}$MIS$_{20}$ (sample **8**).

V-4. CONCLUSIONS

Free radical grafting initiated by DCP via reactive extrusion led to the improvement of the mechanical performances of PHBHV/MIS blends. A total amount of 2.2 wt% of DCP was found to be the optimum content in order to achieve a good adhesion fibers/matrix with consequent improvement in final strength and elongation at break of the biocomposites. Fibers sieved with a 45 μm mesh sieve showed in general a better improvement of the mechanical properties. Although this good result, the great interfacial area exposed by these little particles caused a limitation in the processing step when a lot of these fibers were used. This fact led to the choice of the blend with 20 wt% of long fibers and 2.2% of DCP as the better solution realized in terms of mechanical results obtained, less matrix degradation during the process and no significant change in crystallinity degree due to the presence of fibers or DCP. The evidence of the grafting between the fibers and the matrix proved by FTIR-ATR and SEM analyses and the knowledge of the gel fraction for this composite, led to the implementation of analytical models. However, the Mori-Tanaka model with 3 phases (neat matrix/cross-linked matrix/fibers) overestimates the mechanical behavior of the composite. The mathematical approach used to evaluate the ranges of Young modulus of the cross-linked matrix and of its volumetric fraction agree with the experimental values. However, this result is not true for higher fibers content (typically 20 wt %) in which the presence of a lot of fibers influences the normal reaction of DCP. A threshold effect correlated to the content of fibers is visible on the analyzed specimens. The first behavior is that typical of a material without fibers while the second one of a composite with a high content of fibers that is able to modify the normal reaction occurring between DCP and PHBHV. This fact was also demonstrated by an additional tests with an intermediary composition between those realized in which the mechanical behavior at 10 wt % of fibers is similar to that of composites at 5 wt %. The possibility to substitute a part of the matrix with vegetal fibers, the improvement of the adhesion fiber/matrix and the possibility to process these composites with conventional techniques, all these factors suggests that the functionalization of natural fibers with DCP appears to be a very promising way to improve the mechanical properties of any type of polyesters.

V-5. APPENDIX

V-5A. REALIZATION OF SPECIMENS PHBHV$_{90}$MIS$_{10}$ (2.2 % DCP)

In order to demonstrate the threshold effect due to the fibers when the reaction of PHBHV with DCP occurred, we decide to realize a composite with an intermediate content of short fibers (between 5 and 20 wt %) and 2.2 % of DCP. Note that the realization of a composite with 20 wt % of fibers and the same content of DCP was impossible due to the excessive cross-linking effect in the extruder. Once realized, specimens were tested in the same conditions than the others (See paragraph V-2.4.2 for details). Mechanical properties and results obtained by the mathematical approach are resumed in the table V-A1 and visible in Figure V-A1 respectively.

Sample	E [MPa]	σ_{max} [MPa]	ε_r [%]
PHBHV$_{90}$MIS$_{10}$ (DCP)	1099 ± 65	22 ± 2.0	7 ± 1.0

Table V-A1. Tensile properties of biocomposite PHBHV$_{90}$MIS$_{10}$ (DCP) determined by tensile tests.
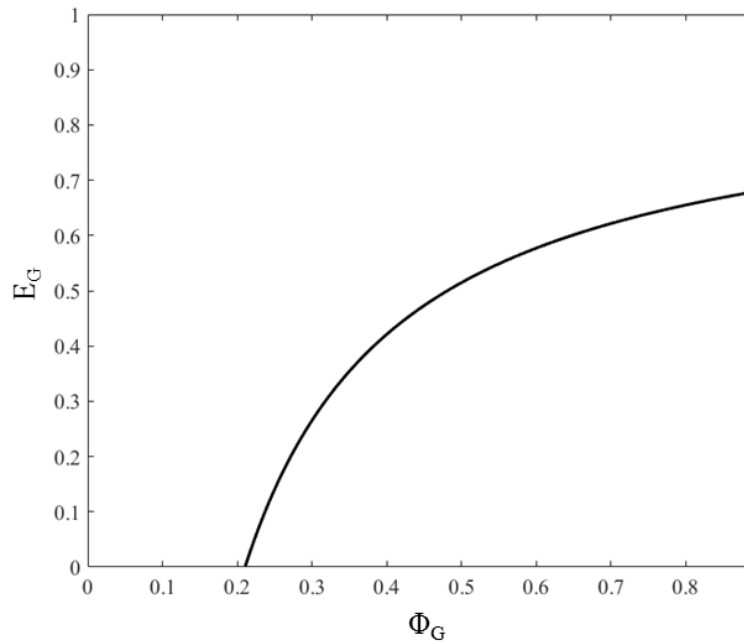
Figure V-A1. Evaluation of E_G as function of Φ_G for composites PHBHV$_{90}$MIS$_{10}$ (DCP).

The properties of PHBHV$_{90}$MIS$_{10}$ (DCP) composite are similar to those realized with 5 wt % of fibers in terms of mechanical behavior and in terms of cross-linking phenomena.

V-6. REFERENCES

1.   Mohanty, A.K. et al., Natural fibers, biopolymers, and biocomposites. CRC press (**2005**).
2.   Mohanty, A. et al., Biofibers, biodegradable polymers and biocomposites: an overview. *Macromolecular materials and Engineering* 276(1), p. 1-24 (**2000**).
3.   Zhang, K. et al., Fully biodegradable and biorenewable ternary blends from Polylactide, Poly(3-hydroxybutyrate-co-hydroxyvalerate) and Poly(butylene succinate) with balanced properties. *ACS Appl. Mater. Interfaces* 4, p. 3091−3101 (**2012**).
4.   Gurunathan, T. et al., A review of the recent developments in biocomposites based on natural fibres and their application perspectives. *Composites Part A: Applied Science and Manufacturing* 77, p. 1-25 (**2015**).
5.   Somleva, M.N. et al., PHA bioplastics, biochemicals, and energy from crops. *Plant biotechnology journal* 11(2), p. 233-252 (**2013**).
6.   Laycock, B. et al., The chemomechanical properties of microbial polyhydroxyalkanoates. *Progress in Polymer Science* 39(2), p. 397-442 (**2014**).
7.   Kai, D. et al., Polyhydroxyalkanoates: Chemical modifications toward biomedical applications. *ACS Sustainable Chemistry & Engineering* 2(2), p. 106-119 (**2013**).
8.   Chen, G.-Q. et al., The application of polyhydroxyalkanoates as tissue engineering materials. *Biomaterials* 26(33), p. 6565-6578 (**2005**).
9.   Chen, G.-Q. et al., Plastics derived from biological sources: present and future: a technical and environmental review. *Chemical reviews* 112(4), p. 2082-2099 (**2011**).
10. Lee, S.Y., Plastic bacteria? Progress and prospects for polyhydroxyalkanoate production in bacteria. *Trends in Biotechnology* 14(11), p. 431-438 (**1996**).
11. Sudesh, K., Molecular design and biosynthesis of biodegradable polyesters. *Polymers for Advanced Technologies* 11(8-12), p. 865-872 (**2000**).
12. Díez-Pascual, A.M. et al., ZnO-reinforced poly (3-hydroxybutyrate-co-3-hydroxyvalerate) bionanocomposites with antimicrobial function for food packaging. *ACS applied materials & interfaces* 6(12), p. 9822-9834 (**2014**).
13. Mekonnen, T. et al., Progress in bio-based plastics and plasticizing modifications. *Journal of Materials Chemistry A* 1(43), p. 13379-13398 (**2013**).
14. Mohanty, A.K. et al., Sustainable Bio-Composites from Renewable Resources: Opportunities and Challenges in the Green Materials World. *Journal of Polymers and the Environment* 10(1), p. 19-26 (**2002**).
15. Bhardwaj, R. et al., Renewable resource-based green composites from recycled cellulose fiber and poly (3-hydroxybutyrate-co-3-hydroxyvalerate) bioplastic. *Biomacromolecules* 7(6), p. 2044-2051 (**2006**).
16. Singh, S. et al., Renewable resource based biocomposites from natural fiber and polyhydroxybutyrate-co-valerate (PHBV) bioplastic. *Composites Part A: Applied Science and Manufacturing* 39(5), p. 875-886 (**2008**).
17. Bledzki, A. et al., Mechanical performance of biocomposites based on PLA and PHBV reinforced with natural fibres–A comparative study to PP. *Composites science and technology* 70(12), p. 1687-1696 (**2010**).
18. Nagarajan, V. et al., Sustainable green composites: Value addition to agricultural residues and perennial grasses. *ACS Sustainable Chemistry & Engineering* 1(3), p. 325-333 (**2013**).
19. Nagarajan, V. et al., New engineered biocomposites from poly (3-hydroxybutyrate-co-3-hydroxyvalerate)(PHBV)/poly (butylene adipate-co-terephthalate)(PBAT) blends and switchgrass: Fabrication and performance evaluation. *Industrial crops and products* 42, p. 461-468 (**2013**).
20. Nyambo, C. et al., Polylactide-based renewable green composites from agricultural residues and their hybrids. *Biomacromolecules* 11(6), p. 1654-1660 (**2010**).
21. Jiang, L. et al., Reinforcing and toughening effects of bamboo pulp fiber on poly (3-hydroxybutyrate-co-3-hydroxyvalerate) fiber composites. *Industrial & Engineering Chemistry Research* 49(2), p. 572-577 (**2009**).

22. Ahankari, S.S. et al., Mechanical behaviour of agro-residue reinforced poly(3-hydroxybutyrate-co-3-hydroxyvalerate), (PHBV) green composites: A comparison with traditional polypropylene composites. *Composites Science and Technology* 71(5), p. 653-657 (**2011**).

23. Shibata, M. et al., Biocomposites made from short abaca fiber and biodegradable polyesters. *Macromolecular Materials and Engineering* 288(1), p. 35-43 (**2003**).

24. Wollerdorfer, M. et al., Influence of natural fibres on the mechanical properties of biodegradable polymers. *Industrial Crops and Products* 8(2), p. 105-112 (**1998**).

25. Avella, M. et al., Poly(lactic acid)-based biocomposites reinforced with kenaf fibers. *Journal of Applied Polymer Science* 108(6), p. 3542-3551 (**2008**).

26. Bogoeva-Gaceva, G. et al., Natural fiber eco-composites. *Polymer composites* 28(1), p. 98-107 (**2007**).

27. Faruk, O. et al., Biocomposites reinforced with natural fibers: 2000–2010. *Progress in Polymer Science* 37, p. 1552-1596 (**2012**).

28. Murnen, H.K. et al., Optimization of ammonia fiber expansion (AFEX) pretreatment and enzymatic hydrolysis of Miscanthus x giganteus to fermentable sugars. *Biotechnology progress* 23(4), p. 846-850 (**2007**).

29. Fischer, G. et al., Biomass potentials of miscanthus, willow and poplar: results and policy implications for Eastern Europe, Northern and Central Asia. *Biomass and Bioenergy* 28(2), p. 119-132 (**2005**).

30. Collura, S. et al., Thermal behaviour of Miscanthus grasses, an alternative biological fuel. *Environmental Chemistry Letters* 5(1), p. 49-49 (**2007**).

31. Dohleman, F.G. et al., More Productive Than Maize in the Midwest: How Does Miscanthus Do It? *Plant Physiology* 150(4), p. 2104-2115 (**2009**).

32. Widholm, J. et al., Miscanthus: a promising biomass crop. *Adv Bot Res* 56, p. 75137Hu (**2010**).

33. Beale, C.V. et al., Can perennial C4 grasses attain high efficiencies of radiant energy conversion in cool climates? *Plant, Cell & Environment* 18(6), p. 641-650 (**1995**).

34. Kaack, K. et al., Morphological and mechanical properties of Miscanthus in relation to harvesting, lodging, and growth conditions. *Industrial Crops and Products* 14(2), p. 145-154 (**2001**).

35. Park, H.-J. et al., Manufacture and properties of Miscanthus–wood particle composite boards. *Journal of wood science* 58(5), p. 459-464 (**2012**).

36. Heaton, E.A. et al., Meeting US biofuel goals with less land: the potential of Miscanthus. *Global Change Biology* 14(9), p. 2000-2014 (**2008**).

37. Bourmaud, A. et al., Investigations on mechanical properties of poly (propylene) and poly (lactic acid) reinforced by miscanthus fibers. *Composites Part A: Applied Science and Manufacturing* 39(9), p. 1444-1454 (**2008**).

38. Avella, M. et al., Review Properties of blends and composites based on poly(3-hydroxy)butyrate (PHB) and poly(3-hydroxybutyrate-hydroxyvalerate) (PHBV) copolymers. *Journal of Materials Science* 35(3), p. 523-545 (**2000**).

39. Raj, R. et al., Use of wood fibers in thermoplastic composites: VI. Isocyanate as a bonding agent for polyethylene–wood fiber composites. *Polymer Composites* 9(6), p. 404-411 (**1988**).

40. Joseph, K. et al., Effect of chemical treatment on the tensile properties of short sisal fibre-reinforced polyethylene composites. *Polymer* 37(23), p. 5139-5149 (**1996**).

41. Wong, S. et al., Interfacial improvements in poly(3-hydroxybutyrate)-flax fibre composites with hydrogen bonding additives. *Composites Science and Technology* 64(9), p. 1321-1330 (**2004**).

42. Lee, S.G. et al. Characterization of surface modified flax fibers and their biocomposites with PHB. in *Macromolecular symposia*. 2003. Wiley Online Library.

43. Kusumi, R. et al., Cellulose alkyl ester/poly (ε-caprolactone) blends: characterization of miscibility and crystallization behaviour. *Cellulose* 15(1), p. 1-16 (**2008**).

44. Wong, S. et al., Properties of Poly (3-hydroxybutyric acid) Composites with Flax Fibres Modified by Plasticiser Absorption. *Macromolecular Materials and Engineering* 287(10), p. 647-655 (**2002**).

45. Carlmark, A. et al., ATRP grafting from cellulose fibers to create block-copolymer grafts. *Biomacromolecules* 4(6), p. 1740-1745 (**2003**).

46. Lönnberg, H. et al., Grafting of cellulose fibers with poly (ε-caprolactone) and poly (l-lactic acid) via ring-opening polymerization. *Biomacromolecules* 7(7), p. 2178-2185 (**2006**).

47. Samain, X. et al., Grafting biodegradable polyesters onto cellulose. *Journal of Applied Polymer Science* 121(2), p. 1183-1192 (**2011**).

48. Mohanty, A.K. et al., *Polyhydroxyalcanoates d'anhydride fonctionnalises, preparation et utilisation associees*. 2005, Google Patents.

49. Srubar, W.V. et al., Mechanisms and impact of fiber–matrix compatibilization techniques on the material characterization of PHBV/oak wood flour engineered biobased composites. *Composites Science and Technology* 72(6), p. 708-715 (**2012**).

50. Wei, L. et al., Grafting of bacterial polyhydroxybutyrate (PHB) onto cellulose via in situ reactive extrusion with dicumyl peroxide. *Biomacromolecules* 16(3), p. 1040-1049 (**2015**).

51. Luo, S. et al., Interfacial Improvements in a Green Biopolymer Alloy of Poly(3-hydroxybutyrate-co-3-hydroxyvalerate) and Lignin via in Situ Reactive Extrusion. *ACS Sustainable Chem. Eng.* 4, p. 3465−3476 (**2016**).

52. Rodi, E.G. et al., Functionalization of Miscanthus by Photoactivated Thiol−Ene Addition to Improve Interfacial Adhesion with Polycaprolactone. *ACS Sustainable Chem. Eng.* 4, p. 5475−5482 (**2016**).

53. Sapieha, S. et al., Dicumyl peroxide-modified cellulose/LLDPE composites. *Journal of Applied Polymer Science* 41(9-10), p. 2039-2048 (**1990**).

54. Suwanda, D. et al., The reactive modification of polyethylene. II: Mathematical modeling. *Polymer Engineering & Science* 33(24), p. 1592-1605 (**1993**).

55. Pedernera, M.N. et al., An improved kinetic model for the peroxide initiated modification of polyethylene. *Polymer Engineering & Science* 39(10), p. 2085-2095 (**1999**).

56. Asteasuain, M. et al., Peroxide modification of polyethylene. Prediction of molecular weight distributions by probability generating functions. *Polymer* 43(8), p. 2363-2373 (**2002**).

57. Brandolin, A. et al., Mathematical Modeling of the Reactive Modification of High− Density Polyethylene. Effect of Vinyl Content. *Industrial & Engineering Chemistry Research* 46(23), p. 7561-7570 (**2007**).

58. Gloor, P. et al., Chemical modification of polyolefins by free radical mechanisms: a modelling and experimental study of simultaneous random scission, branching and crosslinking. *Polymer* 35(5), p. 1012-1030 (**1994**).

59. Tobita, H., Simulation model for the modification of polymers via crosslinking and degradation. *Polymer* 36(13), p. 2585-2596 (**1995**).

60. Zhu, S., Molecular weight distribution in free-radical polymer modification with cross-linking: effect of chain-length-dependent termination. *Macromolecules* 29(1), p. 456-461 (**1996**).

61. Johnston, R.T., *Modelling peroxide cross-linking in polyolefins*, in *SPE ANTEC*. 2002: San Francisco, USA.

62. Berthet, M.A. et al., Impact of fibre moisture content on the structure/mechanical properties relationships of PHBV/wheat straw fibres biocomposites. *Composites Science and Technology* 117, p. 386-391 (**2015**).

63. Cyras, V.P. et al., Relationship between processing and properties of biodegradable composites based on PCL/starch matrix and sisal fibers. *Polymer Composites* 22(1), p. 104-110 (**2001**).

64. Keller, A., Compounding and mechanical properties of biodegradable hemp fibre composites. *Composites Science and Technology* 63(9), p. 1307-1316 (**2003**).

65. Nemat-Nasser, S. et al., Micromechanics: overall properties of heterogeneous materials. Elsevier.Vol. 37. (**2013**).

66. Tan, H. et al., The Mori–Tanaka method for composite materials with nonlinear interface debonding. *International Journal of Plasticity* 21(10), p. 1890-1918 (**2005**).

67. Benveniste, Y., A new approach to the application of Mori-Tanaka's theory in composite materials. *Mechanics of materials* 6(2), p. 147-157 (**1987**).

68. Eshelby, J.D. The determination of the elastic field of an ellipsoidal inclusion, and related problems. in *Proceedings of the Royal Society of London A: Mathematical, Physical and Engineering Sciences*. 1957. The Royal Society.

69. Kaack, K. et al., Variation in morphology, anatomy and chemistry of stems of Miscanthus genotypes differing in mechanical properties. Industrial Crops and Products 17(2), p. 131-142 (**2003**).

Chapter VI

"There are two possible outcomes:
if the result confirms the hypothesis,
then you've made a measurement.
If the result is contrary to the hypothesis,
then you've made a discovery."

(Enrico Fermi)

PROCESSING AND ACCELERATED AGING OF PLA/MISCANTHUS COMPOSITES: CORRELATION BETWEEN MECHANICAL PROPERTIES AND CHEMICAL AND PHYSICAL STRUCTURE OF THE COMPOSITES

The production of biocomposites at large scale requires the use of abundant low cost matrix and reinforcement, their easy availability and their processability by common industrial techniques. In this last chapter, poly (lactic acid) (PLA) was chosen not only as green alternative to conventional plastics such as polypropylene (PP) but also as a real inexpensive bio-based and biodegradable matrix for the realization of PLA/Miscanthus composites. This chapter has essentially three main goals concerning the improvement of fiber/matrix adhesion, the processing of composites and the characterization of the long-term behavior of PLA-based composites. First of all, the chemical modification of fibers based on the use of PMMS and DCP, successfully used in the presence of the other matrixes treated in this work (PCL and PHBHV), was applied here to PLA. This treatment, was used to increase the ductility of these composites and to favor the adhesion between fibers and matrix. Secondly, two different processing methods (extrusion and injection molding vs mixing and compression molding) were compared to identify the most appropriate process in term of matrix structure (and possibly degradation) and consequently the final mechanical properties of the composite. Lastly, the combined effects of different aging conditions such as temperature, UV and humidity were evaluated, allowing to investigate the long term behavior of PLA-based composites in different simulated environments and to well understand the degradation mechanisms of PLA.

VI.1. INTRODUCTION

Plastics derived from petrochemical resources or made from synthetic polymers retain their physical and chemical structure for a very long time, increasing the quantity of waste products in the environment. Many efforts have been made from the R&D sector to substitute conventional plastics with biodegradable ones. Among all the existing polymers, PLA, a bio-based and biodegradable polyester has been widely produced and used in these last years. Due to its renewable origin (corn starch, sugar beet), its easy recyclability and compostability [1] , good mechanical properties and relatively low cost [2], PLA represent a promising candidate to replace synthetic plastics in many applications. Moreover, this polymer can be processed by conventional techniques such as extrusion, compression and injection molding [3, 4].

PLA has been largely used in biomedical applications for drug delivery or scaffolds due to its hydrophobicity and biocompatibility respectively [5-7], and it has also been used for food packaging applications [8, 9]. The polymer has been also mixed to vegetal fibers [10-13] such as kenaf [14, 15], bamboo [16], miscanthus [17], ramie [18], cellulose [19, 20]. These fibers are biodegradable with a low impact on the environment [21-23]. Moreover, they can be treated at processing temperature of PLA without significant degradation or abrasion of processing equipment [24]. Although plant fibers improve the mechanical properties of the final composite and allow to reduce the total costs, the performances of the composite in terms of durability are limited by the external conditions at which the composite is exposed, typically humidity, high temperature and UV exposure, as showed in a previous works [25]. The aging of the composite is caused by a variety of mechanisms involving not only the neat PLA, such as hydrolysis [26-28], thermal oxidation [29-31], photo oxidation [32] and natural aging, but also the hydrophilic fibers which naturally contain moisture and that can accelerate the degradation process [29]. This is the reason why many researchers have tried to study the effect of aging conditions on composites realized with fibers whose surface was previously modified with a chemical agent [33]. Another important point is the sensitivity of PLA to the processing method. Changes in crystallinity may occur for different applied cooling rates and shear stresses levels, causing a great variability of the mechanical properties [34, 35].

This work aims to provide a comparison on the processing (see figure VI-1) and aging methods used for PLA and its composites realized with 20 wt % of Miscanthus *giganteus* (MIS) fibers. Two kinds of chemical treatment of fibers were used: the first one was based on the grafting of PLA to vegetal fibers in the presence of DCP (method A, figure VI-1) and the second one on the grafting of

PLA to the fibers previously impregnated with PMMS (method B, figure VI-1). These specimens were realized using different techniques and they were compared to composites realized with raw fibers, as well as with the reference pure PLA matrix.

One of the main purposes of this work was to investigate the effect of three processing methods, such as compression molding with (MC) and without mixing (C, only used for the neat PLA matrix) and extrusion and injection molding (EI) on the thermal, mechanical and physical properties of neat PLA and PLA/MIS composites, in which fibers were raw or modified using peroxide and siloxane as reactants. The second purpose of this work was to understand the long-term behavior of the neat matrix and its biocomposites under the combined effect of temperature, UV and humidity, establishing relations between the aging conditions and the global mechanical properties of the final materials. To this aim an accelerated photo-aging in the presence of oxygen at $47 \pm 5°C$ and 50% of humidity was carried out for a total time of 500 hours. This study intends to be a systematic and rigorous investigation of processing and accelerated aging effects on PLA and its composites. The profound knowledge of the existing relationships between mechanical strength and changes in the macromolecular structure of the polymer will allow us to determine the optimal process to be used for the preparation of future composite materials and the optimal life conditions of these types of composites.
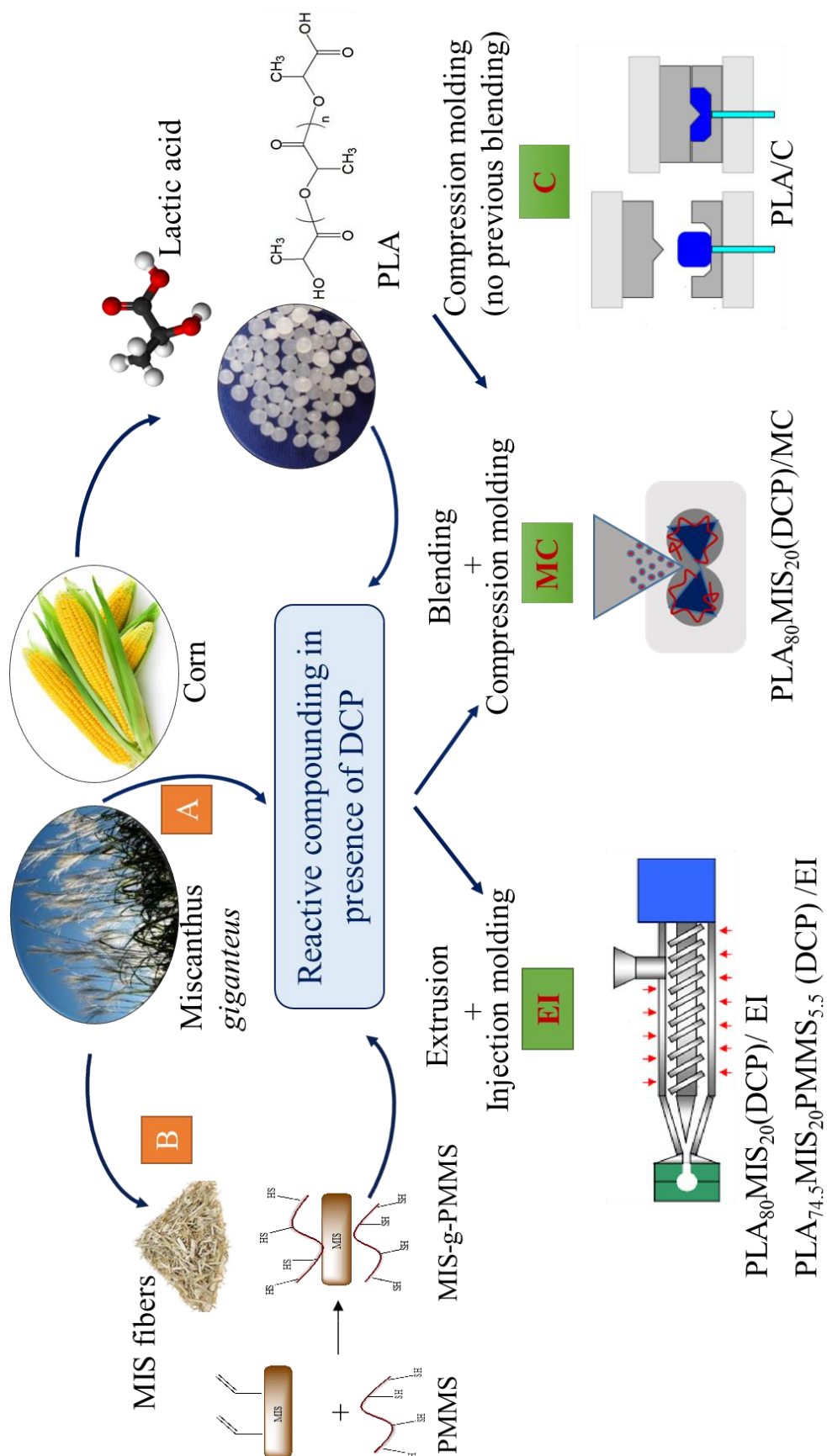
Figure VI-1. Manufacturing methods of PLA-based composites.

VI-2. MATERIALS AND METHODS

VI-2.1 MATERIALS

The poly(lactic acid) (PLA) used for these experiments was the Ingeo2003D purchased by NatureWorks (USA). This grade was recommended by the producer for the extrusion process and packaging applications. The polymer has a MFR of 6 g/10 min at 210°C and 2.16 kg load and a density of 1.24 g/cm^3. Miscanthus *giganteus* (MIS) was provided by Miscanplus (France). It came from a spring crop roughly chopped and subsequently milled and riddled with a 500 μm mesh sieve. Poly(mercaptopropyl)methylsiloxane (PMMS) was purchased from Abcr GmbH & Co. (Germany). The dicumyl peroxide (DCP) at 98% was provided by Sigma Aldrich.

VI-2.2 CHEMICAL TREATMENT OF MISCANTHUS GIGANTEUS FIBERS

Two different reactants were used to treat the surface of vegetal fibers. In the first method, the surface of Miscanthus *giganteus* fibers was modified using the PMMS as chemical agent. Fibers were impregnated in a solution 40 g/l of PMMS in dichloromethane for one hour. More precisely 20 g of PMMS were solubilized in 500 ml of dichloromethane and then 20 g of fibers were added to the solution and stirred at 200 rpm. After impregnation, fibers were filtrated and dried in atmospheric conditions until weight reached a constant value. At the end of the procedure, fibers coated with PMMS had an average weight gain of around 27% (cf. method B in figure VI-1).

The second method consists in an impregnation of the dried fibers in a solution 8 mg/ml of DCP in acetone. Fibers (a total amount of 8 g) were stirred for 30 minutes at 20 rpm in a solution containing 880 mg of DCP solubilized in 110 ml of acetone. They were then dried statically before the preparation of composites (cf. method A in figure VI-1).

VI-2.3 COMPOUNDING WITH INTERNAL MIXER AND MANUFACTURE OF COMPOSITES BY COMPRESSION MOLDING

Before processing, PLA pellets and raw fibers were dried at 80°C under vacuum for 24 hours in order to remove moisture. PLA is very sensible to hydrolysis and as recommended by the producers the moisture content before processing must be less than 0.025%. Matrix and fibers were mixed for 10 minutes using a Brabender W 50 EHT internal mixer operating at 180°C and 50 rpm. The compounding consisted of two steps. At first the polymer pellets were melted in the internal mixer.

After a decrease in the torque value was observed, 20 wt% of fibers, chemically treated or not, were added little by little in order to prevent clustering of fibers. The mixing was continued for 10 minutes for all composites except for those prepared using fibers modified with DCP. For the latter, in order to avoid the crosslinking of the matrix within the Brabender, the mixing time was set to 5 minutes. After mixing, all the blends realized, were dried at 80°C under vacuum for 24 hours and then they were compressed to 1 mm thick plates. During the compression molding, the blends were heated at 200°C for 7 minutes. Two different steps were applied, the first one with a pressure of 20 kg/cm^2 for 10 minutes and the second one at 40 kg/cm^2 for 5 minutes. Mold and samples were cooled down to room temperature with a water cooling system. All specimens were kept in a room with controlled temperature and humidity (23° C and 50% RH) for at least 48 hours prior further testing. In alternative to this procedure, PLA pellets were directly compressed after drying using the same conditions. The objective was to evaluate the influence of the mixing and of the intermediary drying on the mechanical properties of PLA alone. The mixing and compression and the simple compression will be indicated from now with the letters MC and C respectively. Relevant parameters used are listed in the table VI-1.

VI-2.4 COMPOUNDING WITH A TWIN-LAB EXTRUDER AND MANUFACTURE OF SPECIMENS BY INJECTION MOLDING

PLA and raw fibers were dried at 80°C under vacuum for 24 hours before processing. Polymers pellets and treated or untreated fibers were mixed using a lab-scale twin-screw extruder (Minilab Thermo Scientific Haake). The experiments were performed at 180°C with a screw speed of 50 rpm. The retention time for the pure matrix was of 1 minute; this time was increased to 2 minutes in order to well disperse fibers into the matrix. After recirculation, the extruded molten material was transferred and shot in a micro-injection unit (MiniJet Thermo Scientific Haake) operating at 210°C at a fixed injection pressure for 30 seconds. A maintenance pressure, lower than that during the phase of injection, was applied for other 30 seconds. The pressures values were adapted to the viscosity of the molten blends in order to fill completely the mold during the injection molding. Specimens of standard dimensions were then obtained and stored for 48h before testing. This method will be indicated from now by the letters EI and relevant parameters are also listed in table VI-1.

Reference	Method	T_M [°C]	rpm [t*min^{-1}]	t_M [min]	T_I [°C]	T_m [°C]	t_c [min]	P_1 [bar]	t_1 [min]	P_2 [bar]	t_2 [min]
EI	A	180	50	2	210	Variable*	-	Variable*	0.5	Variable*	0.5
MC	B	180	50	10	-	200	7	20	10	40	5
C	C	-	-	-	-	200	7	20	10	40	5

* Variable values depending on the viscosity of the blend

Table VI-1. Processing parameters for the three processing methods: T_M (Melt temperature); rpm (rotation speed); t_M (mixing time); T_I (injection temperature); T_m (mold temperature); t_c (contact time), P_1, P_2 (first and second pressures), t_1 and t_2 (time of contact 1 and 2).

VI-2.5 ACCELERATED AGEING

One of the objective of this study was to evaluate the long-term behavior of neat PLA and its composites. To this aim, the effect of combined parameters, such as temperature, UV and humidity were studied.

At first, specimens of PLA (C) and $PLA_{80}MIS_{20}$ (MC) previously cut and notched on one side (see section VI-2.1 for more details) were UV aged for 250 hours at 32°C in a dried environment. Aging was carried out in a Solarbox 3000e chamber from Erichsen equipped with a filtered Xenon lamp with radiative thermal flux of 550 $W.m^{-2}$. The light of the xenon lamp was filtered under 280 nm with an UV window combined with IR filter glasses. After aging, all specimens were stored in a thermostatic chamber at 23°C and 50% of humidity before fracture tests.

In a second time, another accelerated aging was conducted in the same machine at 47 ± 5°C and 50% of relative humidity for a total exposure time of 500 hours on the neat matrix realized by direct compression of granules (PLA(C)) and also on $PLA_{80}MIS_{20}$ (MC) and $PLA_{80}MIS_{20}$ (DCP) (MC) composites realized by mixing and compression molding. Samples realized with fibers modified with PMMS were not investigated here due to their lower mechanical resistance than the others. This machine can create an accelerated environment of the natural weathering conditions, simulating materials conditions during its lifetime, i.e., daylight exposure to heat, oxygen and humidity. The effect of temperature combined with UV and humidity was then evaluated by tensile tests every 250 hours by thermal and spectroscopy analyses. All specimens realized with different methods and aged according to the procedure described above are summarized in table VI-2 and identified by a reference number in order to simplify the description of future results.

Sample	Method	Composition	DCP [wt %]	Aging
1	C	PLA	-	-
1'	C	PLA	-	250h (47°C, 50%RH)
1''	C	PLA	-	500h (47°C, 50%RH)
1'''	C	PLA	-	250h (32°C, 0% RH)
2	MC	PLA	-	-
3	EI	PLA	-	-
4	MC	$PLA_{80}MIS_{20}$	-	-
4'	MC	$PLA_{80}MIS_{20}$	-	250h (47°C, 50%RH)
4''	MC	$PLA_{80}MIS_{20}$	-	500h (47°C, 50%RH)
4'''	MC	$PLA_{80}MIS_{20}$	-	250h (32°C, 0% RH)
5	EI	$PLA_{80}MIS_{20}$	-	-
6	MC	$PLA_{80}MIS_{20}$ (DCP)	2.2	-
6'	MC	$PLA_{80}MIS_{20}$ (DCP)	2.2	250h (47°C, 50%RH)
6''	MC	$PLA_{80}MIS_{20}$ (DCP)	2.2	500h (47°C, 50%RH)
7	EI	$PLA_{80}MIS_{20}$ (DCP)	2.2	-
8	MC	$PLA_{74.5}MIS_{20}$ $PMMS_{5.5}$(DCP)	2.2	-
9	EI	$PLA_{74.5}MIS_{20}$ $PMMS_{5.5}$(DCP)	2.2	-

Table VI-2. Description of principal samples realized. PLA: poly(lactic acid); MIS: Miscanthus *giganteus* fibers; DCP: dicumyl peroxide; PMMS: poly(mercapropropylmethylsiloxane).

VI-3. MATERIALS CHARACTERIZATION

VI-3.1 MECHANICAL CHARACTERIZATION

The tensile properties of all the specimens realized by simple compression (C) and mixing and compression molding (MC) were studied using an Instron 1121 Universal Testing Machine equipped with a 500N load cell. All types "5 dumb-bell specimens" were obtained using a die cutter according to ISO 527-3. The displacement of the specimens were evaluated using a camera that tracks the position of markers placed on the surface of the test specimens. The recorded video was then converted in a series of frames that were processed with ImageJ software to determine accurately the strain of each specimen.

All samples realized by extrusion and injection molding were tested by an Instron 5965 Universal Testing Machine equipped with cell load of 2 kN. In this case the strain was estimated by the crosshead displacement. All tensile tests were performed at a constant displacement rate of 2 mm/min. In order to evaluate the fracture toughness K_I of PLA (C) and $PLA_{80}MIS_{20}$ (MC) composites aged and not (the index I refers to mode I fracture), LEFM (Linear Elastic Fracture Mechanics) was considered as the best solution. In this case the stress intensity factor K_I completely characterizes the stress field around a crack tip. To this aim, single edge notched tensile (SENT) specimens having dimensions of 50x20x1 mm (HxWxd), with initial notch length of 10 mm (a_0) were realized. Notches were made via automated "chisel-wise" cutting on one side of specimen. Tests were conducted at a constant displacement rate of 2 mm/min and in standard conditions (23°C and 50% RH) using an Instron 1121 Universal Testing Machine. Figure VI-2 shows the specimen used for this type of test, in which H refers to the gauge length, the actual sample being longer to allow for firm gripping.

W=20 mm

H=0.46x2xW

a=10 mm
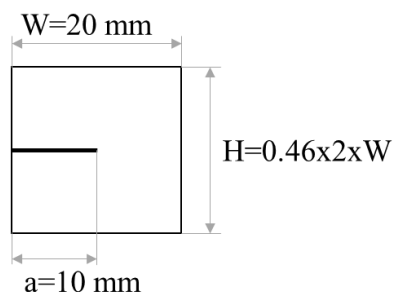
Figure VI-2. In-plane dimensions of the samples used for fracture tests. The value of H refers to the gauge length, with the samples being longer to allow for firm gripping.

The stress intensity factor was calculated using the following equation:

$$K_I = \alpha \sqrt{\pi a} \sigma \qquad\qquad\qquad (VI\text{-}1)$$

Where "α" is a geometry factor, "a" is the notch length and "σ" is the nominal stress applied to the specimens during the tensile test.

VI-3.2 DIFFERENTIAL SCANNING CALORIMETRY (DSC) ANALYSIS

The thermal behavior of neat PLA and PLA–based composites was analyzed using a PerkinElmer Diamond DSC Instruments. Around 10 mg of each sample were introduced into aluminum pans and were then analyzed. The samples were first heated from 20°C to 200°C with a heating rate of 10°C/min, kept isothermal for 1 min at 200°C, then cooled down to 20°C at 100°C/min and finally heated again to 200°C with a heating rate of 10°C/min. The first heating run was considered for determining the melt temperature (T_M) and melting enthalpy (ΔH_M) of samples, while the second run was considered for determining the glass transition temperature (T_g). The crystallinity (X_c) of the PLA phase was calculated by the following equation:

$$X_c\ (\%) = \frac{\Delta H_M}{\Delta H^0 * W_f} * 100 \qquad\qquad\qquad (VI\text{-}2)$$

where ΔH^0 is the enthalpy of melting per gram of 100% crystalline PLA that is 93.6 J/g and W_f is the weight fraction of PLA in the specimen [36].

VI-3.3 X-RAY DIFFRACTION (XRD) ANALYSIS

In order to evaluate structural change due to processing and aging, the neat PLA and its composites were analyzed using a D8 advance Bruker diffractometer operating at 40 kV and 40 mA with a CuKα radiation. The angle range investigated was $2\theta \approx 5\text{-}40°$.

VI-3.4 FOURIER TRANSFORM INFRARED SPECTROSCOPY (FTIR)

Qualitative changes in crystallinity due to the process and to the aging were evaluated using infrared spectroscopy on samples of neat PLA and its composites. All spectra were recorded using a TENSOR27 Bruker apparatus equipped with an attenuated internal reflection accessory using a diamond crystal (Digi Tech DLATGS Detector, 32 scans, 4 cm^{-1}) in the range 500-4000 cm^{-1}.

VI-3.5 SIZE EXCLUSION CHROMATOGRAPHY (SEC)

The changes in molecular characteristics were obtained by size exclusion chromatography (SEC) equipped with a refractive Index detector (Shodex) and a light scattering detector (Wyatt dawn 8+). The calibration of SEC equipment was based on polystyrene standards. All analyses were performed in THF as the eluent at a flow rate of 1 ml*min^{-1}. The PLA solutions in THF (10 mg*ml^{-1}) were prepared and analyzed. Results were treated using Astra V software. At the end of data treatment, the molar mass and the polydispersity index were evaluated.

VI-3.6 SCANNING ELECTRON MICROSCOPY (SEM)

The morphological appearance of tensile fractured surfaces of specimens was investigated using a Merlin Zeiss scanning electron microscopy. Samples were sputter-coated with a thin layer of palladium in a Cressington 208 HR sputter-coater. Images were recorded with an acceleration voltage of 10keV and at different magnifications. Different zones of specimens, with particular attention to the interface fiber/matrix, were observed in order to have information about the effect of processing and aging on the cohesion of fibers to matrix.

VI-4. RESULTS AND DISCUSSIONS: PART I. EFFECT OF PROCESSING ON THE PROPERTIES OF PLA AND PLA-BASED COMPOSITES

VI-4.1 INFLUENCE OF PROCESSING ON THE CHARACTERISTICS OF PLA EVALUATED BY FTIR, XRD, SEC AND DSC

In this work different processing methods (see figure VI-1) already described in paragraph VI-2.3 and VI-2.4 were used to realize specimens of neat PLA and PLA/MIS composites. This matrix is very sensitive to the processing conditions [34, 35] and for this reason it seems necessary to investigate the effect of processing on the microscopic structure of PLA. At first, infrared spectroscopy analysis (FTIR) was used to detect qualitative changes in the crystallinity structure. The principal band assignments for neat PLA were identified according to the literature data [37] and they are listed in more details in table VI-3. Once recorded, spectra were normalized using the peak at 1454 cm^{-1}, corresponding to the methyl group of PLA. This peak was chosen because it doesn't vary

significantly after chemical modification or processing. Specimens of neat PLA realized by different processing were analyzed and spectra were recorded (figure VI-3). Extruded and injected PLA specimens (EI) showed a decrease in C=O ester and in the C-O peaks whereas mixed and compressed ones (MC) showed an increase in the same bands. Evident changes in the zone between 725 and 955 cm^{-1}, which is related to the crystalline zone of PLA that are present for PLA (C) and PLA (MC) samples as showed by the zoom of these zones in figure VI-4. However, these results provide only qualitative information about changes in the crystalline structure of PLA.

v (cm^{-1}) in literature [32, 37, 38]	v (cm^{-1}) in this work	Attribution
3504	-	ν_{OH}
2995	2995	ν_{CH_3}
2945	2945	ν_{CH_3}
1754	1747	$\nu_{C=O}$
1450	1454	δ_{CH_3}
1382	1382	δ_{CH}
1361	1358	δ_{CH}
1263	1261	ν_{COC}
1193	1180	ν_{COC}
1100	1080	ν_{COC}
1045	1042	δ_{C-OH}

Table VI-3. Typical bands assignment for PLA.
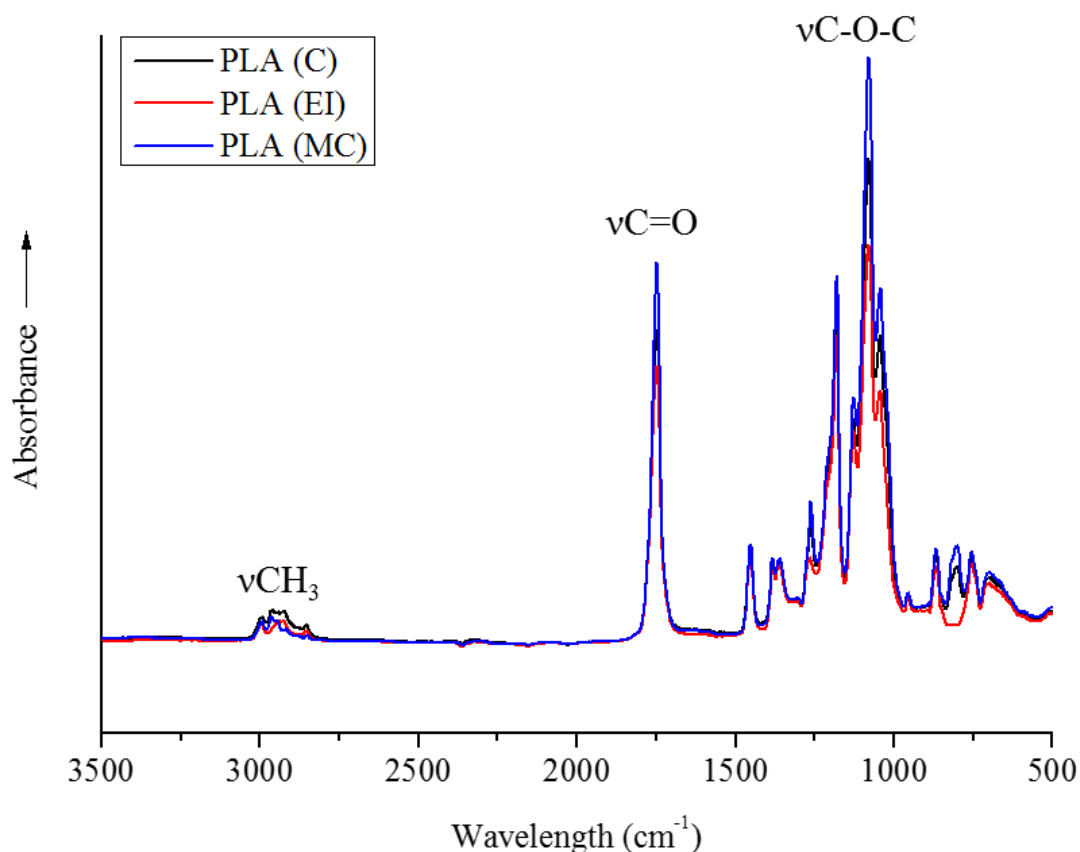
Figure VI-3. FTIR-ATR spectrum of PLA realized by compression (C), mixing and compression (MC) and extrusion and injection (EI). Normalization at 1454 cm^{-1} assigned to δ_{CH3}.
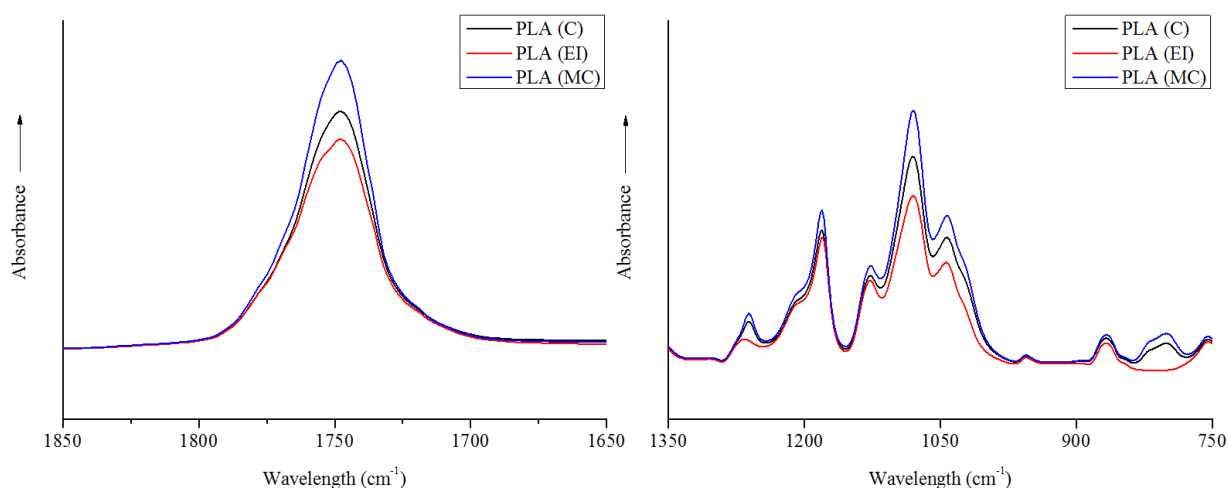
Figure VI-4. FTIR-ATR spectra of PLA processed in different ways in the zones 1650-1850 cm^{-1} and 750-1350 cm^{-1}. Normalization at 1454 cm^{-1} assigned to δ_{CH3}.

Other analyses, such as XRD and DSC analyses can show more precisely a change in the crystalline structure of PLA. From literature, it is known that PLA presents one peak at $2\theta = 16.4°$ corresponding to the 110 reflections and two smaller peaks at 19.1° and 32° corresponding to planes

010 and 203, respectively, in the orthorhombic lattice [39]. XRD of neat PLA specimens realized in different ways were performed and diffractograms were compared in figure VI-5. PLA (C) and PLA (MC) showed a typical amorphous behavior, while the PLA (EI) showed peaks typical of the crystalline structure located at 17.2°. The difference between these XRD results is most certainly induced by the different processing conditions used in each case. The compression molding didn't favor the formation of orderly polymer chains, thus inhibiting the development of polymeric crystals. On the contrary, shear stresses applied during the extrusion or injection molding processes is likely to cause an increase in crystallinity degree.
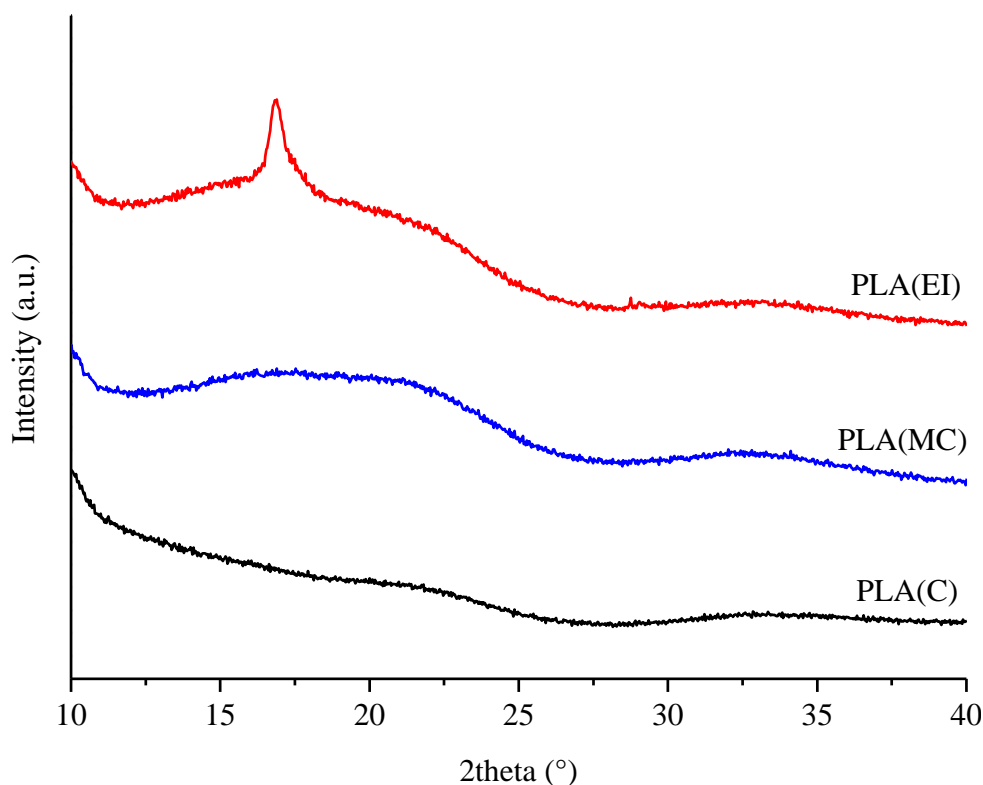
Figure VI-5. XRD of PLA (C) (black curve), PLA (MC) (blue curve) and PLA (EI) (red curve).

The results obtained by XRD and FTIR were confirmed by thermal analysis (see table VI-4). Sheet of neat matrix realized in 3 different ways showed a slight decrease in T_M (from 152°C to 149°C) and also an important increase in crystallinity degree from 2% for the PLA (C) (sample **1**) to 19% for the PLA (MC) (sample **2**) and 32% for the PLA (EI) (sample **3**). Processing methods such as extrusion or injection molding in which high shear stresses are applied are able to enhance the crystallization of PLA. The almost completely amorphous nature of PLA (C) (sample **1**) could be explained by two distinct raisons. First of all, all specimens realized by mixing and compression were dried twice: before mixing and between the two processing steps. In all cases drying was carried out

at a temperature above the T_g of the polymer (80°C for 24 hours). This intermediate drying causes a change in the color of matrix from transparent to white (images are not reported here), the latter occurrence suggesting an increase in crystallinity. Specimens of PLA (C) were not dried a second time, being the dried granules directly compressed. In order to demonstrate that the temperature has a role in the change of the crystalline structure of the polymer, specimens of PLA (C) were annealed for 24 hours at 70°C (T_g +10°C). In this case a slight increase in crystallinity from 2 to 7% was observed. In a second thermal cycle, temperature was increased to 100°C (T_g + 40°C) and the same samples were reheated for 24 hours. In this case, the crystallinity degree finally observed was of 21% The results, presented in table VI-5, show that the thermal history of the polymer plays a role on its ability to crystallize and that the molecular movements of the polymer chains are favored by higher temperatures. Secondly, at high compression pressure the crystallization of PLA can be prevented, despite the low cooling rate.

The composites PLA$_{80}$MIS$_{20}$ (samples **4**, **5**) showed no significant changes in the degree of crystallinity, while those realized in the presence of DCP (samples **6, 7**) showed a decrease in T_M from 151°C (sample **6**) to 147°C (sample **7**), but not in the percentage of crystallinity, showing that for these composites changes in crystallinity concerned the dimensions of crystals that became smaller due to the extrusion and injection processing (See figure VI-6). Comparing the PLA (MC) (sample **2**) with the composite obtained in the same conditions (sample **4**), an increase in crystallinity was observed for the composites (from 19% to 25%). This result could be explained by the formation of trans-crystalline zones formed around the fibers as showed in previous works [17, 40]. The same comparison for the materials realized by injection molding (samples **3** and **5**) showed an opposite trend, indicating that fibers in this case did not act as nucleation points.
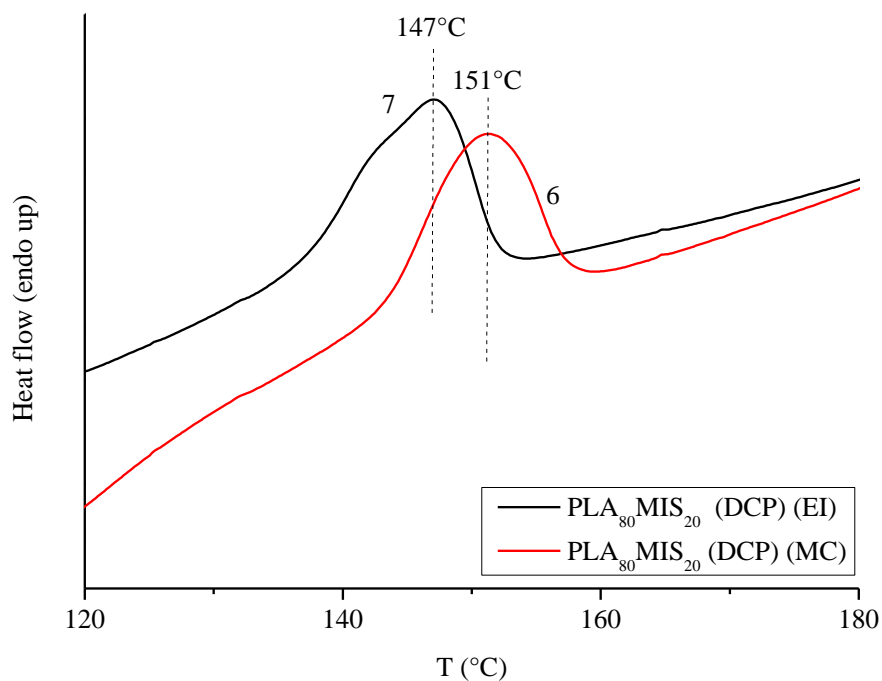
Figure VI-6. DSC curves for PLA$_{80}$MIS$_{20}$ (DCP) (sample **6** and **7**).

	Sample	Method	T$_M$ [°C]	ΔH$_M$ [J/g]	T$_g$ [°C]	X$_C$ [%]
-	Virgin PLA	-	152	29	61	31
1	PLA	C	151	2	61	2*
2	PLA	MC	152	18	61	19
3	PLA	EI	149	30	61	32
4	PLA$_{80}$MIS$_{20}$	MC	151	19	61	25
5	PLA$_{80}$MIS$_{20}$	EI	151	22	61	29
6	PLA$_{80}$MIS$_{20}$ (DCP)	MC	151	21	61	28
7	PLA$_{80}$MIS$_{20}$ (DCP)	EI	147	20	59	27

*The value of this point has been clarified in the table VI-5.

Table VI-4. Effect of process on the thermal properties of neat PLA and its composites.

Sample	T_1 [°C]	t_1 [h]	T_2 [°C]	t_2 [h]	X_c [%]
PLA (C)	-	-	-	-	2
PLA (C)	70	24	-	-	7
PLA (C)	70	24	100	24	21

Table VI-5. Crystallinity degree of PLA(C) after heating at 70°C and 100°C for 24h.

The sensibility to moisture of PLA is a well-known problem affecting the properties of this matrix in particular during the processing step. For this reason SEC analysis was also used to detect all changes in molar mass (M_n) and polydispersity index (PI) of PLA samples realized by different methods and the results are showed in table VI-6. The polydispersity index shows a little increase from 1.2 for a virgin PLA to 1.4 for the PLA (MC/EI) (samples **2**, **3**). A decrease in M_n for specimens of PLA (EI) (sample **3**) is also visible. In general a decrease in molar mass occurred for specimen subjected to high shear stresses, indicating that the processing methods have an direct impact not only on the reduction of fibers aspect ratios (values not reported in this chapter but shown in Chapter III), but also on the degradation of polymer chains.

Reference	Sample	PI	M_n [g/mol]
-	Virgin PLA	1.2	136000
1	PLA (C)	1.4	105000
2	PLA (MC)	1.3	111500
3	PLA (EI)	1.4	98300

Table VI-6. Molar masses (M_n) and polydispersity index (PI) of PLA realized by different processing methods.

VI-4.2 EFFECT OF PROCESSING ON THE MECHANICAL PROPERTIES OF NEAT PLA AND PLA-BASED COMPOSITES

The mechanical properties, which are of fundamental importance in this study, were evaluated through tensile tests on specimens realized by different processing methods already described and resumed in table VI-2. In general, the addition of vegetal fibers caused an increase in elastic modulus and a decrease in elongation at break due to the reinforcing effect of fibers as showed in previous works [17, 41, 42]. In our case we observed an important increase in Young Modulus from 3500 MPa (sample **2**) to 5194 MPa for the composite reinforced with 20 wt % of fibers (sample **4**). The value obtained is higher than that obtained by other researchers for the same compositions and reinforcement type, the latter reaching values of 2422 MPa. Moreover, if compared to poly(propylene), values obtained are much higher (1270 MPa) [41].

The weak adhesion between fibers and matrix, with a consequent inability to transfer stress at the interface between the two phases, was suggested by the decrease in final strength from neat PLA (samples **1**, 2, **3**) to all composites realized (samples **4, 5, 6, 7, 8** and **9**) independently from the production method (figure VI-7). This decrease is more evident in the case of fibers modified with PMMS indicating that this type of fibers modification didn't have the expected result on PLA. PMMS is a more ductile polymer than PLA, but its presence in this case is not sufficient to improve the adhesion fibers/matrix as showed for example in other works in which a strong increase in mechanical properties were found for poly(ε-caprolactone) (PCL)-based composites [43].

Comparing the processing methods, an increase in final strength and at the same time a decrease in Young Modulus occurred for specimens realized by extrusion and injection molding. The increase in final strength could be explained by the fact that shear stresses applied during extrusion and injection molding enhance the crystallinity of PLA [35, 44, 45] . The DSC analyses showed in the previous paragraph are a further confirmation of this result. Moreover, virgin PLA constituted by extruded granules have the same crystallinity of extruded and injected samples. At the same time, the degradation of the polymer matrix suggested by SEC analysis might explain the decrease in Young Modulus.

Torque values and temperature profiles reported in figure VI-A1 (appendix VI-7A), showed that a mixing time of ten minutes is sufficient to homogenize fibers and matrix for all composites realized (torque and temperature profiles reach a constant value) except for composites **6** which tests were stopped at five minutes in order to avoid the cross-linking of the matrix in the Brabender mixer.

Actually, in the case of fibers modified with DCP (samples **6, 7, 8** and **9**), the expected result was an increase in elongation at break and in final strength due to the presence of DCP as showed in

previous works [43, 46, 47]. This increase is essentially due to an improved adhesion between the reinforcement and the matrix that allows the material to resist to a higher stress.

However, in this study, results suggested that DCP had a negative effect on the mechanical properties of composite, resulting in no significant change in final strength and in a decrease in Young Modulus. Similar results were also found elsewhere [34]. In order to understand if this trend is correlated to the DCP quantity, we tried to increase DCP content from 2.2 to 5 wt %. However, the formed product had a totally crumbly texture (see figure VI-B1 in Appendix VI-7B) and it was impossible to use the compression molding technique to obtain convenient specimens.

Despite PLA being an aliphatic polyester such as PCL and PHBHV, the grafting in the presence of DCP is less efficient. In all cases DCP creates radicals able to abstract a hydrogen in the macromolecular chain, promoting grafting, but in the case of PLA β-scission reactions may occur explaining in this way the poor mechanical results obtained. Notwithstanding this remark, figure VI-7 shows that these composites represent a good compromise between high Young Modulus and good final strength. For this reason, in the next section focusing on the aging of these materials, only specimens of $PLA_{80}MIS_{20}$ prepared with and without DCP will be taken into account. These results were than compared to those obtained for the neat matrix. Referring to the latter, no difference in terms of mechanical results were found for samples of neat PLA (MC) and PLA (C) (table VI-B1 in appendix VI-7B).

Actually, one of the aims of this study is to find the best processing method in terms of rapidity, minor cost and low impact on polymer structure and properties. The above results concerning the neat matrix suggests that PLA can be easily processed by direct compression of granules. This procedure allows to optimize time, reducing the degradation of the polymer matrix. However, the direct compression can't be used for the realization of biocomposites for which a homogenization step (mixing or extrusion) is necessary. Although mixing and compression molding method results in polymers with low degree of crystallinity and lower final strength, it has several advantages such as the rapidity and the absence of orientation effect of the fibers, resulting in a more isotropic material. Moreover this process is considered as less aggressive due to lower shear stresses applied during mixing, resulting in a minor reduction of the fibers length (aspect ratio not reported in this work). For all these positive features in the next section all composites subjected to certain aging conditions were prepared by this processing technique.
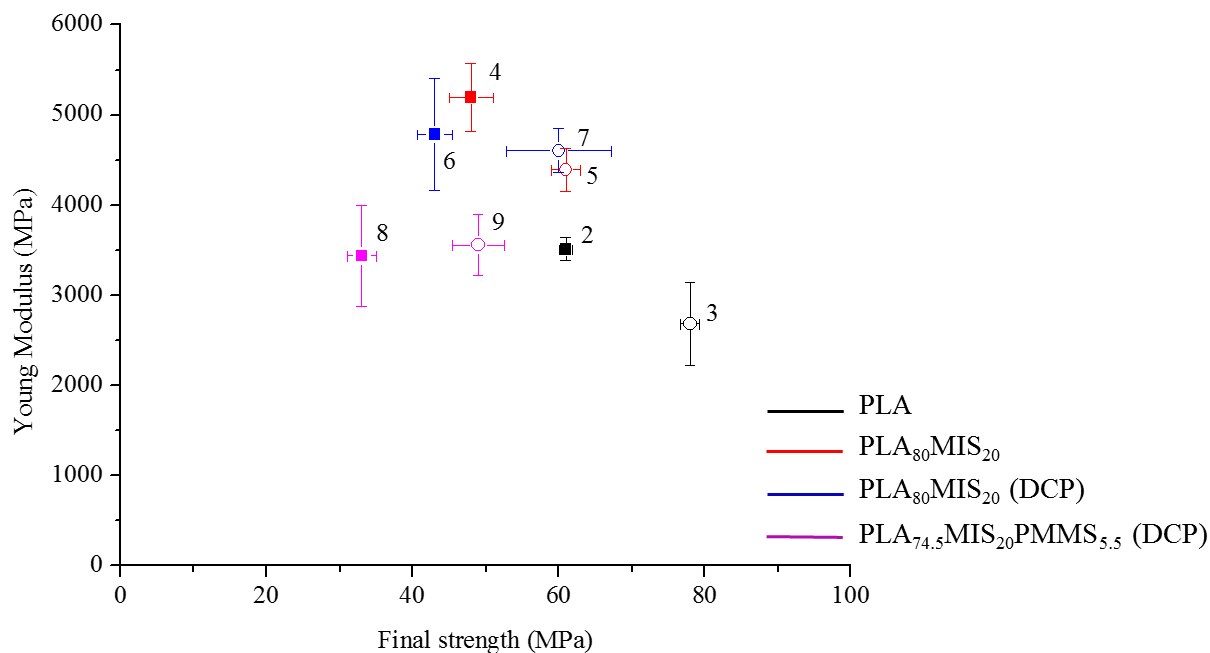
Figure VI-7. Young Modulus vs Final strength for mixed and compressed (■) and extruded and injected (o) specimens.

VI-4.3 ANALYSIS OF FRACTURE SURFACE BY SEM

The effect of different processing can be also evaluated by SEM images recorded on the cross section of samples after traction tests, focusing the attention on the general appearance of the matrix and on the interface fiber/matrix. The failure type and the orientation of fibers into the continuous phase can be evaluated. Figure VI-8 shows the comparison between a composite with 20 wt % of fibers realized by extrusion and injection molding (EI) (figure VI-8 A) and the same composite realized by mixing and compression molding (MC) (figure VI-8 B).

The compressed samples showed a typical brittle failure, while injected samples showed a plastic failure. In all cases fibers were pulled out from the matrix indicating that the adhesion fiber/matrix was poor. In the case of compressed samples it seems that the adhesion of the fibers to the matrix is better than that of injected samples. Moreover the figures show also the different dispersion of fibers in the continuous phase, due to the different processing techniques used. As could be expected, compressed samples seem more isotropic than the injected ones in which an orientation of the fibers in the direction of the material molten flux is firstly due to the extrusion and then to the injection molding. The anisotropy and isotropy of injected and compressed samples respectively were also verified by visual observation on the different samples (images not reported in this work).

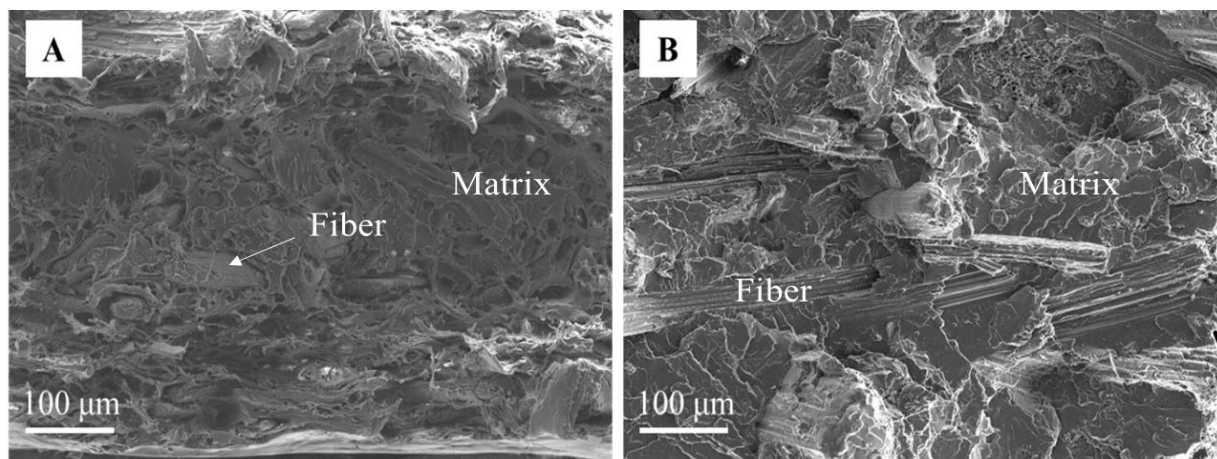Figure VI-8. SEM images of PLA$_{80}$MIS$_{20}$ realized by extrusion and injection molding (A) and by mixing and compression molding (B).

VI-5. RESULTS AND DISCUSSIONS: PART II. EFFECT OF AGING ON THE PROPERTIES OF PLA AND PLA-BASED COMPOSITES

VI-5.1 EFFECT OF AGING ON THE CRYSTALLIZATION BEHAVIOR AND DEGRADATION OF PLA EVALUATED BY FTIR, DRX, DSC AND SEC

In this section the effect of UV, temperature, oxygen and humidity on the properties of PLA and its composites were described. When UV are used at ambient temperature and in the absence of humidity no change in the polymer structure was detected using FTIR, XRD and DSC analyses. Spectra, diffractograms and thermograms of PLA (C) (sample **1'''** in table VI-2) and $PLA_{80}MIS_{20}$ (MC) (sample **4'''** in table VI-2) before and after aging are perfectly superimposed. These results suggest that a UV exposure time of 250 hours has no effect on the crystallinity of PLA and its composites in the absence of humidity and high temperature.

For this reason, a photo-oxidative aging was then carried out at $47 \pm 5°C$ and 50% of humidity. Accordingly to the literature [48] a new band should appear at 921 cm^{-1} indicating the presence of alpha crystals. In our case, we didn't observe this effect on the neat matrix. However, the band at 921 cm^{-1} appears for all composites after 250 hours of aging. Composites showed also the decrease in C=O band, confirming that the hydrolysis of esters bonds can be favored in the presence of humidity at high temperatures. Moreover the C=O ester bonds at 1747 cm^{-1} shift to 1754 cm^{-1} and two C=O distributions are clearly visible after aging (figure VI-C1 appendix VI-7C). These results suggest that the properties of neat PLA are not greatly affected under mild aging conditions, while those of composites changes in the same conditions. More precisely, below the glass transition temperature, the movements of the chains are limited and water cannot diffuse easily in the matrix. On the contrary, the presence of hydrophilic and hygroscopic fibers favored the absorption of water in the blend and the consequent hydrolysis of the matrix.

To support FTIR analysis, XRD was used also in this case to evaluate changes in the crystalline structure of PLA and its composites due to the aging. Figure VI-C2 in the appendix VI-7C showed a comparison between diffractograms in the range 2theta = 5-35° for a PLA (C) and a $PLA_{80}MIS_{20}$ (MC) before and after aging. The comparison revealed an important result: when UV radiation occurred on the neat matrix for relative short time at low temperature, no changes were detected in the crystalline structure. On the other hand, the presence of fibers caused in the same conditions a change in the crystalline structure, the latter going from almost completely amorphous before aging

to semicrystalline after aging. The crystalline peaks of PLA (17°, 19° and 29°) and crystalline cellulose (22.7°) appeared after aging, showing both a change in the crystalline structure of the polymer and in that of lignocellulosic fibers. The parameters of the orthorhombic crystalline lattice were evaluated after XRD analysis. This procedure showed an increase of the lattice volume in the case of composites after aging from 0.465 nm^3 to 0.527 nm^3.

The combined effect of temperature, UV and humidity was also studied using DSC analysis. The neat matrix PLA (C) showed an increase in crystallinity from 2 (sample **1**) to 18% after aging (sample **1'**). The sensitivity of PLA to humidity combined with high temperature, together with the almost amorphous nature of PLA (C), favored changes in crystalline structure. Composites realized with raw fibers did not show significant change in the crystallinity degree. On the contrary, most relevant changes were found for the composites PLA$_{80}$MIS$_{20}$ (DCP) in which the accelerated aging caused a decrease in T_g from 61°C to 56°C and in T_M from 151°C to 142°C for samples **6** and **6'** respectively as showed in figure VI-9. All the thermal results are resumed in table VI-7.

Reference	Sample	Aging time [h]	T_M [°C]	ΔH_f [J/g]	T_g [°C]	X_c [%]
1	PLA (C)	NA	151	2	61	2
1'	PLA (C)	250h	151	17	61	18
1''	PLA (C)	500h	151	13	61	14
4	PLA$_{80}$MIS$_{20}$(MC)	NA	151	19	61	25
4'	PLA$_{80}$MIS$_{20}$(MC)	250h	152	21	61	28
4''	PLA$_{80}$MIS$_{20}$(MC)	500h	152	19	61	25
6	PLA$_{80}$MIS$_{20}$(DCP) (MC)	NA	151	21	61	28
6'	PLA$_{80}$MIS$_{20}$(DCP) (MC)	250h	142	20	56	27
6''	PLA$_{80}$MIS$_{20}$(DCP) (MC)	500h	144	21	59	28

Table VI-7. Effect of UV (λ<280nm), temperature (47±5°C) and humidity (50% RH) on neat PLA, on composite PLA$_{80}$MIS$_{20}$ with and without DCP.
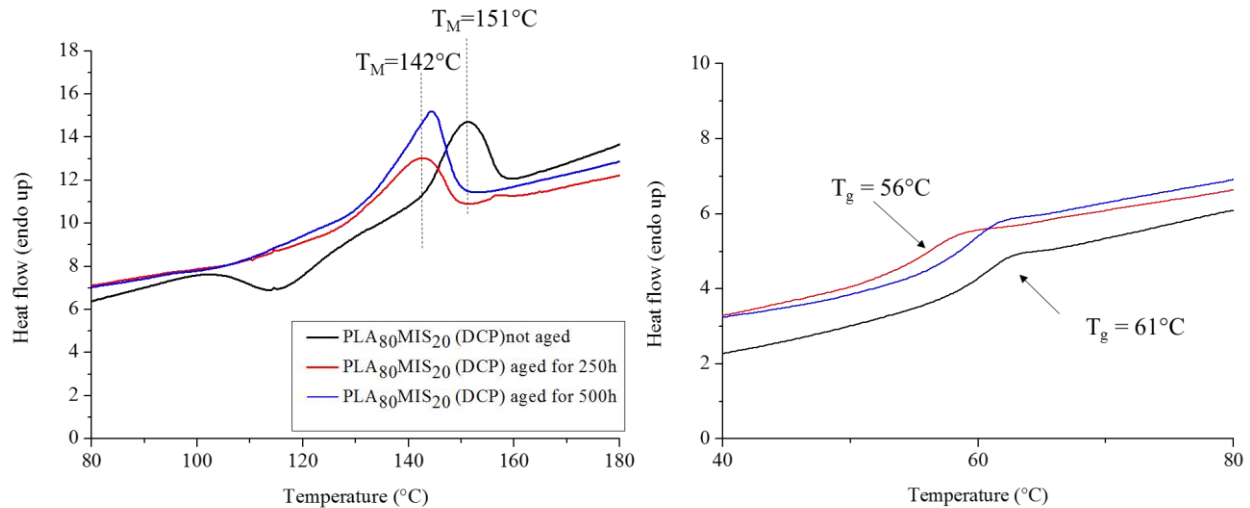
Figure VI-9. DSC curves for PLA$_{80}$MIS$_{20}$ (DCP) specimens not aged (black curve), aged with UV (λ<280nm) for 250h (red curve) and for 500h (bleu curve) at 47±5°C and 50% of humidity.

VI-5.2 EFFECT OF AGING ON THE MECHANICAL PROPERTIES OF NEAT PLA AND ITS COMPOSITES

In a general case fracture will initiate from a given defect when the applied stress intensity factor, K_I, exceeds a critical value K_{IC}, which is the material's fracture toughness. In this study, the stress intensity factor of PLA decreased in two cases. The first one was when vegetal fibers were added to the mix and the second one after 250 hours of UV aging at 32°C. These results showed the reduced ability of the composite to resist crack initiation and propagation (Table VI-8). The weak interfacial adhesion between the two phases caused microvoids and microflows in the composites. In this context each fiber acts as a discontinuity initiating cracks and guiding their propagation [49]. This phenomenon increases during aging.

Reference	Sample	Aging type	K_I [MPa*m^0.5]
1	PLA (C)	NA	3.40 ± 0.34
4	PLA$_{80}$MIS$_{20}$ (MC)	NA	1.84 ± 0.10
1'''	PLA (C)	UV	2.44 ± 0.17
4'''	PLA$_{80}$MIS$_{20}$ (MC)	UV	1.34 ± 0.24

Table VI-8. Stress intensity factor (K_I) values for PLA (C) and PLA$_{80}$MIS$_{20}$ (MC) not aged (NA) and aged for 250 hours with UV (λ<280nm) at 32°C in a dried environment.

Secondly, an accelerated aging was conducted at 47 ± 5°C and 50% of humidity under UV in order to understand the effect of temperature and humidity on the mechanical properties of PLA and its composites. After aging an increase in Young Modulus can be observed for all composites. The materials became more brittle as showed in figure VI-10. For the composites $PLA_{80}MIS_{20}$ (MC) and $PLA_{80}MIS_{20}$ (DCP) (MC) a strong drop in final strength can be also observed (figure VI-11). The neat matrix is not greatly affected by the aging conditions also in this case. All these effects could be explained by the moisture absorption attributed mainly to vegetal fibers. The swelling and shrinking caused by hydration and dehydration caused a decrease in the interfacial interaction with consequent deterioration of the mechanical properties. The highest reduction in final strength occurred for composites realized with DCP. For these composites a yellowish color is noted on the surface of aged samples (images not reported in this work). This last observation might suggest the deterioration of lignin as showed in different works [50, 51]. In particular, many groups present in the lignin structure are able to absorb daylight, acting as preferred sites for photochemical oxidation reactions. Although this effect can be noticed also for composites with raw fibers, probably the deterioration process is accelerated by the presence of unreacted DCP present in the processed materials [52]. Moreover, according to literature, acetophenone, a decomposition product of DCP, can form radicals due to the absorption of UV light under 300 nm, favoring the composites degradation [53].
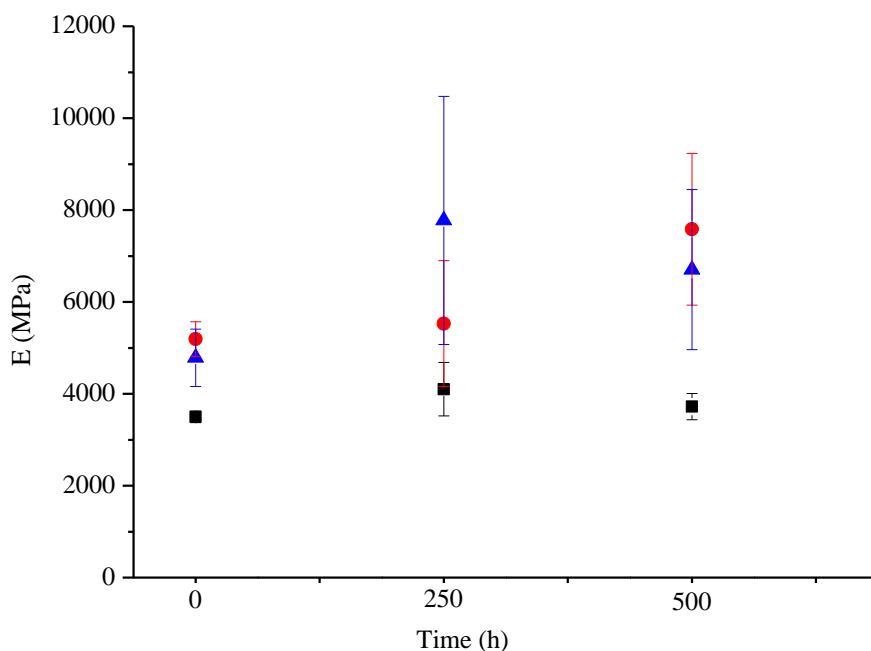

Figure VI-10. Young Modulus (E) for neat matrix (■), $PLA_{80}MIS_{20}$ (MC) (●) and $PLA_{80}MIS_{20}$(DCP) (MC) (▲) after 250h and 500h of UV (λ<280nm) at 47 ± 5°C and 50% of humidity.
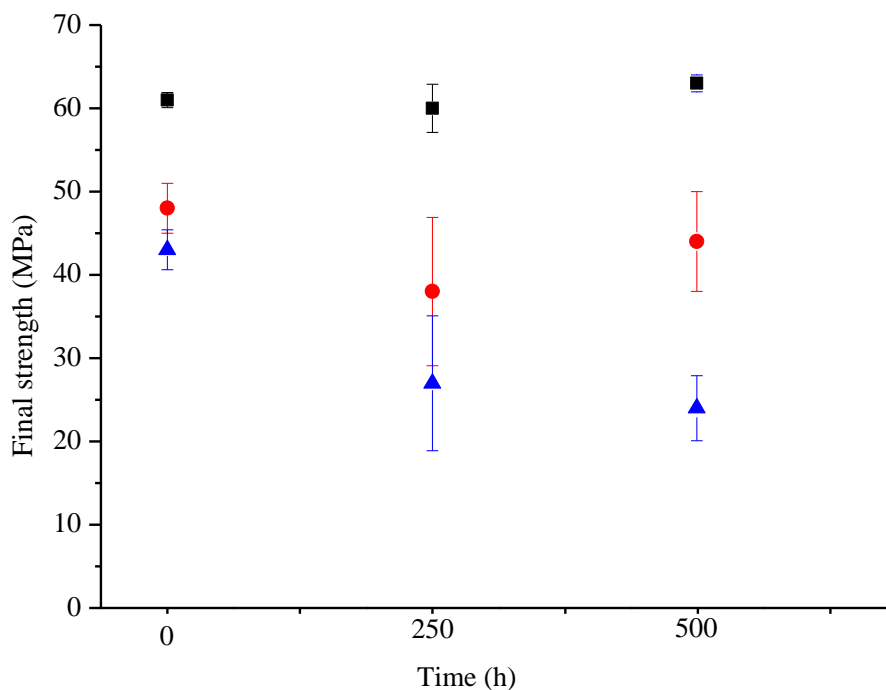
Figure VI-11. Final strength for neat matrix (■), PLA$_{80}$MIS$_{20}$ (MC) (●) and PLA$_{80}$MIS$_{20}$ (DCP) (MC) (▲) after 250h and 500h of UV (λ<280nm) at 47±5°C and 50% of humidity.

VI-5.3 EFFECT OF AGING EVALUATED BY SEM IMAGES

As showed in the previous paragraphs, the effect of aging on the chemical structure of composites, in particular at temperatures higher than the ambient one, combined with UV and humidity is more important for the composites than for the neat matrix. Among all composites realized, those in which DCP is present showed a rapidly degradation. For this reason SEM images were recorded on the cross section of composites realized with raw fibers and fibers modified with DCP before and after aging, in order to show any eventual change in the polymer structure. Figure VI-12 confirmed the results obtained previously. In the case of fibers modified with DCP, the appearance of fibers surface after aging is not the same; the literature reports that at UV light under 300 nm, which correspond exactly to our case, the formation of sub products during the reaction, such as acetophenone [53] can occur. However in our case we believe that this change might be due to the presence of unreacted DCP that at 47°C could continue to crosslink the matrix, forming these peculiar polymer structures on the surface of fibers.
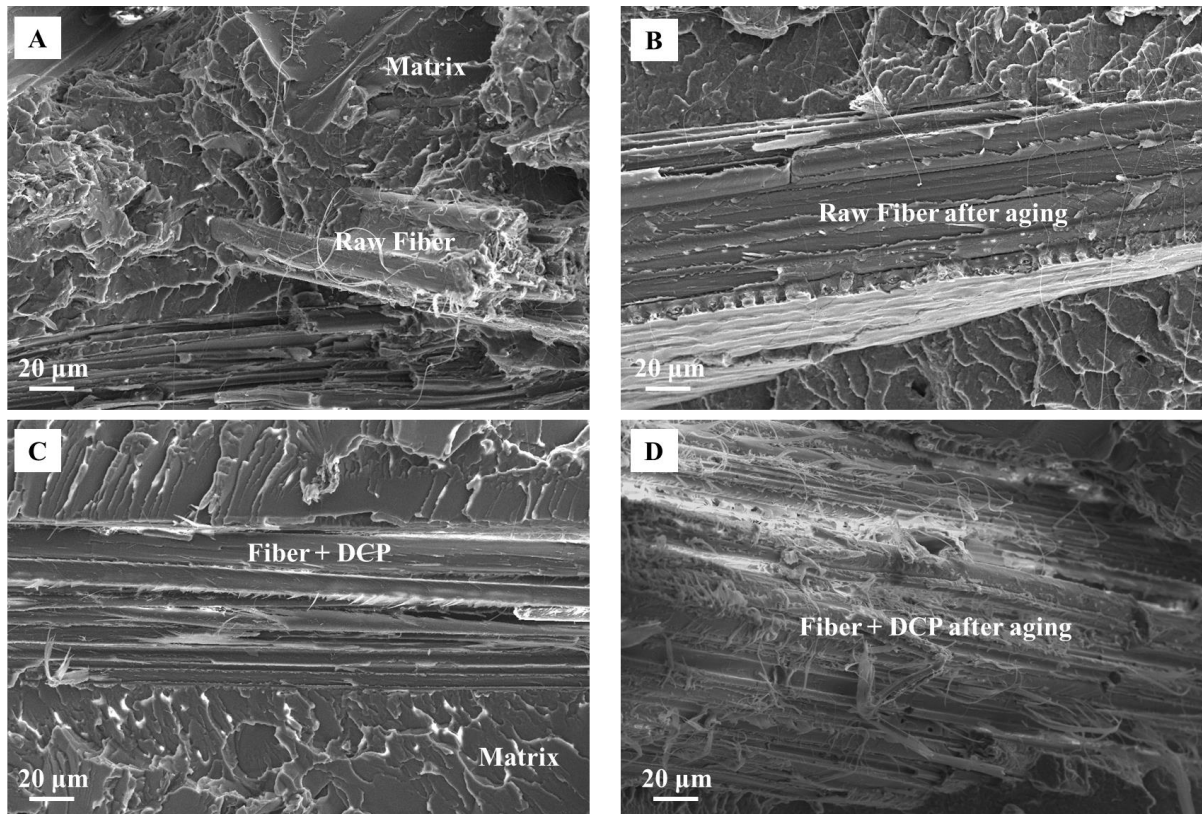
Figure VI-12. SEM images of PLA$_{80}$MIS$_{20}$ (A) PLA$_{80}$MIS$_{20}$ (DCP) (C) not aged and PLA$_{80}$MIS$_{20}$ (B) PLA$_{80}$MIS$_{20}$ (DCP) (D) after aging (UV (λ<280nm) at 47±5°C for 250h at 50% humidity).

VI-6. CONCLUSIONS AND PERSPECTIVES

In this work the effect of different chemical modifications, processing methods and aging conditions were studied on PLA and PLA-based composites. The conditions adopted for processing, in particular the cooling type and the shear stress applied level, have a great impact on the crystallinity of the polymer, changing the mechanical properties of the final materials. All these changes were detected using different analyses.

At a first glance, mixing and compression molding seems to be the most rapid and simple process, and at the same time the less aggressive way to manufacture this type of composites. However, it seems also that resulting polymers structure might be affected, resulting in an almost completely amorphous structure. Moreover, the great advantages described about mixing and compression molding are in contrast with certain mechanical properties, typically the final strength, which is higher in the case of extruded and injected samples and which is the fundamental parameters that have to be taken into account when a chemical treatment of fibers is applied. It is believed that a change in process parameters or secondary heat treatments could yield a different crystalline structure but this will have to be confirmed by further investigations.

In our case, the chemical modification of vegetal fibers surface adopted did not have a significant impact on the mechanical properties of the composites, when compared with results for PCL and PHBHV described in the previous chapters. This fact suggests that probably PLA needs a different chemical treatment before compounding with modified fibers. The dependency of crystallinity, mechanical properties and macromolecular changes on aging conditions confirmed that the tensile properties can be associated with the crystallization of PLA and with the decrease in molar mass. Humidity associated to high temperature and UV accelerate the degradation process, in particular for composites modified with DCP indicating the residual presence of unreacted peroxide which could start various reactions during aging.

Although chemical modification proposed in this work did not give the expected results, composites PLA/MIS realized with raw fibers showed good mechanical properties with a Young Modulus and a tensile strength higher than some fibers-reinforced traditional plastics, such as polypropylene (PP)/MIS composites [54, 55]. The mechanical properties of the materials proposed here remain higher than those obtained with PP also after different aging conditions. These facts suggest that, acting on processing parameters it will be possible to create a defined PLA-based

composite with specific mechanical characteristics and crystallinity that can in the future substitute the traditional plastics.

However, the improvements in mechanical properties might be counterbalanced by a greater sensitivity of the resulting composite to ageing, unless the stability of the latter is improved. At present, it would seem that work in this direction might aim at reducing the effect caused by the hydrophilic nature of the reinforcing fibers.

VI-7. APPENDIX

VI-7A. TORQUE AND TEMPERATURE PROFILES FOR PLA AND PLA-BASED COMPOSITES
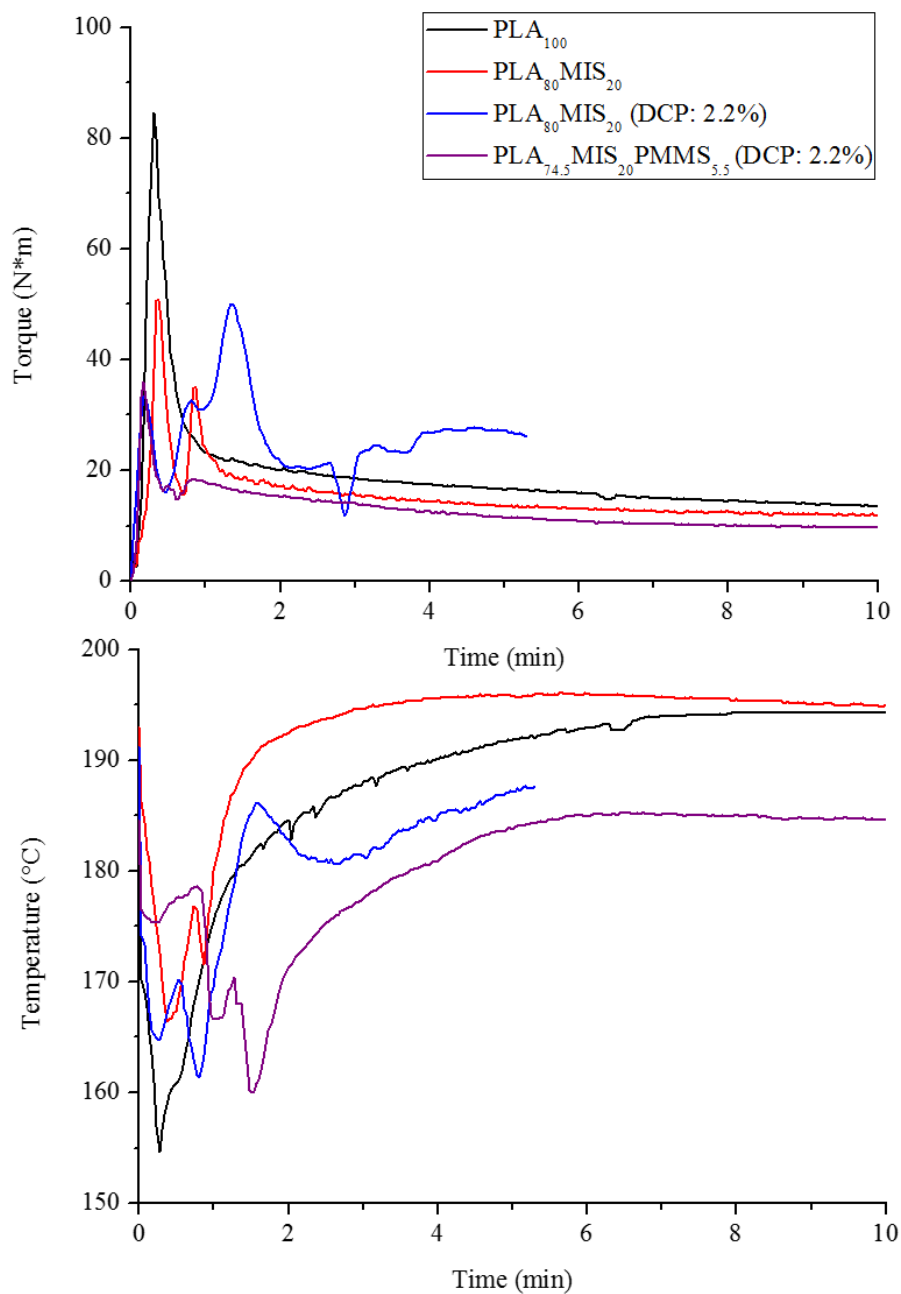
Figure VI-A1. Torque and Temperature profiles vs Time for neat PLA and PLA/MIS composites realized with raw or modified fibers.

VI-7B. PROPERTIES OF PLA-BASED COMPOSITES

Sample	Method	E [MPa]	σ_r [MPa]	σ_{max} [MPa]	ε_r
PLA	C	3707 ± 22	57 ± 0.54	63 ± 0.23	0.07 ± 0.03
PLA	MC	3510 ± 30	56 ± 2.14	61 ± 0.86	0.06 ± 0.03

Table VI-B1. Effect of mixing step on the mechanical properties of neat PLA: compressed granules (C) and mixed and compressed granules (MC).
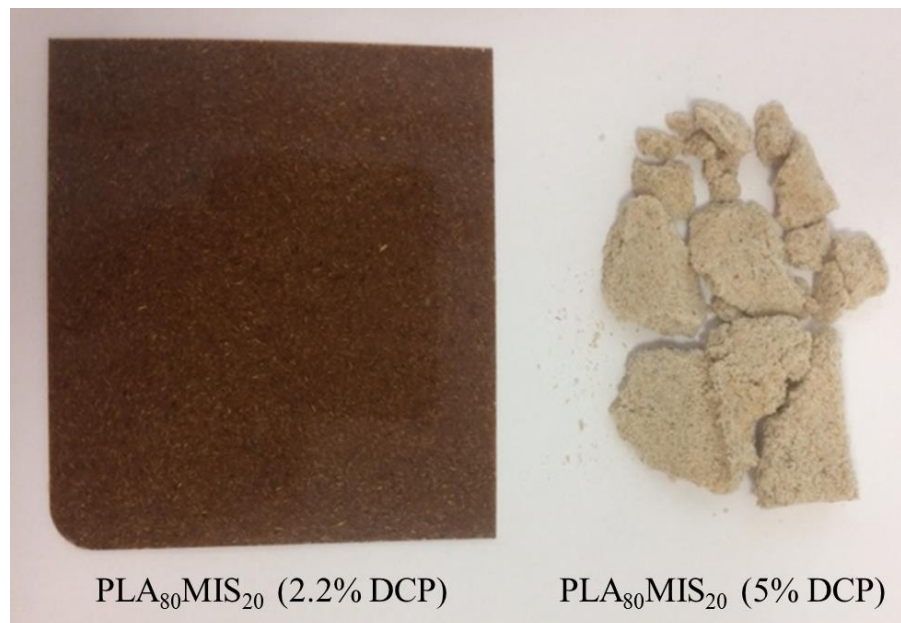
Figure VI-B1. Texture of composites $PLA_{80}MIS_{20}$ at 2.2% DCP (on the left) and 5% DCP (on the right).

VI-7C. CHARACTERIZATION OF PLA AND ITS COMPOSITES AFTER AGING
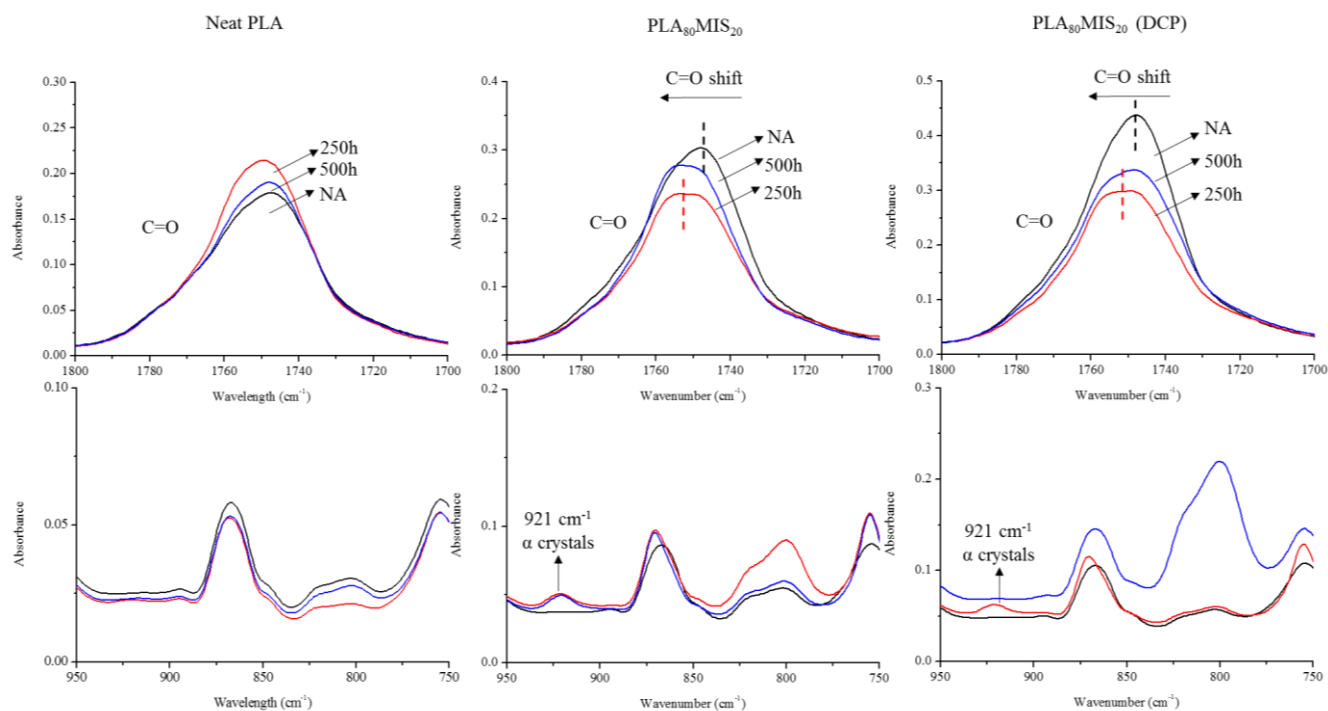
Figure VI-C1. Effect of UV, temperature and humidity on the carbonyl ester group and on the crystalline zone (700-950 cm^{-1}) for neat PLA, composite PLA$_{80}$MIS$_{20}$ and PLA$_{80}$MIS$_{20}$ (DCP).
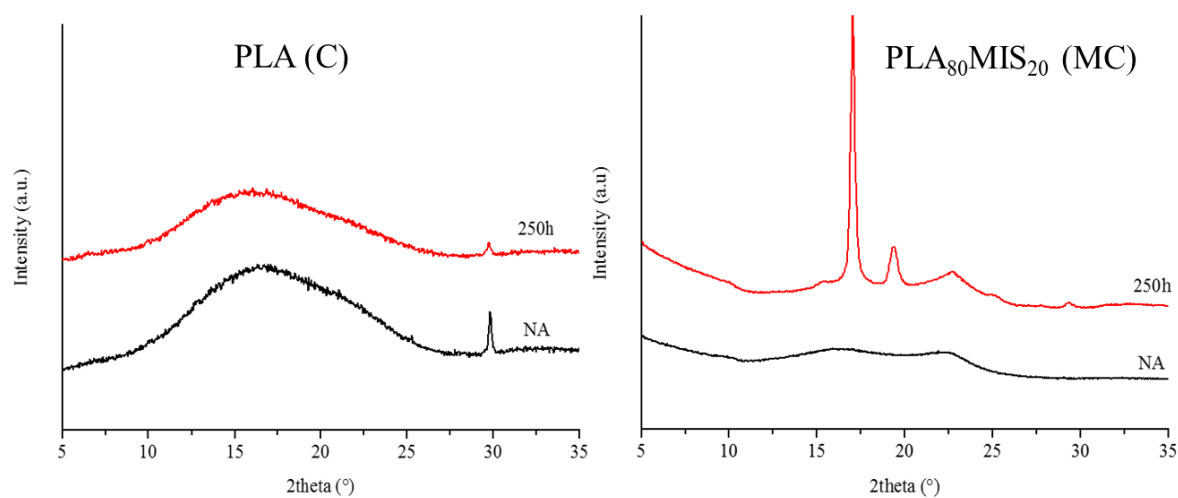
Figure VI-C2. Diffractograms of PLA(C) (on the left) and PLA$_{80}$MIS$_{20}$ (MC) (on the right) before (black curves) and after aging (red curves).

VI-8. REFERENCES

1. Vink, E.T.H. et al., Applications of life cycle assessment to NatureWorks™ polylactide (PLA) production. *Polymer Degradation and Stability* 80(3), p. 403-419 (**2003**).
2. Auras, R. et al., An Overview of Polylactides as Packaging Materials. *Macromolecular Bioscience* 4(9), p. 835-864 (**2004**).
3. Lim, L.T. et al., Processing technologies for poly(lactic acid). *Progress in Polymer Science* 33(8), p. 820-852 (**2008**).
4. Bajpai, P.K. et al., Development and characterization of PLA-based green composites. *Journal of Thermoplastic Composite Materials* 27(1), p. 52-81 (**2012**).
5. Oh, J.K., Polylactide (PLA)-based amphiphilic block copolymers: synthesis, self-assembly, and biomedical applications. *Soft Matter* 7(11), p. 5096-5108 (**2011**).
6. Ignatius, A.A. et al., In vitro biocompatibility of bioresorbable polymers: poly(L, DL-lactide) and poly(L-lactide-co-glycolide). *Biomaterials* 17(8), p. 831-839 (**1996**).
7. Kim, K. et al., Control of degradation rate and hydrophilicity in electrospun non-woven poly(d,l-lactide) nanofiber scaffolds for biomedical applications. *Biomaterials* 24(27), p. 4977-4985 (**2003**).
8. Gruber, P. et al., Polylactides. 'NatureWorksTM PLA', in *Biopolymers. Polyesters III. Applications and Commercial Products*, Y. Doi and A. Steinbuchel, Editors. Weinheim: Wiley-VCH. (**2002**), p. 235-250.
9. Bhatia, A. et al., Compatibility of biodegradable poly (lactic acid)(PLA) and poly (butylene succinate)(PBS) blends for packaging application. *Korea-Australia Rheology Journal* 19(3), p. 125-131 (**2007**).
10. Nishino, T. et al., Kenaf reinforced biodegradable composite. *Composites Science and Technology* 63(9), p. 1281-1286 (**2003**).
11. Finkenstadt, V.L. et al., Poly(lactic acid) green composites using oilseed coproducts as fillers. *Industrial Crops and Products* 26(1), p. 36-43 (**2007**).
12. Cheng, S. et al., Mechanical and thermal properties of chicken feather fiber/PLA green composites. *Composites Part B: Engineering* 40(7), p. 650-654 (**2009**).
13. Yu, T. et al., Preparation and properties of short natural fiber reinforced poly(lactic acid) composites. *Transactions of Nonferrous Metals Society of China* 19, p. s651-s655 (**2009**).
14. Huda, M.S. et al., Effect of fiber surface-treatments on the properties of laminated biocomposites from poly(lactic acid) (PLA) and kenaf fibers. *Composites Science and Technology* 68(2), p. 424-432 (**2008**).
15. Ochi, S., Mechanical properties of kenaf fibers and kenaf/PLA composites. *Mechanics of Materials* 40(4), p. 446-452 (**2008**).
16. Tokoro, R. et al., How to improve mechanical properties of polylactic acid with bamboo fibers. *Journal of Materials Science* 43(2), p. 775-787 (**2008**).
17. Bourmaud, A. et al., Investigations on mechanical properties of poly(propylene) and poly(lactic acid) reinforced by miscanthus fibers. *Composites Part A: Applied Science and Manufacturing* 39(9), p. 1444-1454 (**2008**).
18. Yu, T. et al., Effect of fiber surface-treatments on the properties of poly(lactic acid)/ramie composites. *Composites Part A: Applied Science and Manufacturing* 41(4), p. 499-505 (**2010**).
19. Bledzki, A.K. et al., Mechanical properties of PLA composites with man-made cellulose and abaca fibres. *Composites Part A: Applied Science and Manufacturing* 40(4), p. 404-412 (**2009**).
20. Graupner, N. et al., Natural and man-made cellulose fibre-reinforced poly(lactic acid) (PLA) composites: An overview about mechanical characteristics and application areas. *Composites Part A: Applied Science and Manufacturing* 40(6), p. 810-821 (**2009**).
21. Bleach, N.C. et al., Effect of filler type on the mechanical properties of self-reinforced polylactide–calcium phosphate composites. *Journal of Materials Science: Materials in Medicine* 12(10), p. 911-915 (**2001**).
22. Ikada, Y. et al., Biodegradable polyesters for medical and ecological applications. *Macromolecular Rapid Communications* 21(3), p. 117-132 (**2000**).
23. Dorgan, J.R. et al., Polylactides: properties and prospects of an environmentally benign plastic from renewable resources. *Macromolecular Symposia* 175(1), p. 55-66 (**2001**).

24. Baley, C. et al., Etat de l'art sur les matériaux composites biodégradables. *Revue des composites et des matériaux avancés* 14(2), p. 135-166 (**2005**).

25. Zandvliet, C. et al., Proposition of an Accelerated Ageing Method for Natural Fibre/Polylactic Acid Composite. *Journal of The Institution of Engineers (India): Series D* 96(2), p. 151-158 (**2015**).

26. Ndazi, B.S. et al., Characterization of hydrolytic degradation of polylactic acid/rice hulls composites in water at different temperatures. *Express Polymer Letters* 5(2) (**2011**).

27. Li, S. et al., Further investigations on the hydrolytic degradation of poly (DL-lactide). *Biomaterials* 20(1), p. 35-44 (**1999**).

28. Zhang, X. et al., Morphological behaviour of poly(lactic acid) during hydrolytic degradation. *Polymer Degradation and Stability* 93(10), p. 1964-1970 (**2008**).

29. Badía, J.D. et al., Assessing the MALDI-TOF MS sample preparation procedure to analyze the influence of thermo-oxidative ageing and thermo-mechanical degradation on poly (Lactide). *European Polymer Journal* 47(7), p. 1416-1428 (**2011**).

30. Gupta, M.C. et al., Thermal oxidative degradation of poly-lactic acid. *Colloid and Polymer Science* 260(3), p. 308-311 (**1982**).

31. Rasselet, D. et al., Oxidative degradation of polylactide (PLA) and its effects on physical and mechanical properties. *European Polymer Journal* 50, p. 109-116 (**2014**).

32. Copinet, A. et al., Effects of ultraviolet light (315 nm), temperature and relative humidity on the degradation of polylactic acid plastic films. *Chemosphere* 55(5), p. 763-773 (**2004**).

33. Islam, M.S. et al., Influence of accelerated ageing on the physico-mechanical properties of alkali-treated industrial hemp fibre reinforced poly(lactic acid) (PLA) composites. *Polymer Degradation and Stability* 95(1), p. 59-65 (**2010**).

34. Semba, T. et al., The effect of crosslinking on the mechanical properties of polylactic acid/polycaprolactone blends. *Journal of Applied Polymer Science* 101(3), p. 1816-1825 (**2006**).

35. Wang, J. et al., Shear-induced enhancements of crystallization kinetics and morphological transformation for long chain branched polylactides with different branching degrees. 6, p. 26560 (**2016**).

36. Fischer, E.W. et al., Investigation of the structure of solution grown crystals of lactide copolymers by means of chemical reactions. *Kolloid-Zeitschrift und Zeitschrift für Polymere* 251(11), p. 980-990 (**1973**).

37. Gardette, M. et al., Photooxidation of polylactide/calcium sulphate composites. *Polymer Degradation and Stability* 96(4), p. 616-623 (**2011**).

38. Liu, X. et al., Kinetics of thermo-oxidative and thermal degradation of poly(d,l-lactide) (PDLLA) at processing temperature. *Polymer Degradation and Stability* 91(12), p. 3259-3265 (**2006**).

39. Abdelwahab, M.A. et al., Thermal, mechanical and morphological characterization of plasticized PLA–PHB blends. *Polymer Degradation and Stability* 97(9), p. 1822-1828 (**2012**).

40. Sawpan, M.A. et al., Improvement of mechanical performance of industrial hemp fibre reinforced polylactide biocomposites. *Composites Part A: Applied Science and Manufacturing* 42(3), p. 310-319 (**2011**).

41. Ragoubi, M. et al., Effect of corona discharge treatment on mechanical and thermal properties of composites based on miscanthus fibres and polylactic acid or polypropylene matrix. *Composites Part A: Applied Science and Manufacturing* 43(4), p. 675-685 (**2012**).

42. Oksman, K. et al., Natural fibres as reinforcement in polylactic acid (PLA) composites. *Composites Science and Technology* 63(9), p. 1317-1324 (**2003**).

43. Rodi, E.G. et al., Functionalization of Miscanthus by Photoactivated Thiol–Ene Addition to Improve Interfacial Adhesion with Polycaprolactone. *ACS Sustainable Chemistry & Engineering* 4(10), p. 5475-5482 (**2016**).

44. Fang, H. et al., Shear-Induced Nucleation and Morphological Evolution for Bimodal Long Chain Branched Polylactide. *Macromolecules* 46(16), p. 6555-6565 (**2013**).

45. Wang, J. et al., More Dominant Shear Flow Effect Assisted by Added Carbon Nanotubes on Crystallization Kinetics of Isotactic Polypropylene in Nanocomposites. *ACS Applied Materials & Interfaces* 7(2), p. 1364-1375 (**2015**).

46. Luo, S. et al., Interfacial Improvements in a Green Biopolymer Alloy of Poly(3-hydroxybutyrate-co-3-hydroxyvalerate) and Lignin via in Situ Reactive Extrusion. *ACS Sustainable Chemistry & Engineering* 4(6), p. 3465-3476 (**2016**).

47. Sapieha, S. et al., Dicumyl peroxide-modified cellulose/LLDPE composites. *Journal of Applied Polymer Science* 41(9-10), p. 2039-2048 (**1990**).
48. Meaurio, E. et al., Infrared Spectrum of Poly(l-lactide): Application to Crystallinity Studies. *Macromolecules* 39(26), p. 9291-9301 (**2006**).
49. Afrifah, K.A. et al., Fracture toughness of poly(lactic acid)/ ethylene acrylate copolymer/wood-flour composite ternary blends. *Polymer International* 62(7), p. 1053-1058 (**2013**).
50. Hon, D.N.-S. et al., Wood and cellulosic chemistry, revised, and expanded. CRC Press (**2000**).
51. Heitner, C., Light-Induced Yellowing of Wood-Containing Papers, in *Photochemistry of Lignocellulosic Materials*. American Chemical Society , p. 2-25 (**1993**).
52. Dan R., Visakh P. M., Photochemical Behavior of Multicomponent Polymeric-based Materials. Springer International Publishing (**2016**).
53. Snijders, E.A. et al., Effect of dicumyl peroxide crosslinking on the UV stability of ethylene-propylene-diene (EPDM) elastomers containing 5-ethylene-2-norbornene (ENB). *Polymer Degradation and Stability* 89(3), p. 484-491 (**2005**).
54. Chegdani, F. et al., Fiber type effect on tribological behavior when cutting natural fiber reinforced plastics. *Wear* 332, p. 772-779 (**2015**).
55. Murdy, R.C. et al., An in-depth analysis of the physico-mechanical properties imparted by agricultural fibers and food processing residues in polypropylene biocomposites. *AIP Conference Proceedings* 1664(1), (**2015**).

Conclusions and perspectives

This conclusion represents both a synthesis of the information presented in the course of this study and an overview on the future perspectives. All the considerations and principal results presented in the different chapters will guide the discussion towards possible applications and extensions of this work.

The objective of the first chapter was to give the reader the basic concepts related to the biocomposites world and a global overview of the potential matrixes and fibers, focusing progressively the attention on the principal processing methods and chemical modification of fibers used, which constitute in a certain manner one of the focus point of this work. The materials were treated taking into account both the macroscopic characteristics such as their mechanical and thermal properties and their microstructure by using a micromechanical approach. This part allowed us to choice three aliphatic biodegradable polyesters as matrixes, more precisely poly(caprolactone) (PCL), poly(3-hydroxybutyrate-*co*-3-hydroxyvalerate) (PHBHV) and poly(lactic acid) (PLA) and Miscanthus *giganteus* fibers as reinforcement. Actually, the experimental part was divided in several chapters that focuses on the biocomposites realized with these matrixes.

The aim of the second chapter was to propose an innovative chemical modification of vegetal fibers based on the thiol-ene reaction on the unsaturated bonds of lignin in the presence of peroxides to improve the adhesion matrix/fibers, solving by this way problems related to the hydrophilic character of the fibers, this last being incompatible with the hydrophobic one of the matrix. This part allows to a strong improvement in the mechanical properties of PCL/MIS biocomposites, demonstrating in this way not only the importance to add a reinforcement to the matrix, but also the efficiency of this method and its applicability to other biopolyesters. However, the non-renewable origin of PCL and its low thermal resistance led us to the investigation of other matrixes, most innovative and with a great potential.

For this reason, the third chapter focused on the PHBHV/MIS biocomposites, starting from the effect of the content of fibers on the mechanical properties of this matrix. This study highlighted the advantages and the limits to use a vegetal reinforcement; the use of too much less fibers content results in composites with no great interest from an industrial point of view. At the same time the use of too much high fibers is limited from the processing adopted,

resulting in a poor dispersion and formation of aggregates, these last formed also due to the lack adhesion fiber/matrix. The analytical model of Mori-Tanaka used to predict the elastic behavior of the biocomposites showed promising results for fibers imaged as cylinder aligned in the direction of the stress applied and at the same time showed various limits, including the assumptions of perfect contact and of heterogeneity in fibers dimensions. For these several reasons, the investigation of the effect of fibers dimensions and pathway was the focus of the fourth chapter. 2D and 3D finite element analyses were conducted to study the sensibility of the models to fibers dimensions and orientation in the matrix. The results demonstrated that 3D models better approximate the elastic behavior of the composite. Moreover, the transmission of the stress depends on the fibers pathway and content in the matrix. In this context, composites with aligned fibers induced less stress localization and are more rigid than the others. This result reveals that biocomposites for application in which high performance materials are required have to be realized using other processing methods able to control the orientation of fibers.

The fifth chapter intended to be a sort of synthesis of the previous two, in which the effect of fibers dimension was coupled with a reactive extrusion initiated by peroxides in order to improve the mechanical properties of the PHBHV-based composites. The study highlighted two different phenomena occurring in the biocomposites: the cross-linking of the matrix on one side and the grafting of fibers to matrix on the other side. This result constituted the starting point for the implementation of a numerical model in which the aim was not only to find a model that can predict the elastic properties of the biocomposite, but also to predict the gel fraction formed in the blend after the reactive process. Although the promising and innovative results obtained with PHBHV, its high cost which great limits its use to a very large scale, led us to the investigation of a more economic matrix in which the effect of process and the long term behavior of the material can be studied.

The last chapter was then dedicated to the economical PLA and its composites. The study showed that the processing method and more precisely the thermal treatment had a great impact on the mechanical properties of the biocomposites and also on the crystallinity of the neat matrix. Moreover, the photo-oxidative aging of the PLA-based composites showed a general embrittlement of the material with the time, this last being more important for composites modified with peroxides. The composites manufactured in this last chapter exhibited an extraordinary elastic modulus and final strength when manufactured by mixing and compression molding, maintaining good properties also after aging. These promising results

demonstrated the feasibility to realize economical biocomposites able to concur with traditional plastics reinforced with glass fibers.

The presentation of the macroscopic characteristics of the biocomposites manufactured in this work highlighted not only their dependence from the processing methods, but also from their microstructure. We exposed the limits of some analytical and numerical models in the third and fourth chapters. Nevertheless, microscopic techniques associated to these models seem a promising way for the identification of a model able to predict the elastic properties of the biocomposites. Although, the engine of this work has been that to find an equilibrium between the simplicity of the model and the not simplistic description of the reality, the complexity of this last has constrained us to make some assumptions. Starting from this point, it seems logic that in order to have more precise information about the microstructure, other techniques should to be used such as micro-tomography. By this methods, the real images of any sample could be used for the implementation of more realistic finite element models.

The systematic association of numerical models to the practical realization of the materials seems to be a good method in order to obtain information on the relations existing between macro-properties and microstructure. Therefore, the interdisciplinarity of this work seems to be a good starting point for the concrete realization of biocomposites based on vegetable fiber in the near future. The wide choice of matrixes and fibers will allow us to create composites suitable in the most diverse fields, from that of construction to niche sector for the most expensive matrixes.